409 522

ASD-TDR-63-326

FUNDAMENTAL STUDY OF JET NOISE GENERATION AND SUPPRESSION

VOL I EXPERIMENTAL AND THEORETICAL INVESTIGATIONS OF MODEL JET EXHAUST STREAM NOISE AND THE DEVELOPMENT OF NORMALIZING PARAMETERS FOR SIZE AND TEMPERATURE

TECHNICAL DOCUMENTARY REPORT ASD-TDR-63-326

March 1963

Propulsion Laboratory
Aeronautical Systems Division
Air Force Systems Command
Wright-Patterson Air Force Base, Ohio

Project No. 3066, Task 306601

(Prepared under Contract No. AF 33(657)-8405 by Armour Research Foundation of Illinois Institute of Technology, Chicago, Illinois; William C. Sperry, A. Peter, and R. [illegible], authors)

NOTICES

When Government drawings, specifications, or other data are used for any purpose other than in connection with a definitely related Government procurement operation, the United States Government thereby incurs no responsibility nor any obligation whatsoever; and the fact that the Government may have formulated, furnished, or in any way supplied the said drawings, specifications, or other data, is not to be regarded by implication or otherwise as in any manner licensing the holder or any other person or corporation, or conveying any rights or permission to manufacture, use, or sell any patented invention that may in any way be related thereto.

ASTIA release to OTS not authorized.

Qualified requesters may obtain copies of this report from the Armed Services Technical Information Agency, (ASTIA), Arlington Hall Station, Arlington 12, Virginia.

Copies of this report should not be returned to the Aeronautical Systems Division unless return is required by security considerations, contractual obligations, or notice on a specific document

FOREWORD

This report was prepared by Armour Research Foundation of Illinois Institute of Technology, Chicago, Illinois on Air Force Contract AF 33(657)-8405, "Theoretical and Experimental Study of Jet Noise Generation and Suppression Mechanisms." The work was administered under the direction of the Propulsion Laboratory. Mr. E. E. Buchanan was task engineer of the laboratory.

The work was begun in April 1962, and ended in March 1963. The project leader was W. C. Sperry and other contributors were C. S. Caccavari, R. W. Higgs, D. F. Pernet, H. H. Hall, R. Kamo, A. Peter, P. W. Cooper, S. Dubren, J. Fitzgerald, and B. Glicksberg.

ABSTRACT

Part I

Far-field sound pressure levels were measured in an anechoic room for noise generated by cold air flow through a wide variety of small nozzle configurations including converging, converging-diverging, and annular types with and without center core flow. The results are examined in terms of flow and acoustic power performance, directivity, and power spectral density. Normalization parameters are developed for both size and temperature which show good agreement between flow and acoustic performance of small cold jet nozzles, large hot jet nozzles, and jet engines. A particular configuration of annular plug nozzle exhibited remarkably good acoustic performance with no measurable loss of mass flow performance.

Part II

A simplified theory on the acoustical attenuation qualities of an extended plug nozzle is presented. The theory is based upon similarity relationships and on the location of shock structure, a parameter which remains constant in supersonic flow. Theoretical curves of noise attenuation versus nozzle geometrical parameters show reasonable agreement with our experimental cold jet results for a nozzle exhibiting ten to fifteen decibels reduction over a wide mass flow range. Design criteria is given which indicate that twenty or more decibels reduction may be accomplished by an optimally designed nozzle.

TABLE OF CONTENTS

Part I

TABLE OF CONTENTS (Continued)

TABLE OF CONTENTS (Continued)

LIST OF TABLES

Part I

LIST OF TABLES (Continued)

Part II

LIST OF FIGURES

Part I

LIST OF FIGURES (Continued)

LIST OF FIGURES (Continued)

LIST OF FIGURES (Continued)

LIST OF FIGURES (Continued)

LIST OF FIGURES (Continued)

LIST OF FIGURES (Continued)

LIST OF FIGURES (Continued)

FUNDAMENTAL STUDY OF JET NOISE GENERATION AND SUPPRESSION

Volume I

EXPERIMENTAL AND THEORETICAL INVESTIGATIONS OF MODEL JET EXHAUST STREAM NOISE AND THE DEVELOPMENT OF NORMALIZING PARAMETERS FOR SIZE AND TEMPERATURE

Part I

EXPERIMENTAL INVESTIGATIONS, RELATED THEORY, AND DEVELOPMENT OF NORMALIZATION TECHNIQUE

by

William C. Sperry

SECTION I

INTRODUCTION AND SUMMARY

The research reported in the following sections is a logical extension of the work reported in Refs. 1, 2, and 3. Our objectives were the following:

(1) to establish nozzle design principles for inflight suppression of high velocity jet stream noise;

(2) to describe as much flow and acoustic performance phenomena as possible by means of engineering equations suitable for direct application;

(3) to demonstrate that small cold model jet investigations are both practical and invaluable for preliminary design of jet engine nozzle configurations;

(4) to recommend minimum standards for reporting measured flow and acoustic performance data so that the work of all investigators can be satisfactorily compared;

(5) to contribute toward a better understanding of the mechanisms of jet noise generation and suppression.

As jet aircraft continue to grow larger and faster, the mechanical power of the exhaust jet stream increases as well. A common conception of jet noise is that acoustic power is a variable fraction of the turbulent power of the jet stream which in turn is a small fixed fraction of mechanical power, see Ref. 1, Chapter VI, pp 148. Furthermore, as mechanical power increases, the acoustic power increases at a faster rate until it ultimately equals turbulent power as an upper limit. From then on, acoustic power increases commensurate with mechanical power. This concept, while not established as fact, is quite logical. The question then is, if acoustic power ultimately increases directly as mechanical power, what hope is there for satisfactory jet noise control? We believe that, while there is no foreseeable chance that jet noise can ever be eliminated, there is an excellent chance to effect significant control in a fairly wide mechanical power range below the point where acoustic power would equal turbulent power. Our belief is based upon the concept that initially acoustic power is a variable fraction of turbulent power but with no general agreement as to the exact variable relationship. Consequently, we have approached the problem, primarily in an experimental manner, by investigating the flow and

---

Manuscript released by author 31 March 1963 for publication as an ASD Technical Documentary Report.

acoustic performance of a wide variety of model nozzle configurations in an attempt to see if there is a variation in acoustic performance with no sacrifice in flow performance, and if so, to attempt optimization.

The pessimistic view is that since inflight suppression techniques are handicapped by the need to provide a radical change to a very small portion of jet stream energy without significantly affecting the majority, the problem is hopeless. Our viewpoint is that since very little is known about the performance of various nozzle configurations above the critical pressure ratio, it is wrong to prejudge. Actually our investigations have shown that all nozzles with good flow performance have essentially the same acoustic performance below the critical pressure ratio but vary widely above. Furthermore, at least two nozzle configurations perform acoustically above the critical pressure ratio even better than theoretical extrapolations would indicate. The consequence of this is, that if the results from our small cold jets can be scaled to jet engines, and we believe they can, it is possible by new nozzle configurations to operate jet engines at increased mechanical power with no increase in noise. In other words, it is possible that the existing line can be held for larger and faster jet aircraft.

Section IV of Part I presents theoretical predictions for flow and acoustic performance including spectral character, of jet nozzles. The theory is based upon isentropic conditions and results from combining ideal gas relations and equation of state with the one dimensional Euler equation of motion for steady flow. The manipulations were ultimately put into engineering type equations and graphs suitable for direct application. In general, the experimental results were in excellent agreement with the engineering equations.

One of our main objectives was to demonstrate the extreme usefulness of small cold model jet acoustical investigations with respect to jet engine nozzle design. If this can be verified, the advantages are considerable. First, many nozzle configurations can be investigated at relatively small expense. What is more important, however, is that many more qualified investigators can contribute to basic studies without being limited to those having access to large hot jet facilities. In our estimation, theory alone will not solve the jet noise problem. Experiment is needed, both to corroborate theory and to supply clues for modifying theory as well.

Everyone recognizes the need for model studies since it is far too expensive and time consuming to experiment entirely with jet engines. However, there is no general agreement as to the limitations of size and temperature for models for which the results can be considered applicable in some way to jet engines. Our approach was to design a small cold jet facility which was very flexible, easy and inexpensive to operate, and had the capability of producing precise and repeatable data. We then combined theory and measurement until we were satisfied that our particular cold jet results were adequately explained and size scaled or normalized over our rather limited size range. We then attempted to locate similar measured data by other investigators for large hot jets and jet engines in order to corroborate our size scaling technique and to develop normalizing factors for temperature. We were entirely successful in developing normalizing factors for size and temperature which were in excellent agreement with comparable

results for a four-inch conical nozzle and in fair agreement with some jet engines. This agreement includes flow and acoustic performance and power spectral densities. We make no claims, however, that the validity of our normalizing techniques are conclusive until we can verify them with much more large hot jet data. Nevertheless, we have found no reason to be other than optimistic and it would be remarkable indeed if our cold jet results, which agree so well with theory and with the results of independent investigations for a four-inch hot jet, should abruptly cease to be valid above a four-inch size. There are lower limits to size however and we have attempted to clearly indicate them.

In our search for hot jet data by other investigators we found extreme difficulty in locating sufficient measured results suitable for the development of normalizing techniques. Most experimental investigators of jet noise at least measure total pressure and temperature, mass flow, and acoustic power levels. These factors are relatively easily obtained and should form the basis of minimum standards. Other factors such as thrust and velocity profiles are important but are much more difficult to obtain to satisfactory degrees of accuracy and, consequently, are most often omitted. However, it appears that most investigators do not believe that the four basic factors can adequately represent flow and acoustic performance of jet nozzles and engines and take the rather dubious approach of computing such other factors such as thrust, velocity, acoustic efficiencies, Lighthill parameters, etc. This leads to considerable confusion when attempts are made to compare and use the results of the various investigators, particularly when there is not general agreement as to the methods of computing these additional factors. Furthermore, while most investigators measure the four basic factors, the majority omit reporting one or more of them.

As a consequence, we have considered one of our objectives to be the development of minimum standard methods for data representation which will be suitable for comparison among various investigators. We have chosen graphical as opposed to tabular methods of data representation where both the ordinate and abscissa consist of measured quantities only. Theoretical predicted curves are superposed for comparison.

In our estimation, a portion of our experimental results have turned out to have no direct application to jet noise suppression. However, we have included the results in this report because they were part of our evolutionary approach and did contribute to a better understanding of the mechanisms of jet noise generation and suppression. In fact, whether our normalizing techniques are ultimately proven valid or not, we believe that our small cold jet results can be of assistance to others in contributing to a better basic understanding of jet flow and noise phenomena.

SECTION II

EXPERIMENTAL FACILITY

The jet noise facility is shown in Fig. 1. The facility is of the blow-down type where compressed air was dried, filtered, and stored in tanks having a total volume of about 80-cubic feet at a maximum pressure of 125 psig. The stored air was released by a manually controlled, 3-inch, quick opening ball valve where it then successively passed through a 3-inch pressure reducing valve, a 4-inch flexible tube through the wall of the anechoic room, a calming tank, and a nozzle. The pressure reducing valve is capable of precisely controlling the pressure in the calming tank from 2 to 60-psig. The 16-inch diameter by 39-inch long calming tank contains six fine mesh woven wire screens designed to minimize the turbulence generated by air flow through piping and valves. Temperature and pressure sensors, located in the calming tank between the screens and nozzle, were remotely monitored at the control station located outside the anechoic room. Because of the large ratio of calming tank diameter to nozzle diameter, stagnation conditions were maintained in the tank with an error of less than 0.1 percent.

Mass flow through all nozzles was measured by timing the pressure decrease in the storage tanks. Overall sound pressure levels were measured at seven stations located in a horizontal plane and on a circular arc having a radius of 88-inches measured from the nozzle exit as shown in Fig. 1(d). The stations have an angular separation of 15-degrees and are located at the 15 through 105-degree angles where 0-degrees is considered to be the downstream jet axis. One microphone was used, consequently, seven air flow runs were required for one survey, moving the microphone from station to station between runs. Repeatability of pressure, temperature, and sound was excellent. The acoustic environment was essentially free-field as the air jet exhausted into and the sound pressure measurements were made in an anechoic room having a usable volume of about 1600-cubic feet with a lower cut-off frequency of about 130 cycles per second.

All nozzles investigated for this program are identified in Tables I through IV which include sketches and significant geometrical information. The nozzles are grouped into three general types, (1) basic, (2) annular with center core flow, and (3) annular plug. The basic types consist of a family of four different sizes but geometrically scaled converging nozzles with short extensions, a converging nozzle with no extension, three different converging-diverging types, and four converging nozzles with long extensions. Investigations of these basic types gave much valuable information useful for size scaling and establishment of lower limits of size. Annular with center core flow nozzles were all constructed by combining various basic nozzles. Both primary and by-pass flow were assumed to have the same pressure ratio since both nozzles of the combination were mounted to the same calming tank and subjected to the same stagnation pressure. Annular plug nozzles consisted of the basic types with a center solid straight bar terminated with various solid cones.

SECTION III

PERFORMANCE REPRESENTATION AND MEASUREMENT TECHNIQUE

The quantities of interest for this program are pressure ratio (p_s/p_o), mass flow (m), acoustic power level (PWL), sound pressure level (SPL) at various azimuth stations, frequency (f), and stagnation temperature (T_s). For our cold jet experiments, stagnation temperature is essentially equal to ambient temperature, hence $T_s = T_o$. However, we will refer to hot jet data by others, so that we are concerned with values of T_s other than ambient. It is our objective to utilize the above quantities to 1) determine the noise generating capabilities of various nozzle configurations, 2) determine one or more nozzle configurations which generate significantly less noise with minimum loss in flow performance, and 3) develop normalizing parameters such that our data obtained from small cold jets will be valid for large hot jets.

While our jet nozzles are small, we are concerned with a fairly wide range of sizes. For example, of all nozzle configurations under consideration at the present time, the largest has an exit area over six times that of the smallest. Consequently, in order to be able to determine significant trends of acoustic and flow performance, some sort of size normalization is needed. Our experience to date indicates that, when acoustic power and mass flow are divided by some characteristic nozzle area, size normalization is accomplished. Initially, we chose nozzle exit area as the characteristic area. Subsequent examination, however, indicated that this might not be satisfactory for all cases. For example, consider annular nozzles with center core flow. When the center nozzle exhausts interior to the exit plane of the outer nozzle, the exit area of the composite nozzle is equivalent to that of the outer nozzle. When the center nozzle exhausts at the exit plane of, or exterior to the outer nozzle, the exit area of the composite nozzle is somewhat less than that of the outer nozzle. This difference is due to the finite thickness of the walls of the center nozzle. While the difference between gross and net areas for the various nozzle combinations investigated is not great, the scaling results for acoustic and flow performance have sufficient differences that significant trends could conceivably be masked by normal experimental scatter.

As a result, the characteristic area to be used for scaling center core flow types will, henceforth, be that of the minimum flow cross-section normal to the axis of flow (A_m). For all other nozzles the characteristic area will be the exit area (A).

As mentioned above, a very important part of our experimental effort was to be cognizant of significant trends so that we could direct further investigations in the most optimistic direction. Therefore, the measured data was to be graphed in the most informative manner possible. With our present cold jet facility, we were capable of precisely measuring the following five quantities for all nozzles.

1. pressure ratio

2. mass flow

3. sound pressure levels for various azimuth stations

4. frequency spectrums of sound pressure levels

5. stagnation temperature

These quantities were used to represent nozzle performance by means of the following four types of graphs.

1. mass flow versus pressure ratio

$$m/A \text{ versus } p_s/p_o$$

2. power level versus mass flow

$$PWL - 10 \log A \text{ versus } m/A$$

3. directivity versus mass flow

$$DI \text{ versus } m/A$$

4. power spectral density

In addition normalization techniques were developed with the objective of proving the generality of the results from small cold jet nozzles with respect to large hot jet nozzles.

MASS FLOW MEASUREMENTS

Mass flow through all nozzles was determined by measuring air storage pressures and temperatures and the time rate of change of each for a condition of constant stagnation pressure and temperature. For a blowdown system, the mass flow of the evacuating fluid can be expressed as

$$m = - V \frac{d\rho}{dt} \tag{1}$$

where V is the volume of the storage system, ρ is the density of the stored fluid, t is time, and the negative sign indicates fluid loss. For an ideal gas,

$$\rho = \frac{p}{RT} \tag{2}$$

where p and T are the pressure and temperature of the stored fluid, respectively, and R is the ideal gas constant. Then,

$$m = - \frac{V}{R} \frac{d}{dt} \left(\frac{p}{T} \right) \tag{3}$$

and

$$\frac{d}{dt} \left(\frac{p}{T} \right) = - \frac{mR}{V} = C \tag{4}$$

which is a constant for any controlled blowdown run. Then,

$$\frac{p}{T} = Ct + C_1 \tag{5}$$

When t = 0, then $p = p_2$ and $T = T_2$ where p_2 and T_2 are the pressure and temperature, respectively, in the storage system at the beginning of the constant mass flow run. Therefore,

$$C_1 = \frac{p_2}{T_2} \tag{6}$$

and

$$\frac{p}{T} = Ct + \frac{p_2}{T_2} \tag{7}$$

When $t = \Delta t$, then $p = p_1$ and $T = T_1$ where p_1 and T_1 are the pressure and temperature, respectively, in the storage system at the end of the constant mass flow run. Therefore,

$$C = \frac{1}{\Delta t}\left(\frac{p_1}{T_1} - \frac{p_2}{T_2}\right) = -\frac{mR}{V} \tag{8}$$

and

$$m = 5.83 \times 10^{-4}\ \frac{V}{\Delta t}\left(\frac{p_2}{T_2} - \frac{p_1}{T_1}\right) \tag{9}$$

where

$$R = 1716\ ft^2\ (sec^2 \times {}^\circ R) \tag{10}$$

for air. Hence, the mass flow for any controlled flow condition is readily obtained from measurements of pressures and temperatures of the stored air and the length of time of the controlled run. Of course, the volume of the storage system must be known also.

NOISE MEASUREMENTS

For an axially symmetric but directional source, the sound pressure p is a function of the azimuth angle θ. The procedure for determining the acoustic power is to measure p at a sufficient number of stations to ensure small measurement error and use a numerical integration process. Thus,

$$P = \frac{1}{\rho_o c_o} \sum_{k=1}^{n} p_k^2 s_k \tag{11}$$

where P is the acoustic power and p_k and s_k are the sound pressure and incremental surface area respectively at station k. The total number of equally spaced survey stations around a hemisphere at the equator including those at the poles is given by

$$n = \frac{\pi}{\alpha} + 1 \tag{12}$$

where α is the constant increment angle. For $\rho_o c_o$ in rayles (dyne sec/cm^3), p in dynes per square centimeter, and s in cubic feet,

$$P = \frac{930 \times 10^{-7}}{\rho_o c_o} \sum_{k=1}^{n} p_k^2 s_k \tag{13}$$

For sound pressure level referred to 2×10^{-4} dynes per square centimeter and power level referred to 10^{-13} watts,

$$PWL = 10 \log \left[\frac{37.2}{\rho_o c_o} \sum_{k}^{n} s_k \operatorname{antilog} \frac{SPL_k}{10} \right] \tag{14}$$

The incremental surface areas are given by

$$s_1 = s_n = 2\pi r^2 \left(1 - \cos \frac{\alpha}{2}\right) \tag{15}$$

$$s_k = 4\pi r^2 \sin \frac{\alpha}{2} \sin \theta_k \tag{16}$$

where r is the radius from the nozzle exit to each measurement station and s_1 and s_n represent the polar areas.

For this program, the following conditions were chosen:

$$\left.\begin{aligned} T_o &= 70°F \\ p_o &= 14.7 \text{ psia} \\ \rho_o c_o &= 40.6 \text{ rayles} \\ r &= 88\text{-inches} = 7.33 \text{ feet} \\ \alpha &= 15° \end{aligned}\right\} \tag{17}$$

and stations 2 through 8 were considered to be the only significant contributors to sound. Hence,

$$PWL = 10 \log \sum_{k=2}^{8} s_k \text{ antilog } \frac{SPL_k}{10} \tag{18}$$

where

$$s_k = 88.2 \sin \theta_k \tag{19}$$

DIRECTIVITY

In addition to overall sound power, an important acoustic performance characteristic of jet nozzles is a description of their directional behavior. A measure of this is the directivity index, DI(θ), a function of the directivity or azimuth angle θ, which gives the difference in decibels between the sound pressure level at a given point produced by a directional source and that produced by a non-directional source having the same acoustic power. Mathematically, it is expressed as

$$DI(\theta) = SPL(r,\theta) - SPL(r) \tag{20}$$

where SPL(r, θ) is the sound pressure level (depending upon both distance r and angle θ) for a directional source and SPL(r) is the sound pressure level (depending only upon distance r) for a non-directional source having the same acoustic power as the directional source. For a non-directional source, the power level corresponding to the conditions of Eqs. (17) can be written,

$$PWL = SPL(r) + 28.3 \tag{21}$$

Combining Eqs. (20) and (21), the directivity index is

$$DI(\theta) = SPL(r,\theta) + 28.3 - PWL \tag{22}$$

where the values of SPL(r, θ) and PWL can be taken directly from the sound survey data records.

SECTION IV

THEORETICAL PREDICTIONS

MASS FLOW AND THRUST

Performance data representation will be in graphical form where both ordinate and abscissa will consist of measured quantities uncontaminated by theoretical manipulations. This is not to imply that theoretical considerations are unimportant, to the contrary, they are very important and will be used extensively. However, since no two investigators of jet noise phenomena necessarily agree on any one theoretical approach, all theoretical predictions will be relegated to a position where they have no influence on data representation. This will be accomplished by superposing on performance graphs, various theoretical curves which will be available for comparison only.

The following theoretical development pertains directly to nozzle flow performance but the quantities involved are basic to acoustic performance as well. The resulting equations will be cast into forms where the quantities involved are similar to those measured. Hence, theoretical predictions can be superposed upon measured data graphs.

Flow performance relations will be developed for an isentropic ideal gas utilizing the following basic equations:

Equation of State

$$p = C\rho^{\gamma} \tag{23}$$

Ideal Gas Relations

$$p = R\rho T \tag{24}$$

$$c^2 = \gamma RT \tag{25}$$

Euler Equation of Motion for Steady Flow

$$\frac{\partial U}{\partial x} + \frac{1}{\rho}\frac{\partial p}{\partial x} = 0 \tag{26}$$

From the basic equations, the following isentropic flow relations can be derived.

$$\frac{\rho_s}{\rho} = \left(\frac{p_s}{p}\right)^{\frac{1}{\gamma}} \tag{27}$$

$$\frac{T_s}{T} = \left(\frac{p_s}{p}\right)^{\frac{\gamma - 1}{\gamma}} \tag{28}$$

$$c = (\gamma R T_s)^{1/2} \left(\frac{p_s}{p}\right)^{-\frac{\gamma - 1}{2\gamma}} \tag{29}$$

$$U = \left(\frac{2\gamma R T_s}{\gamma - 1}\right)^{1/2} \left[1 - \left(\frac{p_s}{p}\right)^{-\frac{\gamma - 1}{\gamma}}\right]^{1/2} \tag{30}$$

$$M = \left(\frac{2}{\gamma - 1}\right)^{1/2} \left[\left(\frac{p_s}{p}\right)^{\frac{\gamma - 1}{\gamma}} - 1\right]^{1/2} = \frac{U}{c} \tag{31}$$

$$\frac{p_s}{p} = \left[\frac{\gamma - 1}{2} M^2 + 1\right]^{\frac{\gamma}{\gamma - 1}} \tag{32}$$

$$\frac{m}{A} = \left[\frac{2\gamma}{(\gamma - 1) R T_s}\right]^{1/2} p_o \left(\frac{p_s}{p_o}\right) \left[\left(\frac{p_s}{p}\right)^{-\frac{2}{\gamma}} - \left(\frac{p_s}{p}\right)^{-\frac{\gamma + 1}{\gamma}}\right]^{1/2}$$

$$= \left(\frac{\gamma}{R T_s}\right)^{1/2} p_o \left(\frac{p_s}{p_o}\right) M \left[\frac{\gamma - 1}{2} M^2 + 1\right]^{-\frac{\gamma + 1}{2(\gamma - 1)}} \tag{33}$$

$$\frac{F}{A} = \frac{2\gamma p_o}{\gamma - 1} \left(\frac{p_s}{p_o}\right) \left[\left(\frac{p_s}{p}\right)^{-\frac{1}{\gamma}} - \left(\frac{p_s}{p}\right)^{-1}\right]$$

$$= \gamma p_o \left(\frac{p_s}{p_o}\right) M^2 \left[\frac{\gamma - 1}{2} M^2 + 1\right]^{-\frac{\gamma}{\gamma - 1}} \tag{34}$$

The above relations are general in the sense that they depend upon stagnation temperature and nozzle exit pressure. The equations for mass flow and thrust will now be degenerated to the case where stagnation

temperature and exit pressure are assumed equivalent to ambient conditions. The designations "fully expanded flow" is given to the latter assumption. That is for,

$$\left.\begin{aligned} T_s &= T_o = 530°R \\ p &= p_o = 2117 \text{ psfa (fully expanded)} \\ R &= 1716 \text{ ft}^2/(\text{sec} \times °R) \\ \gamma &= 1.4 \end{aligned}\right] \tag{35}$$

mass flow and thrust are

$$\frac{m}{A} = 2.63 \frac{p_s}{p_o} M_o \left[\frac{M_o^2 + 5}{5}\right]^{-3} \tag{36}$$

$$\frac{F}{A} = 2970 \left(\frac{p_s}{p_o}\right) M_o^2 \left[\frac{M_o^2 + 5}{5}\right]^{-\frac{7}{2}} \tag{37}$$

where

$$M_o = (5)^{1/2} \left[\left(\frac{p_s}{p_o}\right)^{2/7} - 1\right]^{1/2} \tag{38}$$

Graphs of these functions are shown in Fig. 2.

Fully expanded flow assumptions may be realistic below critical pressure ratios but should not be expected to hold above a velocity of Mach 1

except for converging-diverging nozzles operating at design pressure ratios. Now assume, for a converging nozzle, that the assumption fully expanded flow is valid below Mach 1 which is further assumed to be the upper limit of velocity. That is,

$$\frac{m}{A} = 2.63 \frac{p_s}{p_o} M_o \left[\frac{M_o^2 + 5}{5} \right]^{-3} \qquad 0 < M_o \leq 1 \qquad (39)$$

$$\frac{m}{A} = 1.523 \frac{p_s}{p_o} \qquad M_o \geq 1 \qquad (40)$$

The solid curve in Fig. 2(a) represents the above relations; the two curves are tangent at the coordinates shown. This is the theoretical curve that will be superposed on all flow performance graphs consisting of measured m/A versus measured p_s/p_o.

The theoretical curve of Fig. 2(a) turns out to be in excellent agreement with measured cold jet data for converging nozzles as can be seen in Fig. 3(a). It therefore provides an excellent basis for comparison for all other nozzles. Furthermore, the results of the normalizing procedure show that it is applicable for large hot jets as well. The relationships for converging-diverging nozzles would not be expected to be the same as for converging nozzles. The former would be expected to exhaust at ambient pressure (fully expanded flow) at their design Mach number. All converging-diverging types investigated for this program did, in fact, have measured results which intersected the broken curve of Fig. 2(a) very near the predicted value, e.g. see Fig. 3(c).

Using the same reasoning for thrust as was used for mass flow, the expressions for thrust are

$$\frac{F}{A} = 2970 \frac{p_s}{p_o} M_o^2 \left[\frac{M_o^2 + 5}{5} \right]^{-\frac{7}{2}} \qquad 0 < M \leq 1 \qquad (41)$$

$$\frac{F}{A} = 1570 \frac{p_s}{p_o} \qquad M \geq 1 \qquad (42)$$

Unlike, the comparable expressions for mass flow, these two curves are never tangent, but intersect at the two sets of coordinates shown in Fig. 2(b). These coordinates are equivalent to values of M_o equivalent to 1 and 1.93. We have no substantiating measured data for this hypothesis of thrust behavior because thrust was not measured. The results shown in Fig. 2(b) are presented only because they are logical extensions of mass flow behavior for which there is substantiating experimental data.

The additional graphs, Fig. 2(c) through (f) are presented for reference; included are significant coordinate points. Portions of the curves are labeled (1) converging nozzles and (2) converging-diverging nozzles at design. These are the predicted portions of the curves applicable to each type of nozzle. Of particular interest is Fig. 2(f) which shows the predicted relationship between thrust and mass flow. The converging nozzles are assumed to perform as the solid curve indicates. Converging-diverging nozzles operating at design pressure ratios only are assumed to perform as the broken curve indicates. No conclusions will be made concerning CD nozzle performance at pressure ratios off design or below critical.

It must be emphasized that these predicted curves are only speculative except for Fig. 2(a) which ultimately proves to be in excellent agreement with the measured performance of converging nozzles and with design values of CD nozzles. It is interesting to note from Fig. 2(f) that a CD nozzle may have a lower mass flow but greater thrust than a comparable size converging nozzle. This, of course, sheds doubt on the use of m/A as a size scaled performance variable for CD nozzles.

ACOUSTIC POWER

The philosophy for acoustic power representation is precisely the same as was discussed for flow performance. That is, the data will be graphed with the ordinate and abscissa consisting of measured quantities uncontaminated by theoretical manipulations. Theoretical curves will be superposed for comparison only. Four theoretical expressions for acoustic power will be used, each dependent upon the eighth power of velocity (Ref. 1, Chapter VI) but with individual differences dependent upon pressure ratio. They are,

Relation 1

$$\frac{P}{A} = K \frac{\rho_o U^8}{c_o^5} \tag{43}$$

Relation 2

$$\frac{P}{A} = K \frac{\rho^2 U^8}{\rho_o c_o^5} \tag{44}$$

Relation 3

$$\frac{P}{A} = K \frac{\rho^2 U^8}{\rho_o c_o c^4} \tag{45}$$

Relation 4

$$\frac{P}{A} = K \frac{\rho^2 c_o^3 U^8}{\rho_o c^8} \tag{46}$$

The first two relations are in common usage (Ref. 1) and the latter two are logical extensions. When the isentropic flow relations previously developed are used, and when,

$$
\left.
\begin{aligned}
K &= 4.5 \times 10^{-5} \\
T_s &= T_o = 530°R \\
p &= p_o = 2117 \text{ psfa (fully expanded)} \\
R &= 1716 \text{ ft}^3/(\text{sec} \times °R) \\
\gamma &= 1.4
\end{aligned}
\right\} \qquad (47)
$$

the expressions for acoustic power are,

$$\left(\frac{P}{A}\right)_1 = 204 \left(\frac{p_s}{p_o}\right)^{-8/7} M_o^{\,8} \qquad (48)$$

$$\left(\frac{P}{A}\right)_2 = 204 \left(\frac{p_s}{p_o}\right)^{-4/7} M_o^{\,8} \qquad (49)$$

$$\left(\frac{P}{A}\right)_3 = 204\, M_o^{\,8} \qquad (50)$$

$$\left(\frac{P}{A}\right)_4 = 204 \left(\frac{p_s}{p_o}\right)^{4/7} M_o^{\,8} \qquad (51)$$

Comparing relations 2, 3, and 4 to 1, which is most commonly used, the interrelationships are

$$\frac{\text{relation 2}}{\text{relation 1}} = \left(\frac{p_s}{p_o}\right)^{4/7} \qquad (52)$$

$$\frac{\text{relation 3}}{\text{relation 1}} = \left(\frac{p_s}{p_o}\right)^{8/7} \tag{53}$$

$$\frac{\text{relation 4}}{\text{relation 1}} = \left(\frac{p_s}{p_o}\right)^{12/7} \tag{54}$$

Hence, it is seen that relations 2, 3, and 4, successively place more emphasis upon pressure ratio than is placed by relation 1.

One might expect that these fully expanded flow relations would be valid below critical pressure ratios and in fact they are. However, above critical, there is no reason to assume that choking affects acoustic power in the same way as mass flow. Consequently, no attempt will be made to develop new relations above the critical pressure ratio as was done for mass flow. Instead these four relations are plotted in Fig. 2(g) in the form of acoustic power versus mass flow and one or more of them will be superposed on all acoustic performance graphs consisting of measured PWL - 10 log A versus m/A.

STROUHAL AND MODIFIED STROUHAL NUMBER

A very important factor of jet noise is spectral character, particularly if the results of model studies are to be used for predicting full scale counterparts. A commonly used scaling term is the dimensionless Strouhal number defined as,

$$S = \frac{fD}{U} \tag{55}$$

where f is the frequency, D is a characteristic length such as exit diameter for converging nozzles, and U is the average exit velocity. Since exit velocity was not measured, the Strouhal number will be reworked into a form containing measured quantities.

Using relations previously developed, velocity can be expressed as

$$U = \frac{m}{A\rho} = \frac{RT_o}{p_o} \frac{m}{A} \left(\frac{p_s}{p_o}\right)^{-1} \left(\frac{p_s}{p}\right)^{1/\gamma} \left(\frac{T_s}{T_o}\right) \tag{56}$$

Then, the Strouhal number can be written

$$S = \frac{p_o}{RT_o} \frac{fD}{\left[\frac{m}{A} \frac{T_s}{T_o}\right]} \frac{p_s}{p_o} \left(\frac{p_s}{p}\right)^{-1/\gamma} \tag{57}$$

and for fully expanded flow ($p = p_o$),

$$S_o = \frac{p_o}{RT_o} \frac{fD}{\left[\frac{m}{A} \frac{T_s}{T_o}\right]} \left(\frac{p_s}{p_o}\right)^{\frac{\gamma - 1}{\gamma}} \tag{58}$$

Hence, the Strouhal number is in terms of measurable quantities.

Subsequent results will show, however, that S_o as developed above is not an optimum normalizing or scaling parameter. Therefore, a modified Strouhal number will be defined below which will prove to be most useful. That is,

$$S_m = C_2 f \left(\frac{p_s}{p_o}\right)^{\frac{\gamma - 1}{\gamma}} \tag{59}$$

where

$$C_2 = \left[\frac{m}{AD^2} \frac{T_s}{T_o} \right]^{-1/2} \tag{60}$$

SECTION V

MEASURED RESULTS

MASS FLOW

The mass flow performance of all nozzles is shown in Figs. 3, 4, and 5 categorized as basic, annular with center core flow, and plug nozzles, respectively.

Basic Nozzles

Figure 3(a) shows the results for the geometrically matched set of converging nozzles. Data cluster about the solid theoretical curve is excellent although it appears that nozzle 100 is about the lower limit in size. Nozzle 110, Fig. 3(b), converging with no extension performs about the same as the matched set.

The converging-diverging nozzles shown in Fig. 3(c) do not, as expected, follow the theoretical curve except at very low pressure ratios. The measured results intersect the fully expanded flow curve at a pressure ratio of about 3.4. This would correspond to a Mach number of about 1.45 which is very near the design value of 1.5. This result and others for converging-diverging type nozzles formed by tapered plugs is shown in Table V.

The effect of nozzle length on flow performance can be seen by examining Figs. 3(d) through (h) which relate to five nozzles identical in every respect except length. Note that nozzle 100 is also one of the geometrically matched set of converging nozzles. The performance of nozzle 100 is slightly inferior to theoretical prediction and also to the other nozzles of the geometrically matched set (101, 102, and 103). This probably indicates that the lower limit of size has been reached, possibly because of boundary layer effects. The performance of nozzle 140 is very similar to 100 which indicates that the slight increase in length is not significant. However, the performance of the remainder of the nozzles becomes increasingly inferior with length. It is interesting to note that the flow performance of nozzle 143 is very similar to that of the CD nozzles shown in Fig. 3(c). It does not seem logical that 143 ultimately becomes an efficient CD type at a particular pressure ratio, hence, the judgment is made that it is an inferior converging type due in all probability to the excess internal drag resulting from a large L/D ratio.

Annular Nozzles with Center Core Flow

Figures 4(a) through (h) show the mass flow performance for the annular nozzles with center core flow. The area used for scaling was the minimum area (A_m) for the reason discussed in Section III. All results are very close to predicted theoretical performance which indicates that they are behaving like converging types.

Annular Plug Nozzles

Figures 5(a) through (j) show the flow performance of the plug nozzles. Four of these nozzles, 301, 305, 601, and 621, shown in Figs. 5(a), (b), (i), and (j) respectively are CD types in the sense that they have an interior area less than exit. Comparison of their performance with respect to predicted and measured Mach numbers assuming CD behavior is shown in Table V. Nozzle 301 is excepted from the table because of insufficient data. Measured Mach numbers were determined by noting the pressure ratio corresponding to the intersection of the performance data with the theoretical curve and assuming fully expanded flow conditions.

The remainder of the nozzles except for 421 and 423 performed very nearly as predicted. Nozzles 421 and 423 appear to have too small an annulus to perform well. As was done with the basic nozzles with large L/D ratios, these are judged as inferior converging types, probably because of excess internal drag.

ACOUSTIC POWER

The acoustic power performance of all nozzles is shown in Figs. 6, 7, and 8 categorized as basic, annular with center core flow, plug nozzles, respectively.

Basic Nozzles

Figure 6(a) shows the results for the geometrically matched set of converging nozzles. Data cluster about the predicted theoretical curve of relation 1 is excellent below critical flow and deviates considerably above.

The broken curve is the extension of relation 1, Eq (48), plotted in terms of power level and mass flow. The solid curve is the best fit line and coincides with relation 1 for values of m/A below about 2.4. These two curves, the solid best fit line and the broken theoretical line will be superposed upon all other acoustic power curves for comparison purposes.

The scatter of the data in Fig. 6(a) beyond critical flow can be attributed in part to the effects of screech, Ref. 1, Chapter VI. This is a rather unstable highly directional phenomenon that produces intense discrete sounds and will be examined in more detail when directivity and power spectral density are discussed. However, our investigations have shown that screech can increase acoustic power by as much as four decibels which would imply that the solid curve of Fig. 6(a) above critical might actually be a scatter band four decibels broad.

Figure 6(b) shows that the acoustic performance of the converging nozzle with no extension is slightly inferior to the standard set for values of m/A between four and five.

The converging-diverging nozzles of Figs. 6(c), (d), and (e) show radically different performance from that of the standard set. They all behave as theory would indicate for very low mass flows but then radically depart and go through an intense sound phase near the critical flow condition. We have frequency analyzed this phase and found the spectrum consisted of a number of very high discrete frequency peaks very similar to those of screech but with greater relative amplitudes. This phenomenon does not satisfy the requirements for screech because it occurs at or below critical flow while screech is generally assumed to be a result of shock formation occurring above critical flow.

Superposed on Figs. 6(c), (d), and (e) are additional theoretical relations beside relation 1. These were included to see if the acoustic performance of the CD nozzles tended to be optimized at some fully expanded flow condition. It is interesting to note that nozzles 120 and 121, which are a geometrically matched pair with relatively short extensions, tend to be tangent to relation 3. Nozzle 122 which has a relatively long extension tends to be tangent to relation 1 and shows smoother and better performance than the other two. Finally, all three CD nozzles tend to tangency at a value of m/A of about 4.5 which corresponds to a pressure ratio of 3.4 and Mach number of 1.45 which are the identical results obtained from Fig. 3(c) and listed in Table V. Hence, these results indicate that CD nozzles have optimum acoustic performance at the fully expanded flow condition which corresponds very closely to nozzle design Mach number.

Figures 6(f) through (i) show the acoustic performance of the converging nozzles with long extensions. The performance is very erratic being most so for the longest nozzle.

Annular Nozzles with Center Core Flow

All nozzles with center core flow show some degree of acoustic superiority over the standard converging set. The best, however, are nozzles 274 and 293, Figs. 7(f) and (h) respectively. These nozzles show a remarkable tendency to perform in accordance with theoretical relation 1.

An interesting acoustic effect is shown in Fig. 7(g) for nozzle 275. Unusually high acoustic power levels occurred in the subsonic region which we ultimately attributed to aeolian tone generation for the following reasons. Reference 4 indicates that the phenomenon called aeolian tones occurs when fluid flows over a body and that the frequency of sound generation is given by.

$$f_n = \frac{nkU}{d} \tag{61}$$

where n is an integer pertaining to frequency harmonics, k is a constant dependent upon Reynold's number and body shape, d is body diameter or plate thickness, and U is velocity. Rearranging this formula into a fully expanded flow form, there results,

$$f_n = \frac{nk}{d} (\gamma R T_s)^{1/2} \left(\frac{p_s}{p_o}\right)^{-\frac{\gamma - 1}{2\gamma}} M_o \tag{62}$$

and for cold air flow,

$$f_n = 1128 \frac{nk}{d} \left(\frac{p_s}{p_o}\right)^{-1/7} M_o \tag{63}$$

where M_o is given by Eq (38). Considering d to represent the thickness of the wall of the inner nozzle of Nozzle 275, then for

$$\left.\begin{aligned} d &= 0.1265 \text{ inches} \\ n &= 1 \\ k &= 0.2 \text{ (commonly accepted value)} \end{aligned}\right\} \qquad (64)$$

the first harmonic is

$$f_1 = 21400 \left(\frac{p_s}{p_o}\right)^{-1/7} M_o \qquad (65)$$

For pressure ratios of 1.14 and 1.279, computed aeolian tones would be 9.2 and 12.5 kcps respectively while measured values were 10.4 and 13.3 kcps respectively. These results are sufficiently close as to indicate that the unusually high acoustic power levels in the subsonic region of nozzle 275 are due to aeolian tone generation.

No other nozzles with center core flow exhibited aeolian tones probably because of the thinness of the inner nozzle wall. That is for d = 0.05 inches,

$$f_1 = 54200 \left(\frac{p_s}{p_o}\right)^{-1/7} M_o \qquad (66)$$

Then, for a pressure ratio of 1.14, the computed aeolian tone would be 23.3 kcps which is above the range of our acoustic measuring system. Larger pressure ratios, of course, would result in higher frequency tones.

This discussion of aeolian tones illustrates that care should be taken in nozzle design to insure that these tones do not occur in the frequency range of interest.

Annular Plug Nozzles

The acoustic performance of annular plug nozzles is shown in Figs. 8(a) through (o). Nozzles 301, 305, 601, and 621, Figs. 8(a), (b), (n), and (o) respectively have CD configurations due to the taper of the plug tip interior to nozzle exit plane. The latter three are listed in Table V and correspondence between theoretical and measured Mach numbers is quite good. Nozzle 301 was not included because the CD effect was too slight to be observed in the flow performance curve, Fig. 5(a). All other plug nozzles have the plug tapered portion beginning exterior to nozzle exit plane.

Nozzles 327 and 375, Figs. 8(f) and (i), respectively, are a geometrically matched pair and have excellent acoustic power performance being superior to predicted eighth power relation 1. There may be some doubt as to the validity of 375 because of the small annular flow area and because the flow performance, Fig. 5(e), is slightly inferior to theoretical. On the other hand 327 shows excellent flow performance and practically the same acoustic power performance. A normalized spectral analysis of nozzle 327 is given in Fig. 11.

It is interesting to note that poor flow performance is at least partially compensated for by plotting m/A as the abscissa. Consider nozzle 421, Fig. 8(j), which has a very small annular flow area and poor flow performance, Fig. 5(f). The acoustic power performance is not nearly as good as for nozzle 327 although for a given pressure ratio, there is less mass flow per unit area than for 327. If pressure ratio were used for the abscissa, the difference in acoustic power performance would not be as great.

The effect of plug taper can be seen by comparing Figs. 8(e) and (f). The only difference between these nozzles is the presence or absence of tapered tip. Furthermore, comparing Figs. 8(j) and (k), it is seen that the longer taper is superior.

The cross-section configuration of nozzle 327 appears to be optimum considering the ratio of outer nozzle diameter to plug diameter. Larger and smaller ratios than that of 327 result in inferior acoustic power performance.

A most interesting result occurred from increased projection of the plug beyond the nozzle exit plane as seen in Fig. 8(g). Nozzle 347 is identical to 327 except for increased length. Acoustic power performance is as much as five decibels better than eighth power relation 1 predicts except for values of m/A between four and five. It is possible that screech occurs in this range although most plug nozzles appear to be relatively free of screech. Furthermore, there is no sacrifice in flow performance as seen in Fig. 5(d) since nozzle 347 performs very close to the theoretical mass flow curve. To a lesser extent, this phenomena is seen by comparing Figs. 8(l) and (m). A possible explanation for the increase in acoustical performance resulting from an increase in plug length beyond the exit plane is that the contribution of noise due to shock formation is somehow minimized or eliminated. However, this may not be the complete explanation since, if shock noise only were eliminated, it would seem logical to expect the resulting turbulent noise to

behave as the predicted eighth power relation 1. Additional discussions and theory concerning this effect is presented in Part II of this report.

DIRECTIVITY

The directional character of the geometrically matched set of nozzles is shown in Figs. 9(a) through (g). Above a value for m/A of about 2.88 (critical), there is considerable data scatter which we attribute to screech. It is interesting to note that screech exhibits directional character being expecially pronounced at angles of 90 and 105-degrees. The most intense noise occurs at the 30 and 45-degree azimuth stations which are least sensitive to screech or where screech does occur, it is of relatively low level. This indicates that while screech is a phenomenon of cold jets, it does not necessarily make too great a contribution to overall acoustic power.

POWER SPECTRAL DENSITY

Figures 10(a) through (e) show the results of a one third octave band analysis of the standard converging nozzle 101 for three different pressure ratios. The curves are partially normalized by plotting as the ordinate, the difference between power spectrum level and sound power level. The purpose of including the first four figures is to show the significance of screech. For the lower two pressure ratios, screech is nonexistant. For the highest pressure ratio, screech is indicated by the wide scatter of data in the upper frequency range of Fig. 10(c). Figure 10(d) shows the results when screech was ignored in the analysis and reduction of data. For this case, the removal of screech amounted to a four decibel reduction in sound power level. However, not all nozzles exhibited screech to this extent, and the judgment is made that four decibels is about all that can be attributed to screech.

Figure 10(e) shows the combined results for all three pressure ratios excluding screech at the highest pressure ratio. The abscissa is normalized by means of the modified Strouhal number, Eq (59), and the ordinate by incorporating the factor C_2, Eq (60). This normalizing technique was developed by a trial and error process beginning with the unmodified Strouhal number.

Figure 11 shows the comparable normalized results for plug nozzle 327. It is interesting to note that the results for the highest pressure ratio have maximum levels significantly higher (about three decibels) than those for the lower two pressure ratios. We attribute this effect to the omission of some high frequency data in measuring PWL.

SECTION VI

NORMALIZATION

Previous sections pertained to flow and acoustic performance of small cold jet nozzles. Size normalization was attempted by plotting such factors as m/A, p_s/p_o, PWL - 10 log A, and a modified Strouhal number. The results were excellent but certainly not conclusive since the range of sizes was relatively narrow. Jet model studies can have only limited value unless the results can be scaled to full size jet engines including the effects of elevated temperatures.

Despite the wealth of published data for flow and acoustic performance of large hot jet nozzles including jet engines, very little is complete enough for even satisfactory comparison much less for the development of normalization parameters. One exception, however, is the work done by Lee, Tatge, and Wells, concerning a four-inch diameter conical nozzle at cold and elevated temperatures, reported in complete detail in Refs. 5 and 6. Their work will be used in this section, the cold jet data to be compared with ours and their hot jet data for the development of normalization parameters for temperature.

MASS FLOW

Figure 12(a) shows flow performance of the four-inch nozzle before any attempt has been made to include temperature effects. Only the cold jet data performs in accordance with the theoretical prediction for converging nozzles, which confirms, however, that size scaling has been accomplished by plotting m/A versus p_s/p_o.

Temperature normalization was accomplished by examining Eq (33) for its temperature dependent properties which are stagnation temperature (T_s) and specific heat ratio (γ). Usually γ is not considered very temperature sensitive, and a constant value is chosen applicable to a large temperature range. However, we have found that while its effect is not great, it is significant enough to be included. Hence, instead of γ being considered as a constant in Eq 33, we chose it to be the value of specific heat ratios corresponding to total or stagnation temperature (γ_s). Thus Eq (33) can be rewritten,

$$\frac{m}{A} = \left[\frac{2\gamma_s}{(\gamma_s - 1) RT_s}\right]^{1/2} p_o \left(\frac{p_s}{p_o}\right)\left[\left(\frac{p_s}{p}\right)^{-\frac{2}{\gamma_s}} - \left(\frac{p_s}{p}\right)^{-\frac{\gamma_s + 1}{\gamma_s}}\right]^{1/2} \tag{67}$$

which is now temperature dependent in γ_s as well as T_s. Normalization factors can now be determined by rewriting Eq (67) as follows,

$$\frac{m}{A} C_1 C_3 = \left[\frac{2\gamma_o}{(\gamma_o - 1) RT_o}\right]^{1/2} p_o \left(\frac{p_s}{p_o}\right)\left[\left(\frac{p_s}{p}\right)^{-\frac{2}{\gamma_s}} - \left(\frac{p_s}{p}\right)^{-\frac{\gamma_s + 1}{\gamma_s}}\right]^{1/2} \tag{68}$$

where γ_o is specific heat ratio corresponding to ambient temperature and C_1 and C_3 are temperature dependent normalization factors given by

$$C_1 = \left(\frac{T_s}{T_o}\right)^{1/2} \tag{69}$$

$$C_3 = \left[\frac{\gamma_o (\gamma_s - 1)}{\gamma_s (\gamma_o - 1)}\right]^{1/2} \tag{70}$$

For a cold jet, C_1 and C_3 become unity and Eq (68) degenerates to the expression used for our cold jet experiments.

Figure 12(b) shows the effect of considering C_1 only. It is a major effect as all data has very nearly collapsed onto the theoretical curve for converging nozzles. Figure 12(c) shows the effect of including both C_1 and C_3. The effect of C_3 is not nearly as great as that of C_1 but it is significant; for

all practical purposes, size and temperature normalization has been accomplished. The relation between specific heat and temperature used for C_3 is shown in Fig. 13 which is based upon tabulated data in Ref. 7.

ACOUSTIC POWER

Figure 14(a) shows the acoustic power performance of the four-inch nozzle before any attempt has been made to include temperature effects. The cold jet data agrees well with the solid curve representing the best fit line through our geometrically matched set of converging nozzles while there is no agreement at all with the elevated temperature data. However, we concluded that size scaling has been accomplished by plotting PWL - 10 log A versus m/A.

The development of temperature normalization factors for acoustic power did not result from obvious manipulations of any one of the theoretical eighth power relations. Instead, a "brute force" trial and error technique was used which resulted in the following rather simple factor.

$$C_4 = 5\left(\frac{\frac{T_s}{T_o} - 1}{\frac{p_s}{p_o} - 1}\right) \tag{71}$$

Referring to Fig. 14(b), excellent correspondence between cold and hot jet data has been achieved when C_4 is incorporated in a plot of

$$\text{PWL} - 10 \log A - C_4 \quad \text{versus} \quad \frac{m}{A} C_1 C_3$$

At this time we have no theoretical explanation for the effectiveness of the above normalization technique. The fact is, it works and there might well be an explanation, still to be found. Another alternative is, that a factor can be developed from theoretical considerations which bears little resemblance to Eq (71) but has the same effect. Note that C_4 as well as C_1 and C_2 vanishes for cold jet flow.

POWER SPECTRAL DENSITY

The power spectral density of the four-inch conical nozzle can be effectively normalized in precisely the same manner as was done for our cold jet results as shown in Fig. 11. That is, by plotting SL - PWL- 10 log C_2 versus the modified Strouhal number S_m, where S_m and C_2 are given by Eqs (59) and (60) respectively.

Figures 15(a) through (d) show the results for the four-inch nozzle for various runs reported in Refs. 5 and 6. There is considerable scatter in the cold jet data of Fig. 15(a), possibly due to screech, and very little for the elevated temperature data. It is interesting to note that all four-inch nozzle data both cold and hot and our three quarter-inch nozzle cold data show a maximum level of (- 20) to (- 30) decibels occurring within an S_m range of 100 to 200. This is better correspondence than we have been able to find where the unmodified Strouhal number has been used.

SECTION VII

JET ENGINE DATA

Proof of the validity of the normalization techniques can only be conclusive when they are found to be satisfactorily applicable to jet engines. Consequently, we have attempted to collect engine data for corroboration. Unfortunately, we have been unable to locate sufficient information to make a conclusive judgment at this time. This does not mean that engine data is unavailable only that the majority of what we found was not complete enough for our purposes. What we did use however is plotted in Figs. 16, 17, and 18 and the pertinent information used for normalization is given in Table VI (a) and (b). For every case in Table VI (a), at least one of the pertinent properties was based upon someone's recollection without documentation.

MASS FLOW

All performance data for which we had sufficient information, is plotted in Fig. 16. Data cluster is fairly good and it is conceivable that some of the engines had relatively poor performance in the sense that mass flow was less than the solid theoretical curve would indicate.

ACOUSTIC POWER

Normalized acoustic power data for the standard engines is plotted in Fig. 17(a). Data cluster is not good nor does the data conform well to the solid curve representing model converging nozzles. Three possibilities exist: (1) the normalization technique does not extend to jet engines, (2) the data of Table VI (a) is not accurate, and (3) actual acoustic power performance of the engines is poor and scattered.

We are not willing to accept the first possibility at this time because of the excellent correspondence obtained between small cold jet nozzles (the largest being 1.375-inches in diameter) and 4-inch nozzles, cold and hot. These involved area ratios in excess of twelve and temperature ratios of nearly four. The second possibility is apt to be true because of the lack of documentation. The third possibility can also be true because there is no reason to assume a fabricated type nozzle such as the exit portion of a jet engine should perform as smoothly as machined nozzles.

Figure 17(b) shows the performance of special engines for which there is documentation although there is some question of interpretation of some of the listed quantities such as temperature. The results are much closer to predicted performance and the scatter is logical since various suppression devices were utilized. The rank ordering of the performance of each type of suppression device as stated in Ref. 9 is identical to that shown in Fig. 17(b). We judge these results to be about as good as can be expected for normalized jet engine data.

POWER SPECTRAL DENSITY

Figure 18 shows the normalized power spectral density results for a J79 engine. Like the previous analyses for model data the J79 engine spectrum has a maximum level between (- 20) and (- 30) decibels occurring within an S_m range of 100 to 200. The shape of an average curve through the data points is very similar to those of the model data as well. At least for this one case, the normalization technique for power spectral density has proven to yield excellent results for a jet engine.

SECTION VIII

CONCLUSIONS AND RECOMMENDATIONS

As a result of this research concerning flow and acoustic performance of high velocity jet streams, the following conclusions and recommendations are made.

CONCLUSIONS

(1) Normalizing techniques were developed for scaling small cold model jets to large hot jets for flow and acoustic power performance and power spectral densities.

(2) The validity of the normalizing techniques will not be conclusive until more corroborating evidence is available. However, we have found no reason to be other than optimistic.

(3) There are lower limits to size. When this is so indications occur in either or both flow performance and power spectral density results. Flow performance may be significantly lower than theoretical and the power spectral density may indicate that higher frequencies than measured must be included.

(4) Plug nozzles 327 and 347 evidenced remarkable superiority over all other nozzles and the theoretical predicted curve as well. There is some evidence in the power spectral density analysis of 327, that some significant frequency contributions have been omitted due to the upper limit of our measuring system. We judge this effect small, one or two decibels of acoustic power at most. There was no evidence of inferior flow performance.

(5) A great deal of flow and acoustic performance results can be expressed by engineering equations suitable for direct application.

RECOMMENDATIONS

(1) More information is needed concerning large hot jet models and jet engines to verify the normalising techniques.

(2) Nozzles similar to 327 and 347 should be scaled with sufficiently larger annuli to conclusively eliminate any size limitation. Furthermore, these nozzles are not necessarily optimized and that should be done.

(3) When optimization has been accomplished, further benefit may be achieved by adding an ejector configuration. This suggestion is made because of the benefit reported in Ref. 9 and indicated in Fig. 17(b).

(4) Further research could profit from acoustic measuring and analysing equipment with a higher frequency cut-off than the 16 kcps used for the experiments reported here.

ACKNOWLEDGMENT

The author wishes to express his appreciation to the following: C. S. Caccavari for most of the data acquisition and reduction; R. W. Higgs for bibliography compilation and assistance in the development of normalizing techniques; D. F. Pernet for general assistance, investigations of aeolian tone phenomena, and assistance in the development of normalizing techniques; A. Peter for suggestions for improving nozzle acoustic performance; and H. H. Hall, deceased, for instrumentation.

LIST OF REFERENCES

1. Sperry, W. C. (Editor), Fundamental Study of Jet Noise Generation and Suppression, WADD Technical Report 61-21, Volume I, Wright Air Development Division, Wright-Patterson Air Force Base, Ohio, December, 1960

2. Emmitt, Margaret, Fundamental Study of Jet Noise Generation and Suppression, Volume II -- Bibliography, Wright-Patterson Air Development Division, Wright-Patterson Air Force Base, Ohio, December, 1960

3. Sperry, W. C., Kamo, R., and Peter, A., Experimental and Theoretical Studies of Jet Noise Phenomena, Technical Documentary Report ASD-TDR-62-303, Aeronautical Systems Division, Wright-Patterson Air Force Base, Ohio, February, 1962

4. Blokhintsev, D. I., Acoustics of a Nonhomogeneous Moving Medium, NACA TM 1399, February, 1956

5. Lee, R., et al, Research Investigation of the Generation and Suppression of Jet Noise, General Electric Co., U.S.N., Bureau of Weapons, Contract NOas 59-6160c, January, 1961

6. Tatge, R. B., Wells, R. J., "Model Jet Noise Study at Alplaus Facility," General Electric Co., Report No. 61 GL 25, January, 1961

7. Morrison, Richard B., Design Data for Aeronautics and Astronautics, John Wiley and Sons, Inc., N. Y., 1962

8. Crane, F. E., Ahern, P. A., "Jet Engine Exhaust Noise Suppression Investigation. Report of Survey of PWA J57-P-2B Engine," Aeronautical Engine Laboratory, NAMC-AEL-1587, November, 1958

9. Coles, W. D., et al, "Turbojet Engine Noise Reduction with Mixing Nozzle-Ejector Combinations," NACA Technical Note 4317, August, 1958

LIST OF IMPORTANT SYMBOLS

The English system of units will be used and those assigned to the symbols are directly applicable to theoretical formulation and graphical coordinates unless specifically stated otherwise.

Symbol	Units	Definition
A	ft^2	Exit area of nozzle
A_a	ft^2	Annulus area of nozzle
A_c	ft^2	Center core area of nozzle
A_{cr}	ft^2	Critical area of nozzle
A_m	ft^2	Minimum area of nozzle
C_1	---	Normalization factor, Eq (69)
C_2	---	Normalization factor, Eq (60)
C_3	---	Normalization factor, Eq (70)
C_4	---	Normalization factor, Eq (71)
c	fps	Velocity of sound at nozzle exit
c_o	fps	Velocity of sound for ambient conditions
D	ft	Diameter of nozzle exit
D_{cr}	ft	Diameter of nozzle critical section
F	lb	Thrust

LIST OF IMPORTANT SYMBOLS (Continued)

Symbol	Units	Definition
f	kcps	Frequency
K	---	Constant for eighth power relations (assumed equal to 4.5×10^{-5})
k	---	Sound survey azimuth station number
L	ft	Nozzle length
M	---	Mach number
M_o	---	Mach number in terms of fully expanded flow pressure ratio, Eq (38)
m	slugs/sec	Mass flow
n	---	Total number of sound survey stations
P	watts	Acoustic power
PWL	decibels re 10^{-13} watts	Sound power level
p	psfa	Pressure at nozzle exit
p_k	dynes/cm^2	Sound pressure at azimuth station k
p_o	lb/ft^2	Ambient pressure
p_s	psfa	Stagnation or total pressure
R	$ft^2/(sec \times {}^\circ R)$	Ideal gas constant

LIST OF IMPORTANT SYMBOLS (Continued)

Symbol	Units	Definition
SL	decibels re 10^{-13} watts	Sound power spectrum level
SPL	decibels re 0.0002 dynes/cm^2	Sound pressure level
s_k	ft^2	Incremental surface area at azimuth station k
T	°R	Temperature at nozzle exit
T_o	°R	Ambient temperature
T_s	°R	Stagnation or total temperature
U	fps	Average nozzle exit velocity
V	ft^3	Volume of air storage system
α	degrees	Incremental azimuth angle
γ	---	Specific heat ratio
γ_o	---	Specific heat ratio at ambient temperature
γ_s	---	Specific heat ratio at stagnation temperature
θ	degrees	Azimuth direction angle
ρ	slugs/ft^3	Density at nozzle exit
$\rho_o c_o$	rayles	Characteristic impedance of air

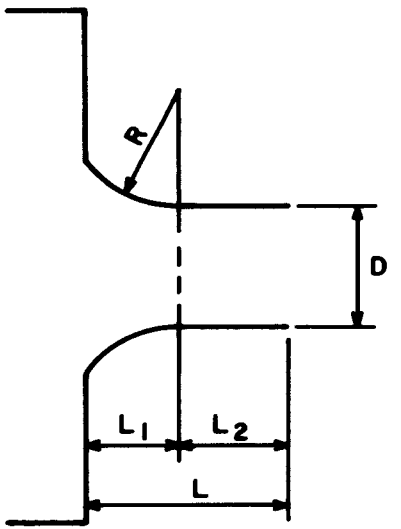

Nozzle no.	D in.	R in.	L_1 in.	L_2 in.	L in.	A $in.^2$	$\frac{L_1}{L}$	$\frac{L_2}{L}$	$\frac{L}{D}$
100	0.533	0.533	0.422	0.484	0.906	0.223	0.466	0.534	1.700
101	0.750	0.750	0.600	0.681	1.281	0.442	0.468	0.531	1.708
102	1.000	1.000	0.792	0.908	1.700	0.785	0.466	0.534	1.700
103	1.375	1.375	1.094	1.250	2.344	1.485	0.468	0.534	1.705

Table I. Details of Basic Nozzles

(a) Geometrically Matched Converging Nozzles with Short Extensions

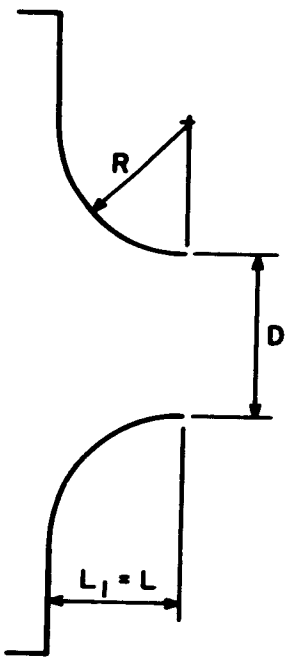

Nozzle no.	D in.	R in.	L_1 in.	L_2 in.	L in.	A $in.^2$	$\frac{L_1}{L}$	$\frac{L_2}{L}$	$\frac{L}{D}$
110	1.000	1.000	0.792	0	0.792	0.785	1.000	0	0.792

Table I. Details of Basic Nozzles

(b) Converging Nozzle with No Extension

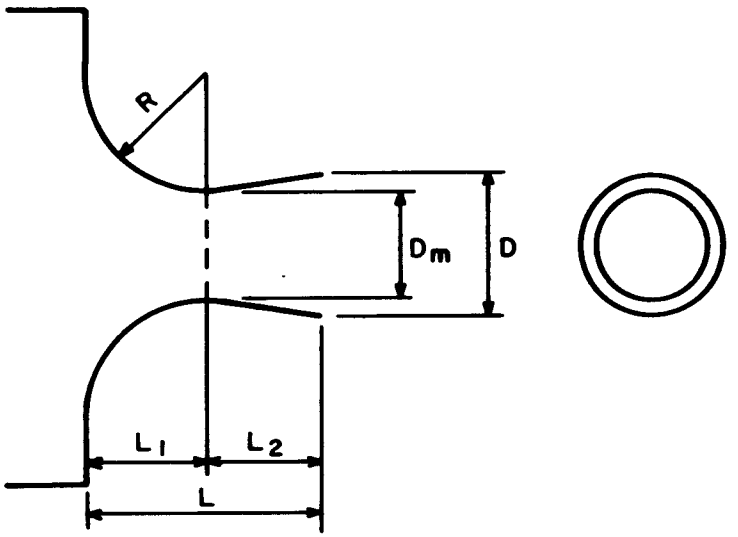

						exit				critical		
Nozzle no.	D in.	R in.	L_1 in.	L_2 in.	L in.	A $in.^2$	$\frac{L_1}{L}$	$\frac{L_2}{L}$	$\frac{L}{D}$	D_{cr} in.	A_{cr} $in.^2$	$\frac{A}{A_{cr}}$
120	0.75	0.75	0.600	0.681	1.281	0.442	0.468	0.531	1.708	0.691	0.375	1.178
121	1.00	1.00	0.792	0.908	1.700	0.785	0.466	0.534	1.700	0.922	0.667	1.178
122	0.75	0.75	0.600	2.073	2.673	0.442	0.223	0.776	3.564	0.691	0.375	1.178

Table I. Details of Basic Nozzles

(c) Converging-Diverging Nozzles

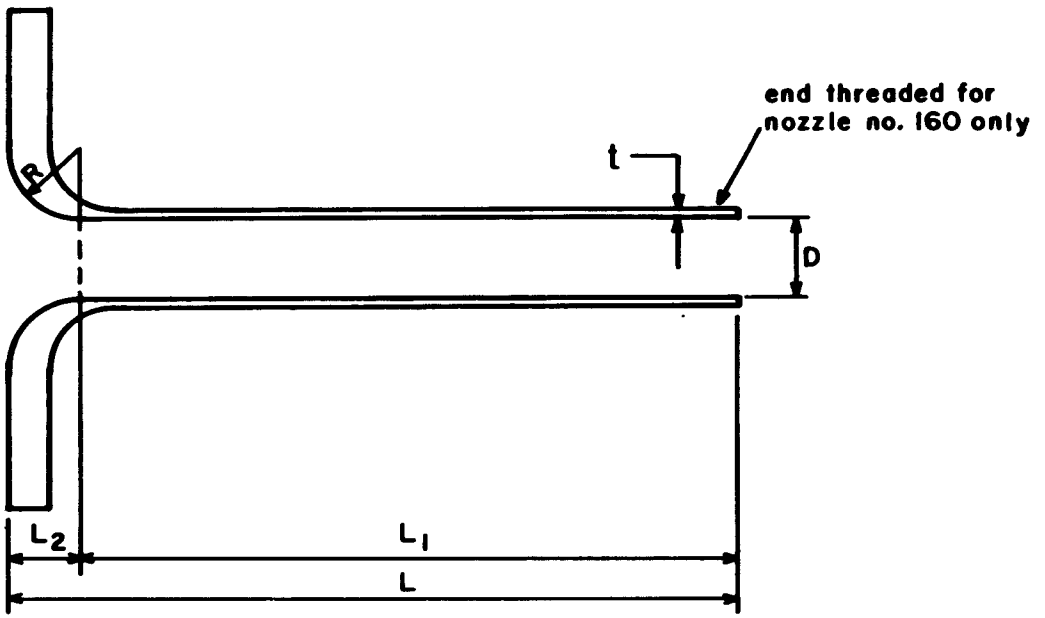

Nozzle no.	D in.	R in.	L_1 in.	L_2 in.	L in.	A $in.^2$	$\frac{L_1}{L}$	$\frac{L_2}{L}$	$\frac{L}{D}$	t
140	0.533	0.533	0.422	1.922	2.344	0.223	0.180	0.820	4.40	0.050
141	"	"	"	2.922	3.344	"	0.126	0.875	6.27	0.050
142	"	"	"	3.922	4.344	"	0.973	0.904	8.15	0.050
143	"	"	"	4.922	5.344	"	0.790	0.920	10.02	0.050
160	"	"	"	3.922	4.344	"	0.973	0.904	8.15	0.126

Table I. Details of Basic Nozzles

(d) Converging Nozzles with Long Extensions

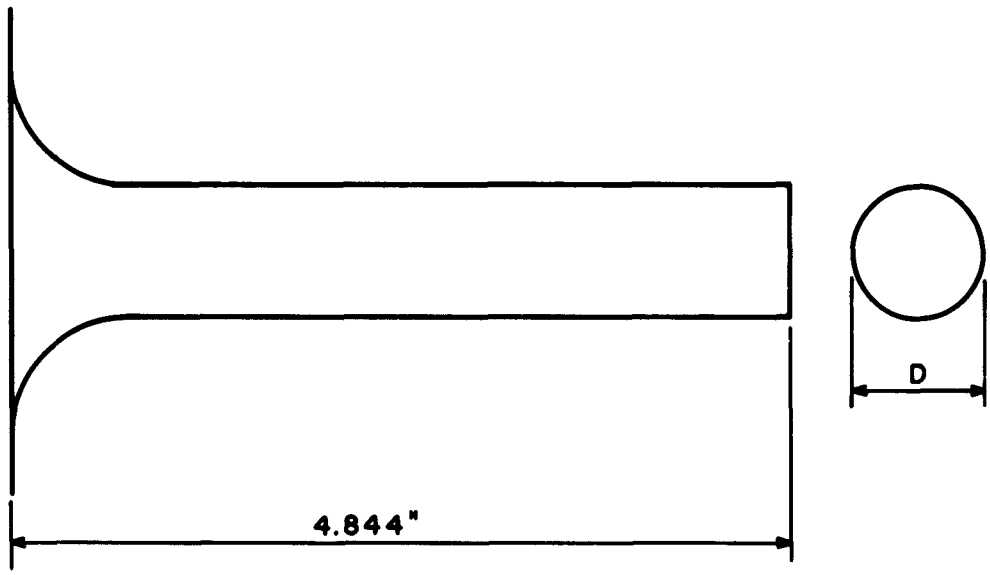

bar no.	D in.	A $in.^2$
B 10	0.318	0.0794
B 20	0.786	0.4850
B 30	1.080	0.9159

Table II. Details of Nozzle Appurtenances
(a) Solid Bars

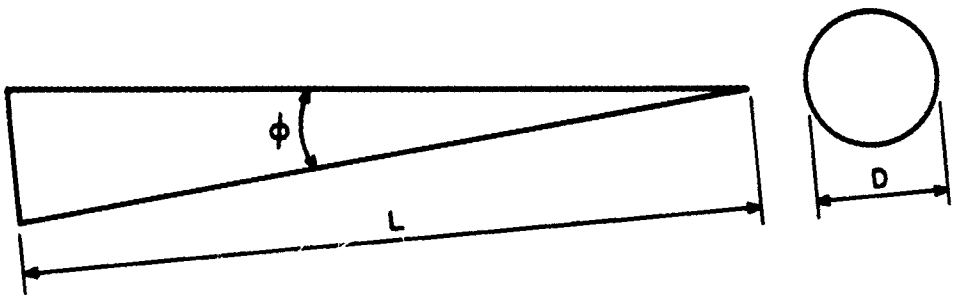

Termination no.	D in.	L in.	ϕ deg.
BT 10	0.318	1.817	10.0
BT 11	"	0.902	20.0
BT 12	"	0.594	30.0
BT 20	0.786	4.82	9.33
BT 30	1.080	6.18	9.33

Table II. Details of Nozzle Appurtenances
(b) Bar Terminating Cones

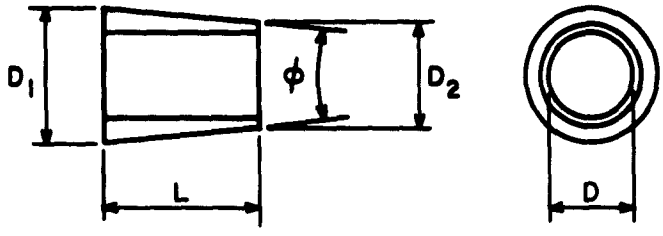

Termination no.	D in.	L in.	ϕ deg.	D_1 in.	D_2 in.
NT 20	0.533	1.000	9.33	0.786	0.618
NT 21	0.533	1.000	—	0.786	0.786

Table II. Details of Nozzle Appurtenances
(c) Nozzle Terminations

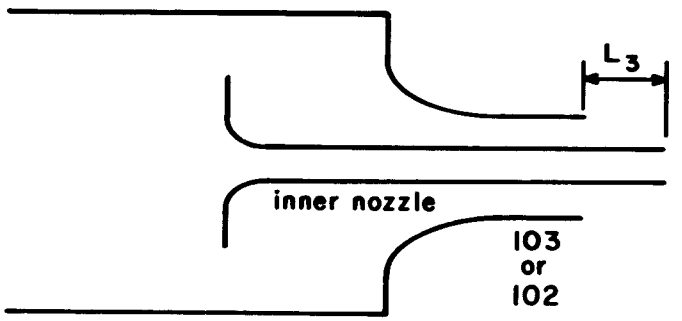

Composite Nozzle No.	Outer Nozzle No.	Inner Nozzle No.	Inner Nozzle Tip	L_3 in.	exit A $in.^2$	core A_c $in.^2$	annulus A_a $in.^2$	minimum A_m $in.^2$	$\frac{A_c}{A_m}$
200	103	140	–	−1.0	1.485	0.223	1.171	1.394	0.16
203	103	143	–	−1.0	1.485	0.223	1.171	1.394	0.16
210	103	141	–	−0.5	1.485	0.223	1.171	1.394	0.16
212	103	143	–	−0.5	1.485	0.223	1.171	1.394	0.16
223	103	160	NT20	0	1.223	0.223	1.000	1.223	0.182
274	102	160	NT20	0	0.523	0.223	0.300	0.523	0.427
275	102	160	NT21	0	0.523	0.223	0.300	0.523	0.427
293	102	143	–	+1.0	0.693	0.223	0.470	0.693	0.322

Table III. Details of Annular Nozzles with Center Core Flow

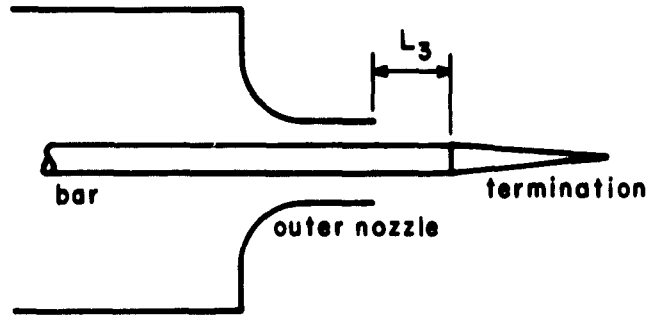

Composite Nozzle no.	Outer Nozzle no.	bar no.	termination no.	L_3 in.	exit A $in.^2$	minimum A_m $in.^2$	$\frac{A}{A_m}$
301	103	B10	BT10	−1.0	1.476	1.406	1.050
305	103	B20	BT20	−1.0	1.178	1.000	1.178
321	103	B10	BT10	0	1.406	1.406	1.000
325	103	B20	BT20	0	1.000	1.000	1.000
326	103	B30	none	0	0.569	0.569	1.000
327	103	B30	BT30	0	0.569	0.569	1.000
371	102	B10	BT10	0	0.706	0.706	1.000
375	102	B20	BT20	0	0,300	0.300	1.000
421	100	B10	BT10	0	0.144	0.144	1.000
423	100	B10	BT12	0	0.144	0.144	1.000
471	101	B10	BT10	0	0,363	0.363	1.000
491	101	B10	BT10	+2.53	0.363	0.363	1.000

Table IV. Details of Plug Nozzles

(a) Converging Nozzles

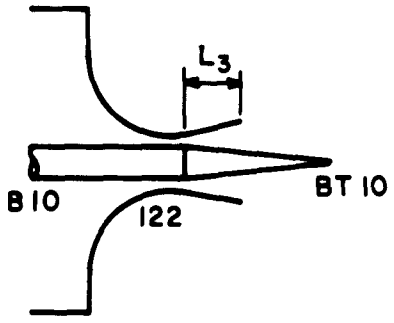

Composite Nozzle no.	Outer Nozzle no.	bar no.	termination no.	L_3 in.	exit A $in.^2$	minimum A_m $in.^2$	$\frac{A}{A_m}$
601	122	B10	BT 10	1.0	0.431	0.296	1.455
621	122	B10	BT 10	0	0.363	0.296	1.226

Table IV. Details of Plug Nozzles

(b) Converging-Diverging Nozzles

				Theoretical		Measured	
Nozzle no.	A $in.^2$	A_{cr} $in.^2$	$\frac{A}{A_{cr}}$	$\frac{P_s}{P_o}$	M	$\frac{P_s}{P_o}$	M
120	0.442	0.375	1.178	3.67	1.50	3.4	1.45
121	0.785	0.667	1.178	3.67	1.50	3.4	1.45
122	0.442	0.375	1.178	3.67	1.50	3.4	1.45
305	1.178	1.000	1.178	3.67	1.50	3.35	1.44
601	0.431	0.296	1.455	5.88	1.815	5.6	1.783
621	0.363	0.296	1.226	4.07	1.57	4.15	1.583

Table V. Comparison Between Theoretical and Measured Mach Numbers for Converging-Diverging Nozzles

Symbols PWL	Symbols m/A	Engine Type	P_S / P_0	T_S °R	m slugs/sec	A $ft.^2$	PWL re 10^{-13} w	Ref.
○	○	J 57 Engine A/B Conf. Military Power	2.16	1600	5.59	2.739	172.5	*
□	□	J 57-P-2B Eng. A/B Conf. Military Power	2.25	1396	5.34	2.40	178.9	8
▽	▽	J 79 Engine A/B Conf. Military Power	2.04	1525	4.78	2.765	178.0	*
◇	◇	CJ-805-3 Eng. Conical Nozzle	2.406	1544	4.62	2.255	175.0	*
◊	◊	CJ-805-3 Eng. Daisy Nozzle	2.39	1529	4.64	2.30	169.5	*
⊔	⊔	1/7 Scale Model J 57	2.16	1610	0.978	0.0554	156.5	*

T_0 = 530 °R
P_0 = 14.7 psia
} Assumed for all cases

* Private Communication

Table VI. Jet Engine Data

(a) Standard Engines

Symbols PWL m/A	Nozzle	P_s / P_o	T_s °R	m slugs/sec	A $ft.^2$	PWL re 10^{-13} w
○ ◁	Engine A Conical Nozzle	2.30	1360	5.29	2.56	169.3
□	Engine A 12 Lobe Nozzle	2.30	1360	5.19	2.56	166.3
◇	Engine A 12 Lobe Nozzle Ejector $D_1/D_2 = 1.4$	2.30	1360	5.38	2.56	163.6
▽	Engine A 12 Lobe Nozzle Ejector $D_1/D_2 = 1.7$	2.30	1360	5.48	2.56	161.6
◺ ◇	Engine B Conical Nozzle	1.70	1735	2.94	2.07	168.1
D	Engine B 8 Lobe Nozzle	1.70	1735	2.85	2.07	164.1
Ω	Engine B 8 Lobe Nozzle Ejector D /D =1.6	1.70	1735	3.21	2.07	160.4

T = 530 °R
P = 14.7 psia
} Assumed for all cases

Table VI. Jet Engine Data
(b) Special Engines (Ref. 9)

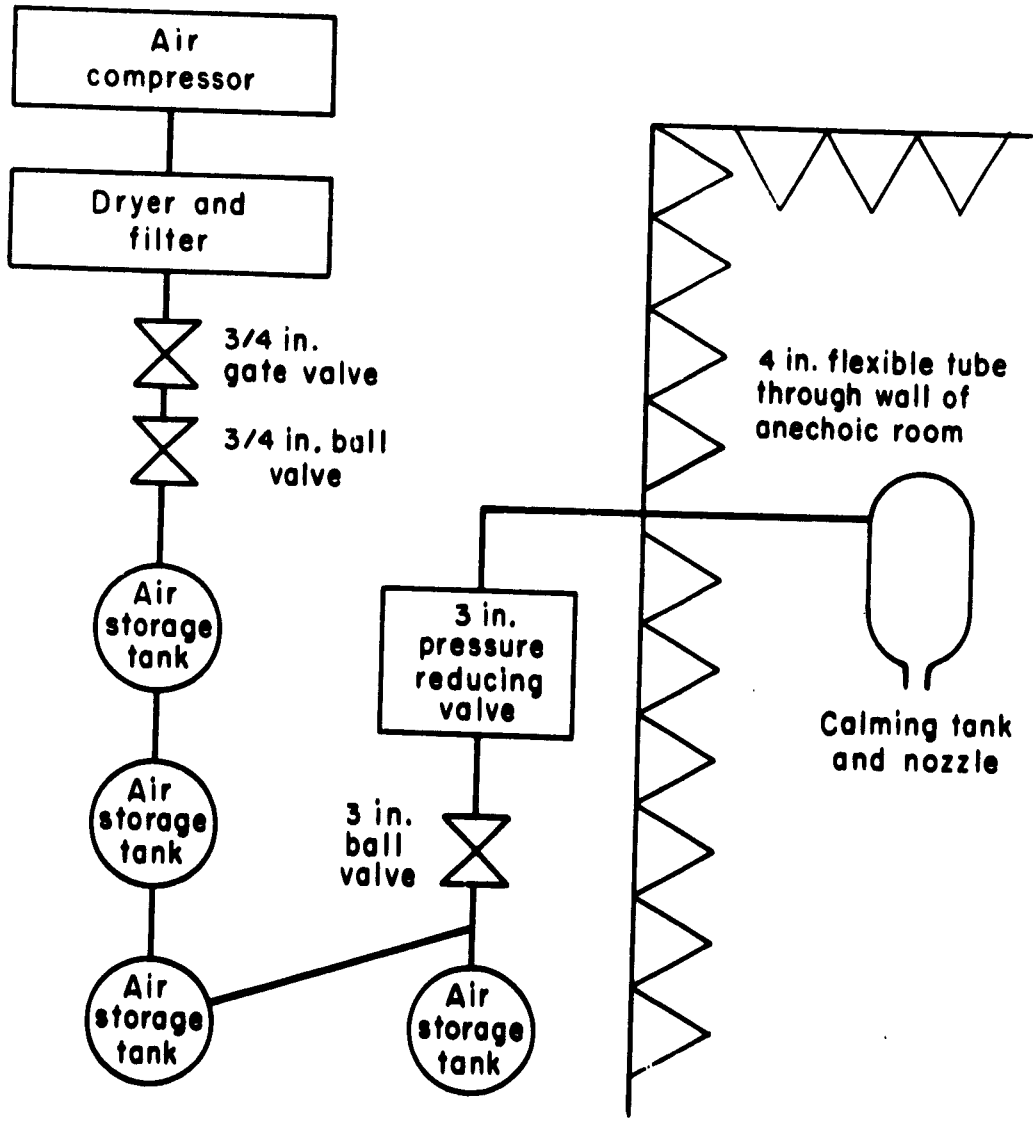

Figure 1. Jet Noise Facility
(a) Air Supply Equipment

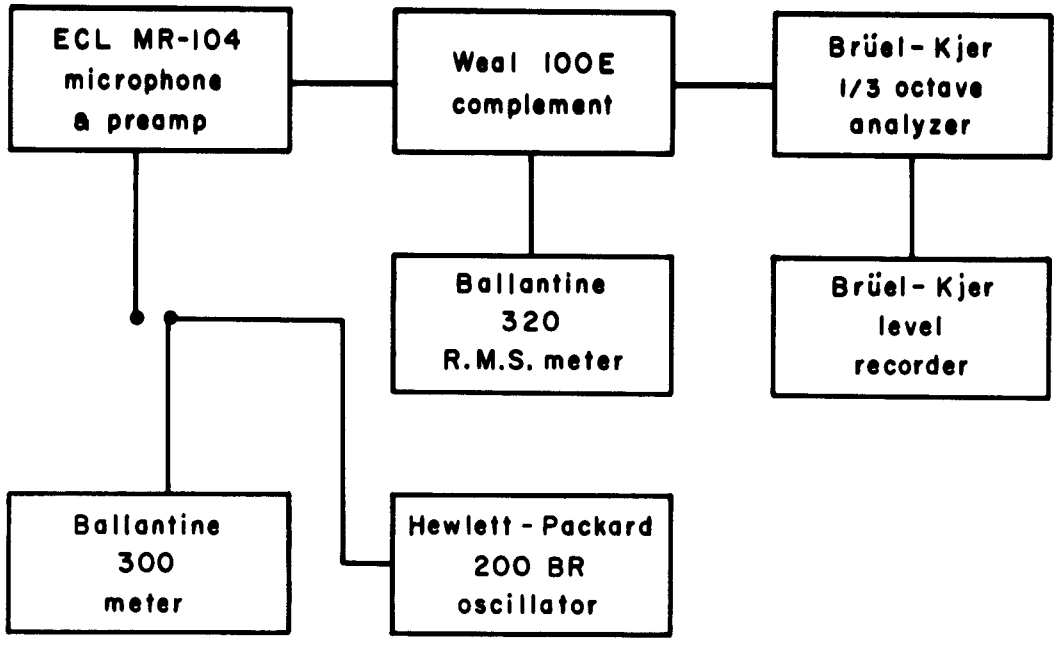

Figure 1. Continued

(b) Noise Measuring Equipment

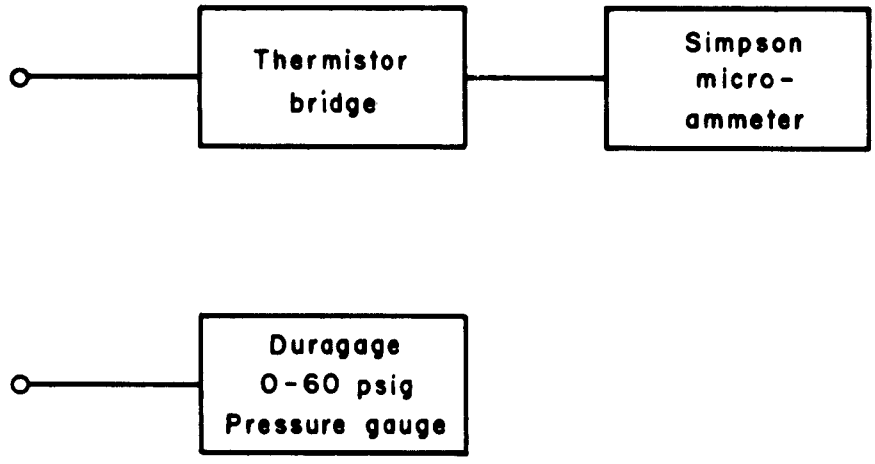

Figure 1. Continued

(c) Pressure and Temperature Measuring Equipment

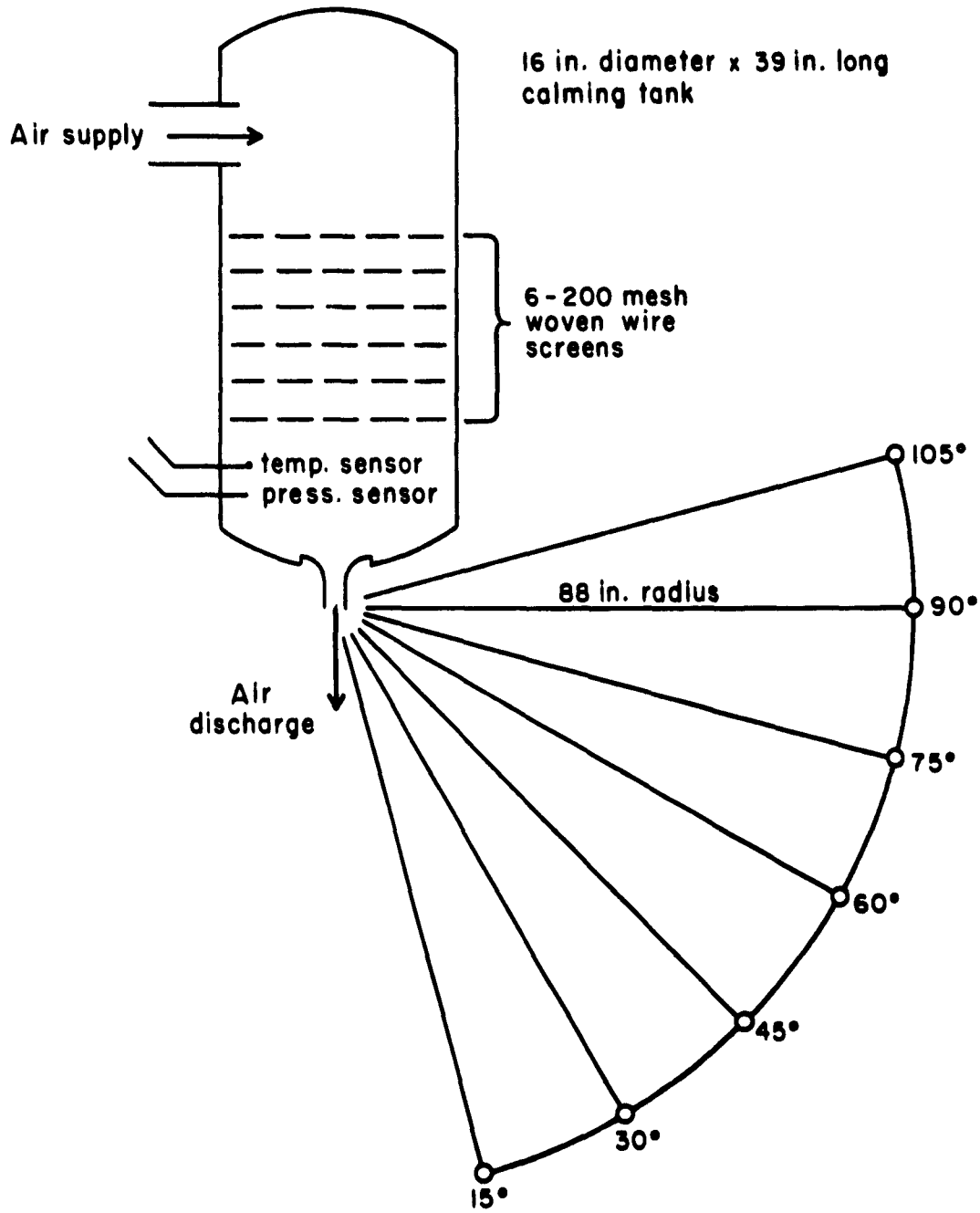

Figure 1. Jet Noise Facility
(d) Calming Tank Details and Noise Survey Stations

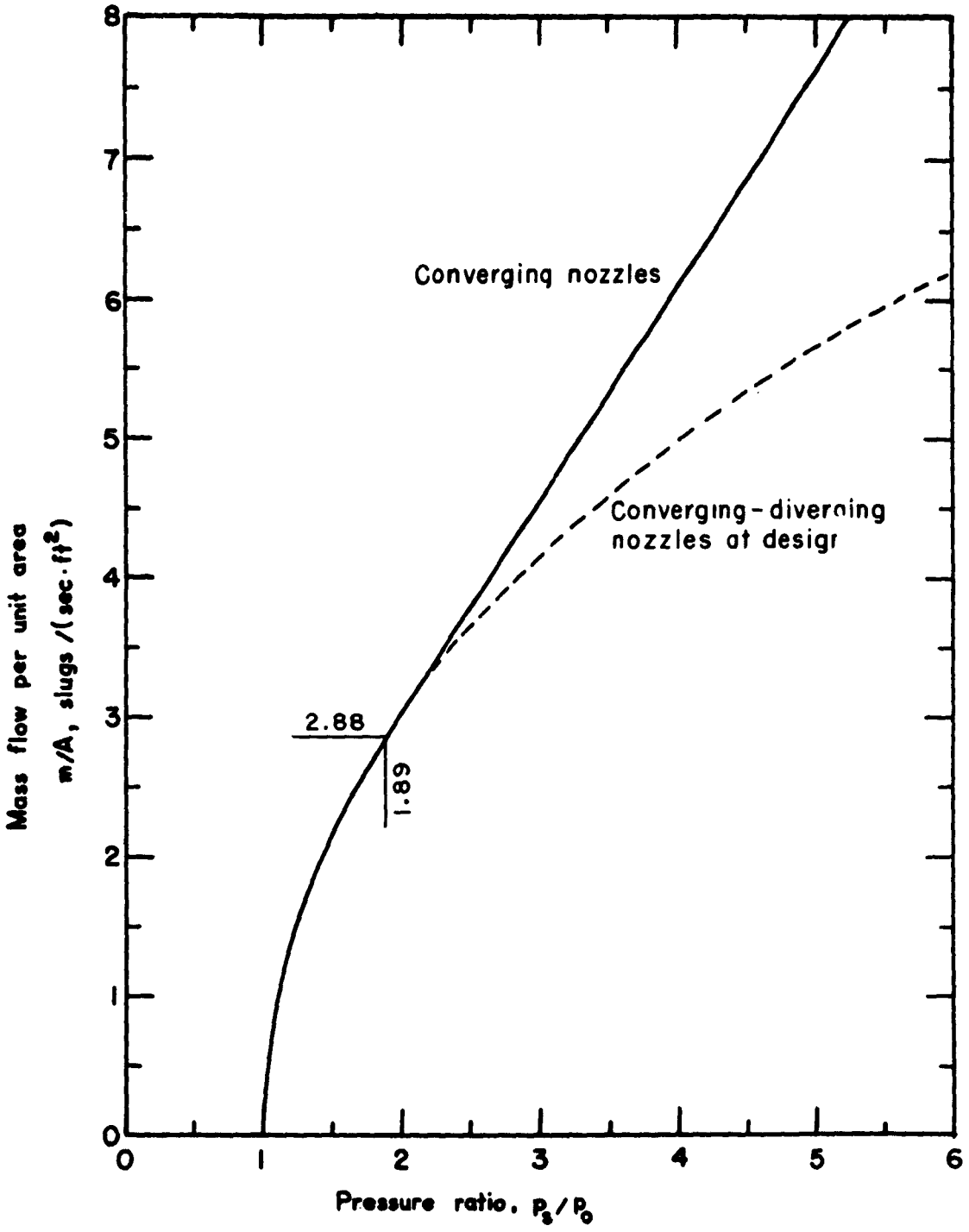

Figure 2. Theoretical Performance
(a) Mass Flow versus Pressure Ratio

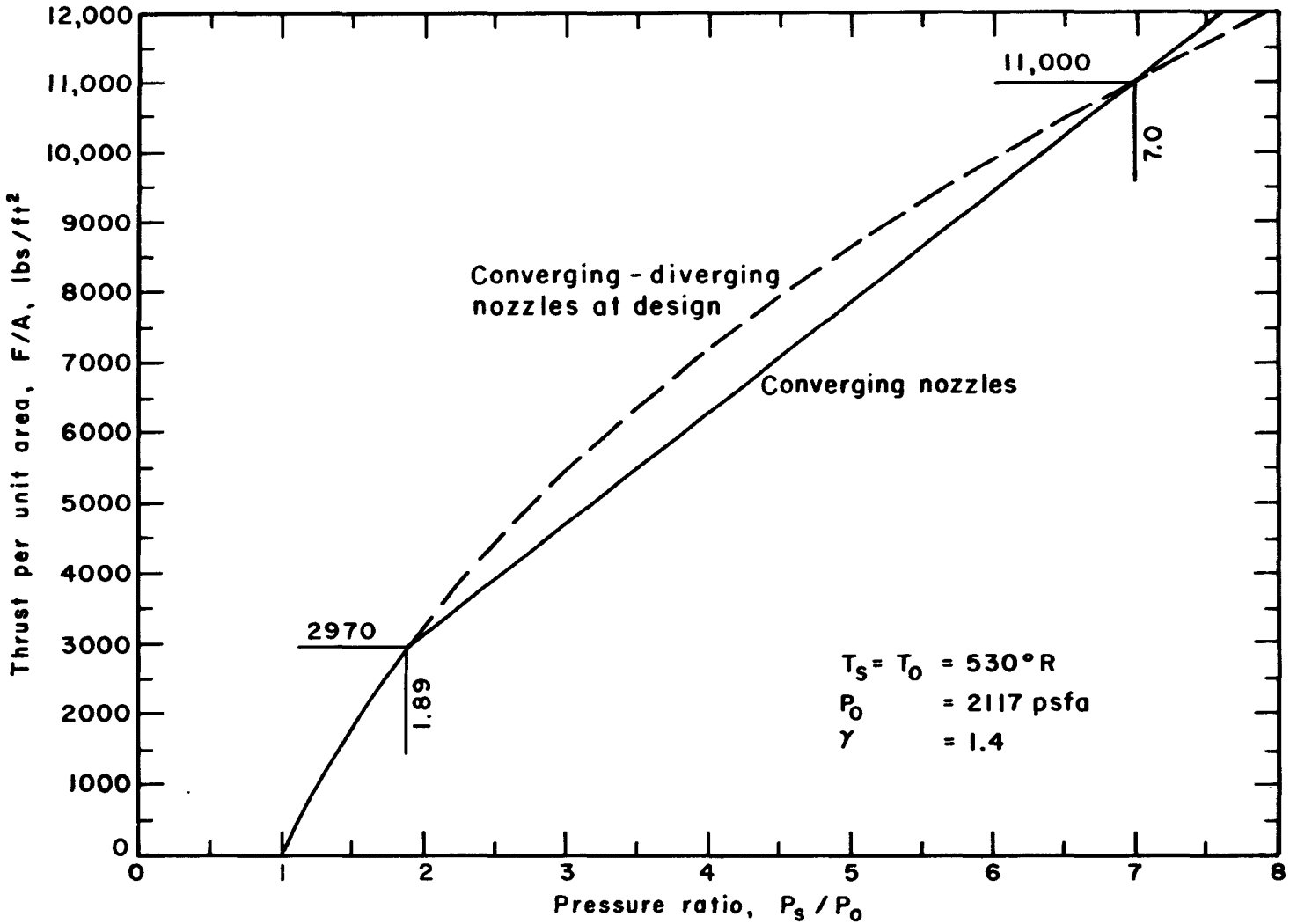

Figure 2. Theoretical Performance
(b) Thrust versus Pressure Ratio

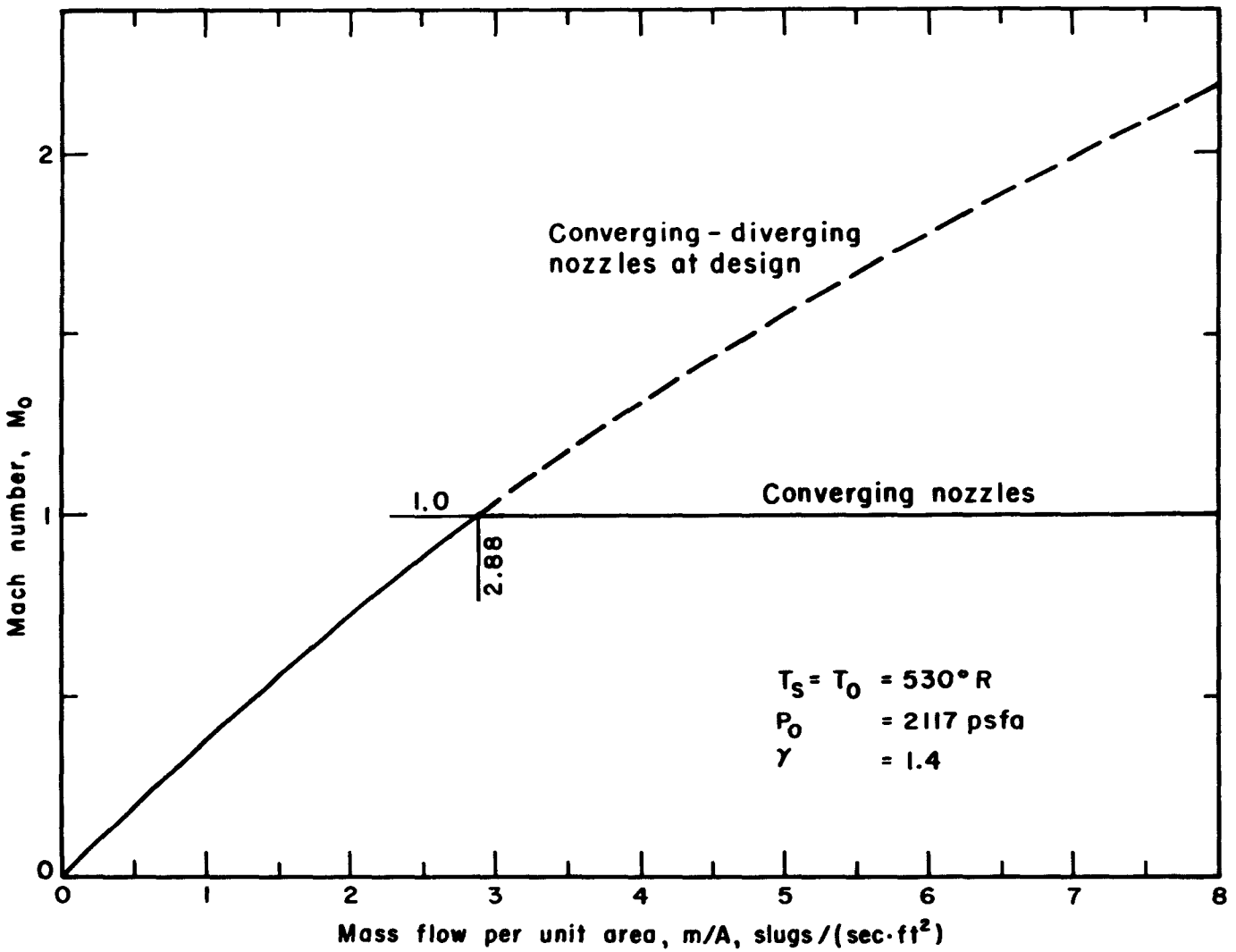

Figure 2. Theoretical Performance
(c) Mass Flow versus Mach Number

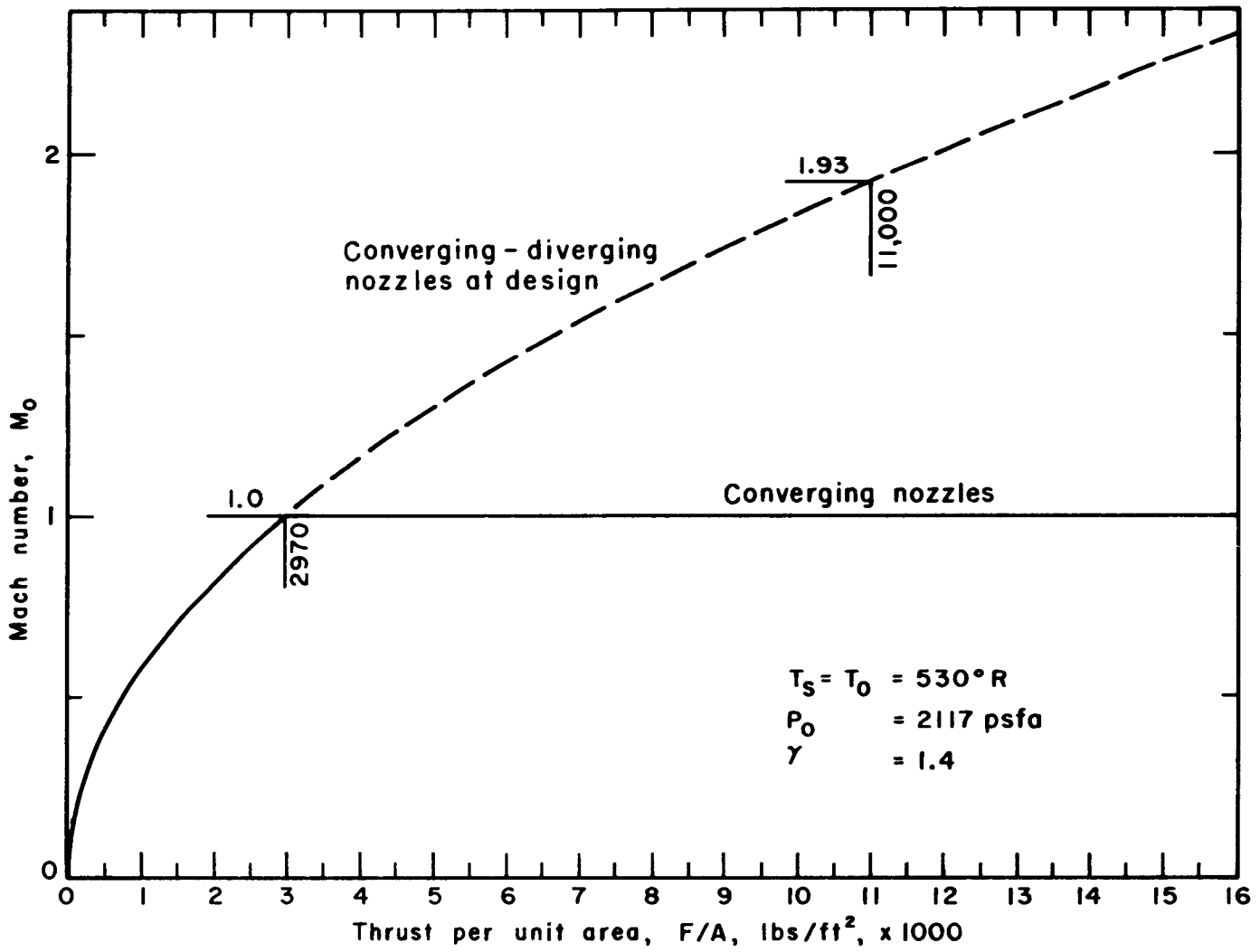

Figure 2. Theoretical Performance

(d) Thrust versus Mach Number

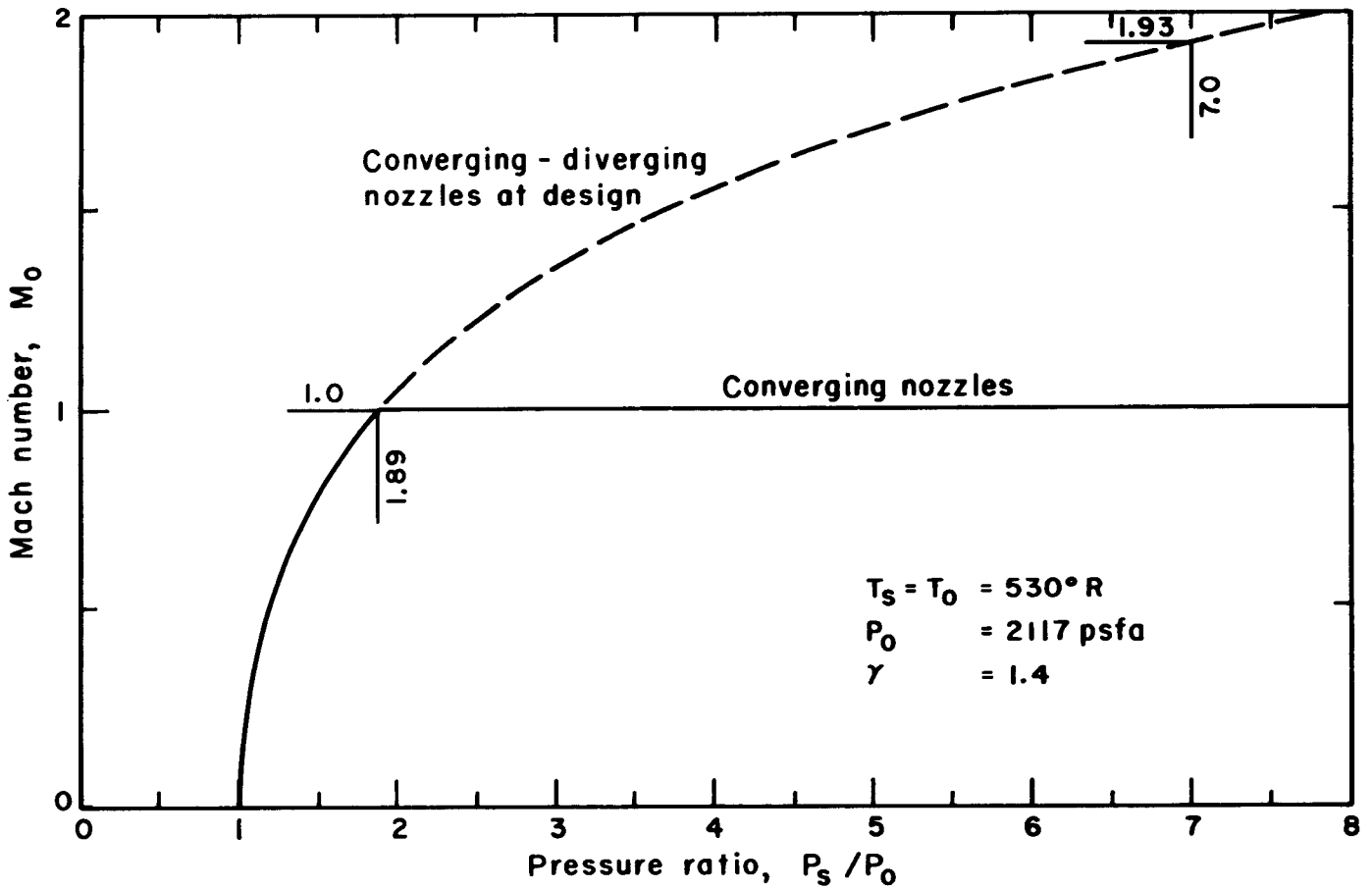

Figure 2. Theoretical Performance
(e) Mass Flow versus Pressure Ratio

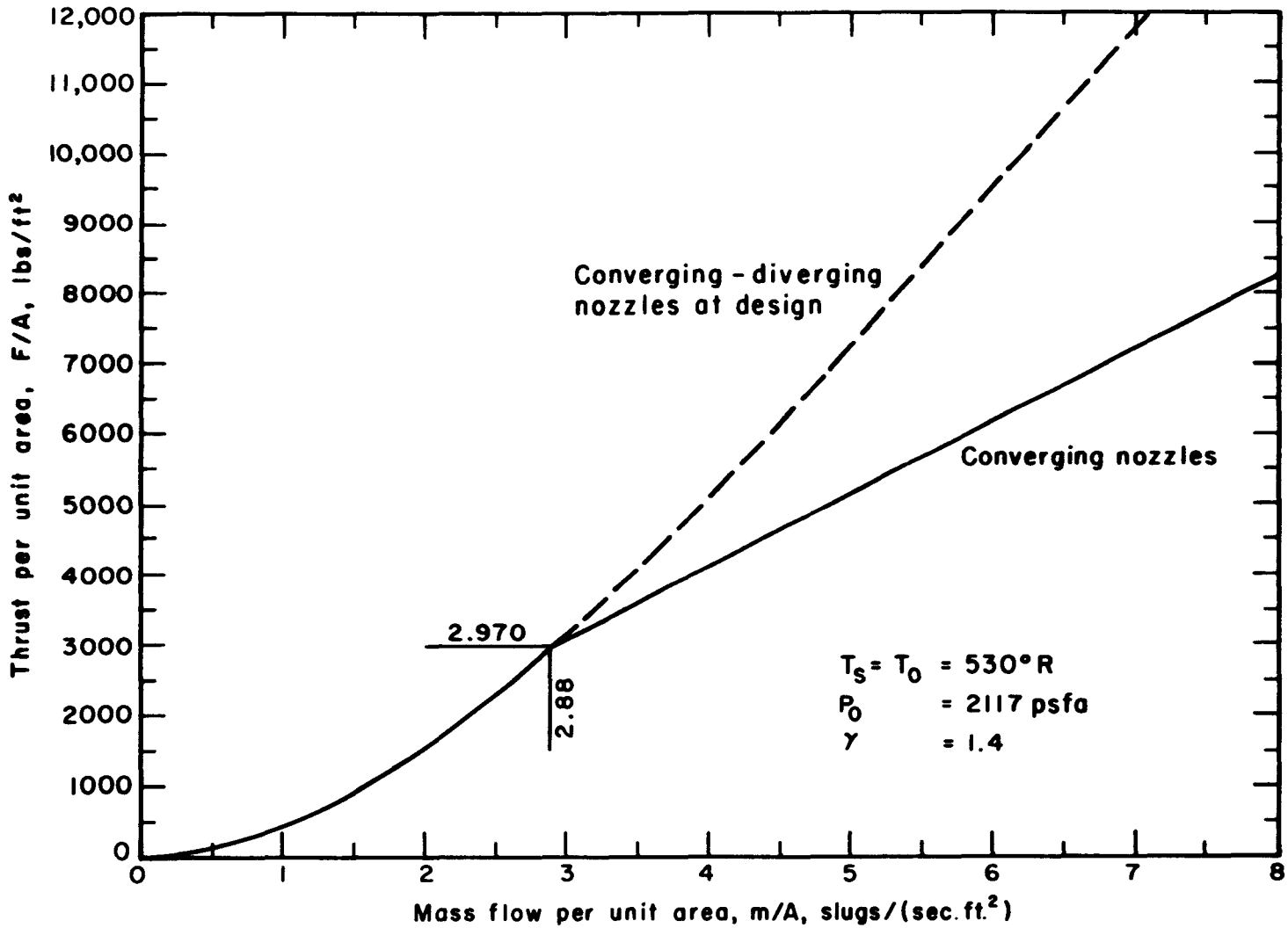

Figure 2. Theoretical Performance

(f) Thrust versus Mass Flow

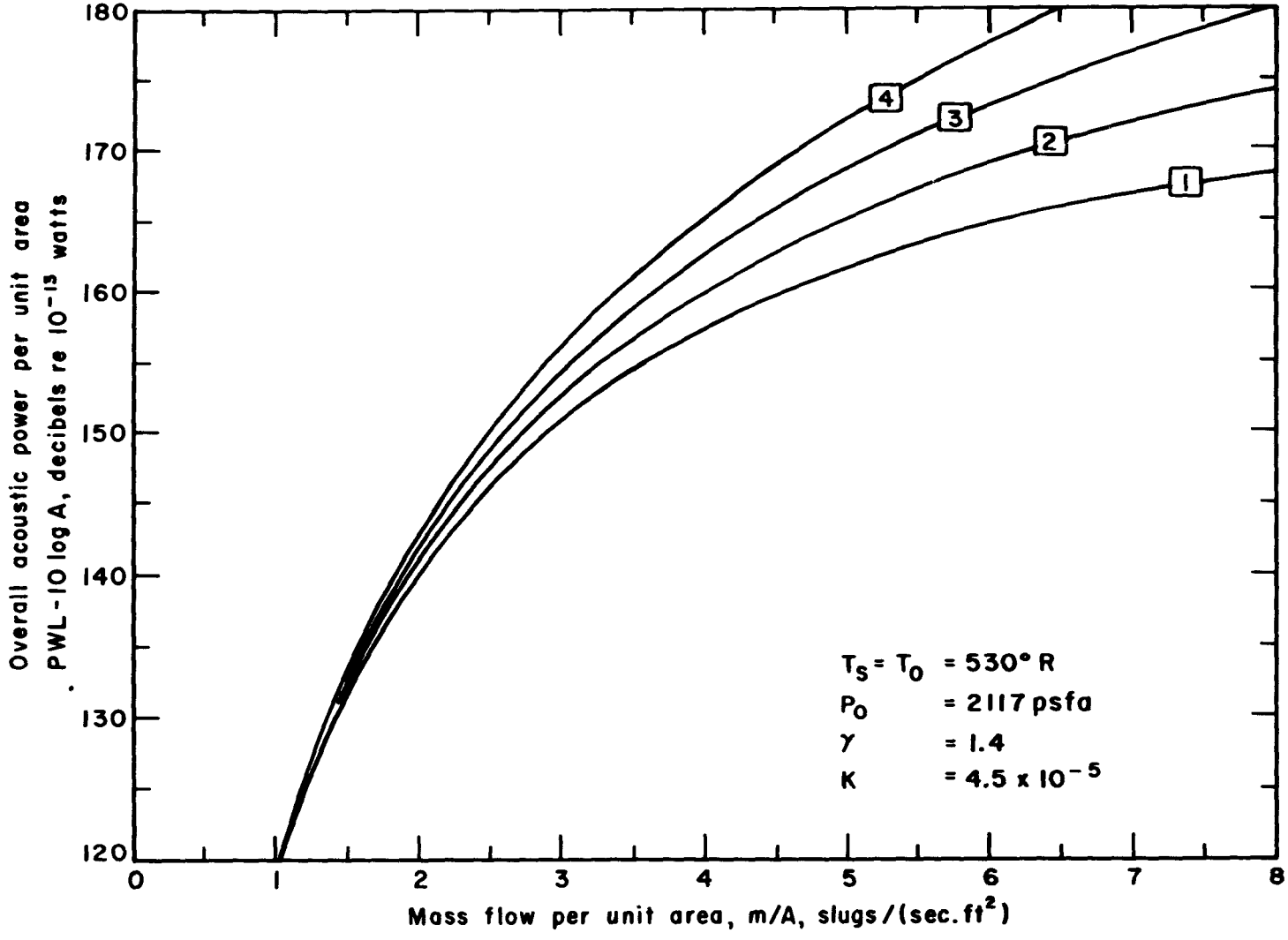

Figure 2. Theoretical Performance
(g) Acoustic Power versus Mass Flow

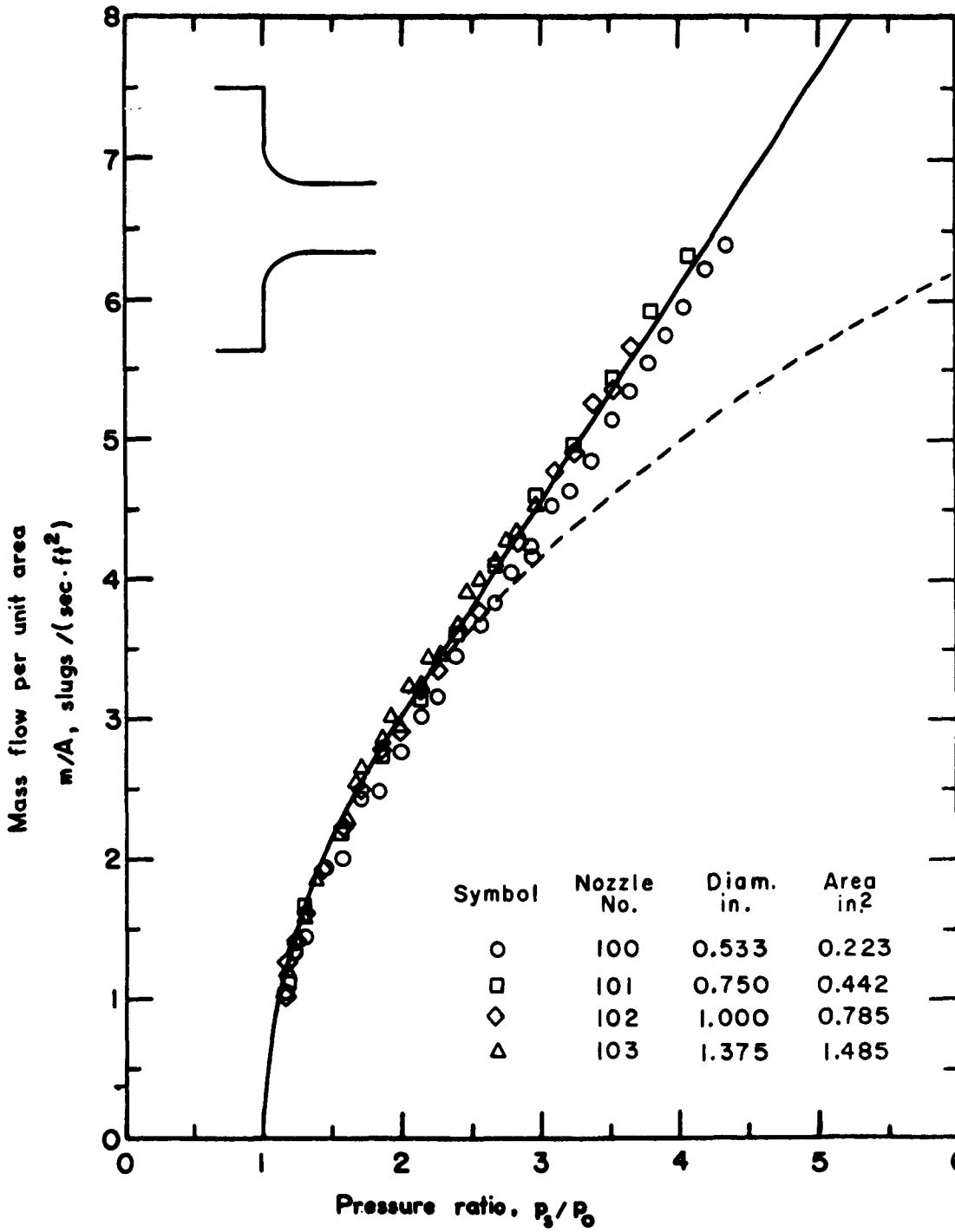

Figure 3. Flow Performance of Basic Nozzles

(a) Nozzles No. 100, 101, 102, and 103

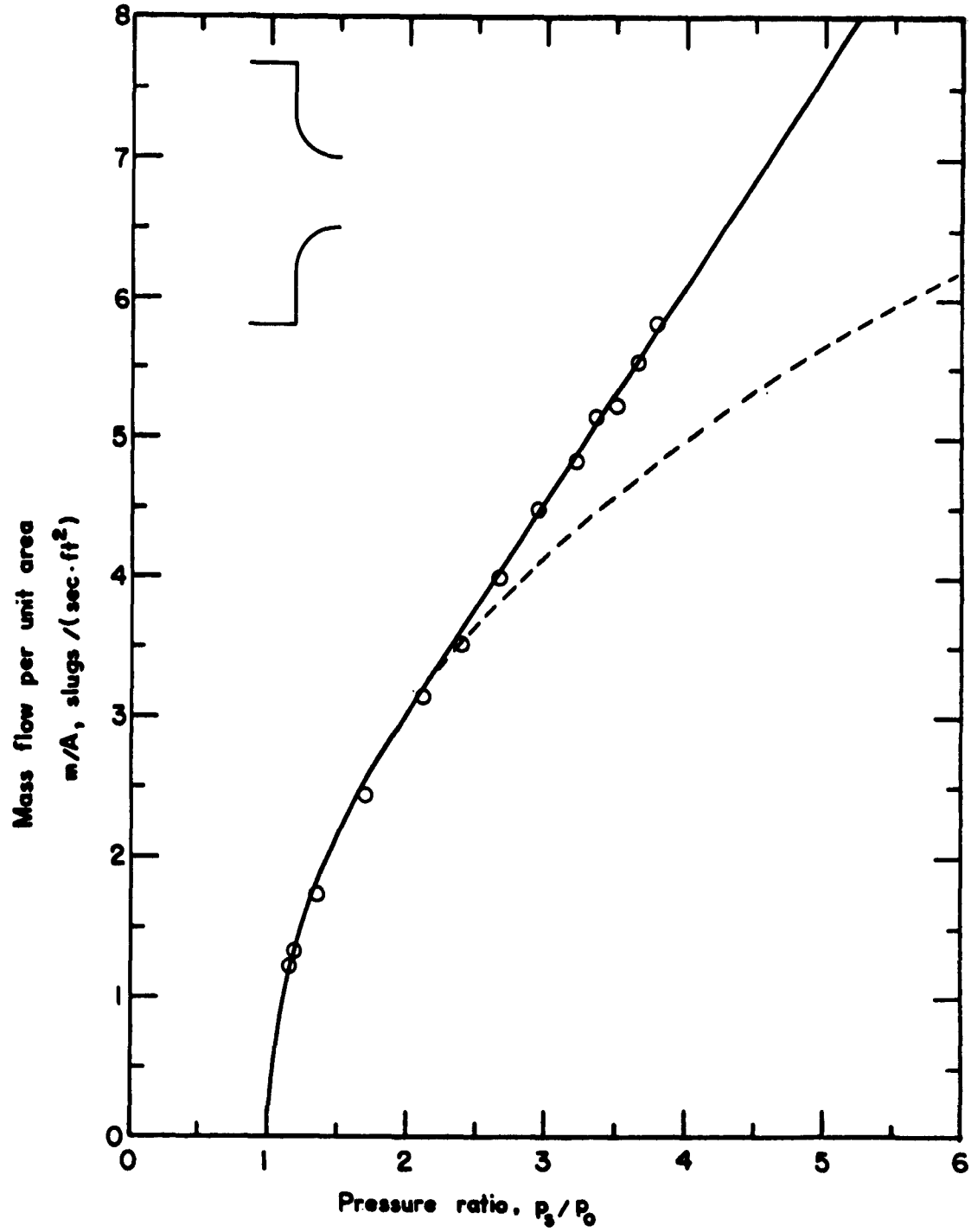

Figure 3. Flow Performance of Basic Nozzles
(b) Nozzle No. 110

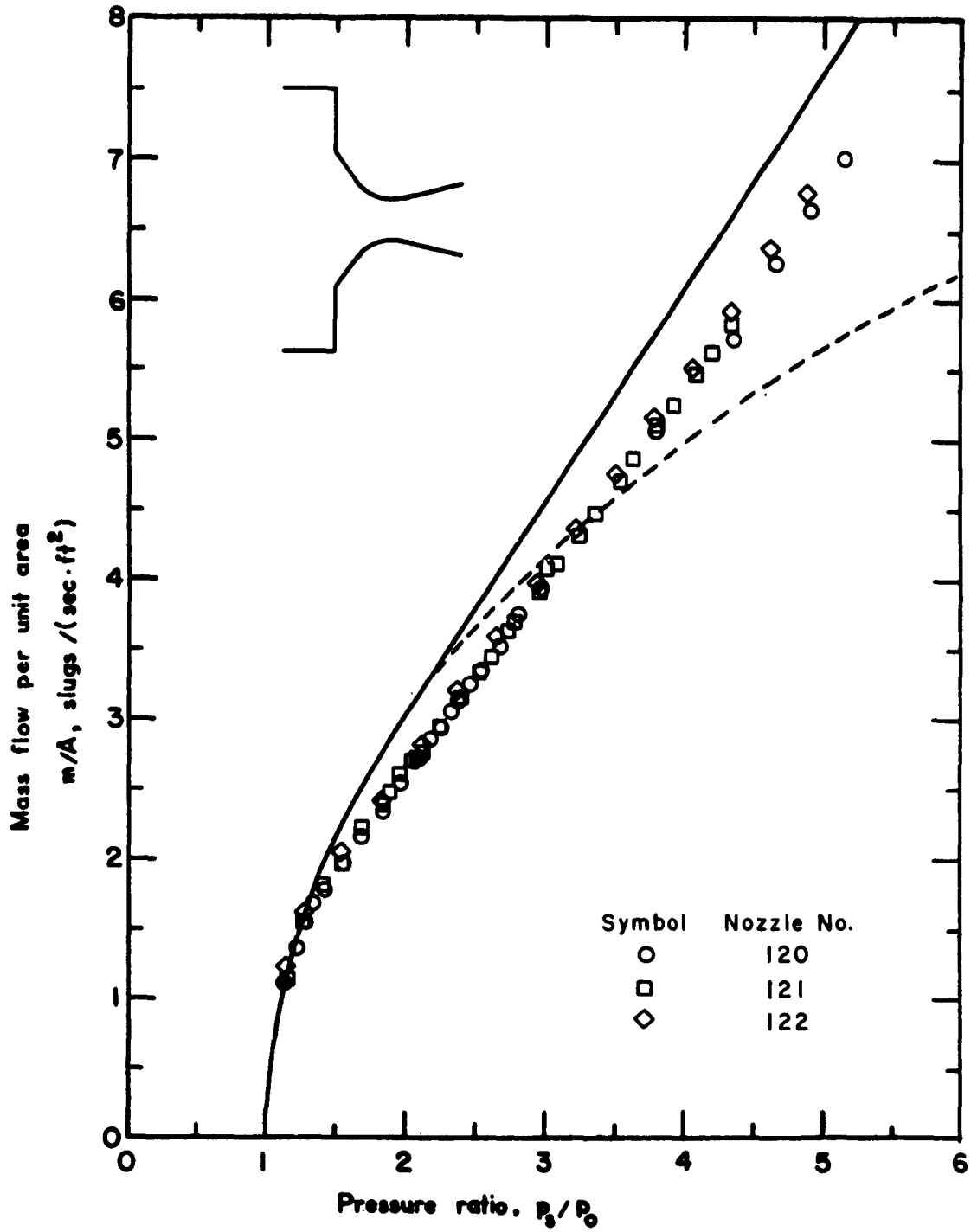

Figure 3. Flow Performance of Basic Nozzles
(c) Nozzles No. 120, 121, and 122

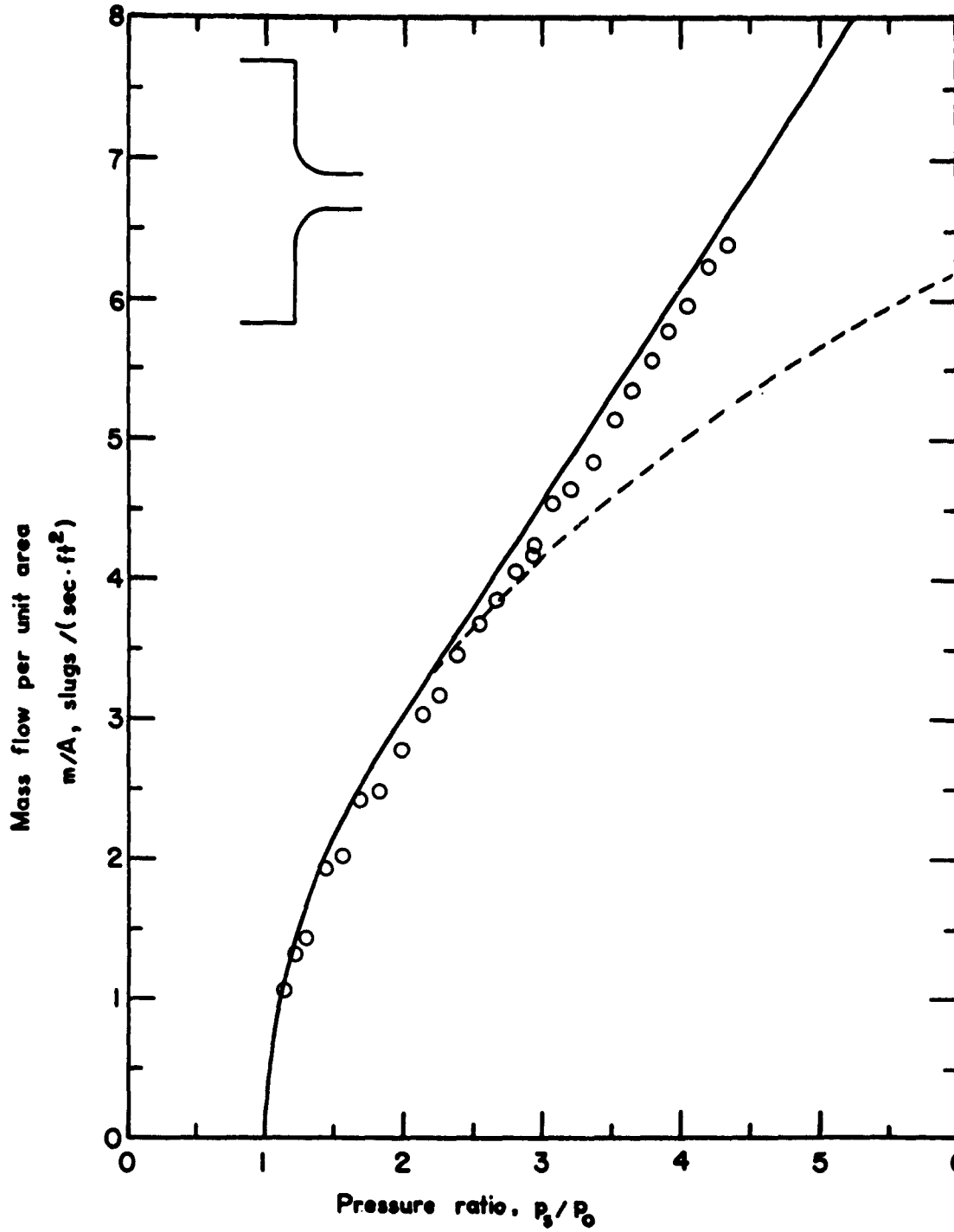

Figure 3. Flow Performance of Basic Nozzles
(d) Nozzle No. 100

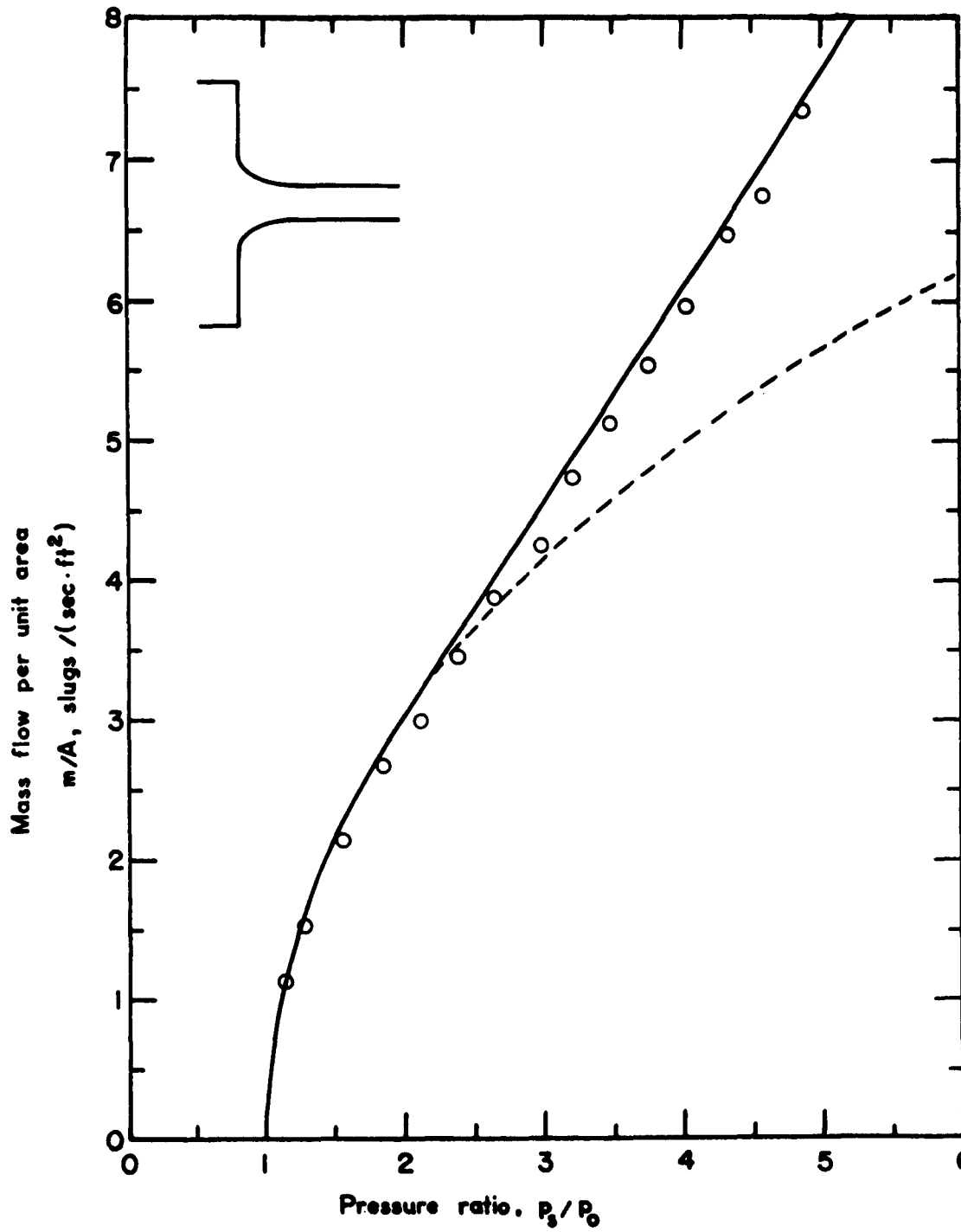

Figure 3. Flow Performance of Basic Nozzles
(e) Nozzle No. 140

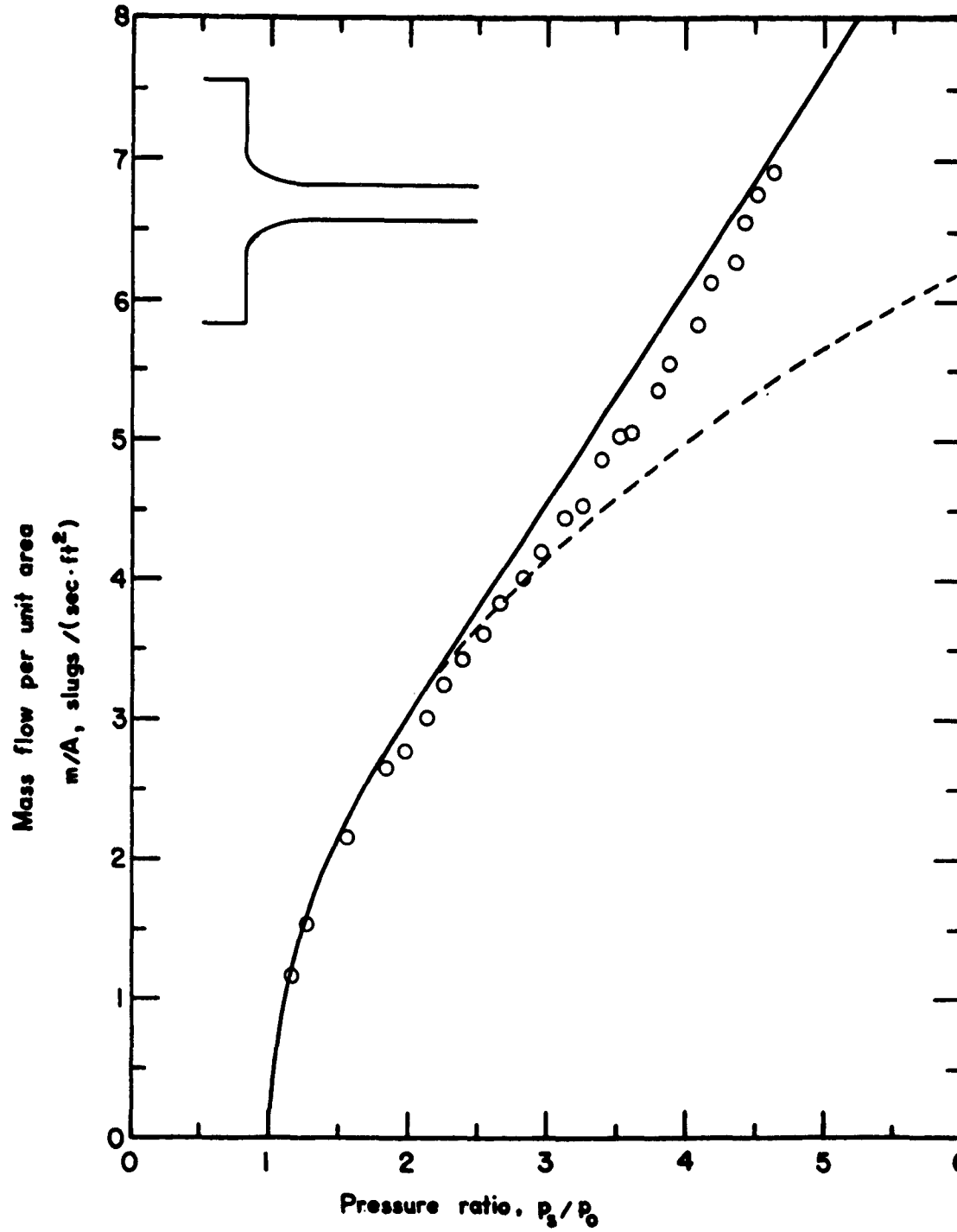

Figure 3. Flow Performance of Basic Nozzles
(f) Nozzle No. 141

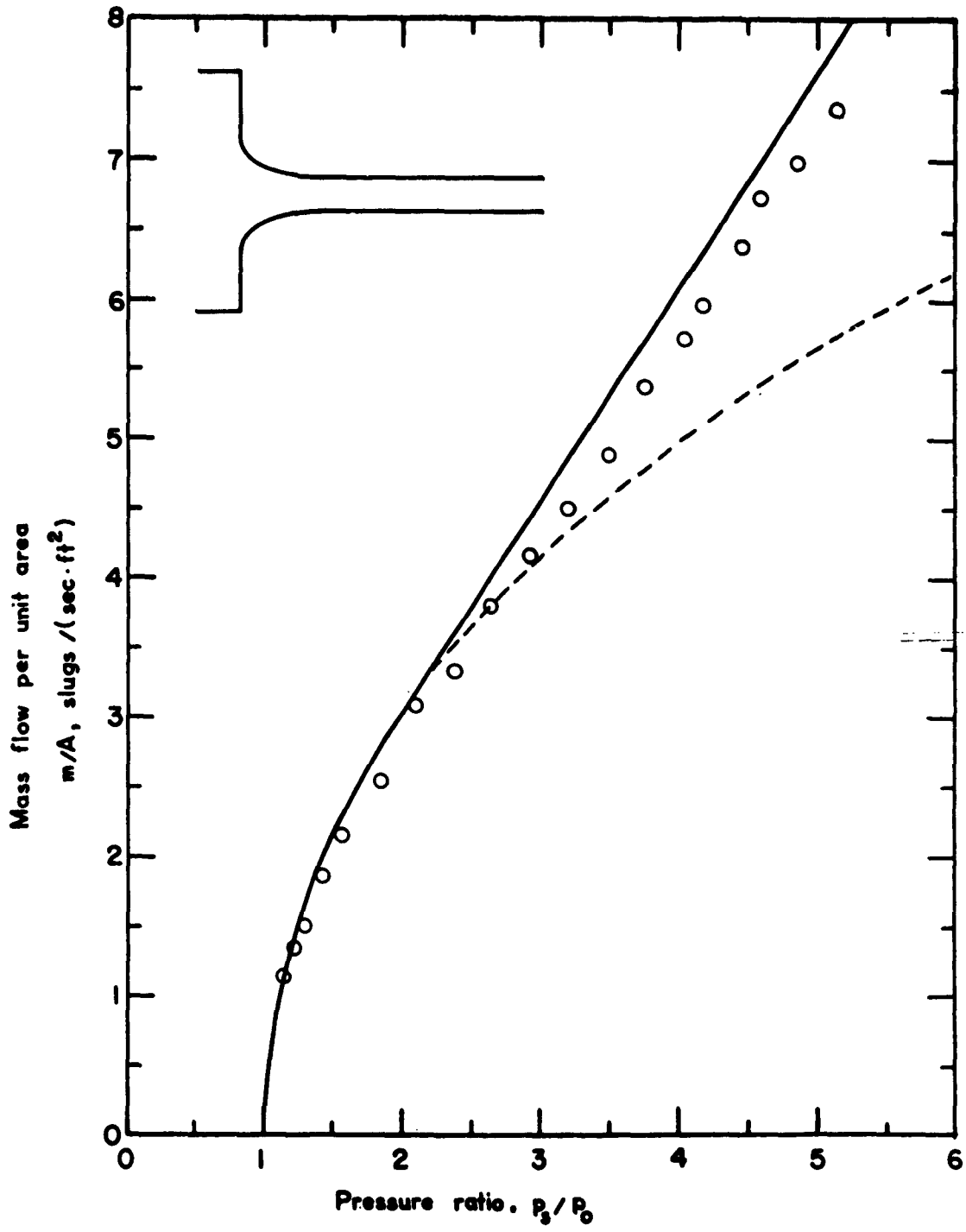

Figure 3. Flow Performance of Basic Nozzles
(g) Nozzle No. 142

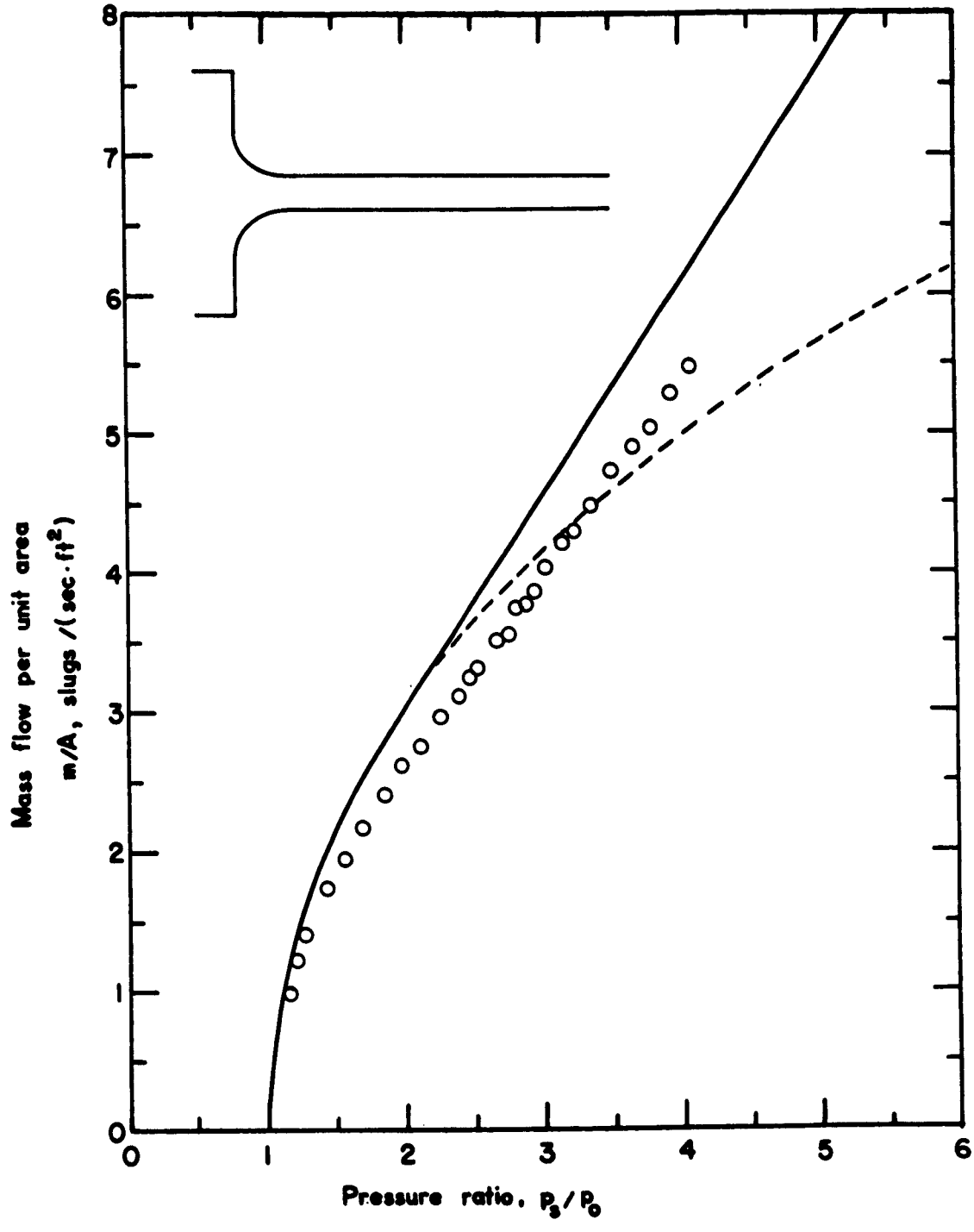

Figure 3. Flow Performance of Basic Nozzles
(h) Nozzle No. 143

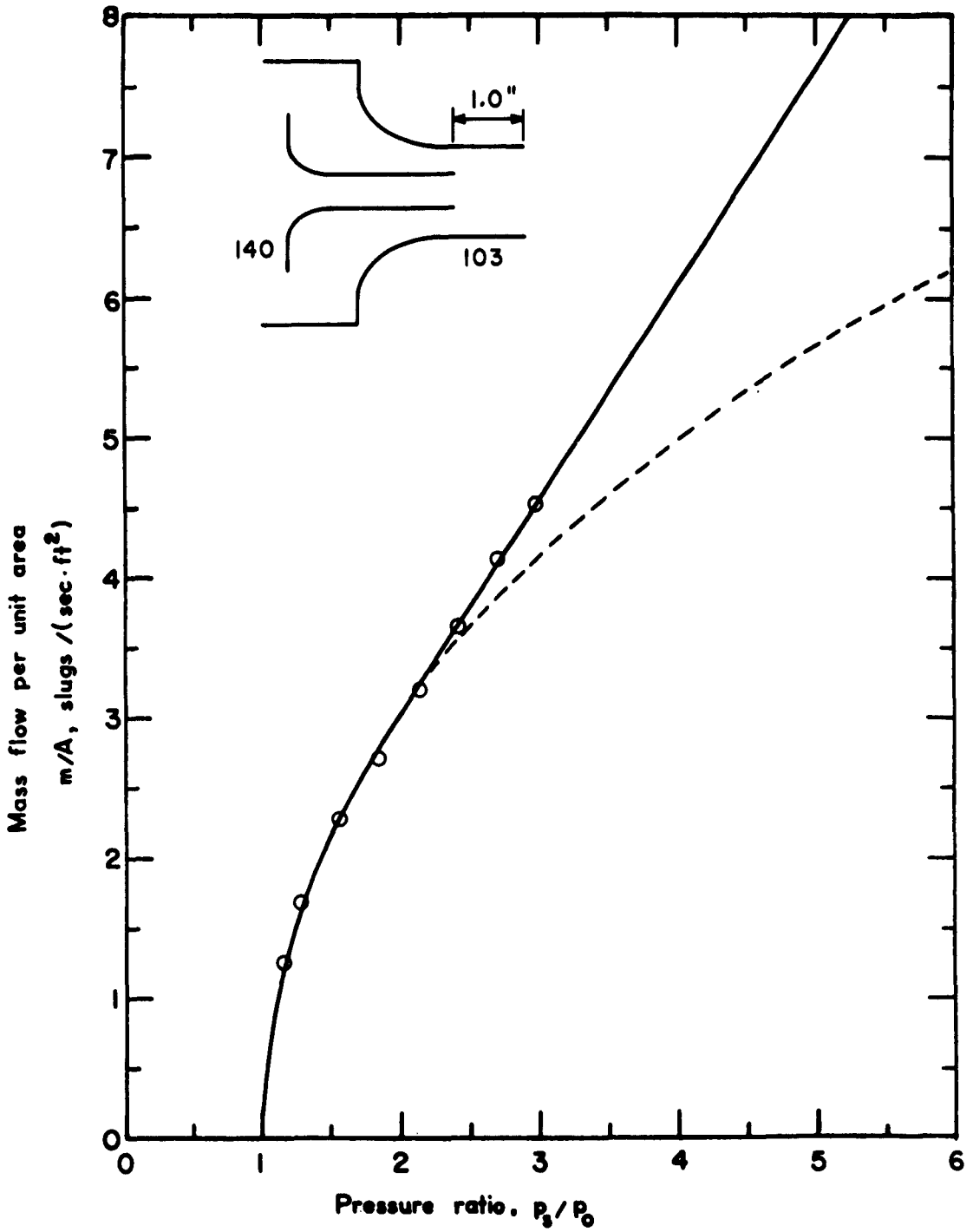

Figure 4. Flow Performance of Annular Nozzles with Center Core Flow

(a) Nozzle No. 200

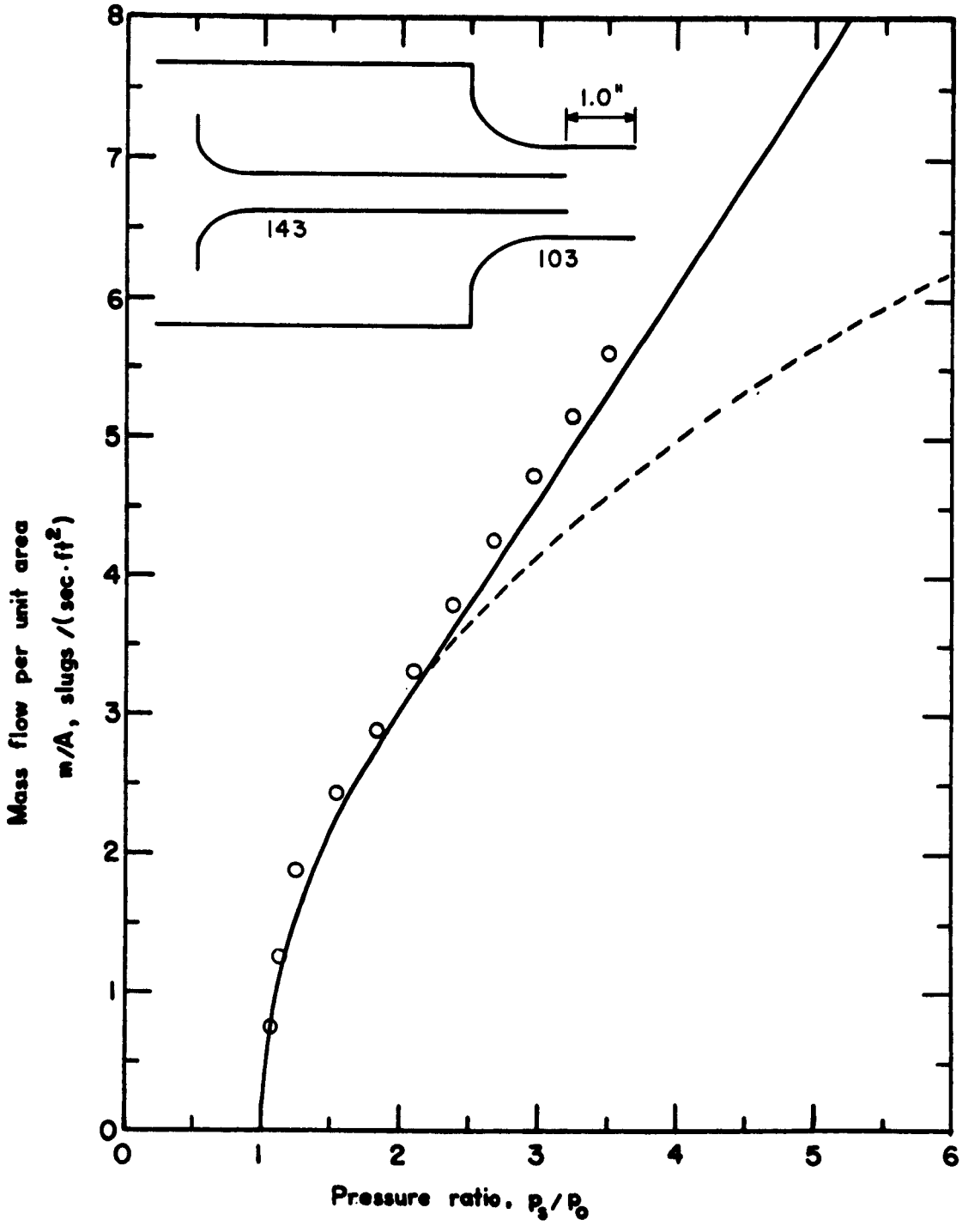

Figure 4. Flow Performance of Annular Nozzles with Center Core Flow

(b) Nozzle No. 203

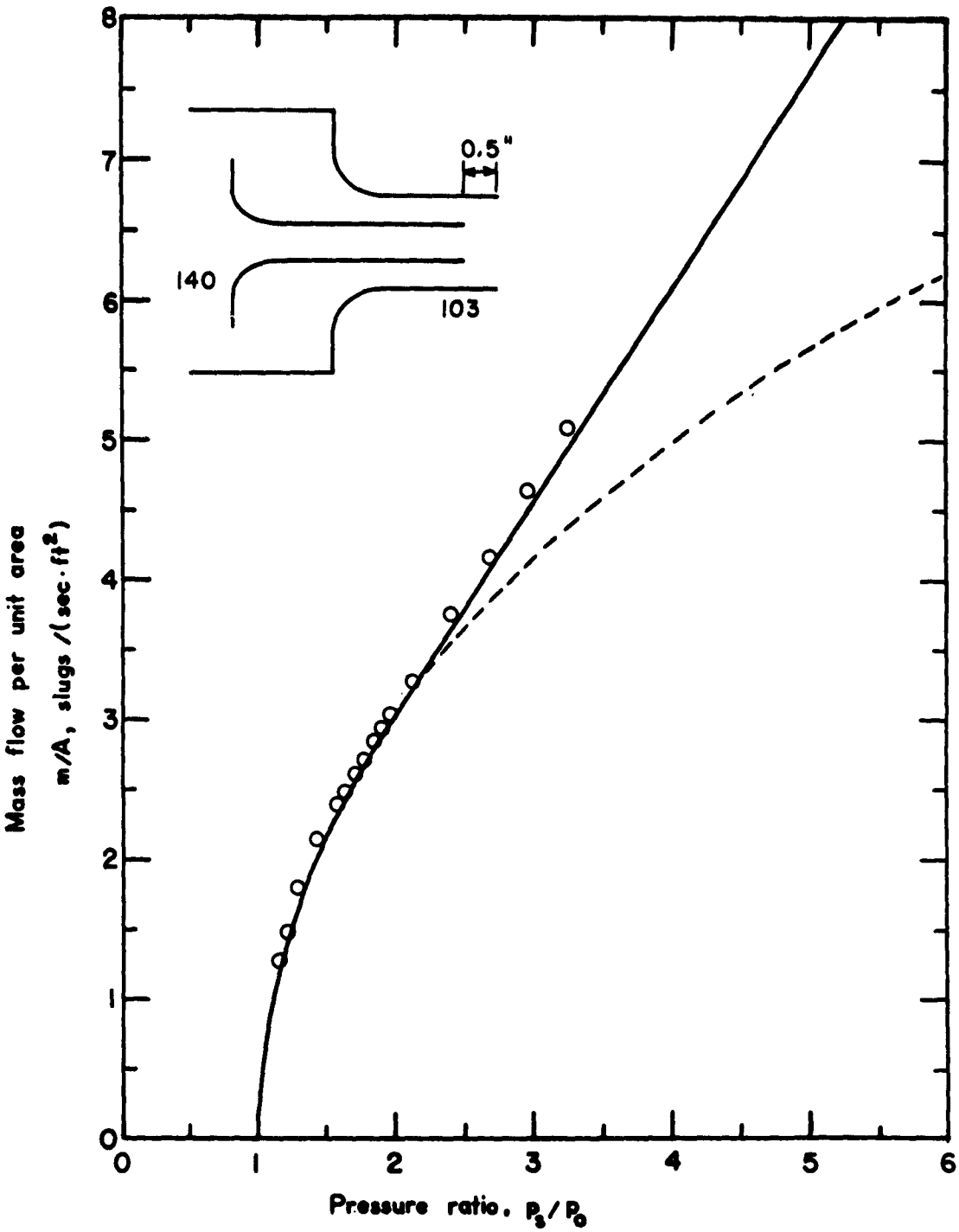

Figure 4. Flow Performance of Annular Nozzles with Center Core Flow

(c) Nozzle No. 210

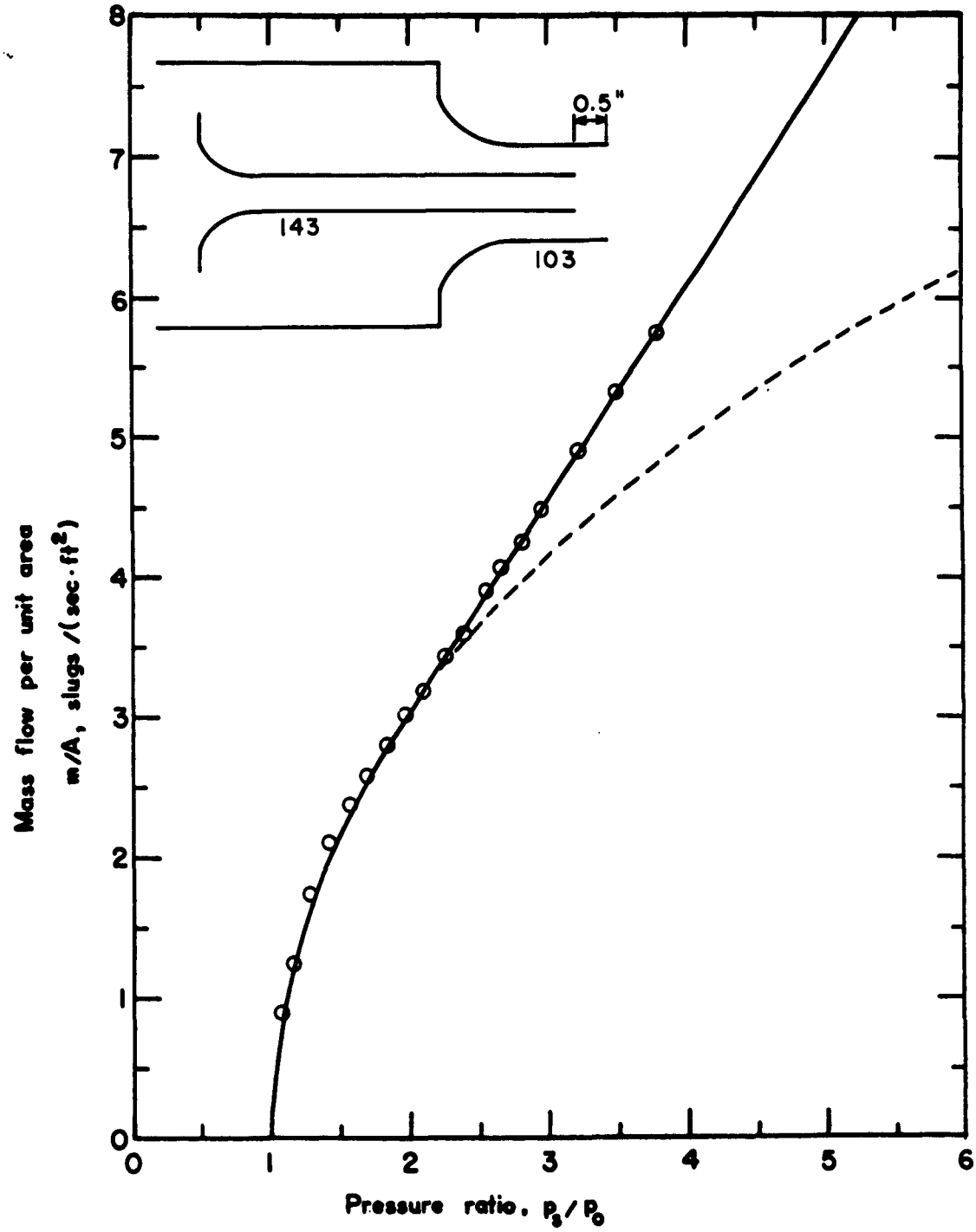

Figure 4. Flow Performance of Annular Nozzles with Center Core Flow

(d) Nozzle No. 212

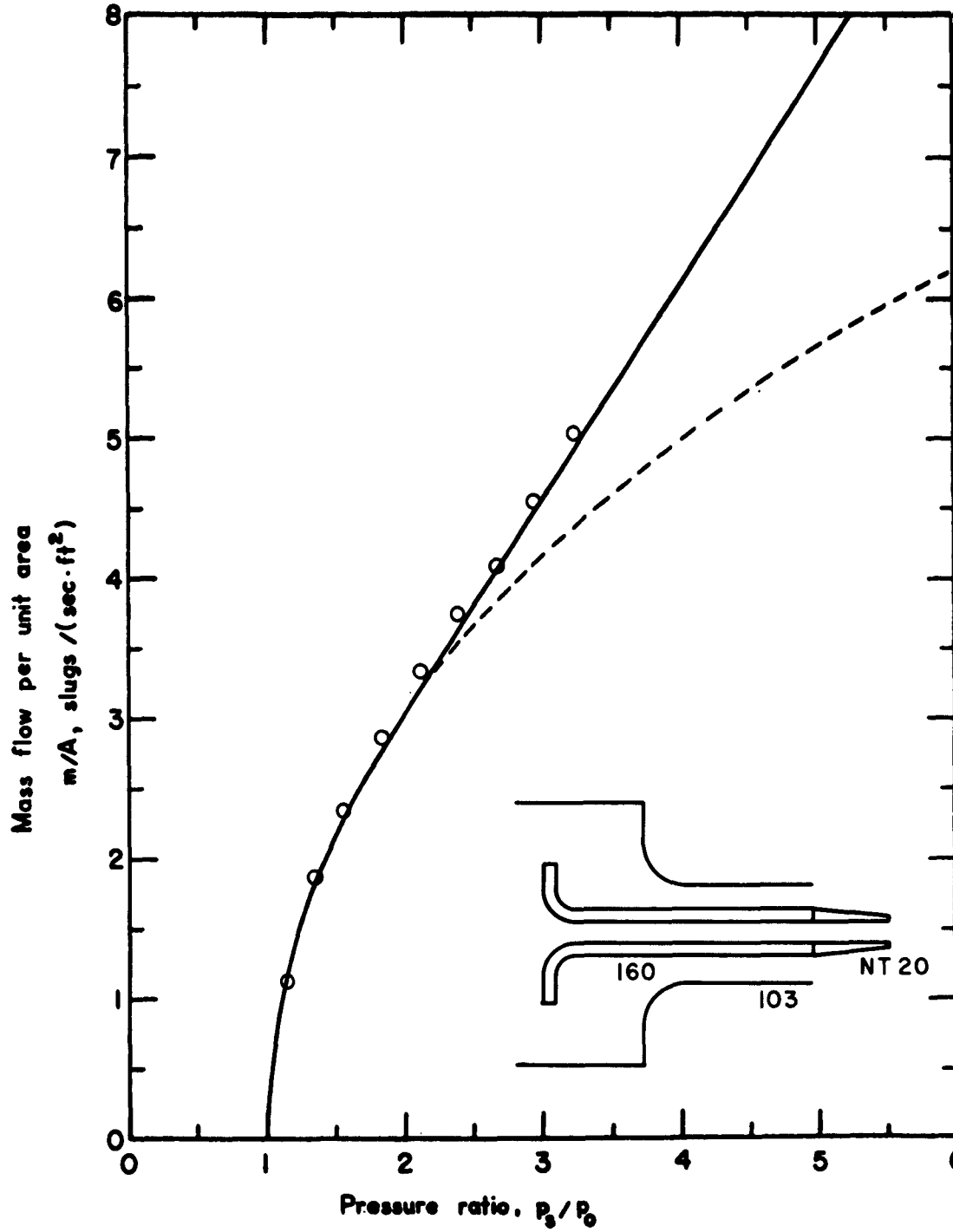

Figure 4. Flow Performance of Annular Nozzles with Center Core Flow

(e) Nozzle No. 223

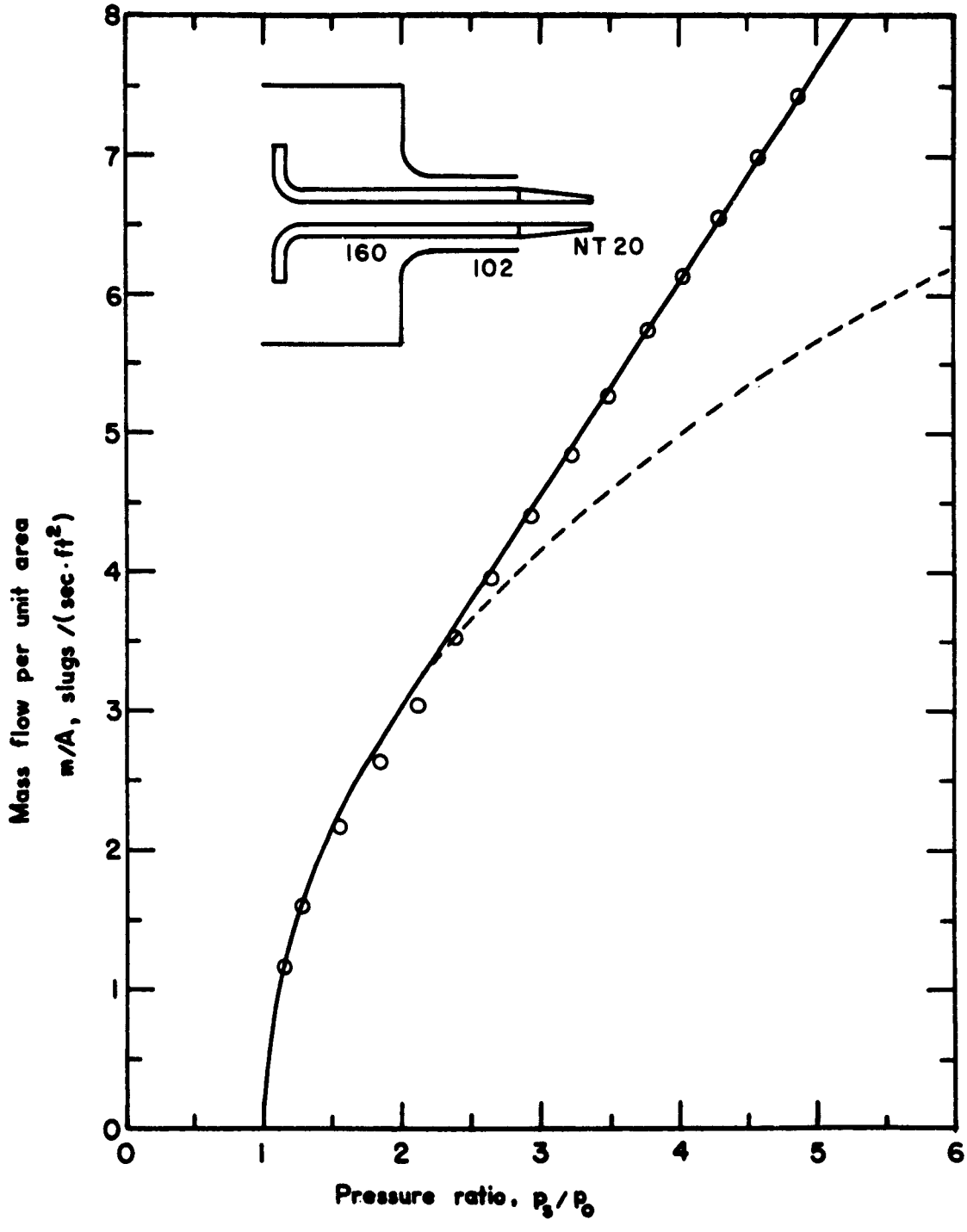

Figure 4. Flow Performance of Annular Nozzles with Center Core Flow

(f) Nozzle No. 274

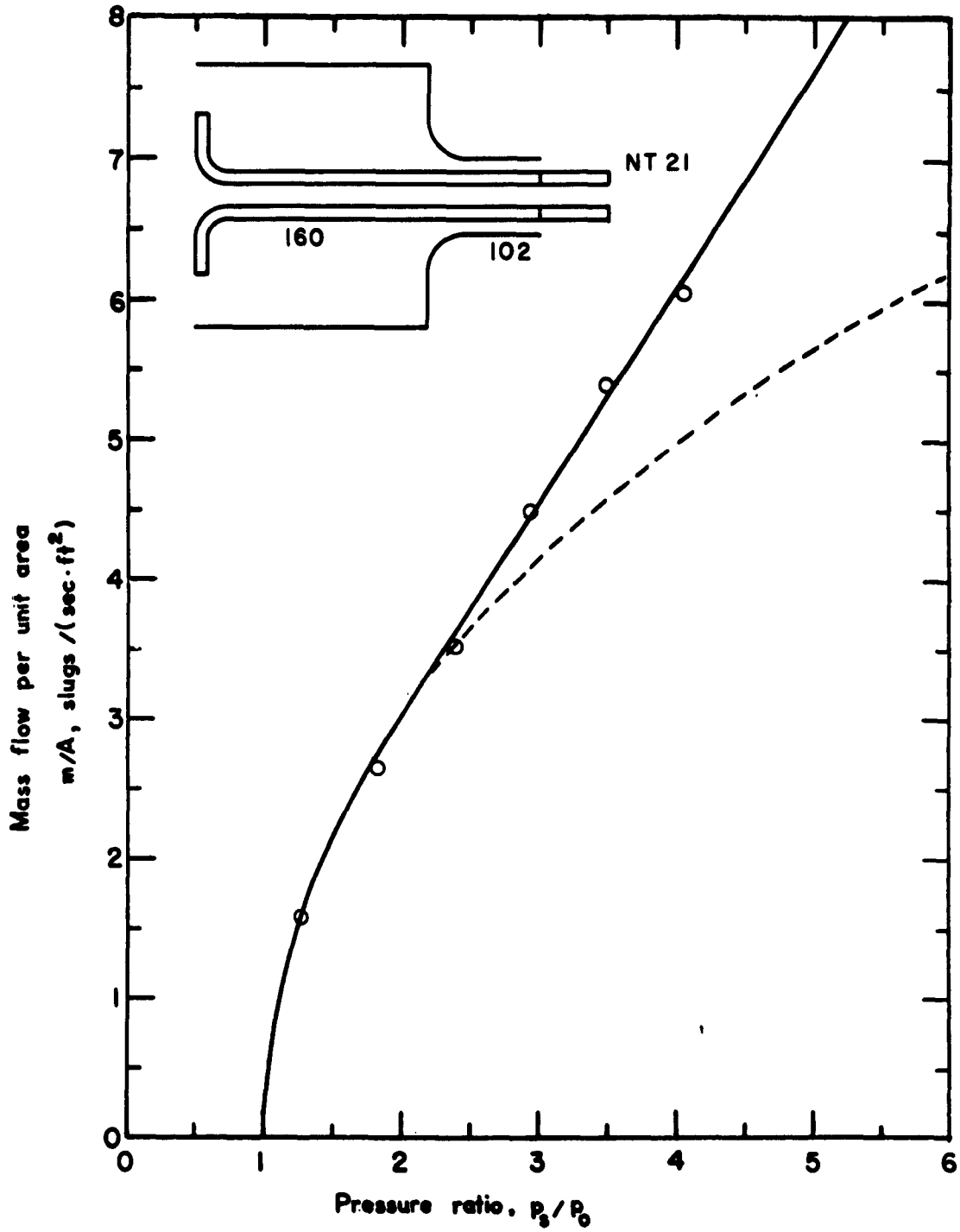

Figure 4. Flow Performance of Annular Nozzles with Center Core Flow

(g) Nozzle No. 275

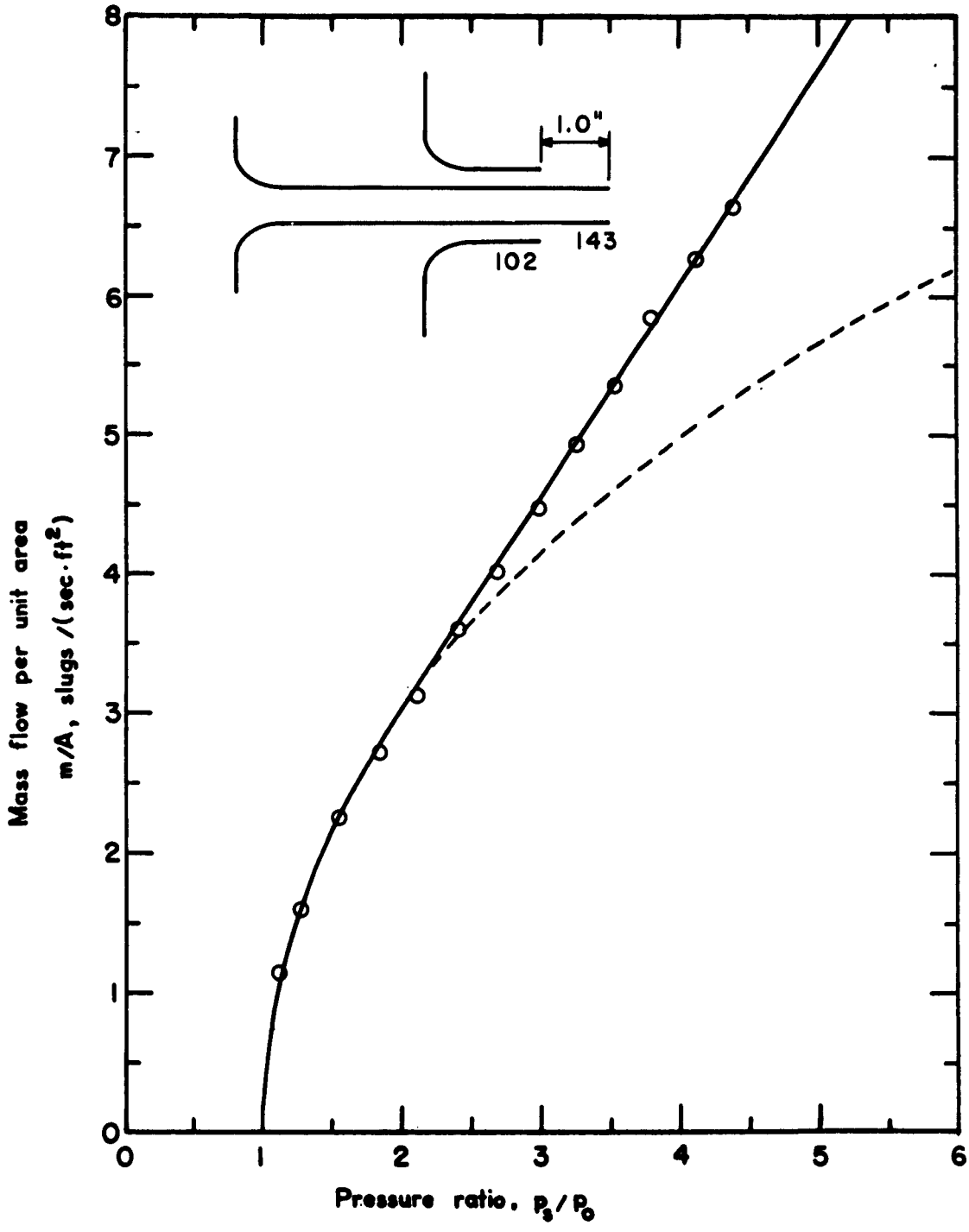

Figure 4. Flow Performance of Annular Nozzles with Center Core Flow

(h) Nozzle No. 293

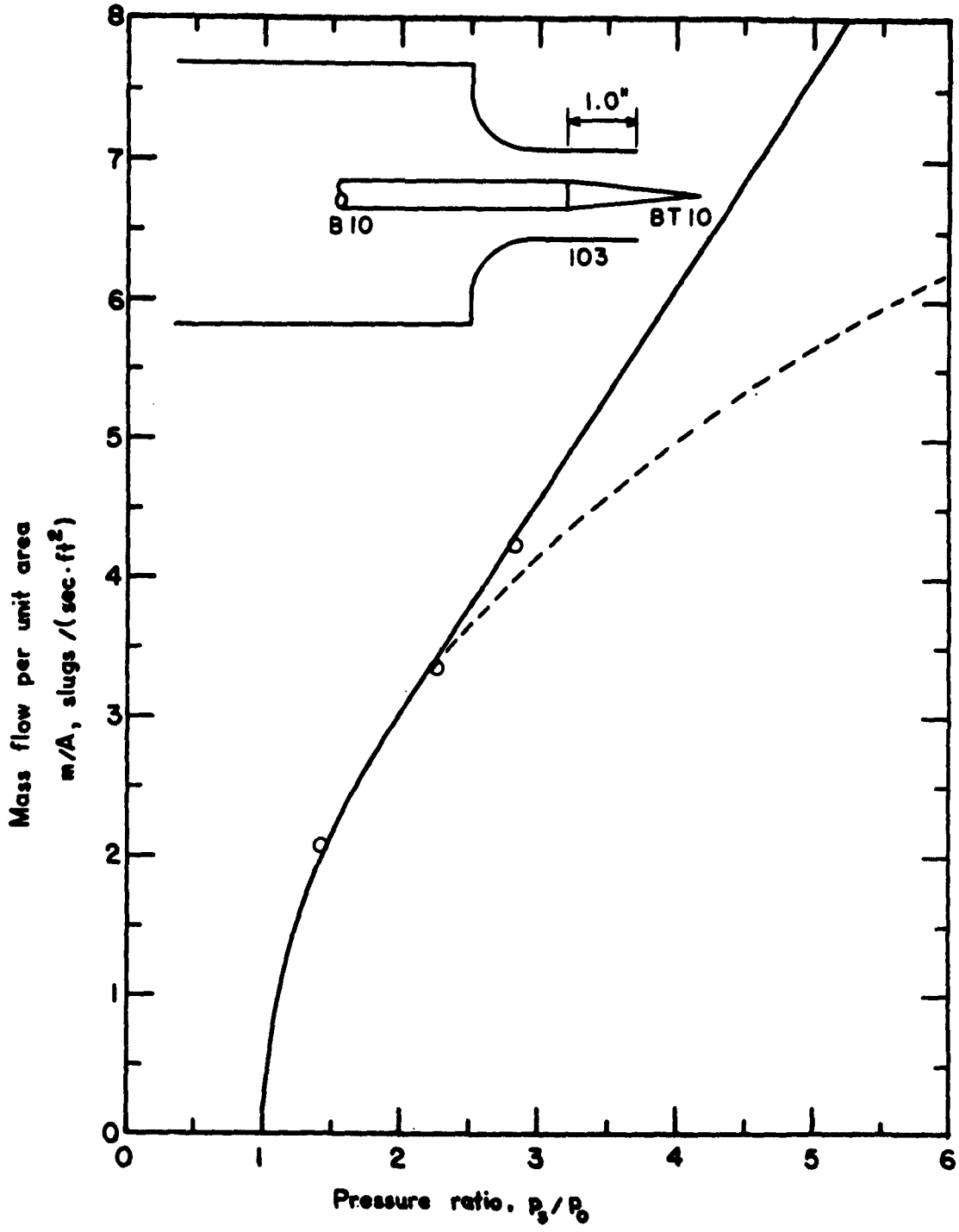

Figure 5: Flow Performance of Plug Nozzles
(a) Nozzle No. 301

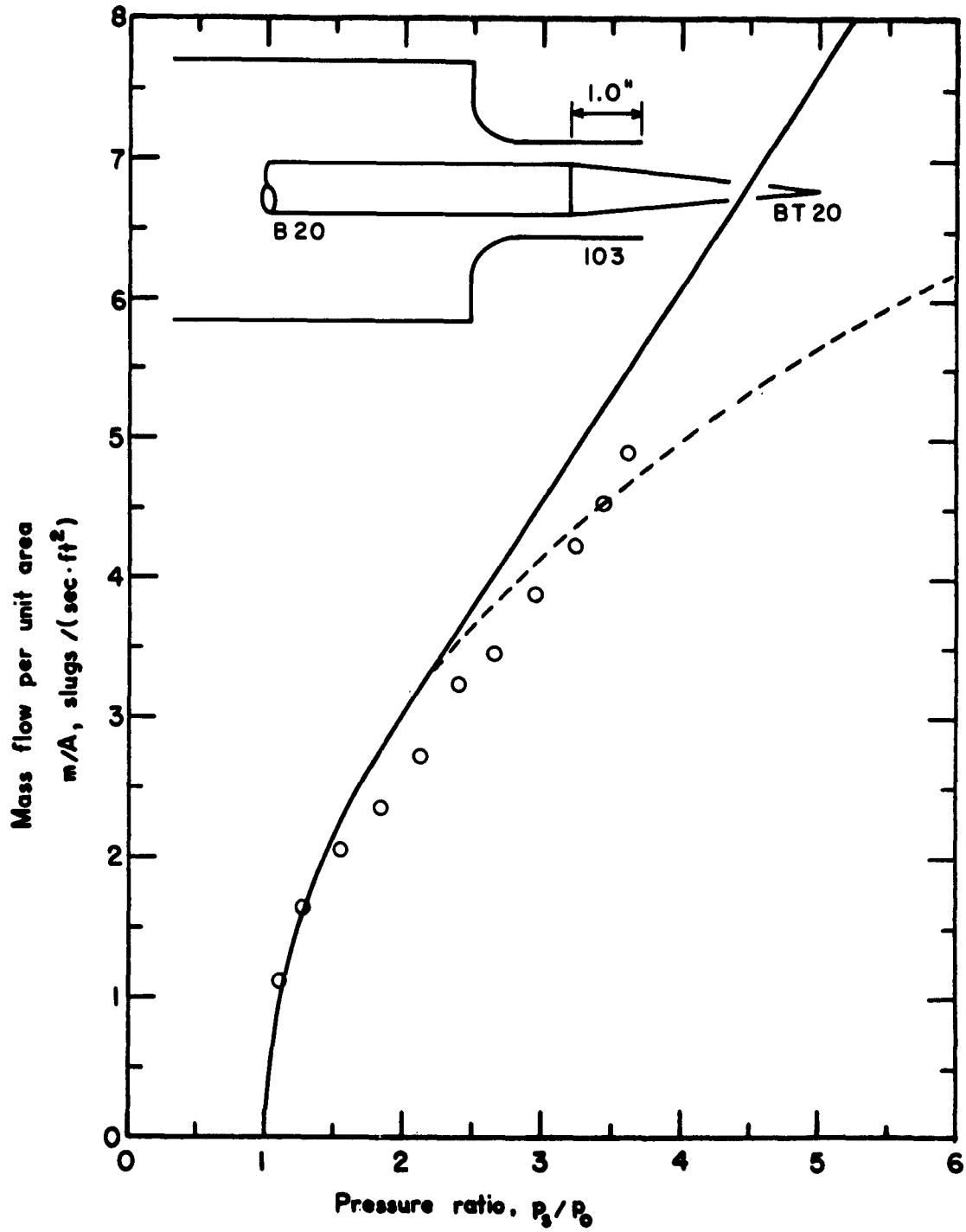

Figure 5. Flow Performance of Plug Nozzles
(b) Nozzle No. 305

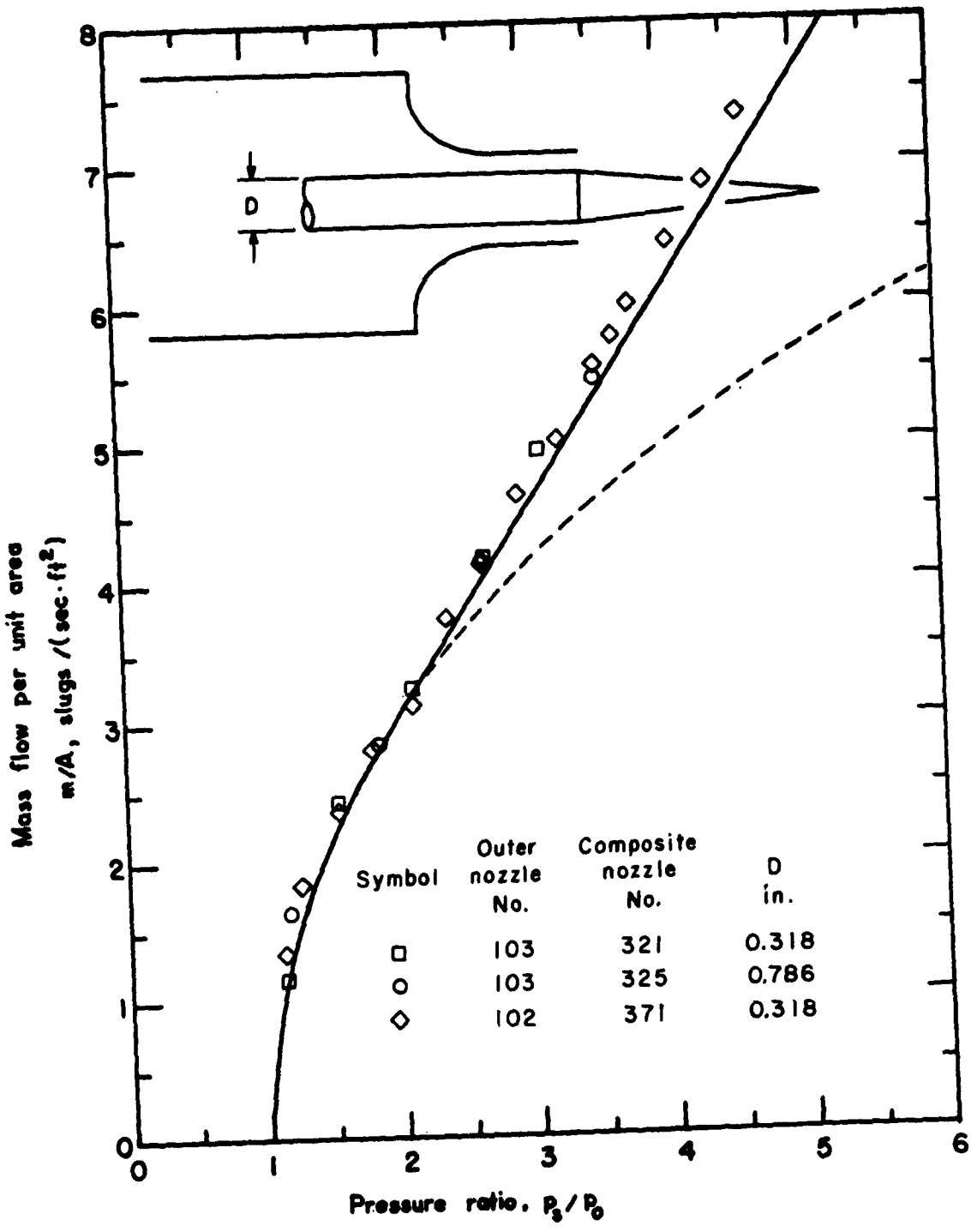

Figure 5. Flow Performance of Plug Nozzles
(c) Nozzles No. 325, 321, and 371

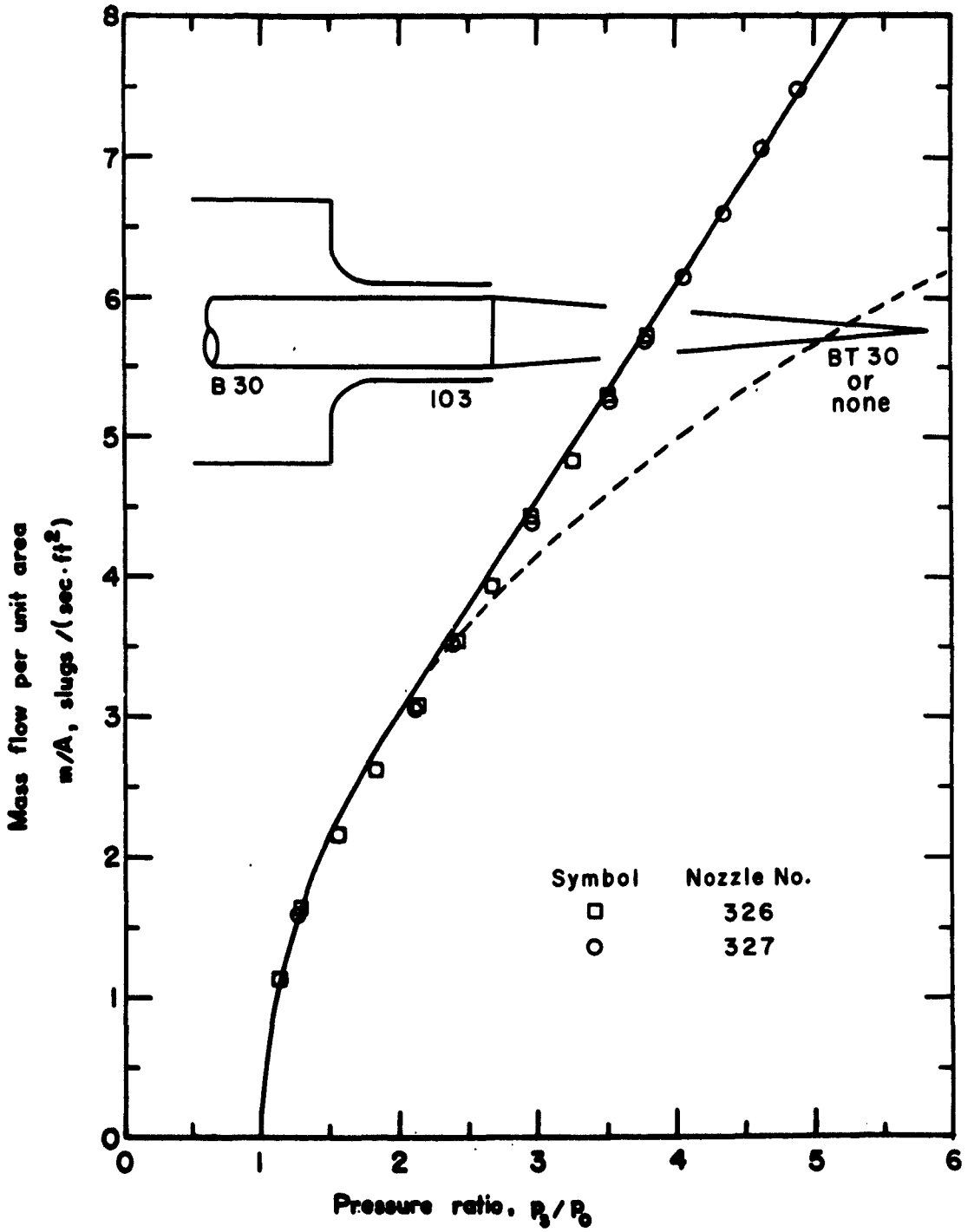

Figure 5. Flow Performance of Plug Nozzles
(d) Nozzles No. 326 and 327

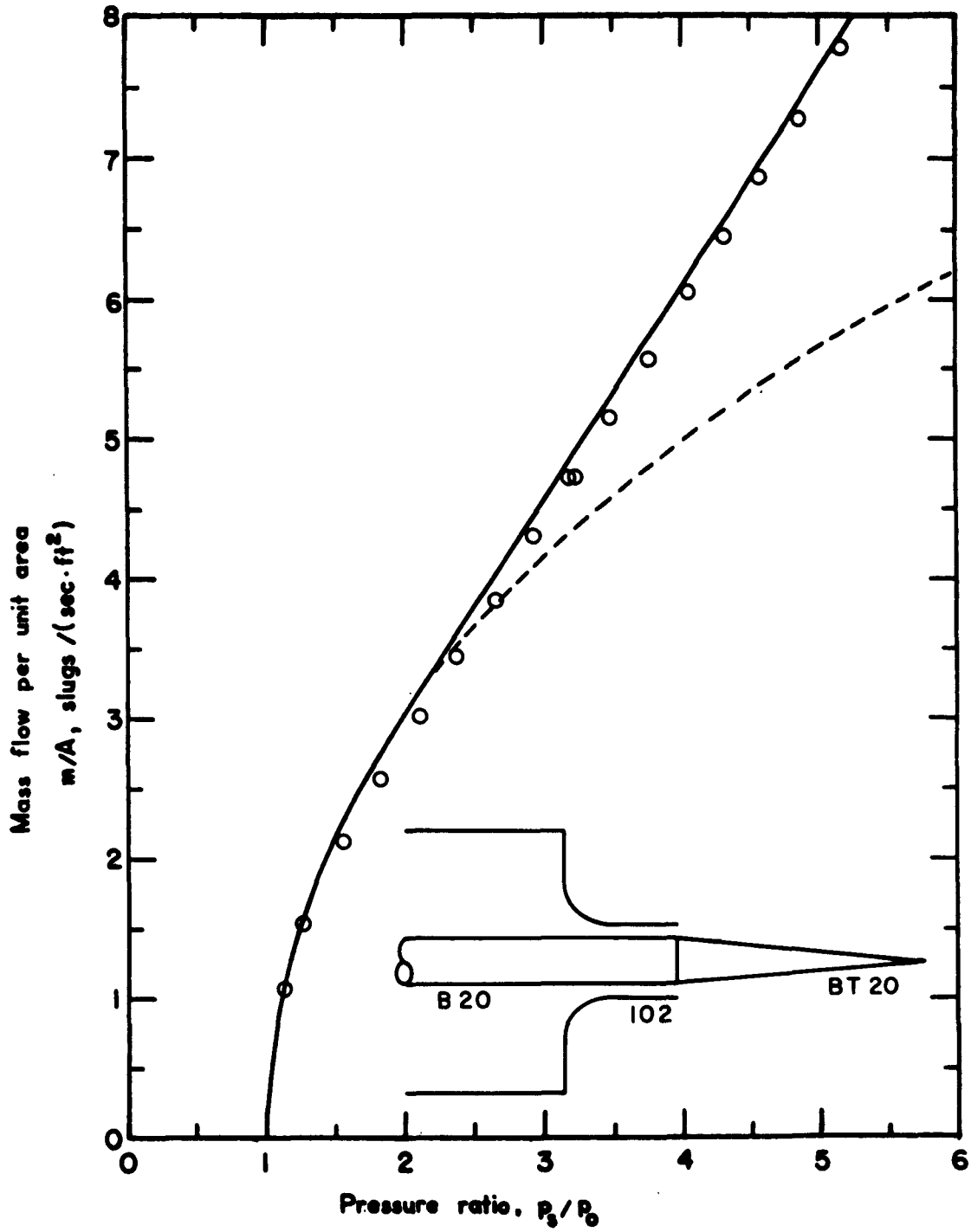

Figure 5. Flow Performance of Plug Nozzles
(e) Nozzle No. 375

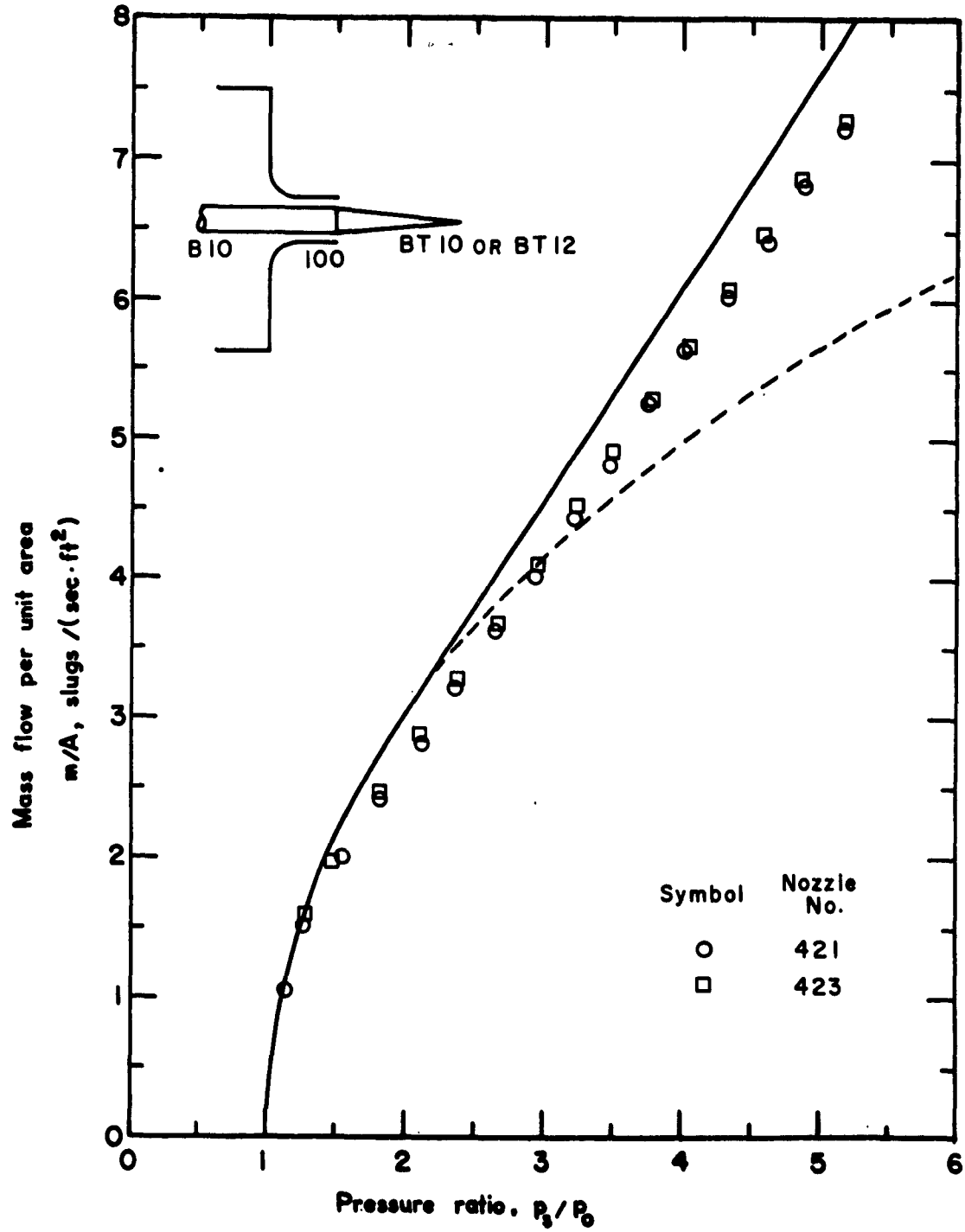

Figure 5. Flow Performance of Plug Nozzles
(f) Nozzles No. 421 and 423

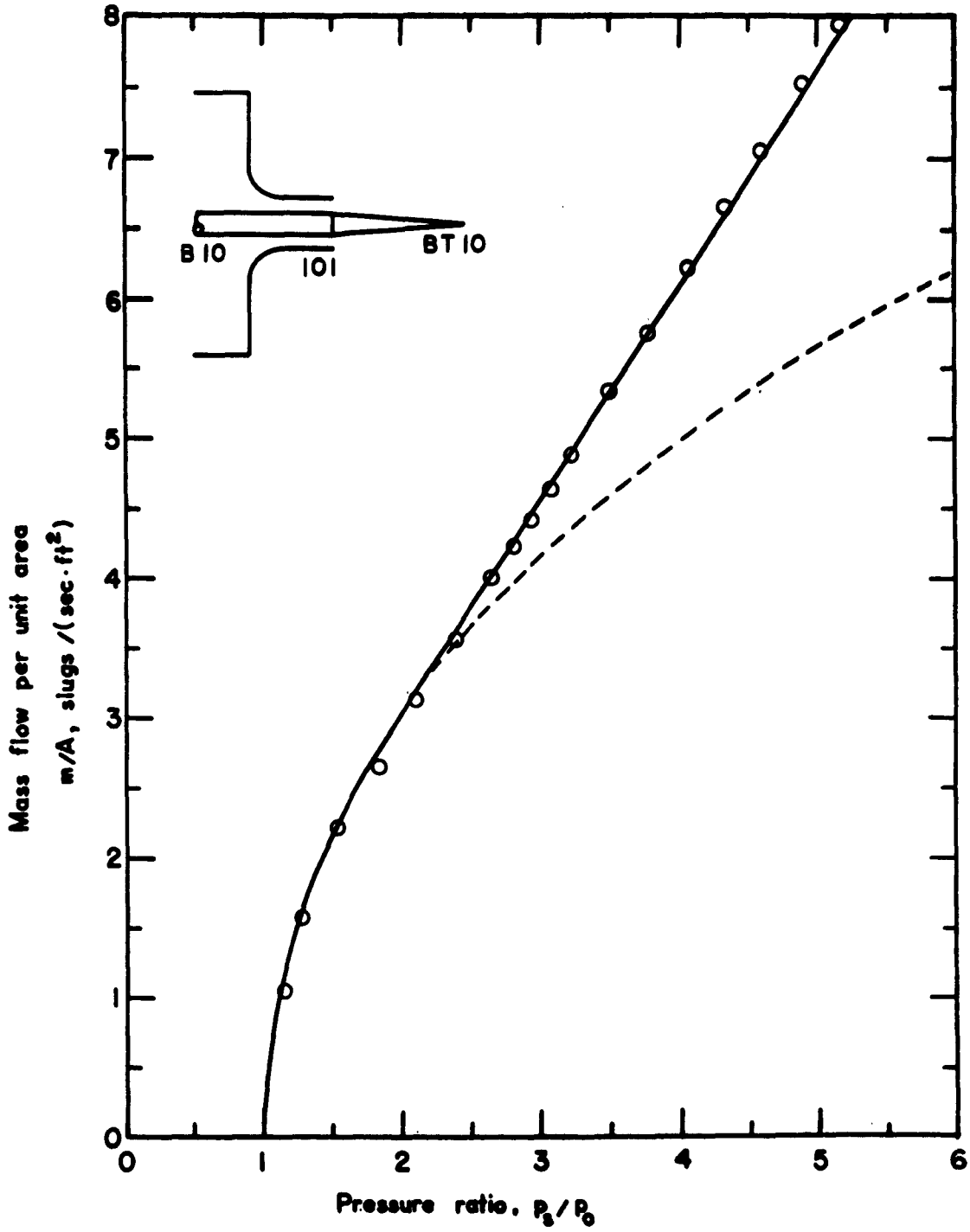

Figure 5. Flow Performance of Plug Nozzles
(g) Nozzle No. 471

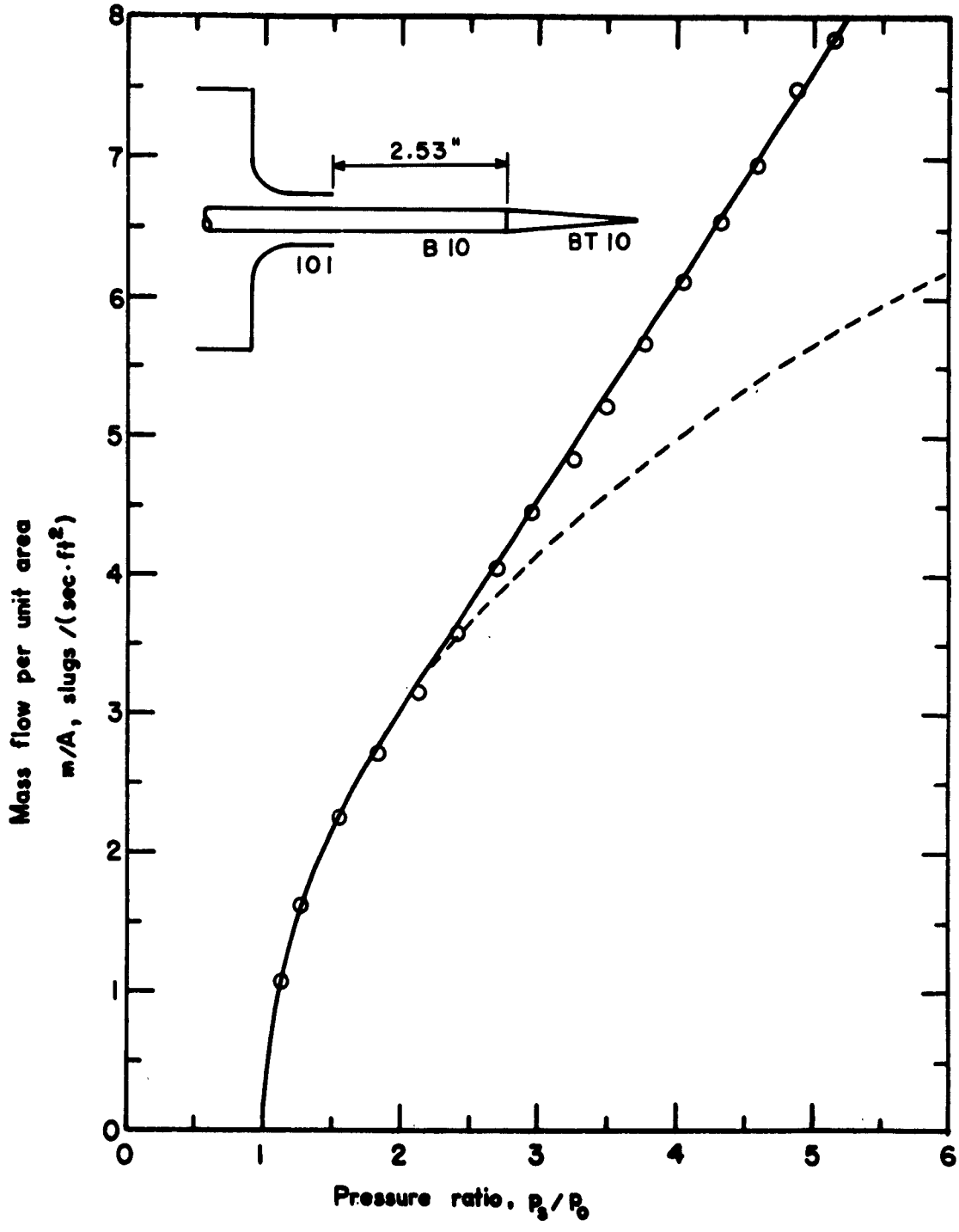

Figure 5. Flow Performance of Plug Nozzles
(h) Nozzle No. 491

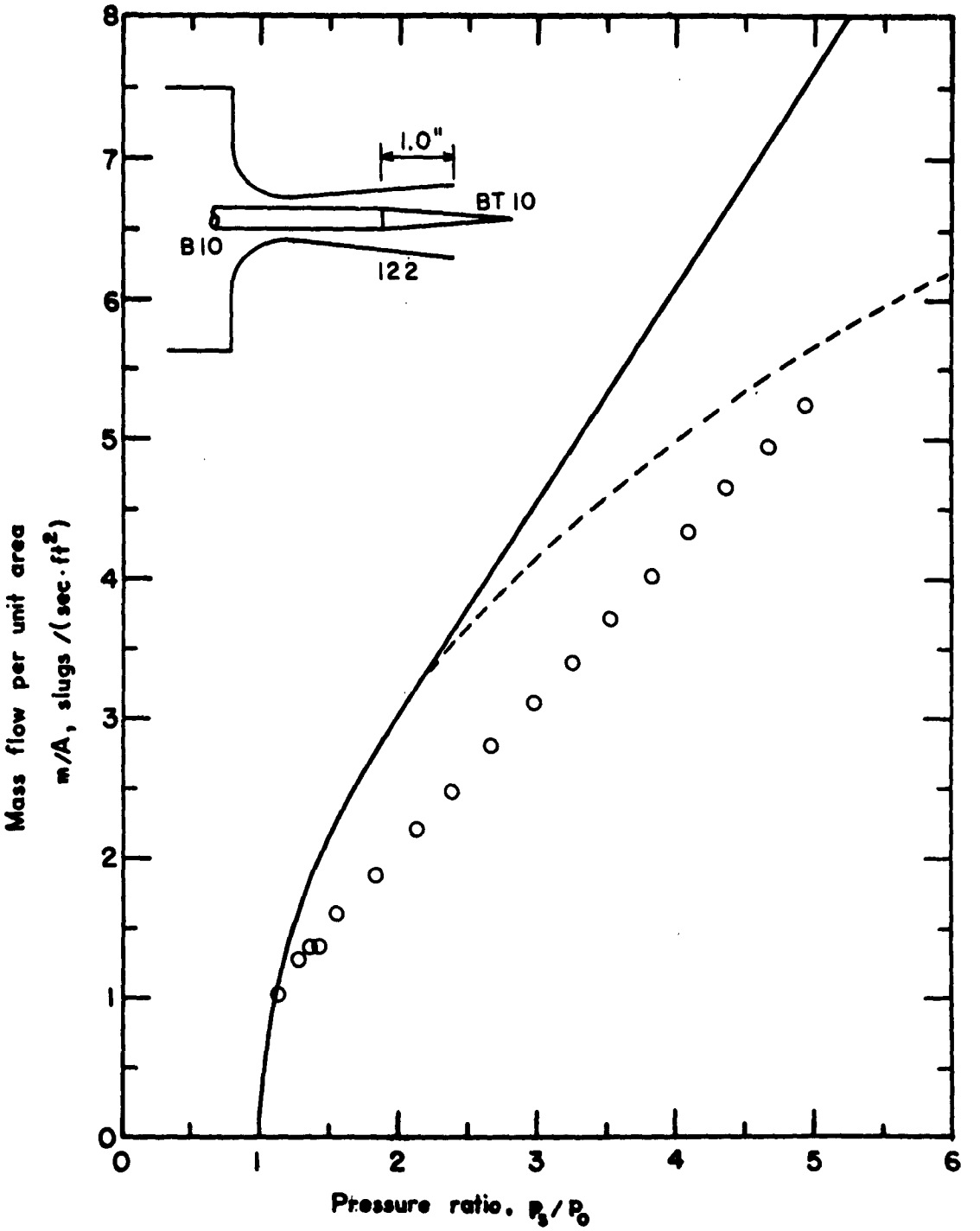

Figure 5. Flow Performance of Plug Nozzles

(i) Nozzle No. 601

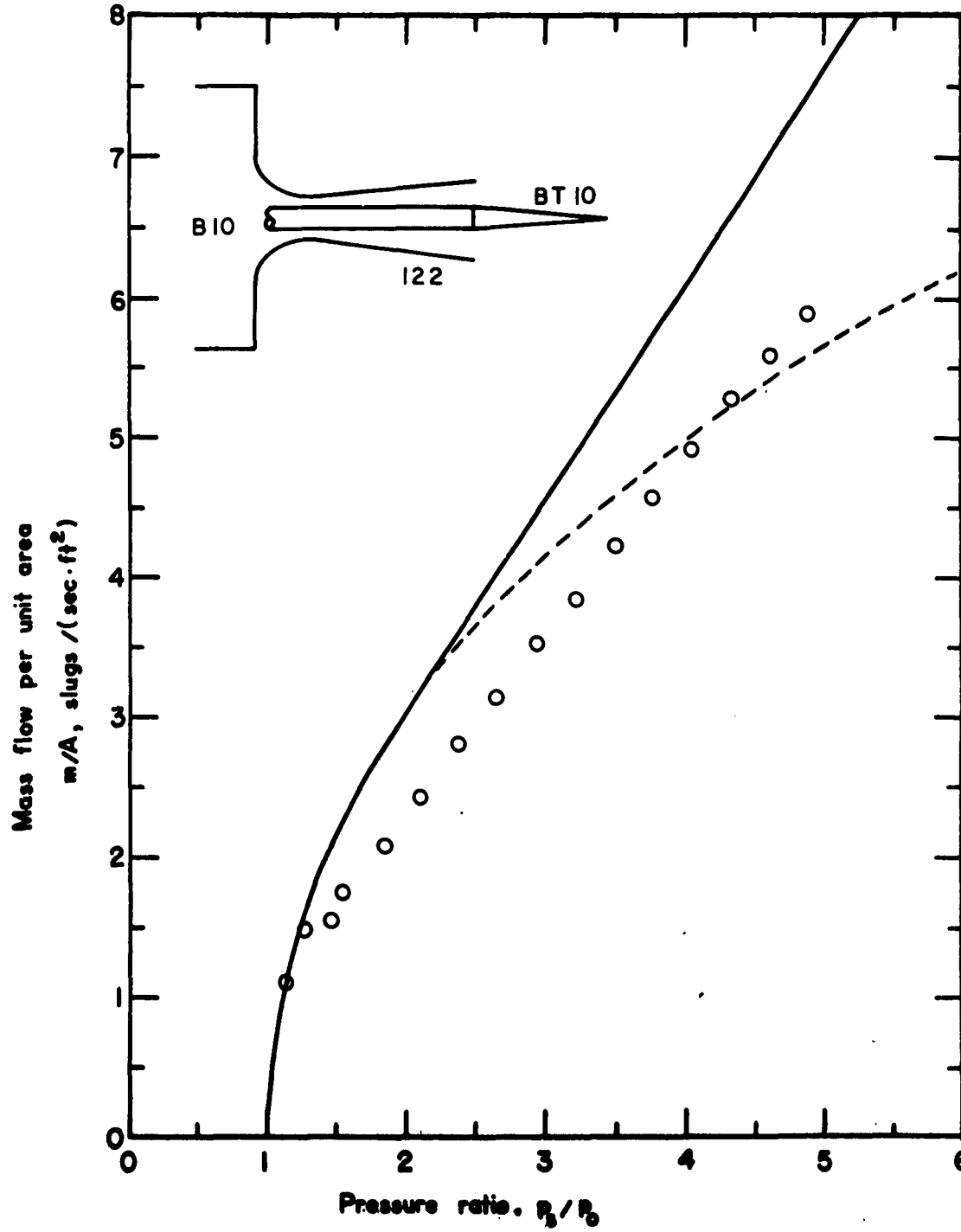

Figure 5. Flow Performance of Plug Nozzles
(j) Nozzle No. 621

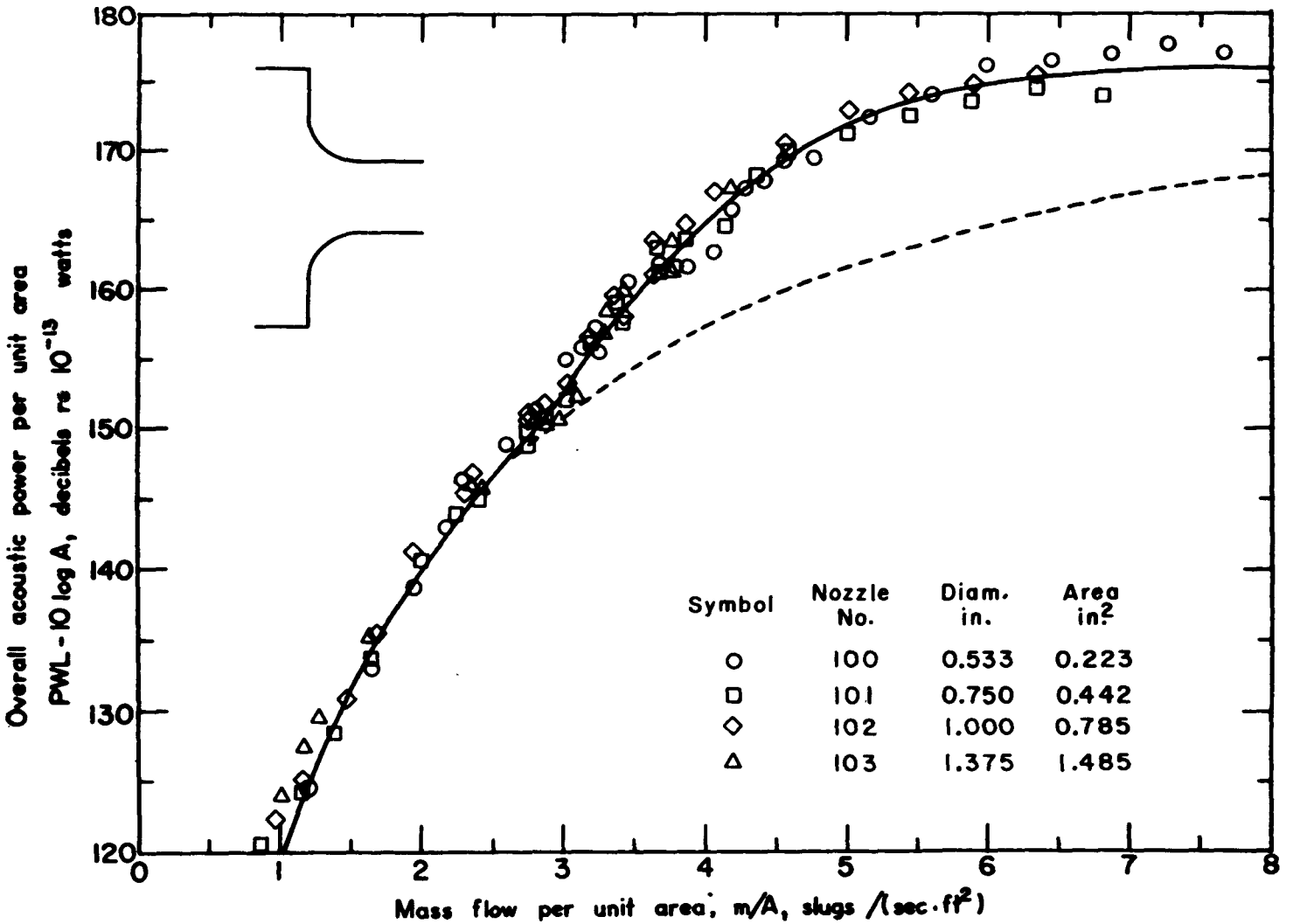

Figure 6. Acoustic Performance of Basic Nozzles
(a) Nozzles No. 100, 101, 102, and 103

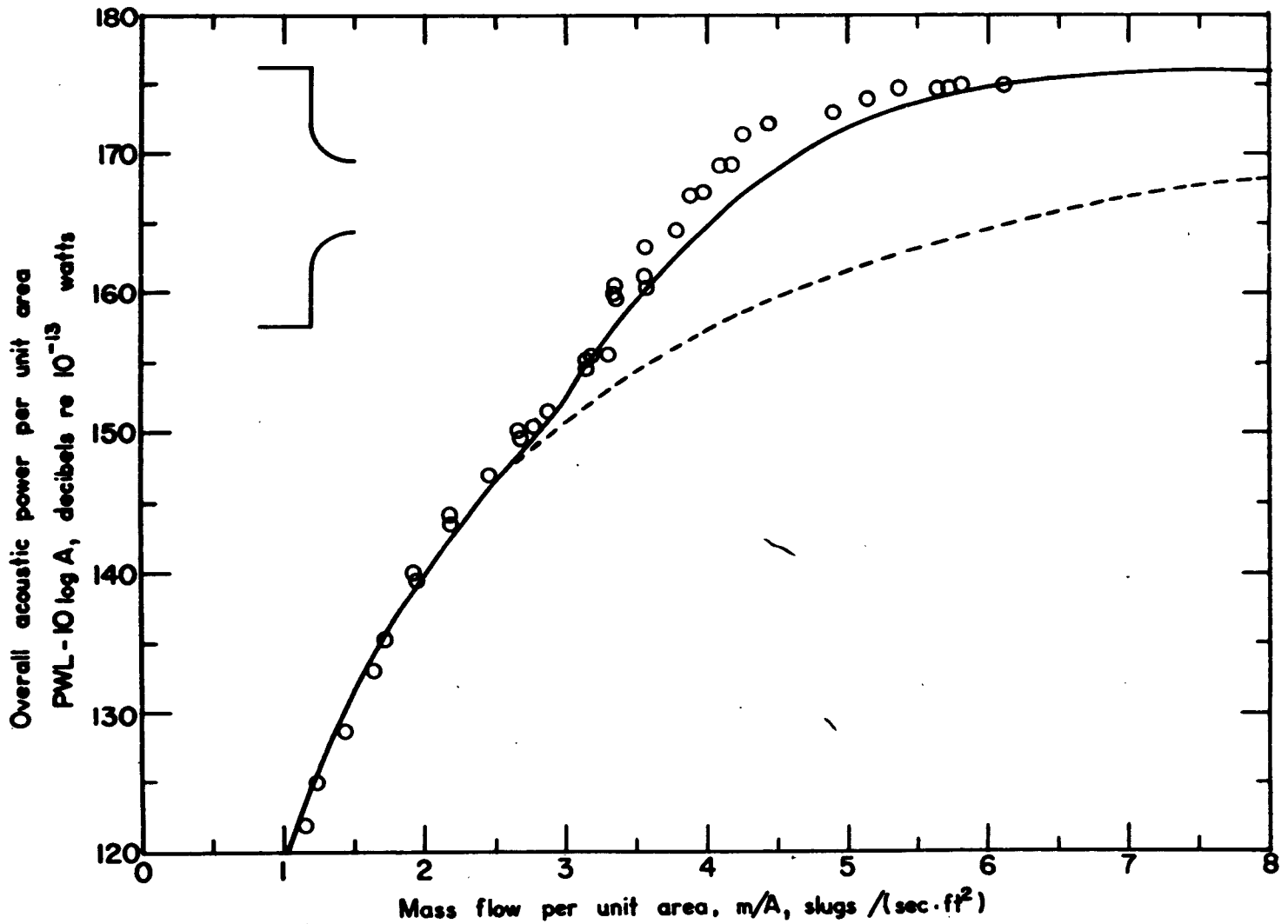

Figure 6. Acoustic Performance of Basic Nozzles

(b) Nozzle No. 110

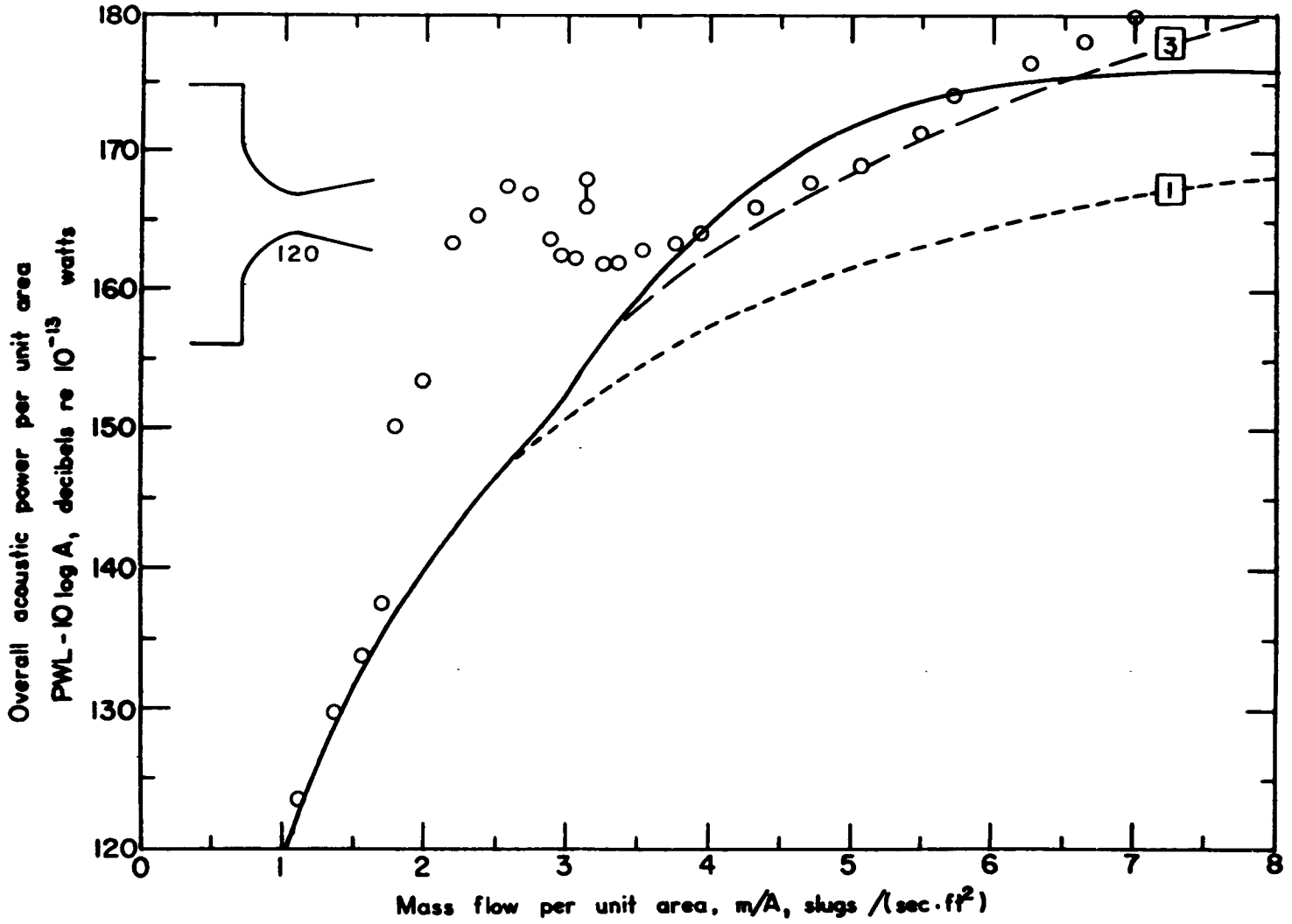

Figure 6. Acoustic Performance of Basic Nozzles
(c) Nozzle No. 120

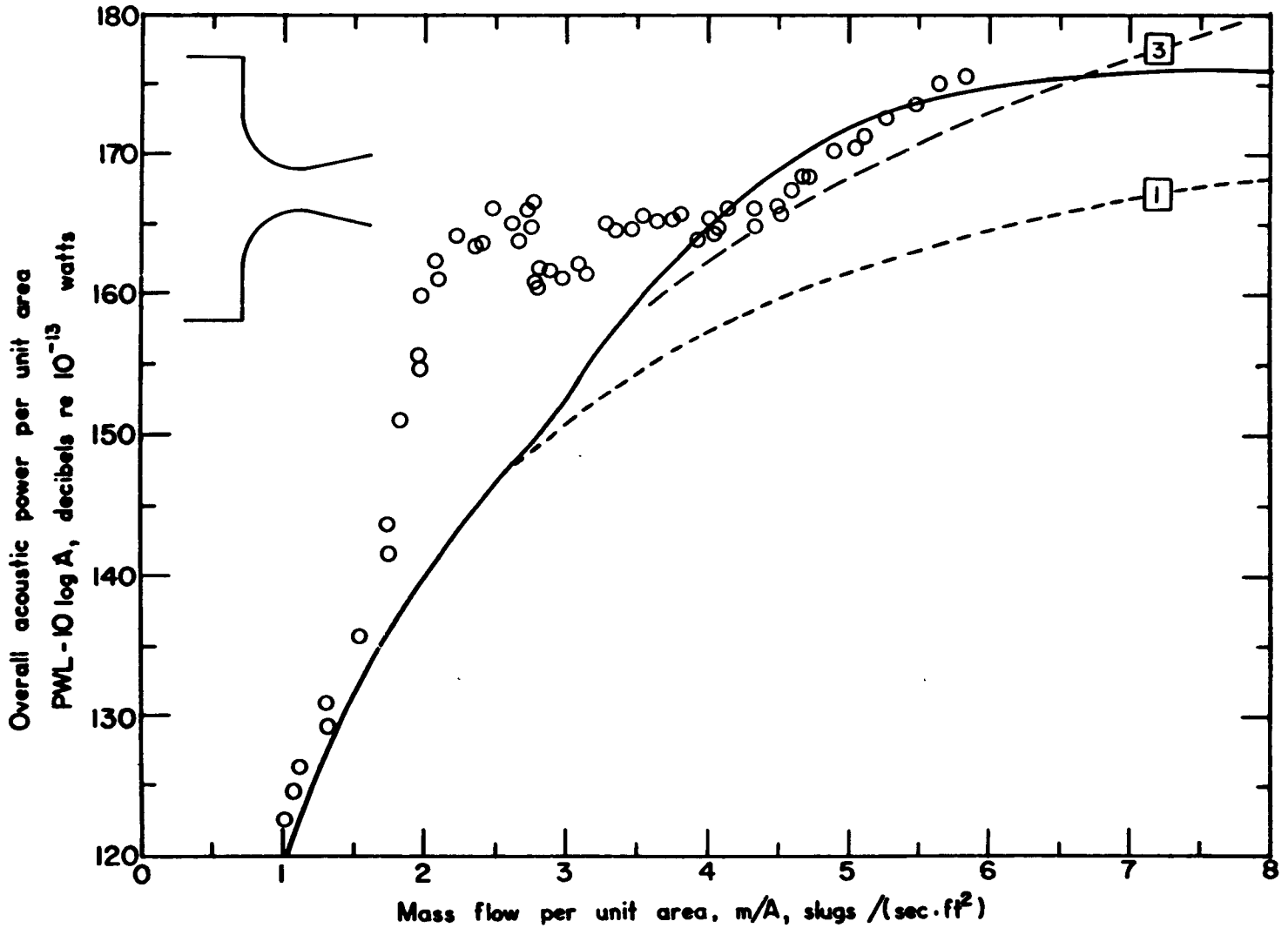

Figure 6. Acoustic Performance of Basic Nozzles

(d) Nozzle No. 121

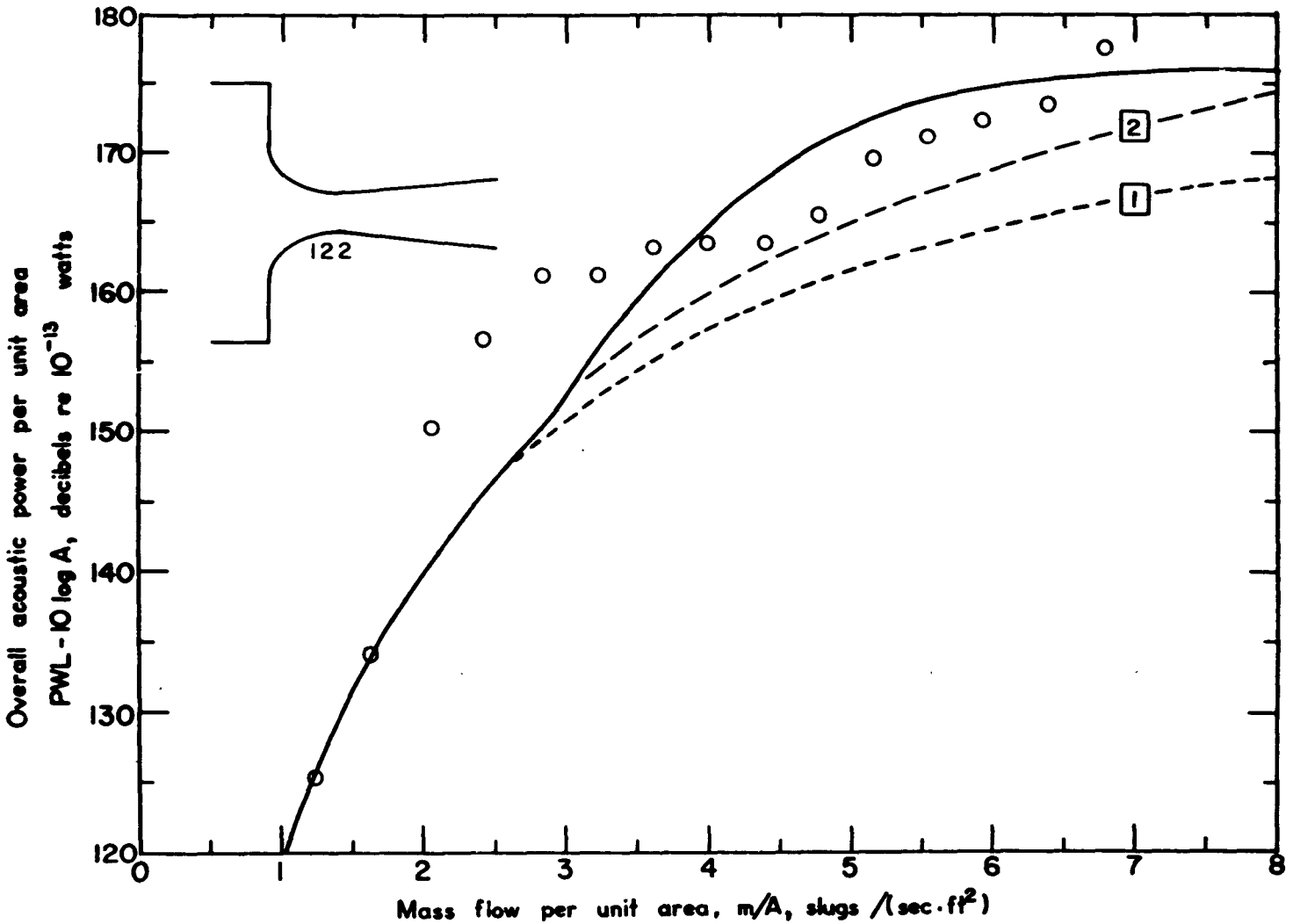

Figure 6. Acoustic Performance of Basic Nozzles

(e) Nozzle No. 122

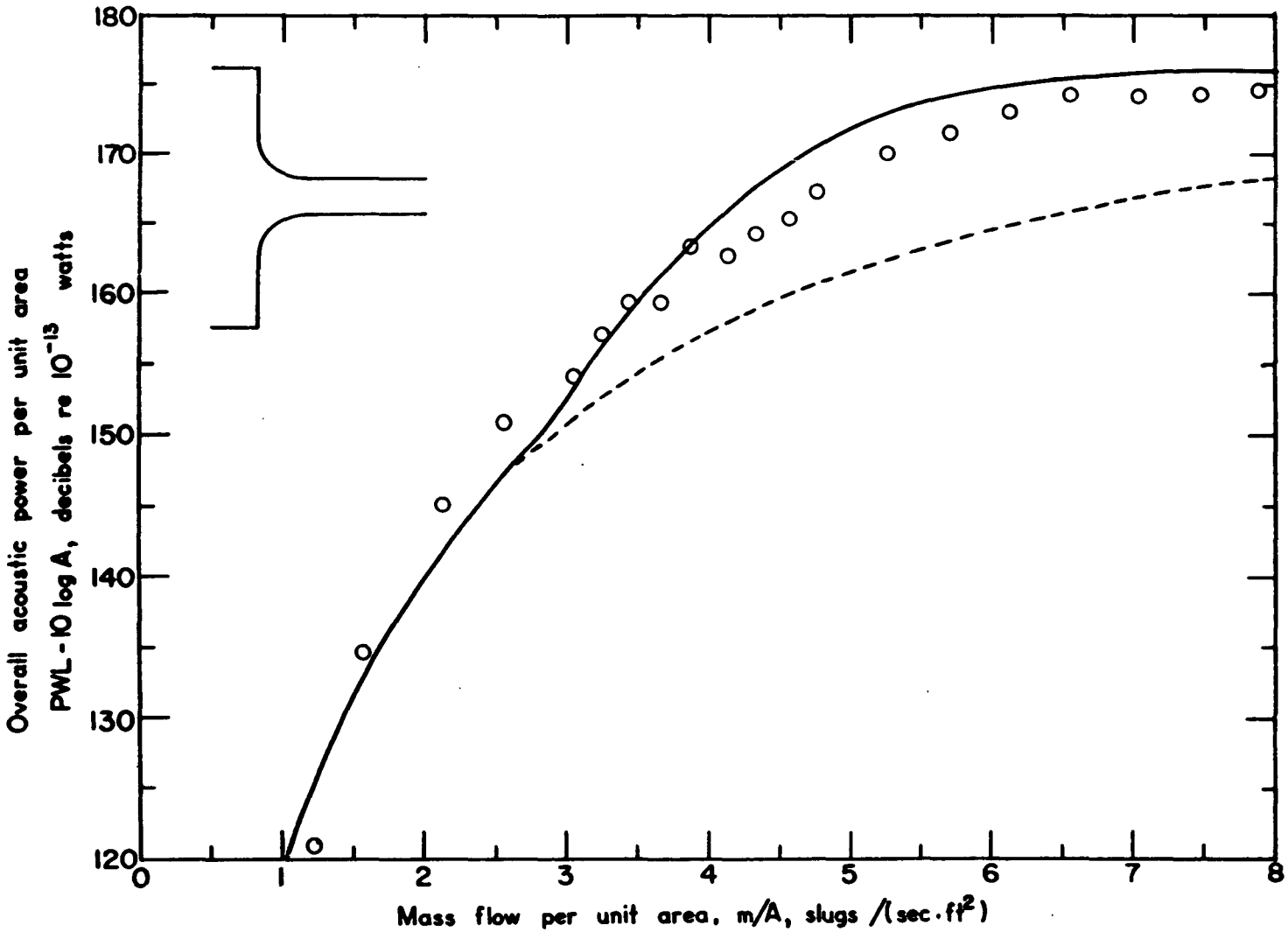

Figure 6. Acoustic Performance of Basic Nozzles

(f) Nozzle No. 140

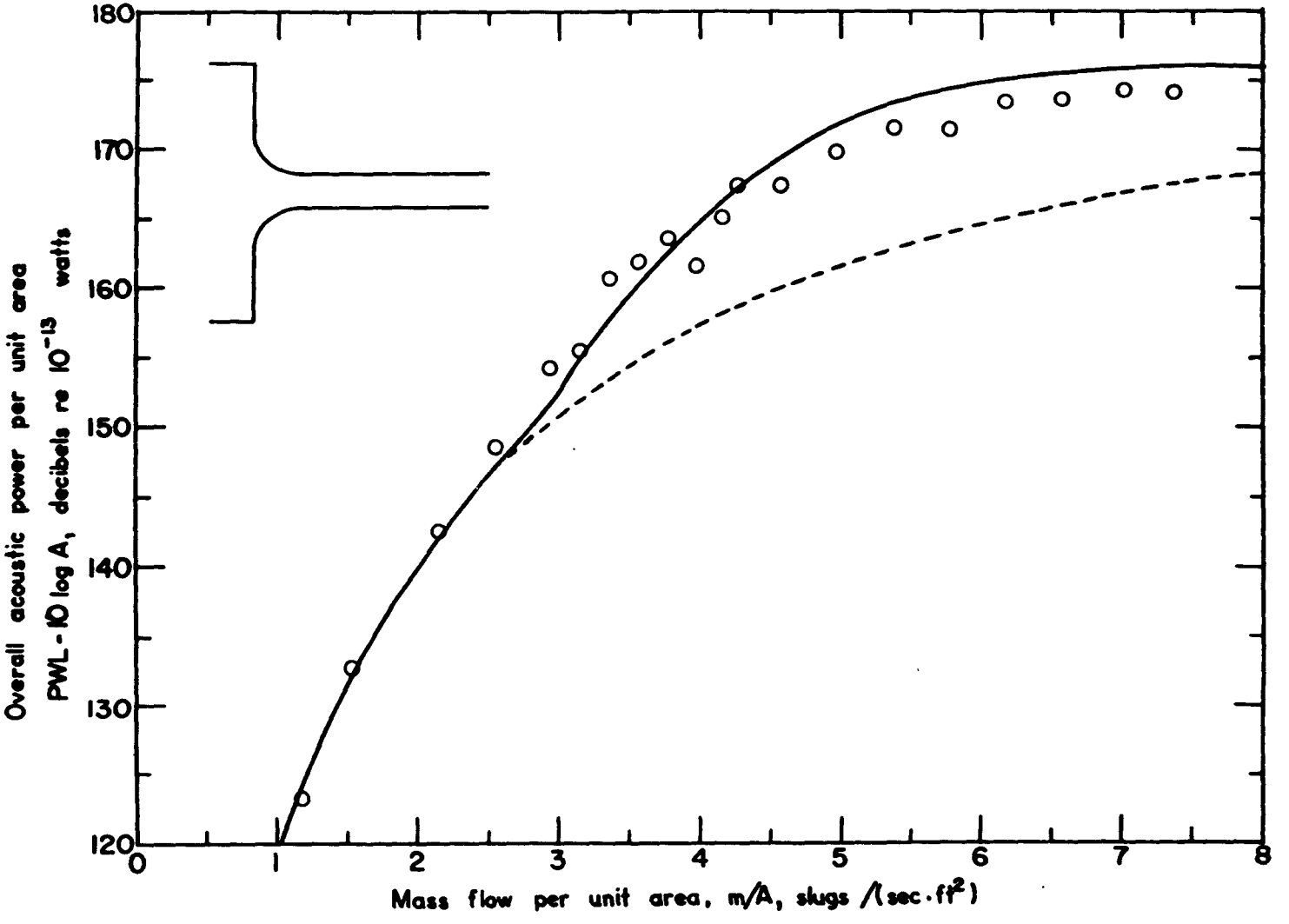

Figure 6. Acoustic Performance of Basic Nozzles

(g) Nozzle No. 141

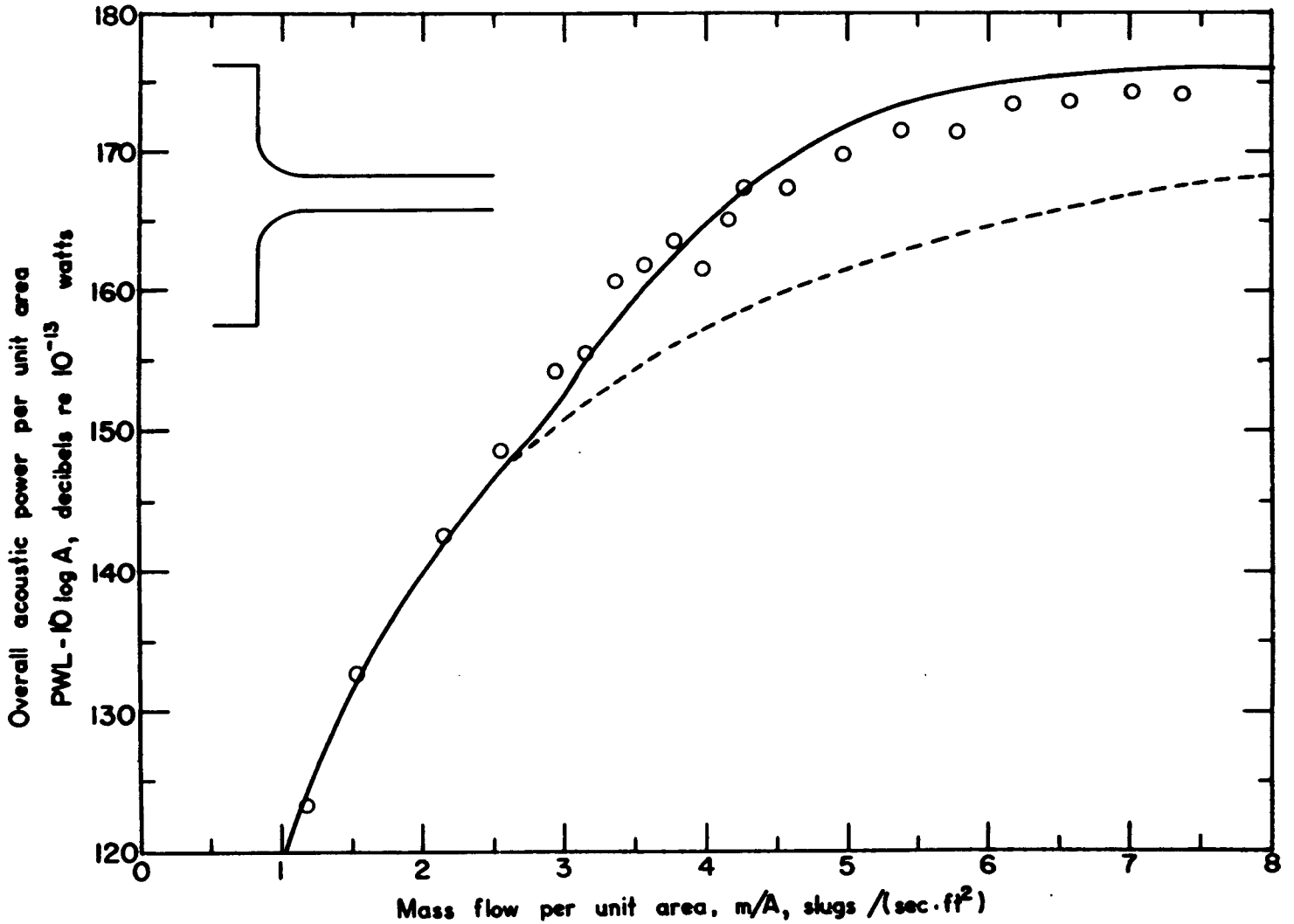

Figure 6. Acoustic Performance of Basic Nozzles

(g) Nozzle No. 141

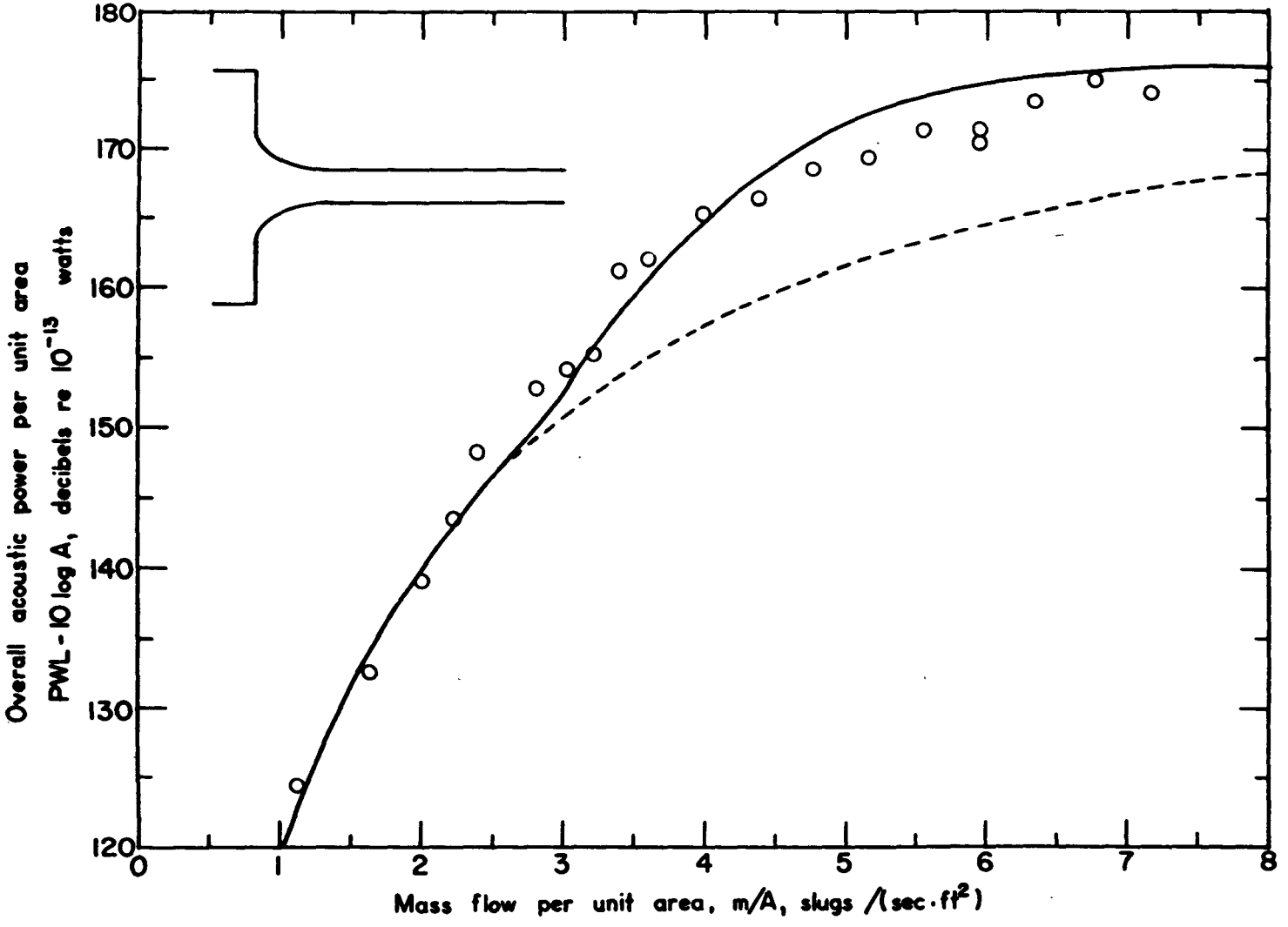

Figure 6. Acoustic Performance of Basic Nozzles

(h) Nozzle No. 142

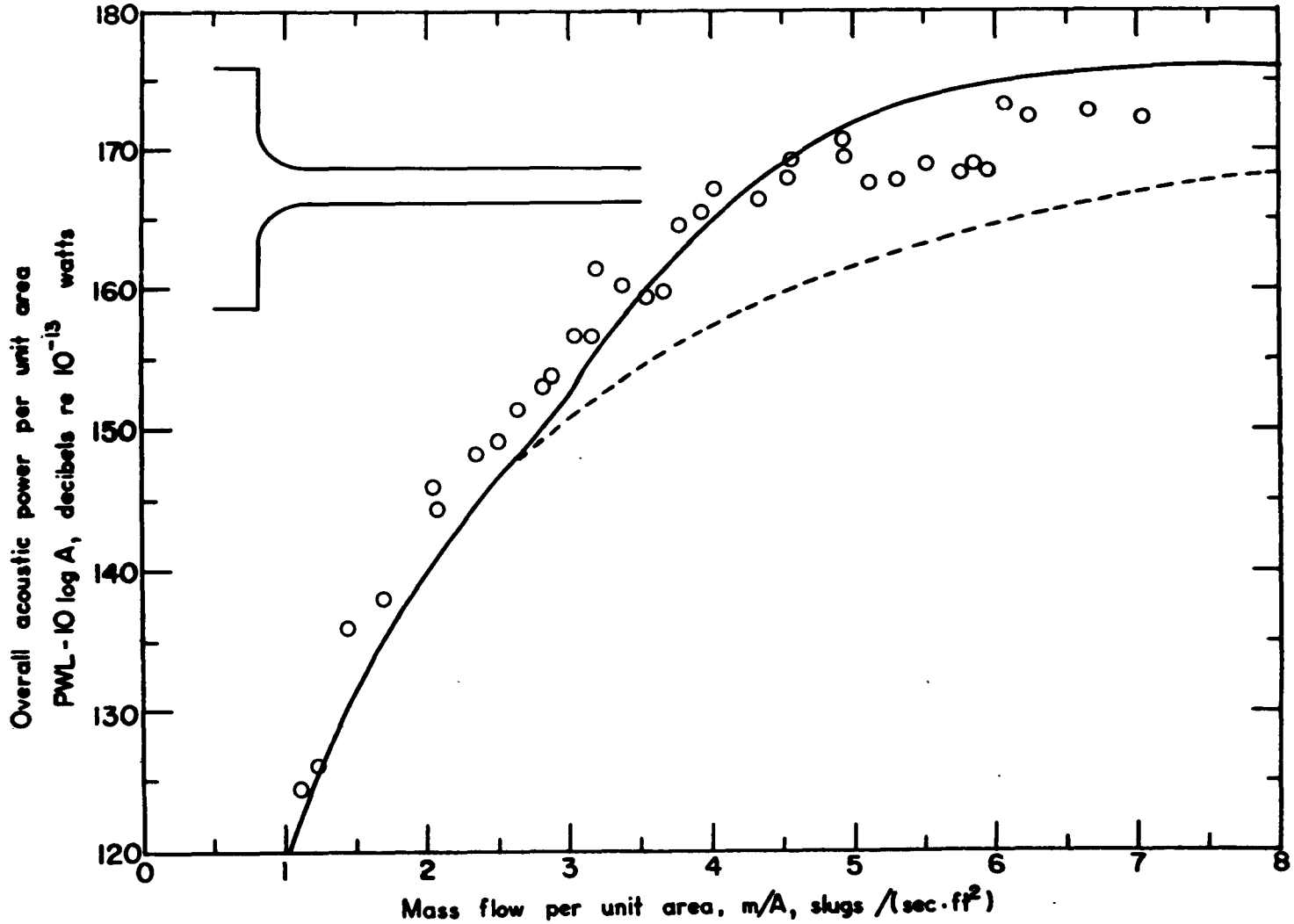

Figure 6. Acoustic Performance of Basic Nozzles

(i) Nozzle No. 143

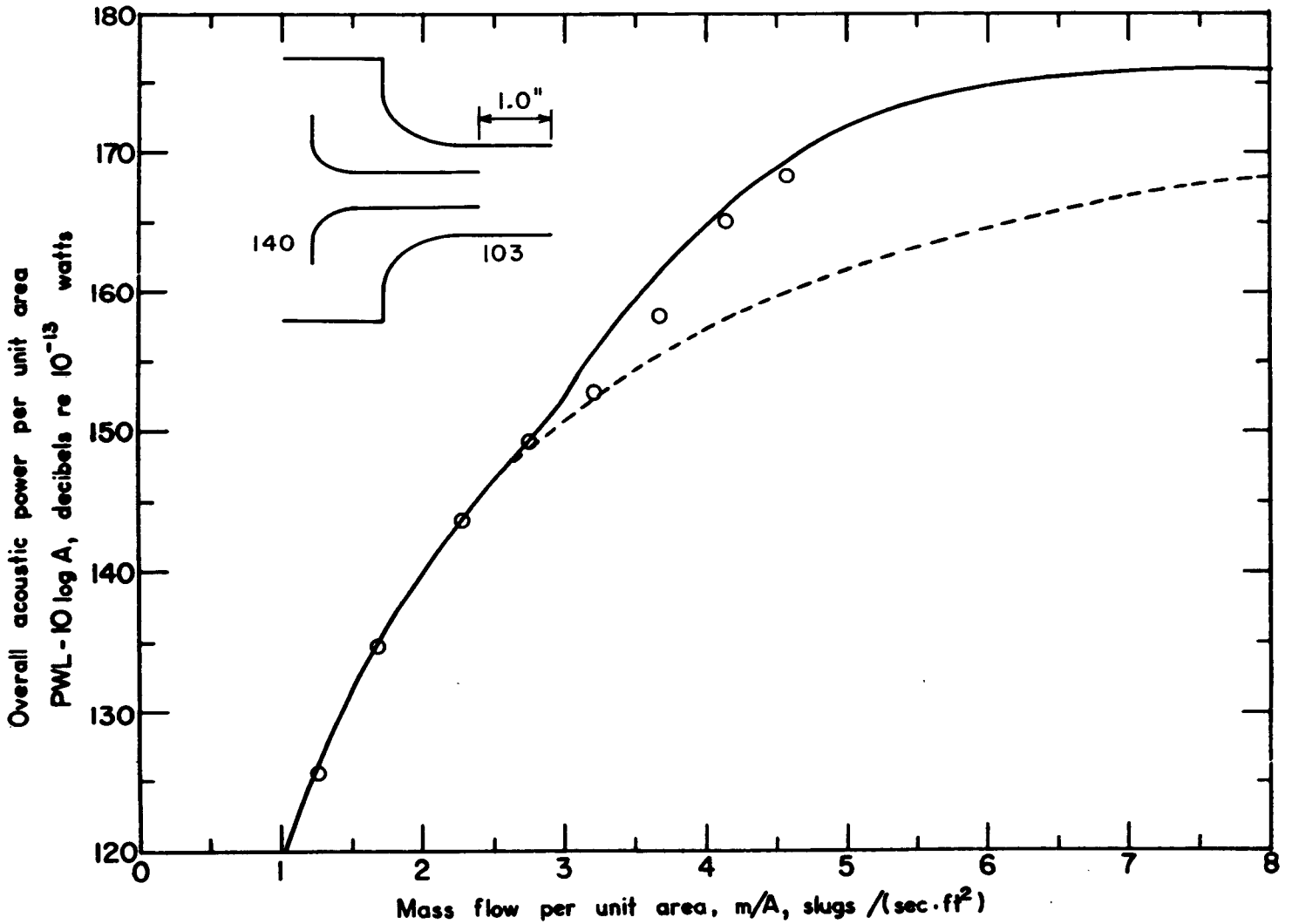

Figure 7. Acoustic Performance of Annular Nozzles with Center Core Flow

(a) Nozzle No. 200

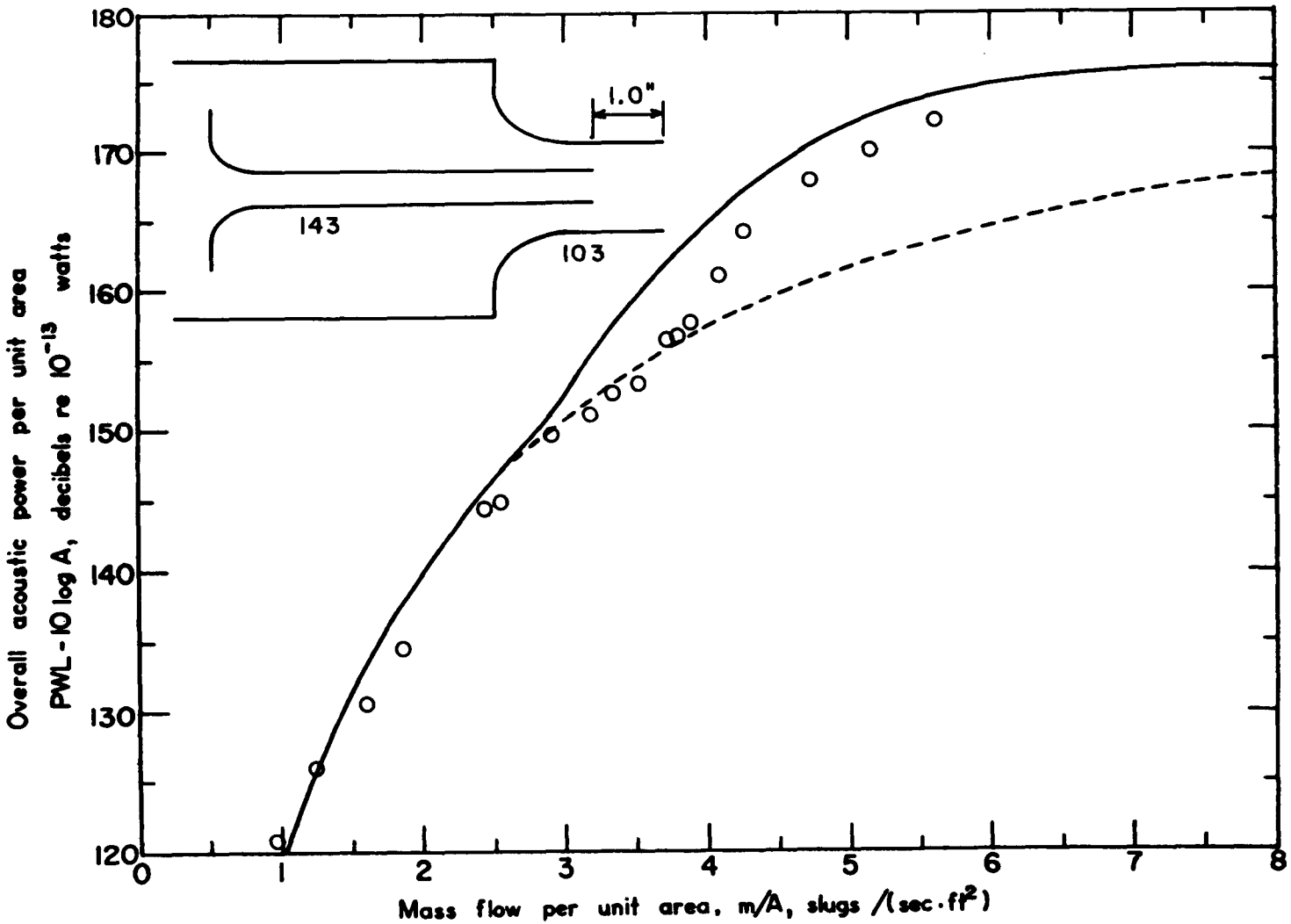

Figure 7. Acoustic Performance of Annular Nozzles with Center Core Flow

(b) Nozzle No. 203

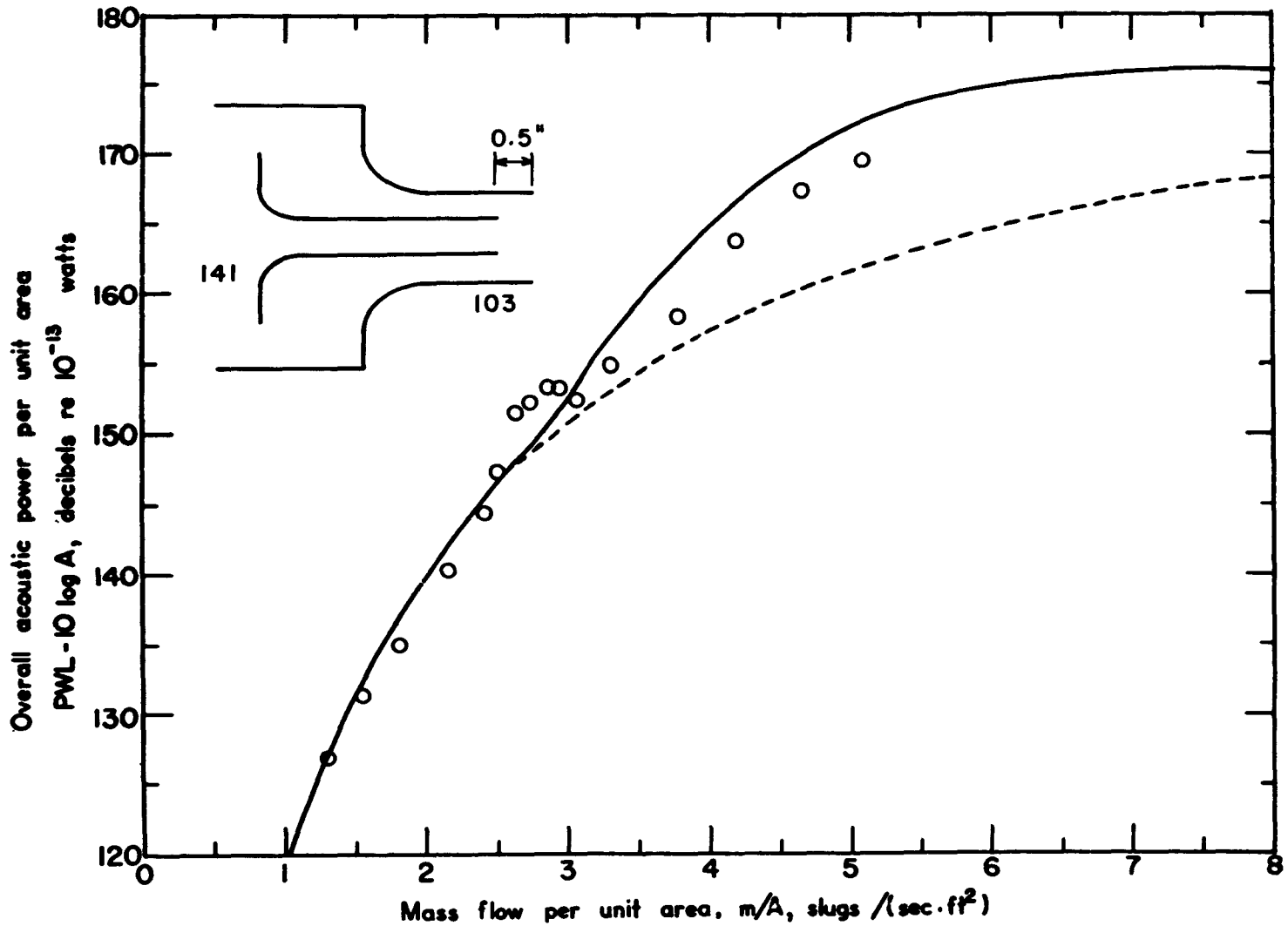

Figure 7. Acoustic Performance of Annular Nozzles with Center Core Flow

(c) Nozzle No. 210

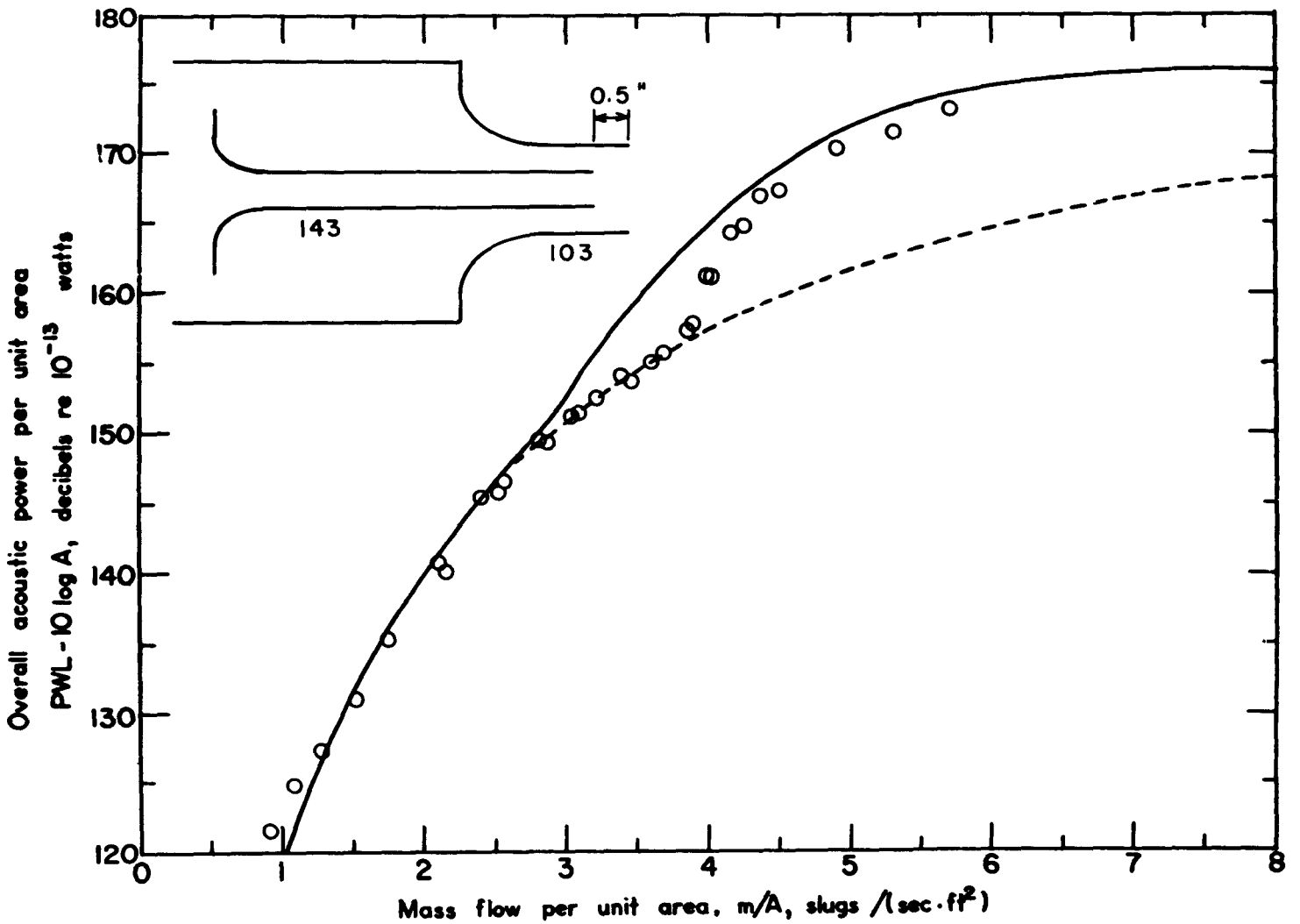

Figure 7. Acoustic Performance of Annular Nozzle with Center Core Flow

(d) Nozzle No. 212

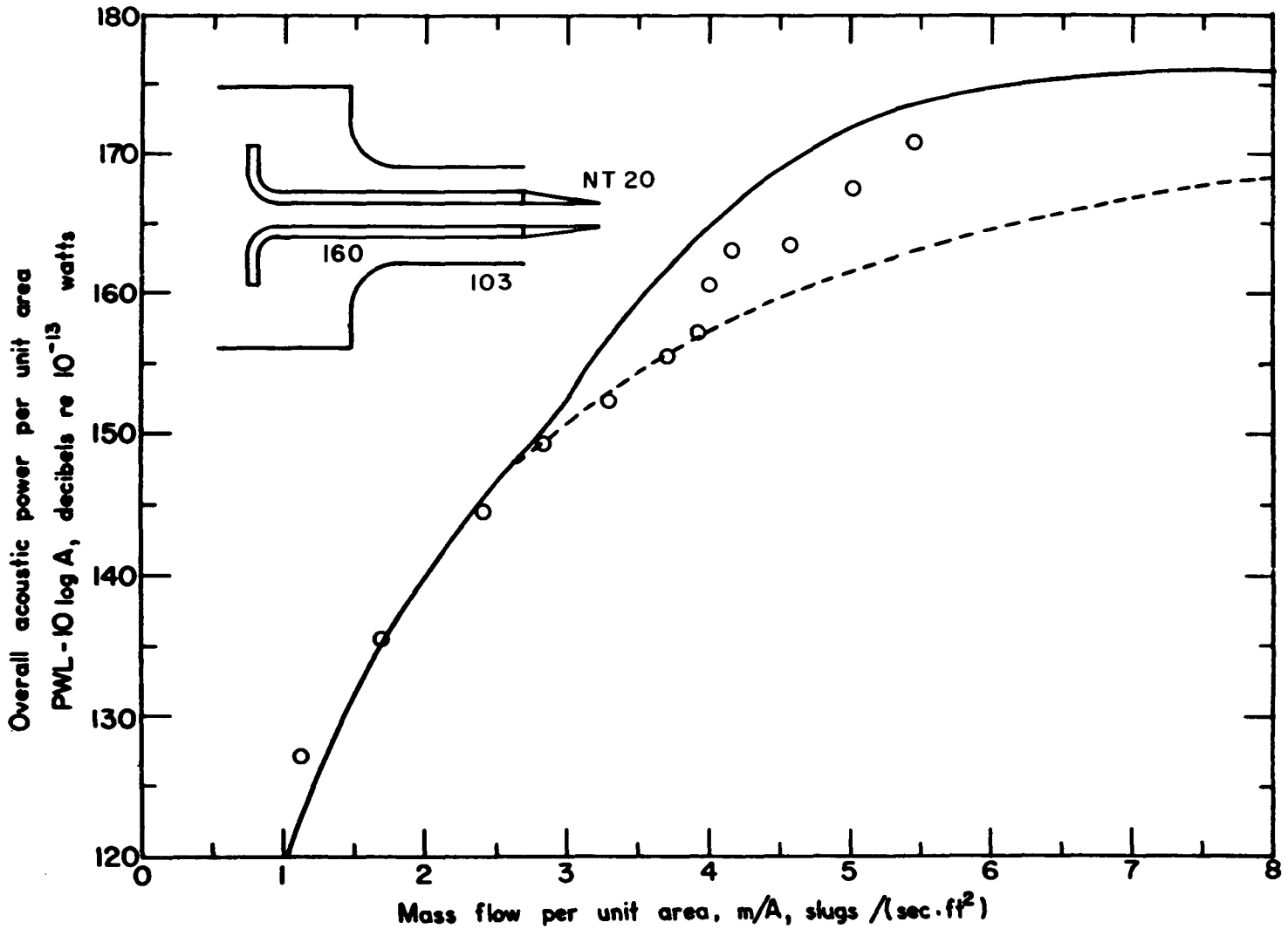

Figure 7. Acoustic Performance of Annular Nozzles with Center Core Flow

(e) Nozzle No. 223

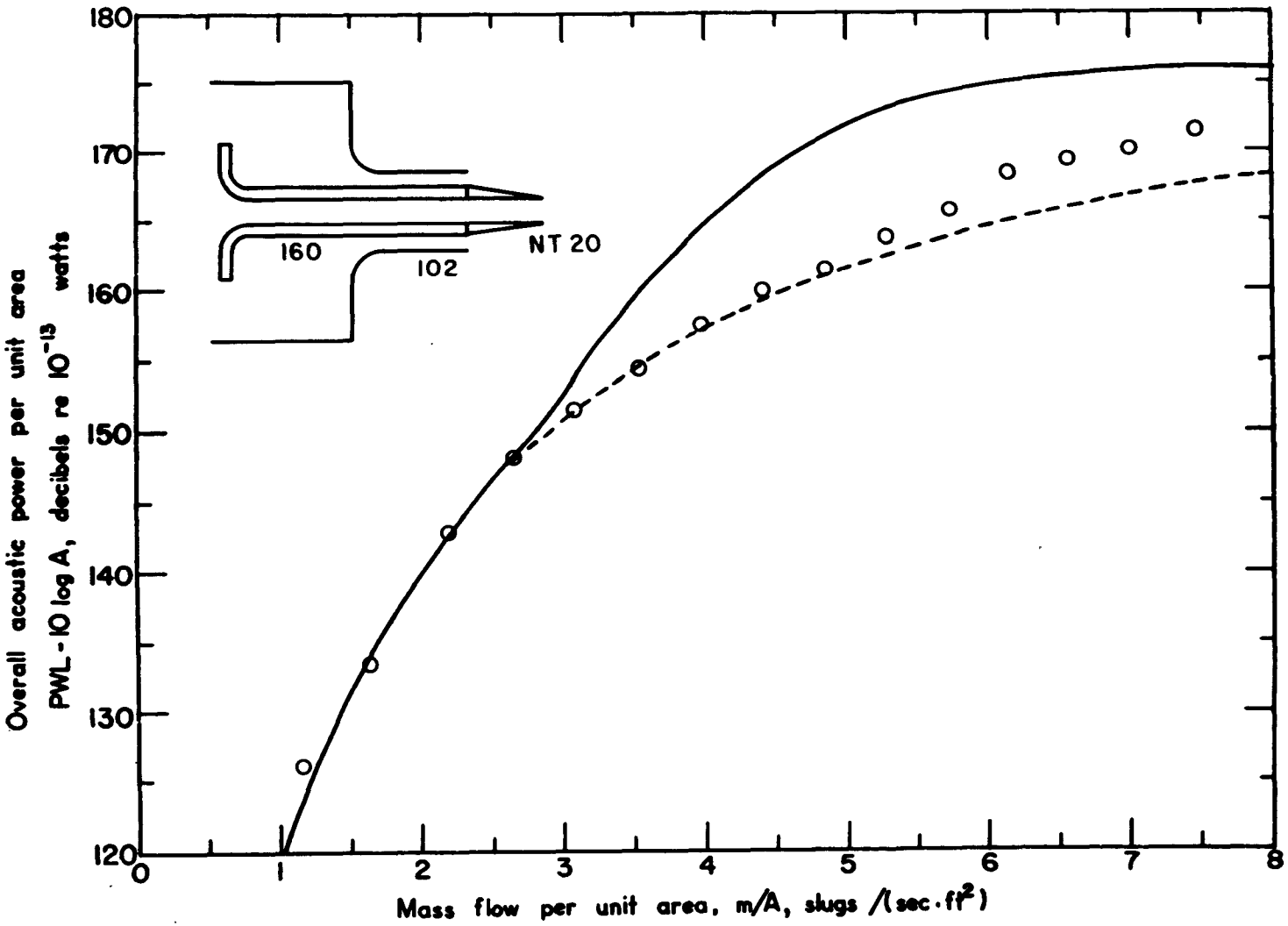

Figure 7. Acoustic Performance of Annular Nozzles with Center Core Flow

(f) Nozzle No. 274.

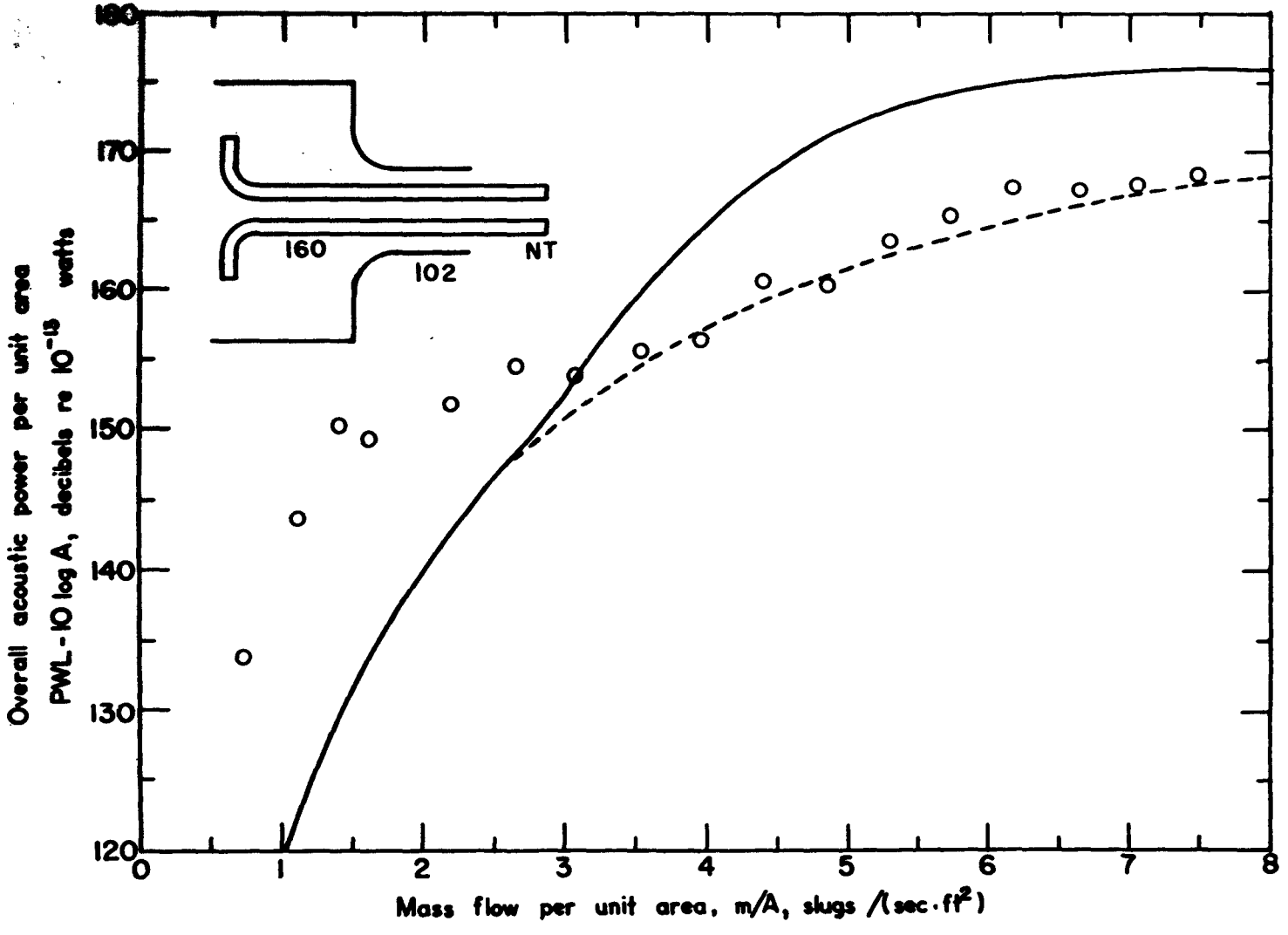

Figure 7. Acoustic Performance of Annular Nozzles with Center Core Flow

(g) Nozzle No. 275

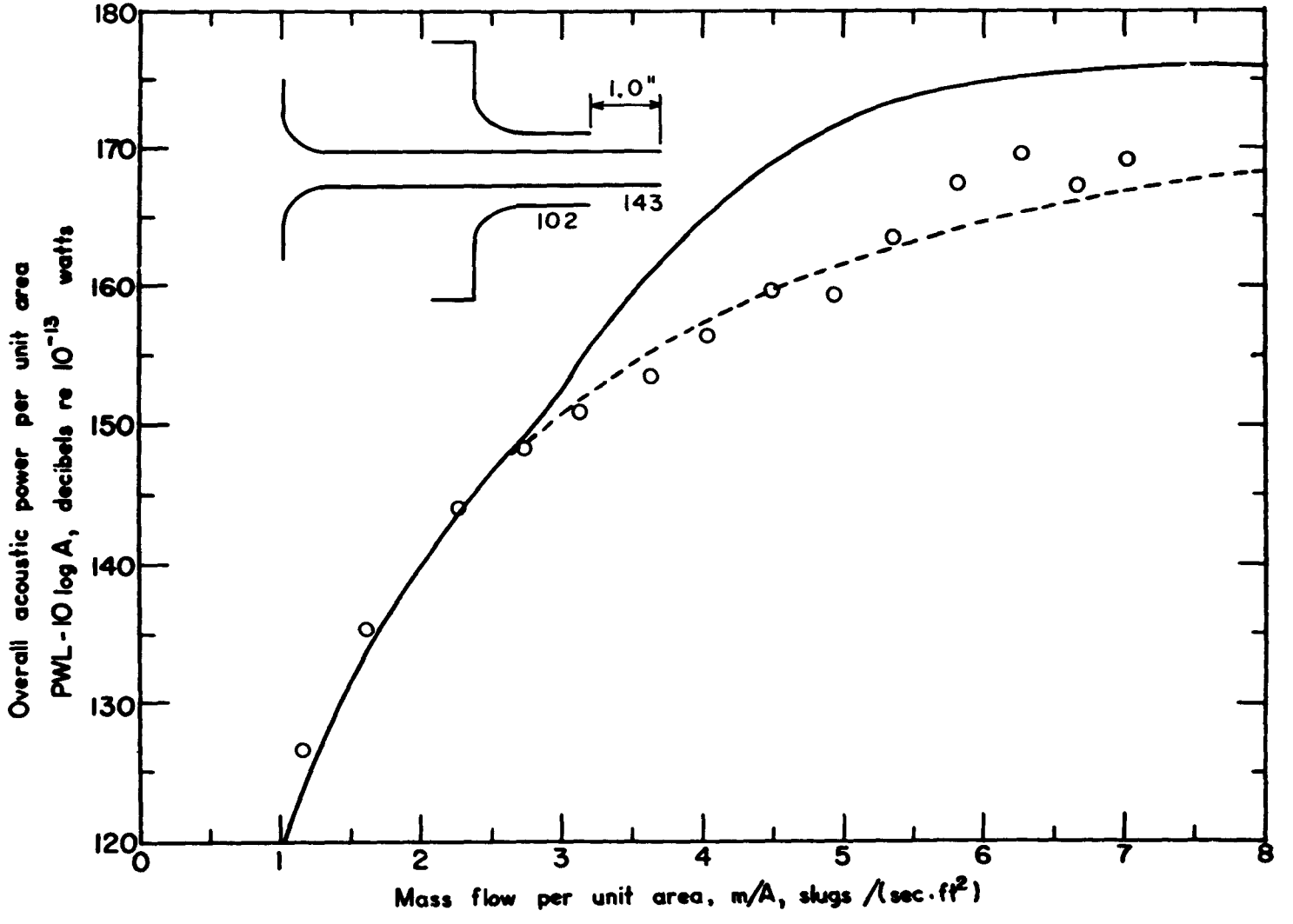

Figure 7. Acoustic Performance of Annular Nozzles with Center Core Flow

(h) Nozzle No. 293.

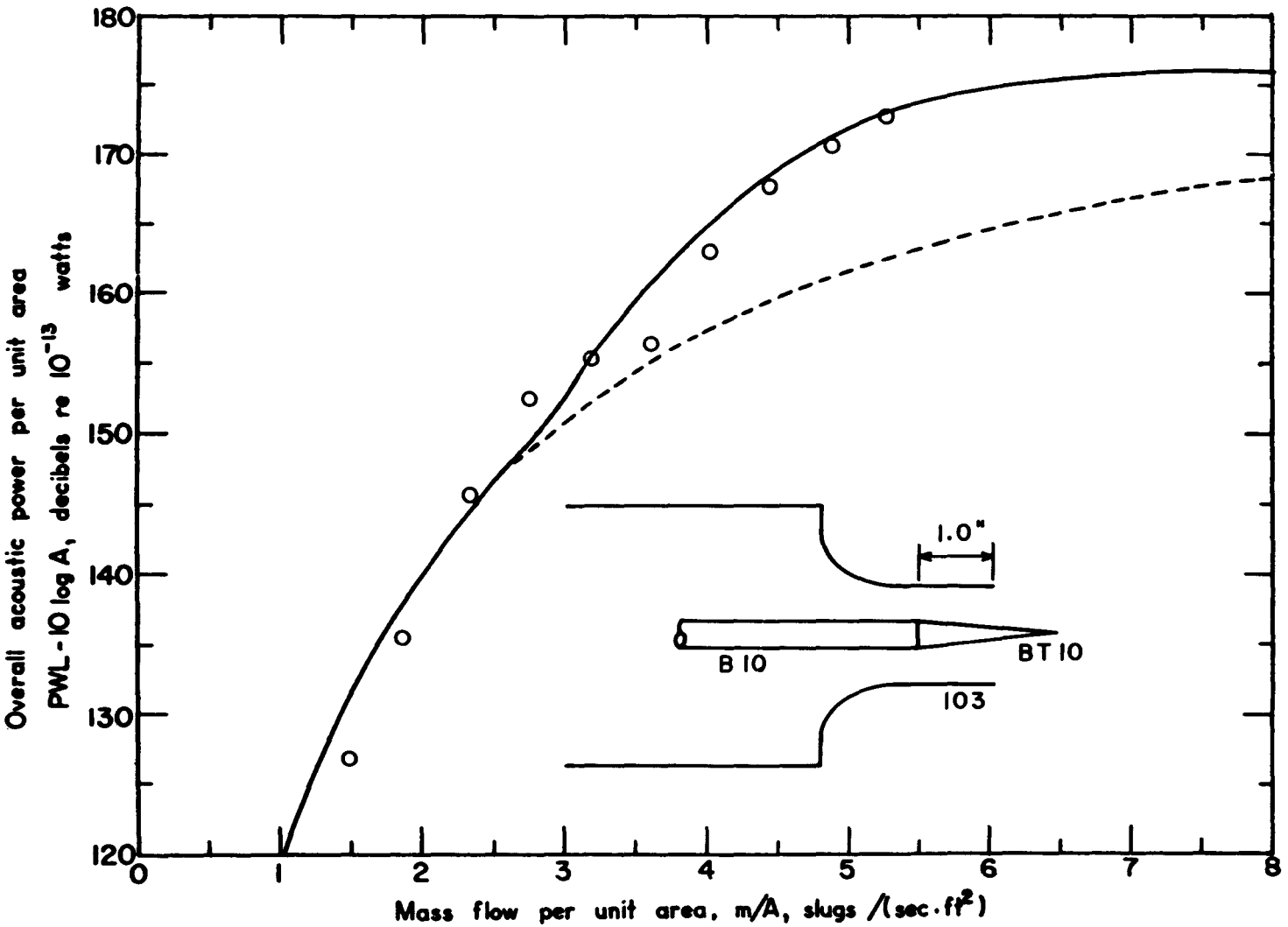

Figure 8. Acoustic Performance of Plug Nozzles

(a) Nozzle No. 301

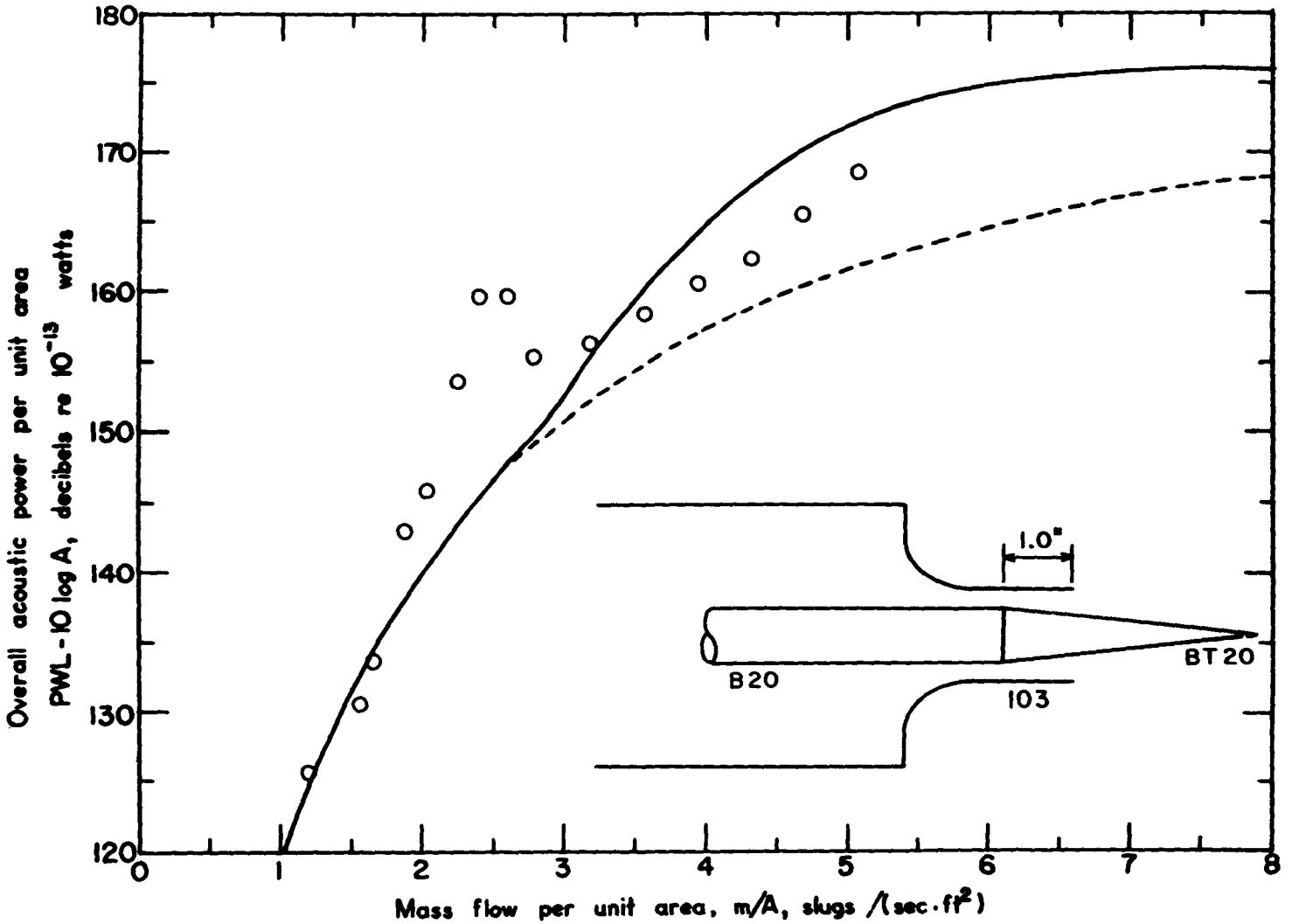

Figure 8. Acoustic Performance of Plug Nozzles
(b) Nozzle No. 305

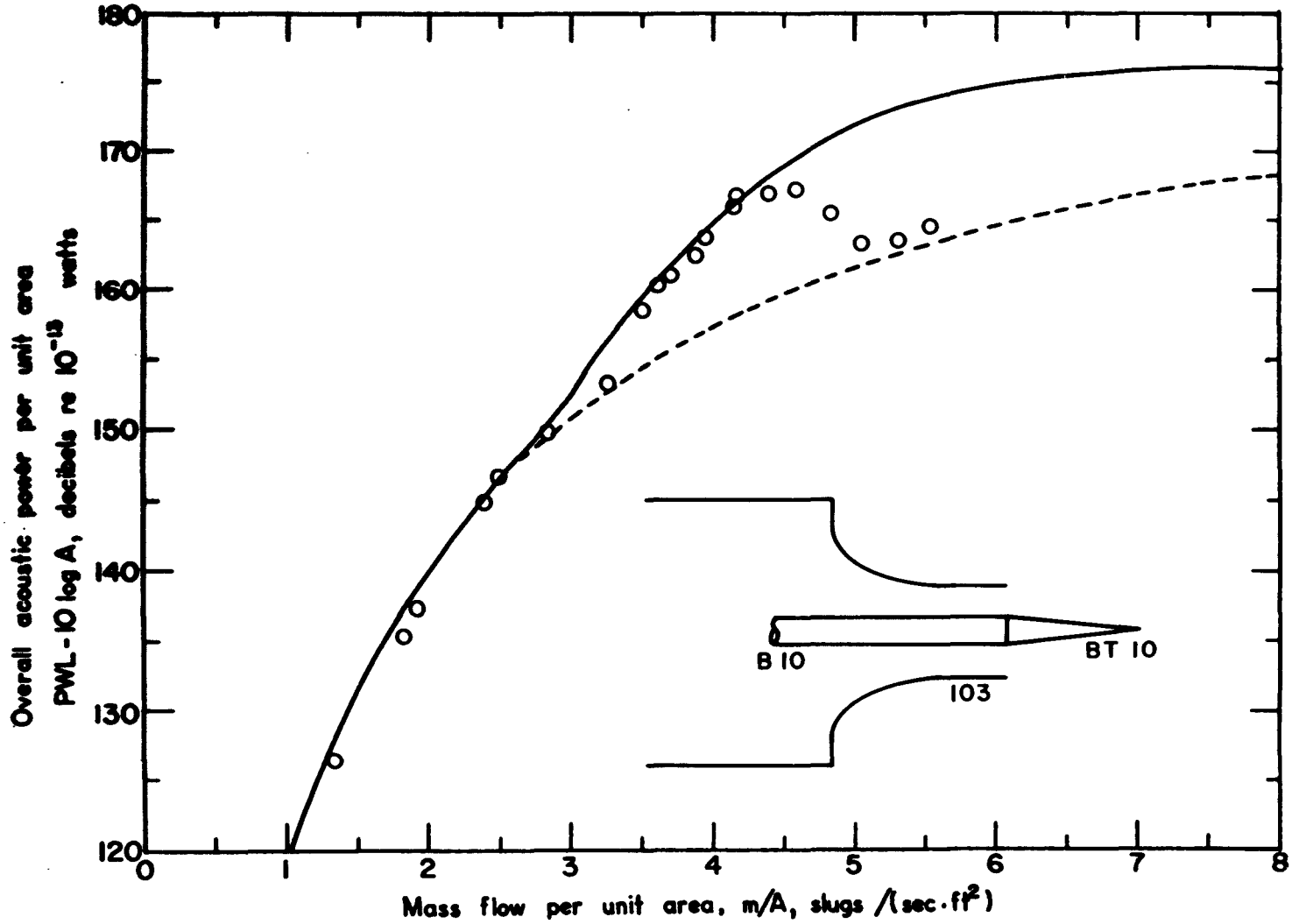

Figure 8. Acoustic Performance of Plug Nozzles

(c) Nozzle No. 321

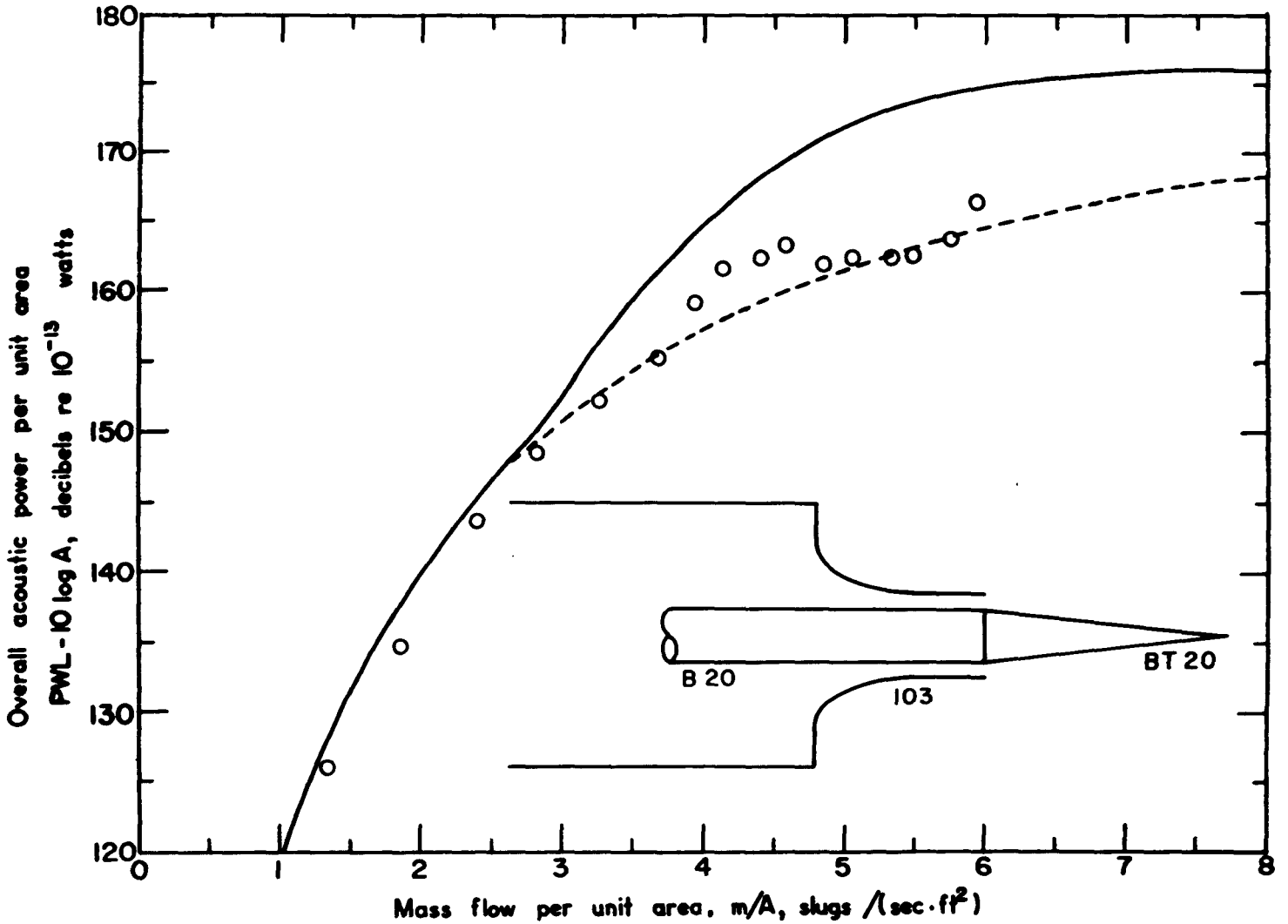

Figure 8. Acoustic Performance of Plug Nozzles

(d) Nozzle No. 325

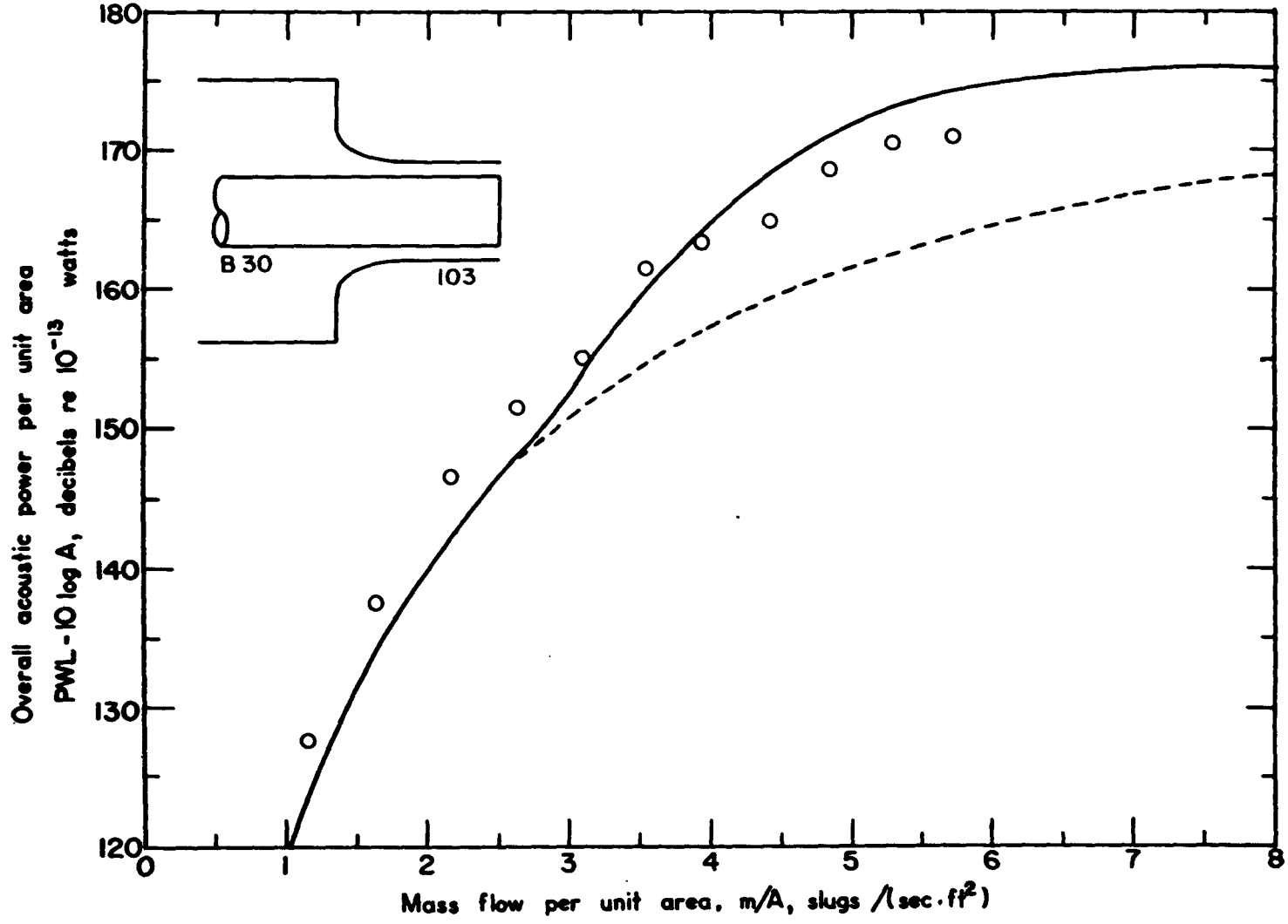

Figure 8. Acoustic Performance of Plug Nozzles

(e) Nozzle No. 326

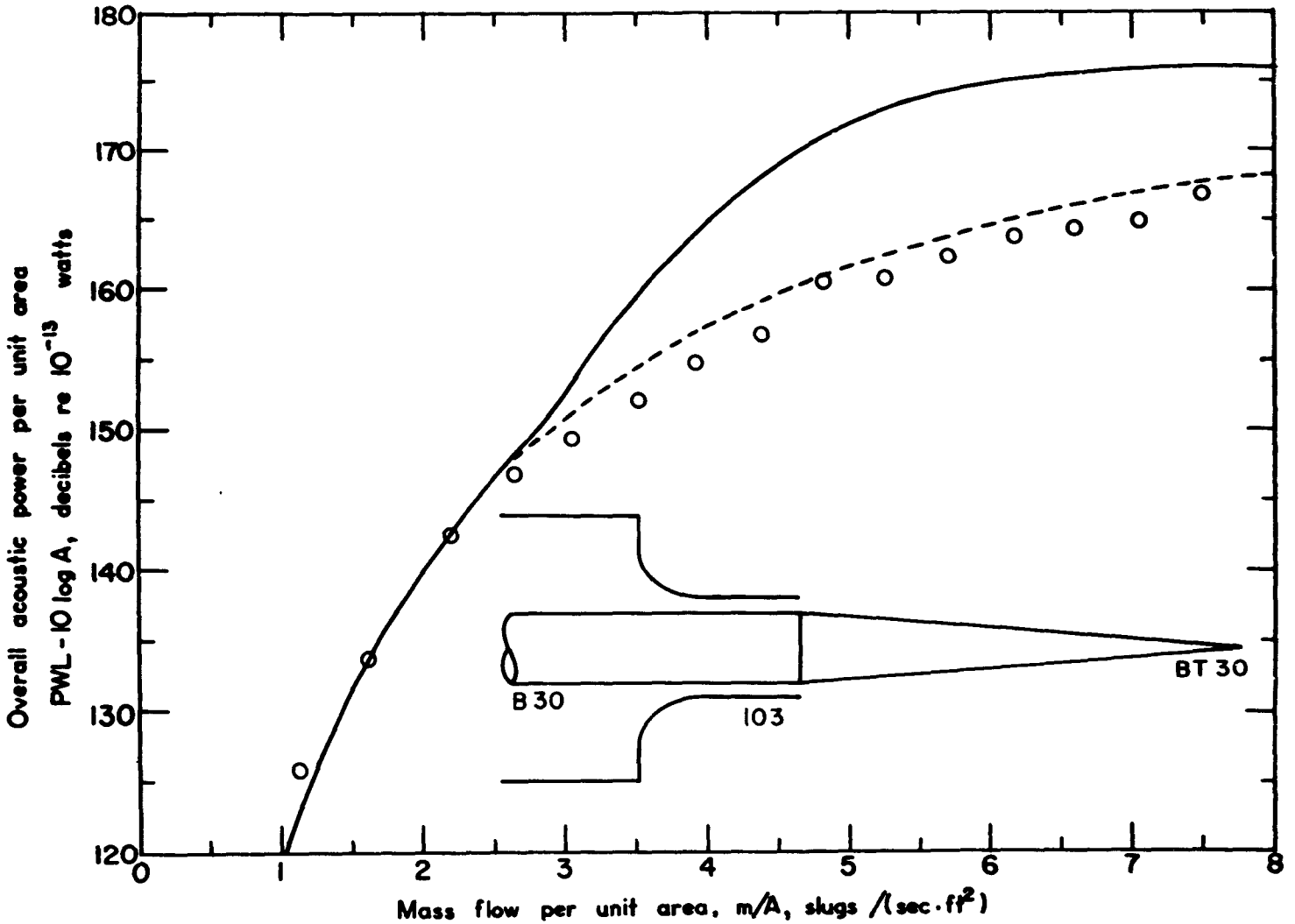

Figure 8. Acoustic Performance of Plug Nozzles

(f) Nozzle No. 327

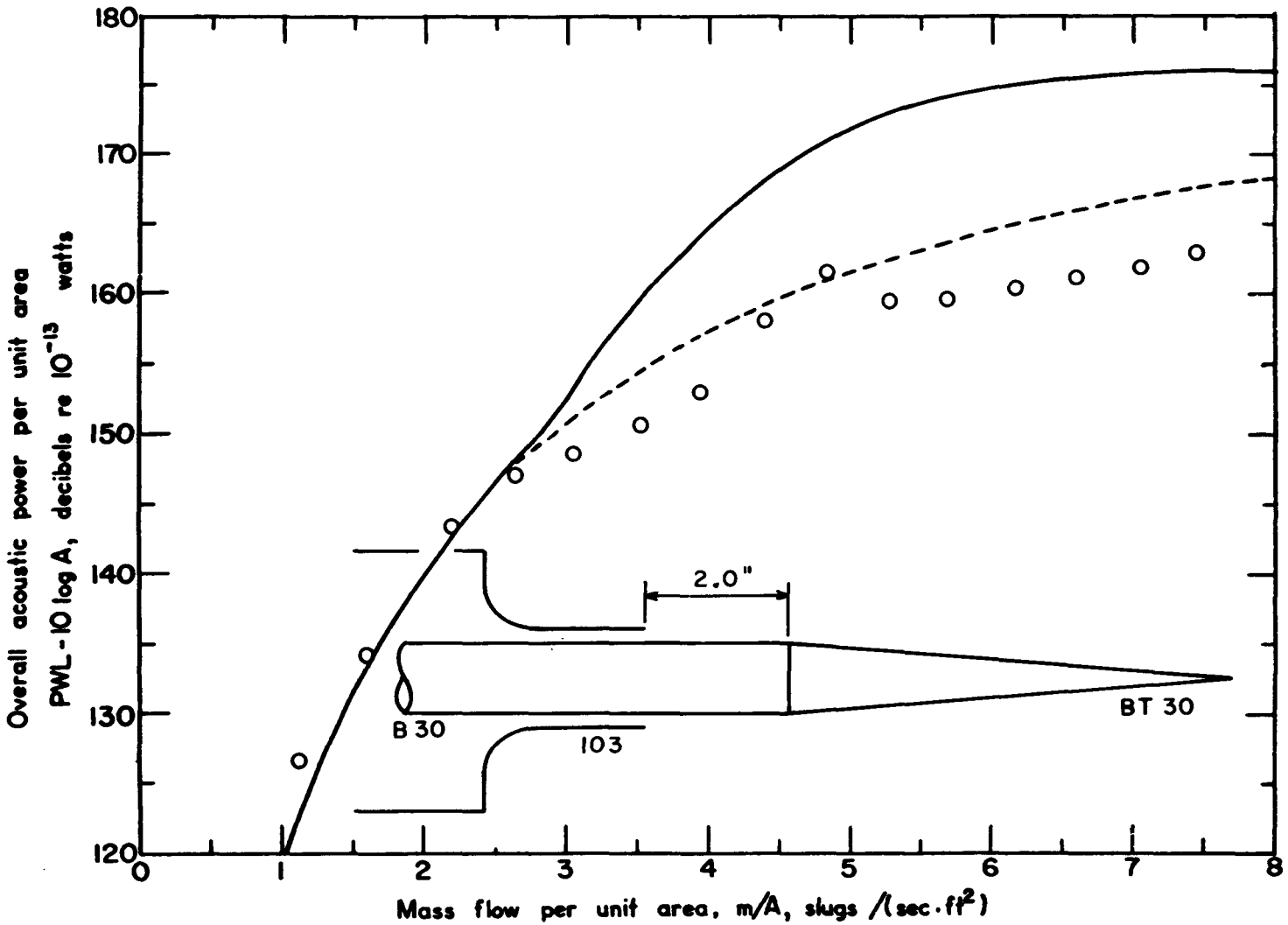

Figure 8. Acoustic Performance of Plug Nozzles

(g) Nozzle No. 347

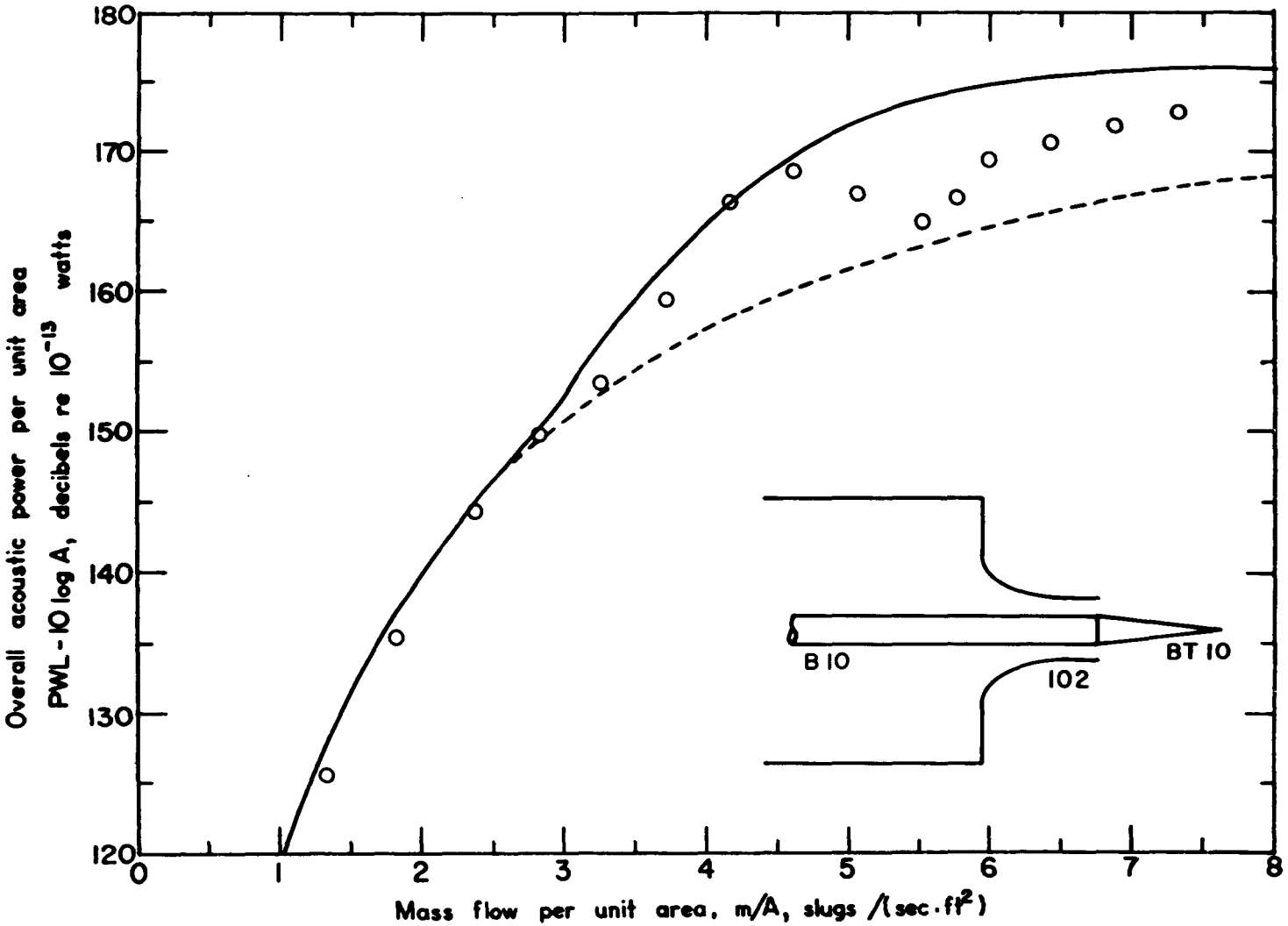

Figure 8. Acoustic Performance of Plug Nozzles
(h). Nozzle No. 371

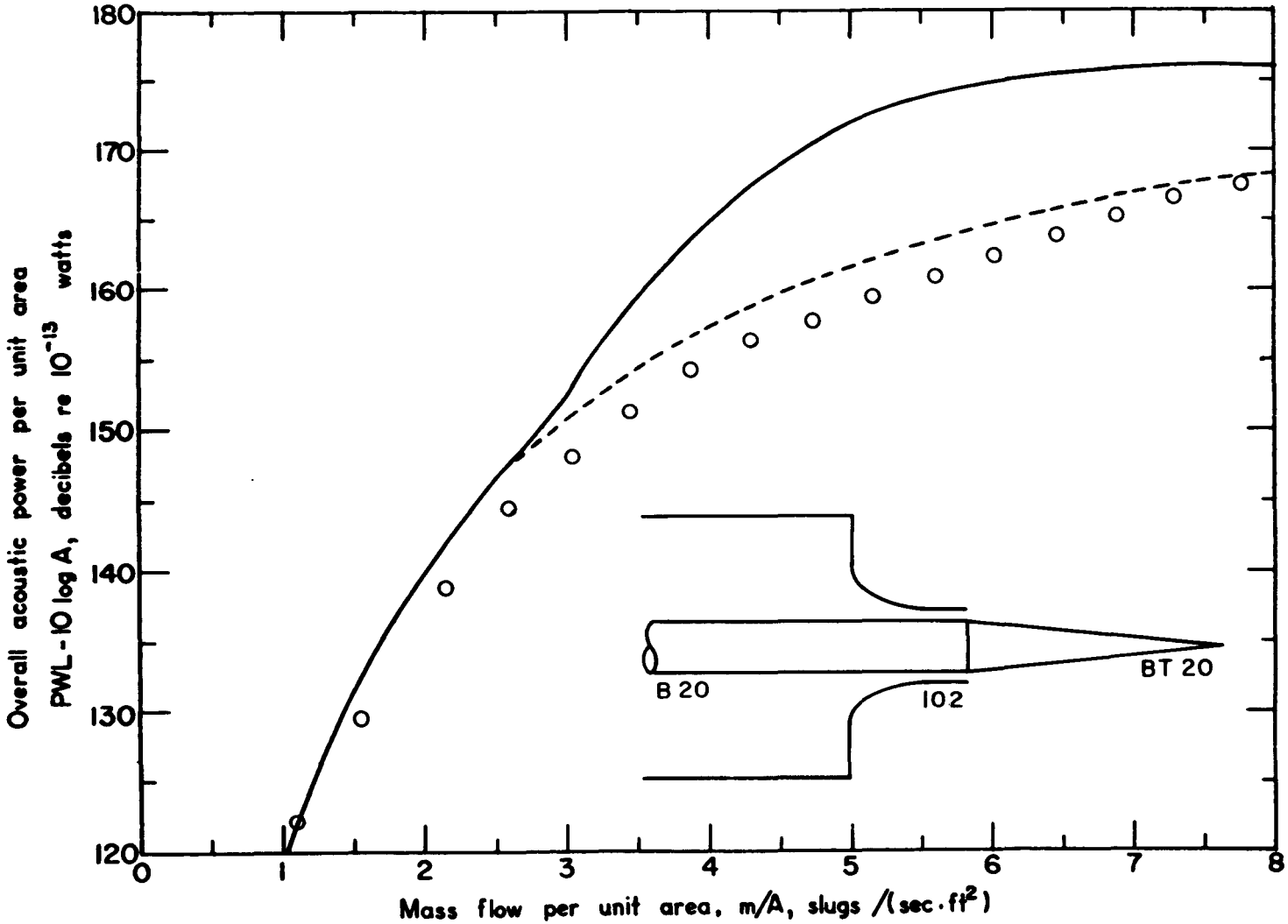

Figure 8. Acoustic Performance of Plug Nozzles

(i) Nozzle No. 375

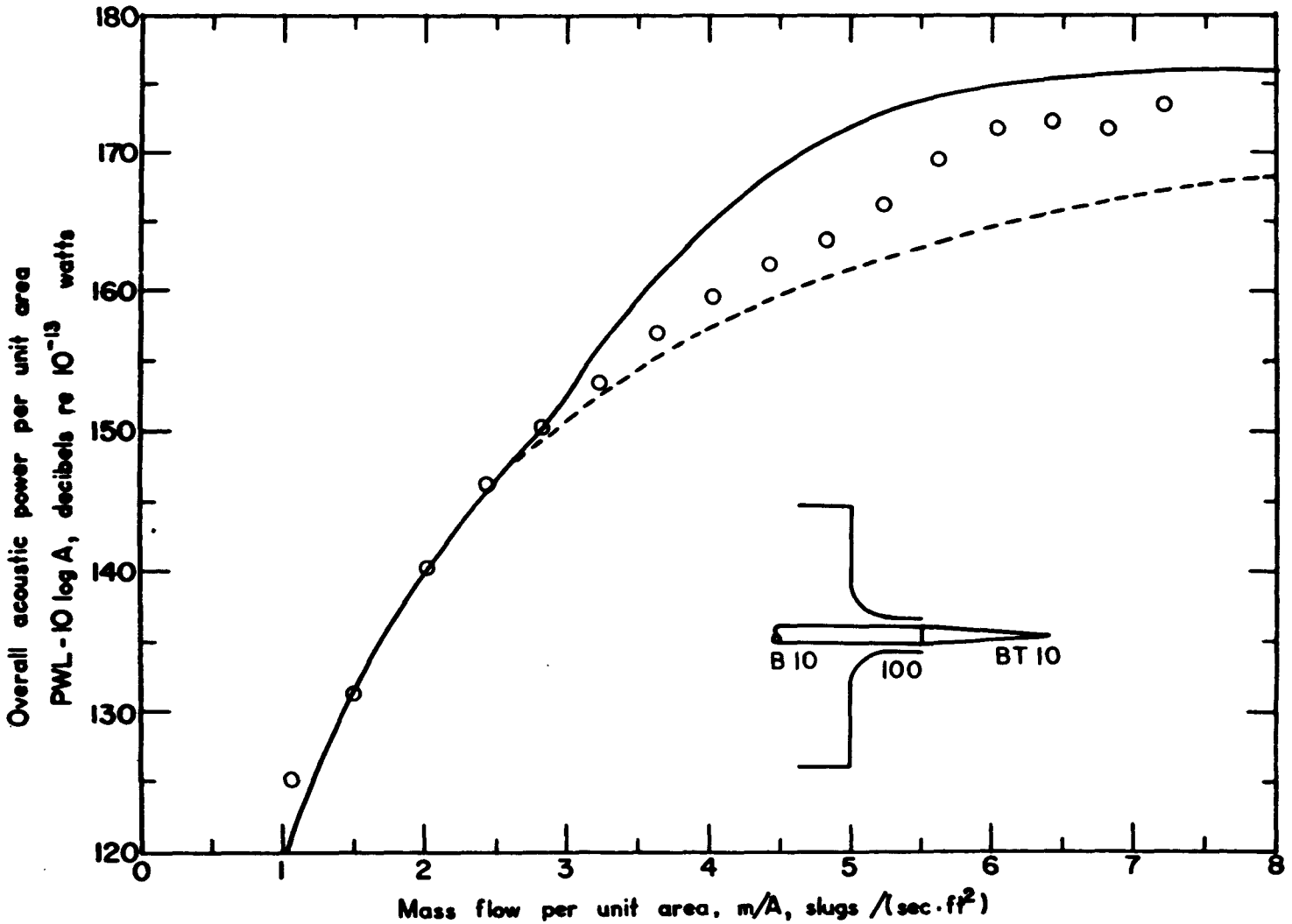

Figure 8. Acoustic Performance of Plug Nozzles

(j) Nozzle No. 421

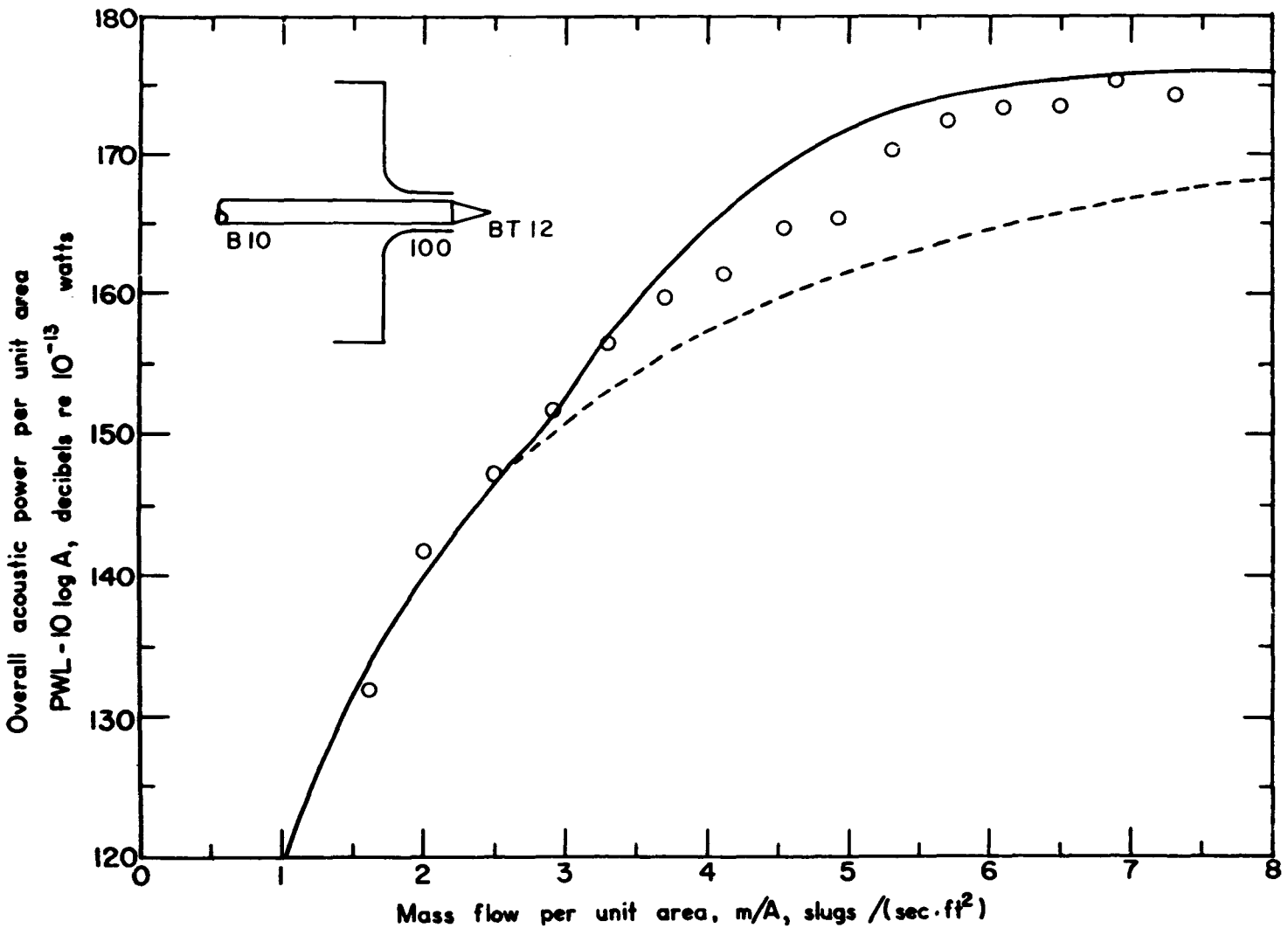

Figure 8. Acoustic Performance of Plug Nozzles

(k) Nozzle No. 423

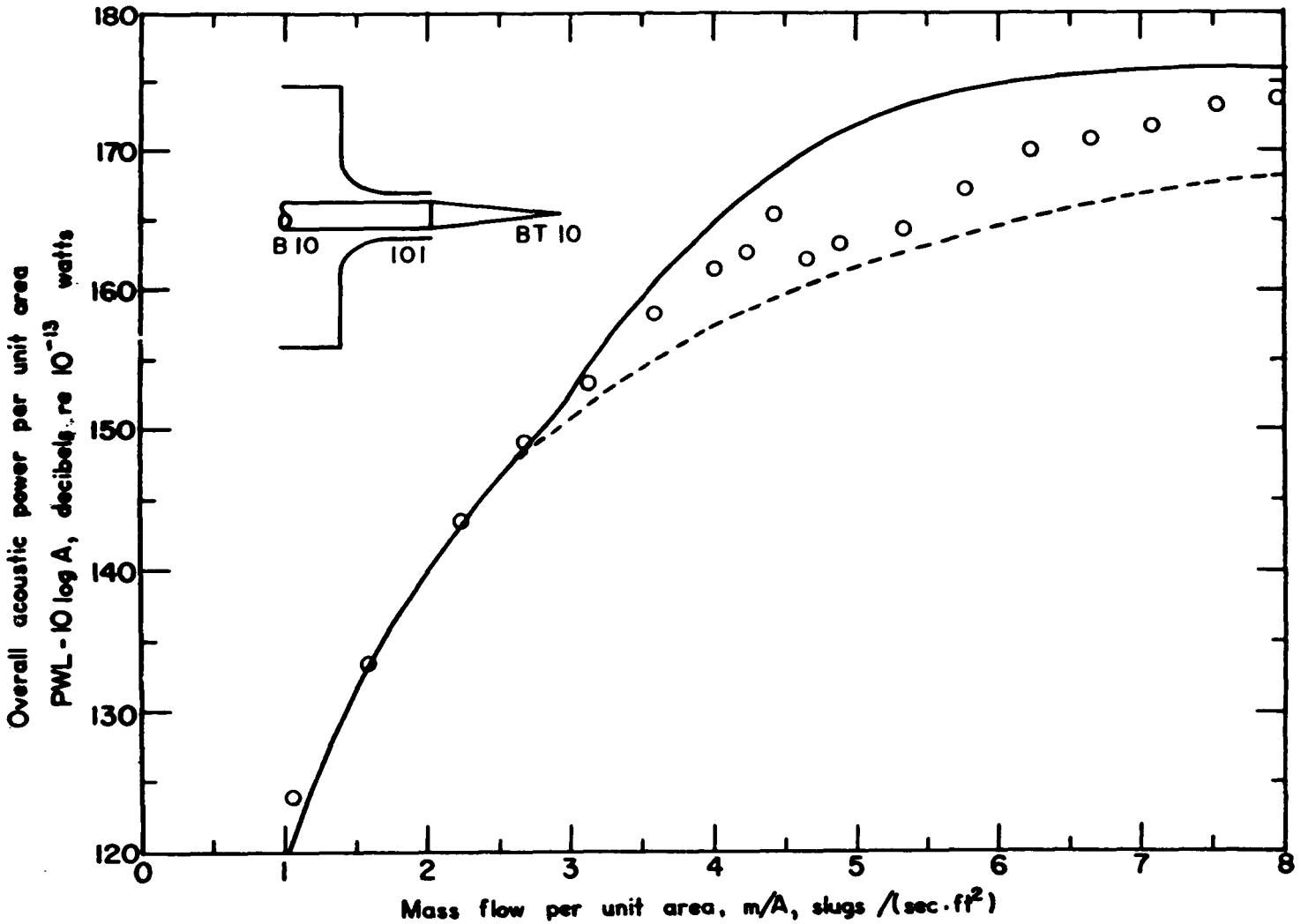

Figure 8. Acoustic Performance of Plug Nozzles

(1) Nozzle No. 471

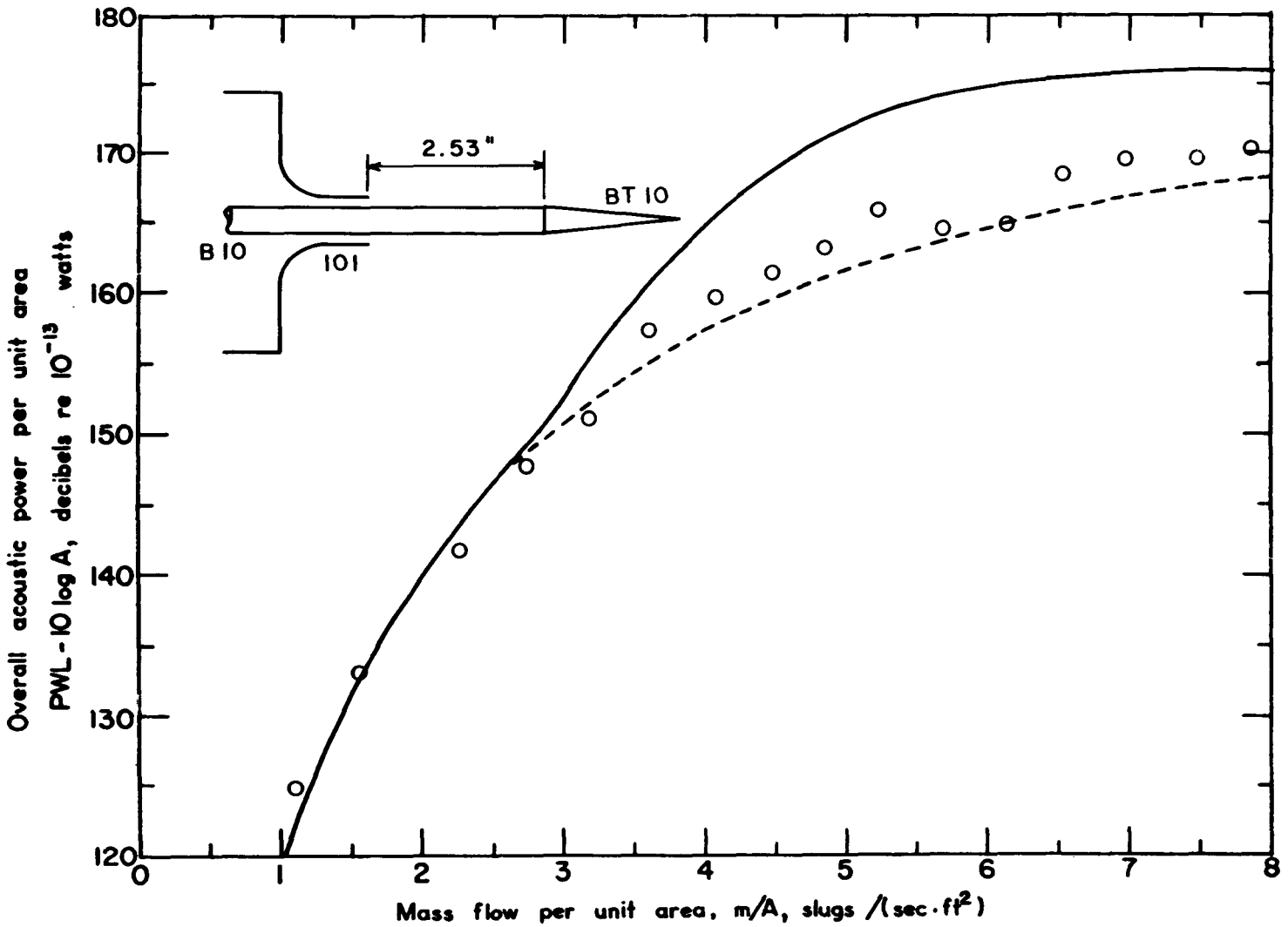

Figure 8. Acoustic Performance of Plug Nozzles
(m) Nozzle No. 491

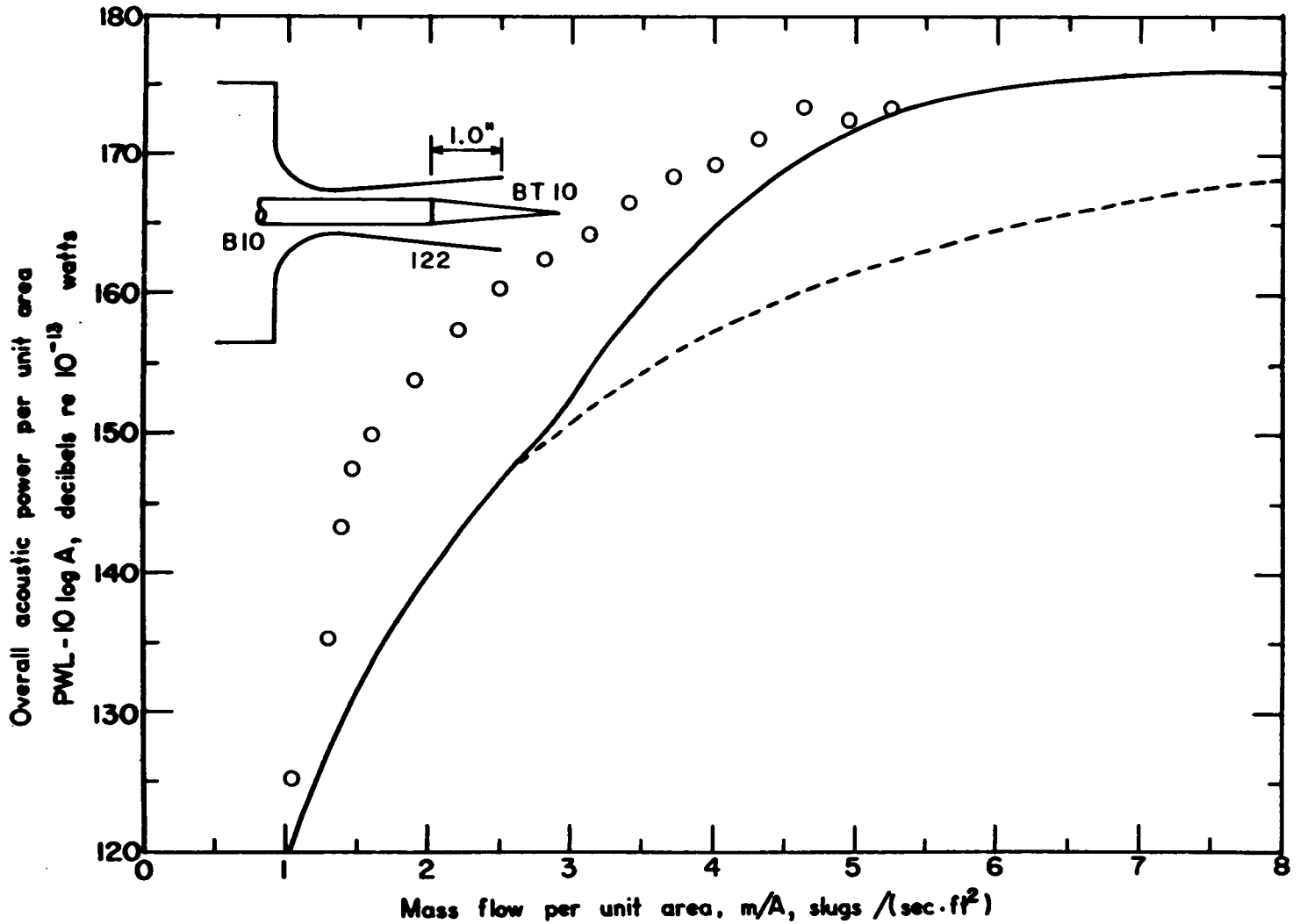

Figure 8. Acoustic Performance of Plug Nozzles
(n) Nozzle No. 601

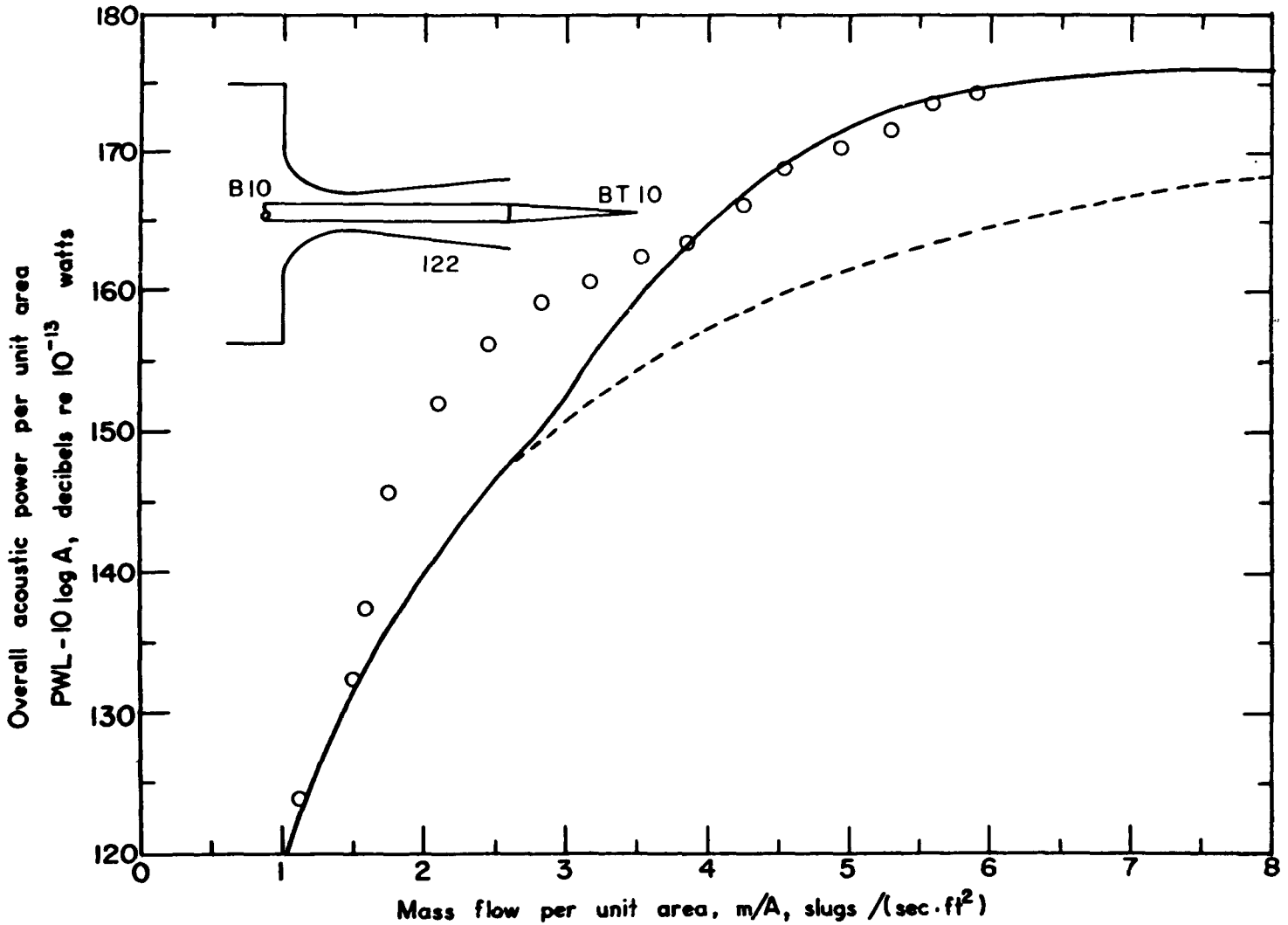

Figure 8. Acoustic Performance of Plug Nozzles

(o) Nozzle No. 621

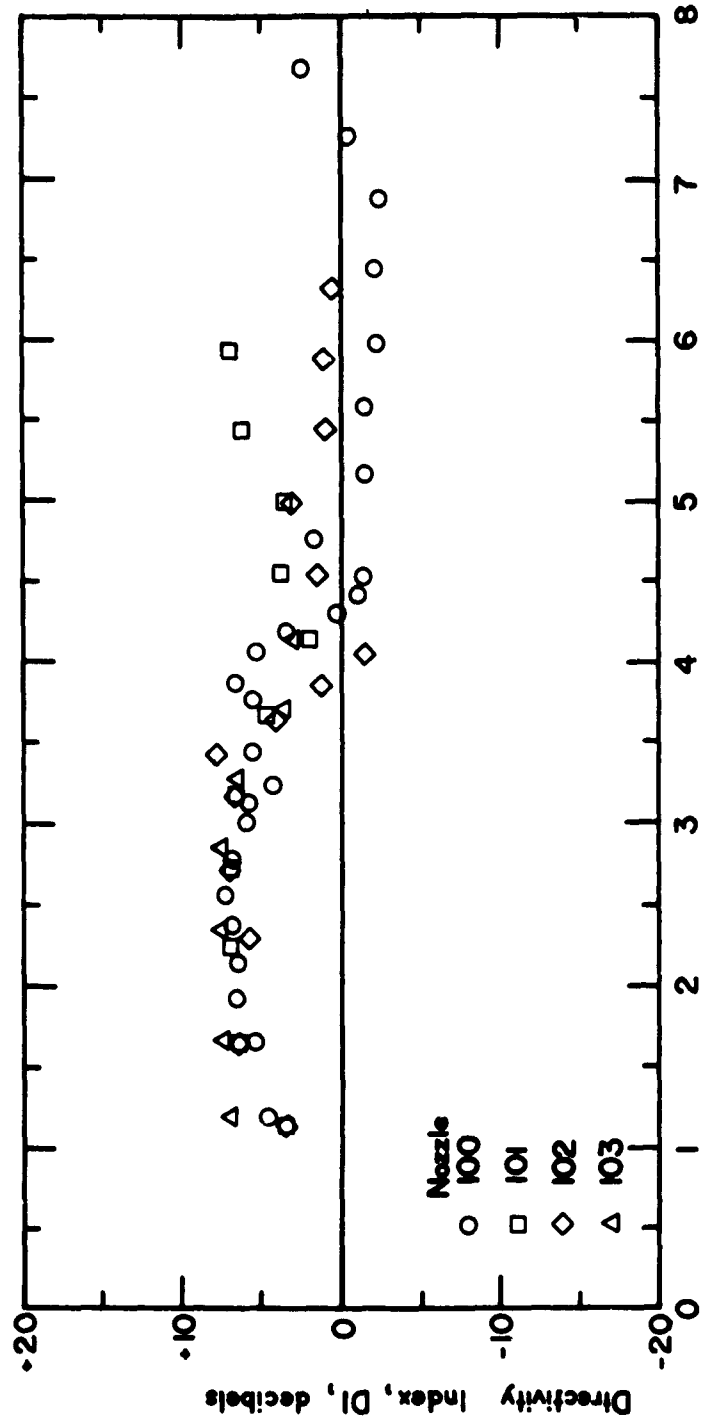

Figure 9. Noise Directional Character for Geometrically Matched Converging Nozzles.
(a) Direction Angle, $\theta = 15^{\circ}$

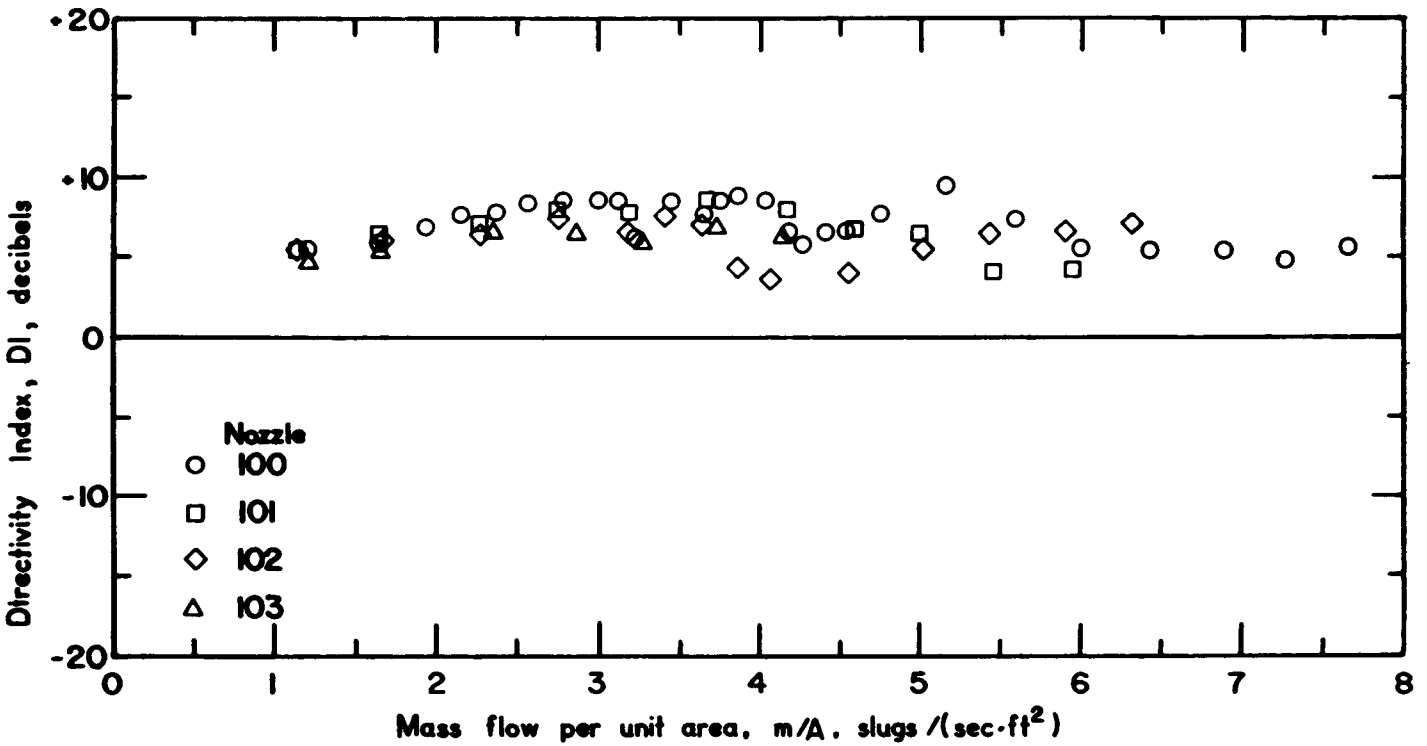

Figure 9. Noise Directional Character for Geometrically Matched Converging Nozzles. (b) Direction Angle, $\Theta = 30^{\circ}$

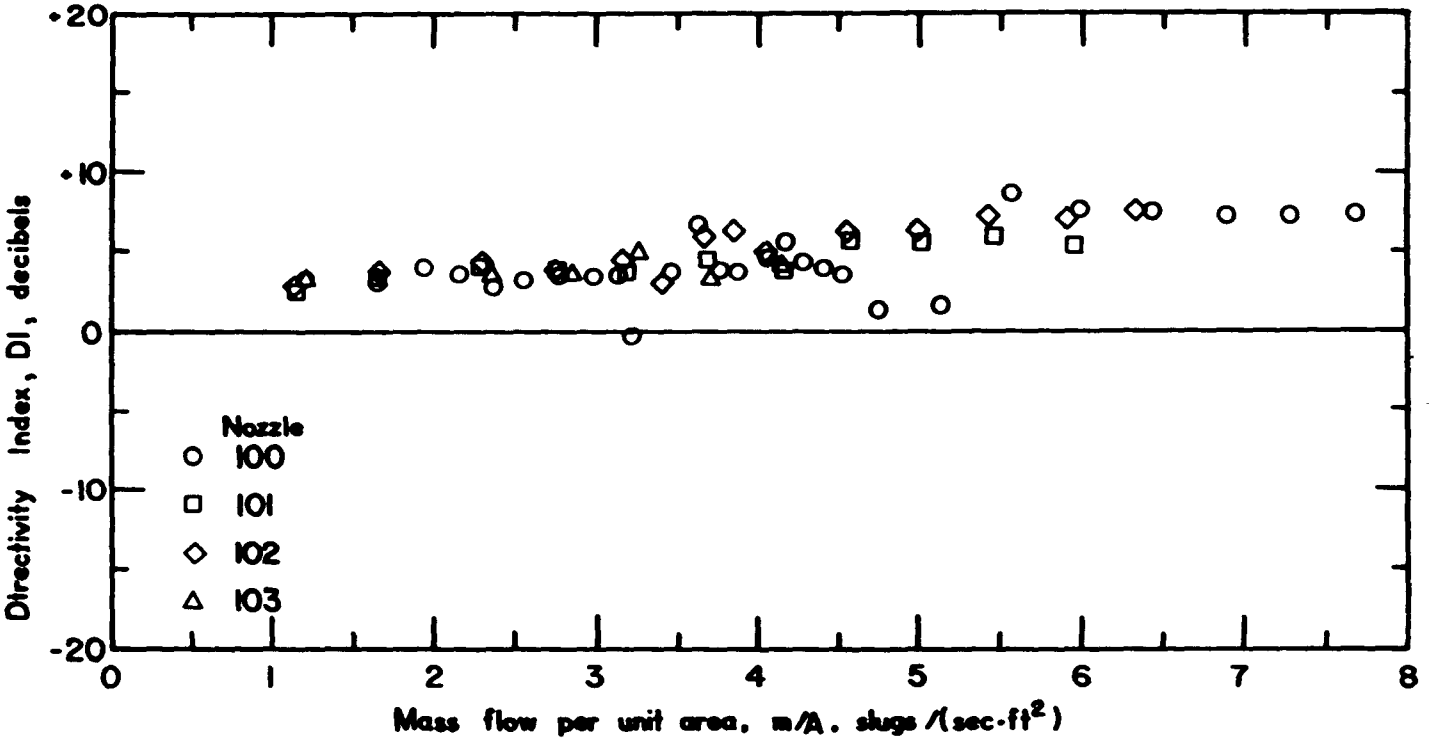

Figure 9. Noise Directional Character for Geometrically Matched Converging Nozzles. (c) Direction Angle, $\Theta = 45^{\circ}$

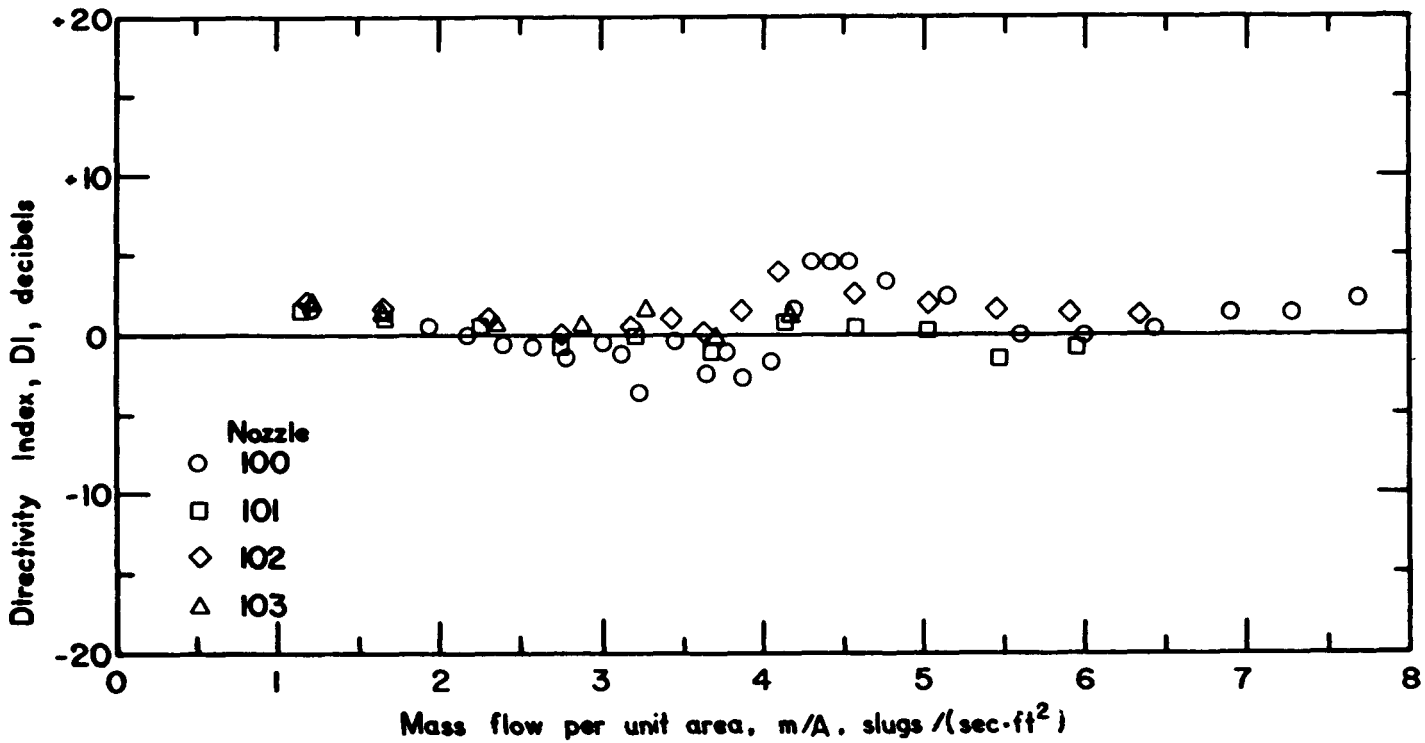

Figure 9. Noise Directional Character for Geometrically Matched Converging Nozzles. (d) Direction Angle, $\Theta = 60^{\circ}$

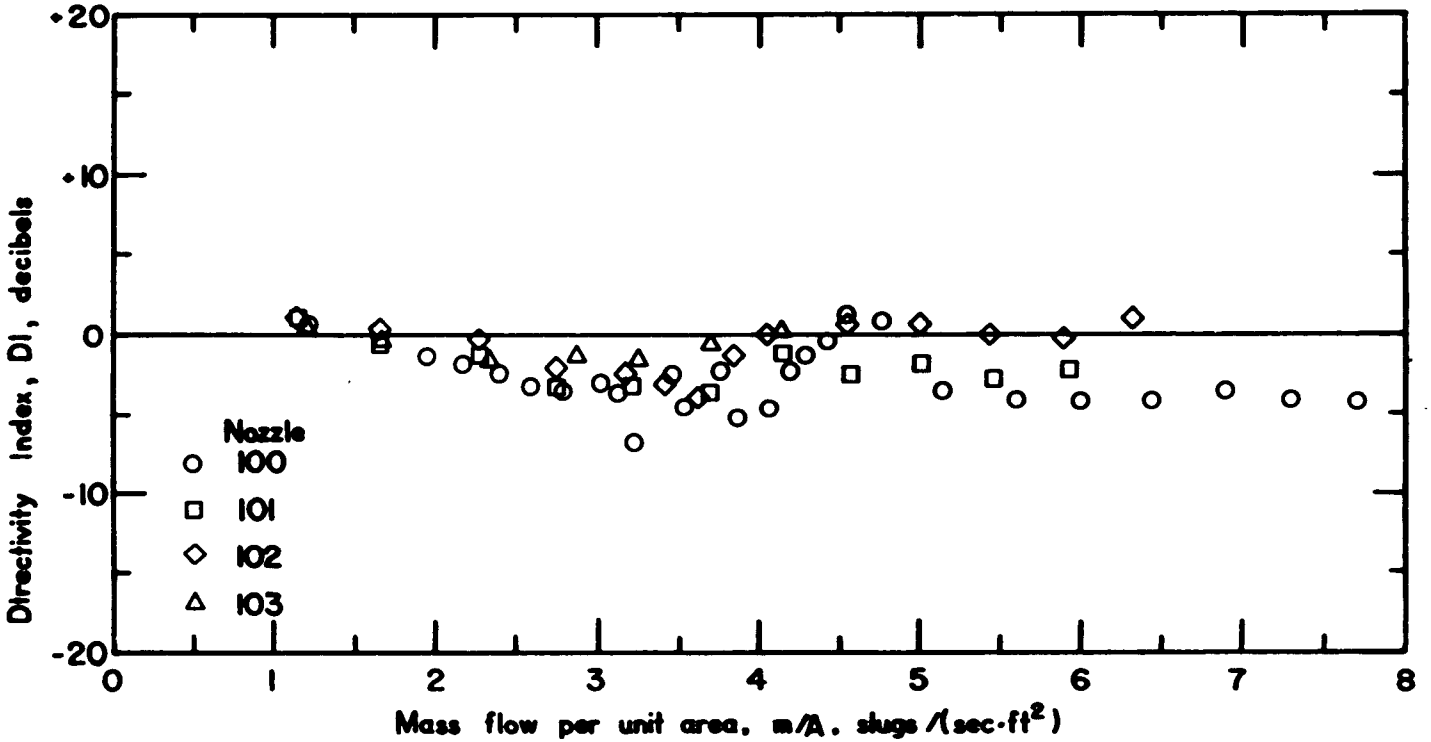

Figure 9. Noise Directional Character for Geometrically Matched Converging Nozzles.
(e) Direction Angle, $\Theta = 75^{\circ}$

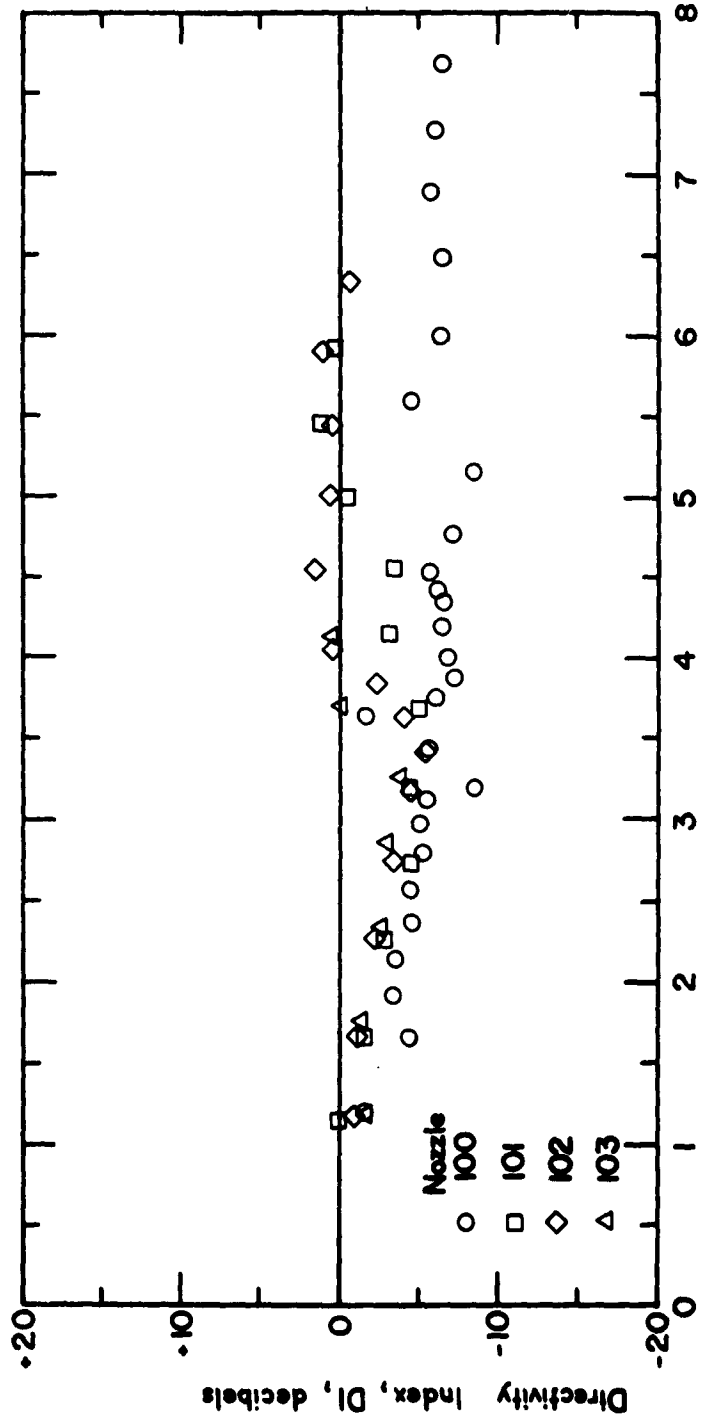

Figure 9. Noise Directional Character for Geometrically Matched Converging Nozzles.
(f) Direction Angle, $\theta = 90^\circ$

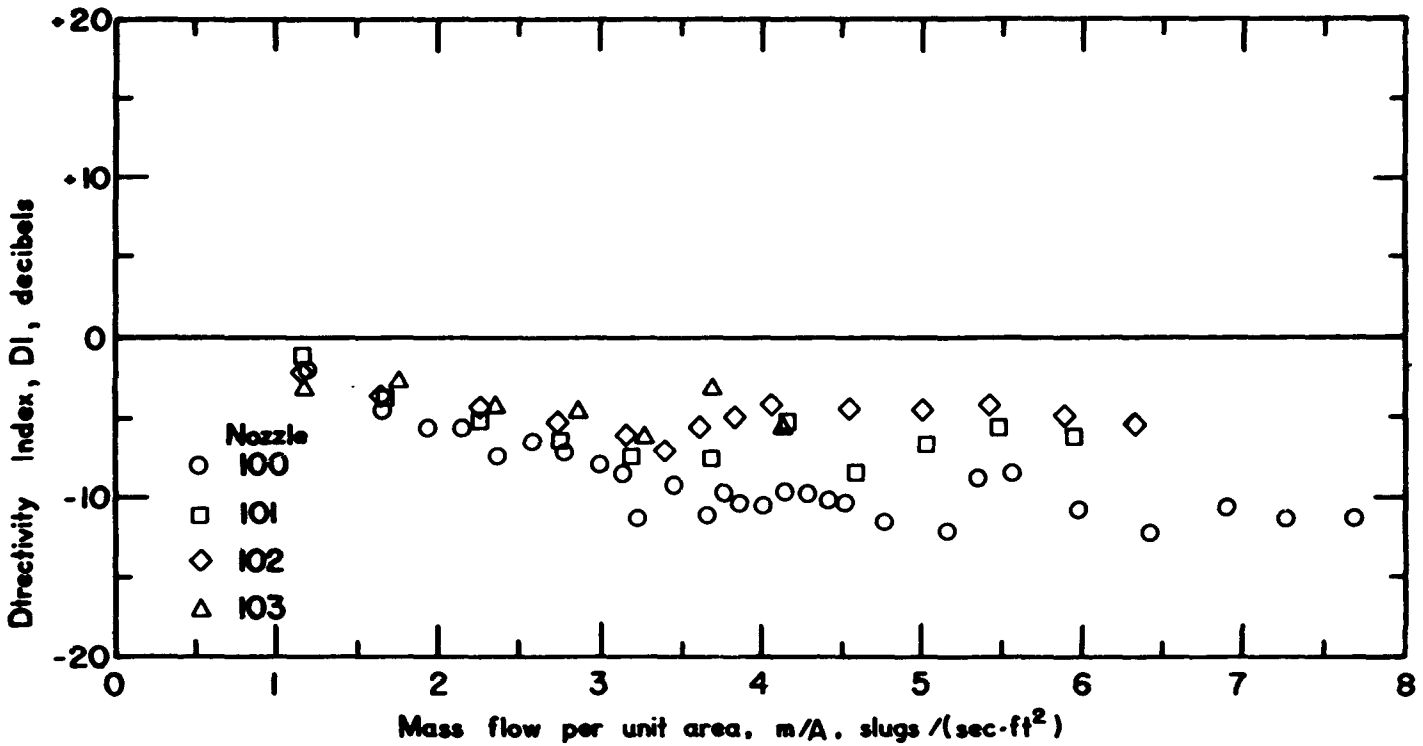

Figure 9. Noise Directional Character for Geometrically Matched Converging Nozzles. (g) Direction Angle, $\Theta = 105^{\circ}$

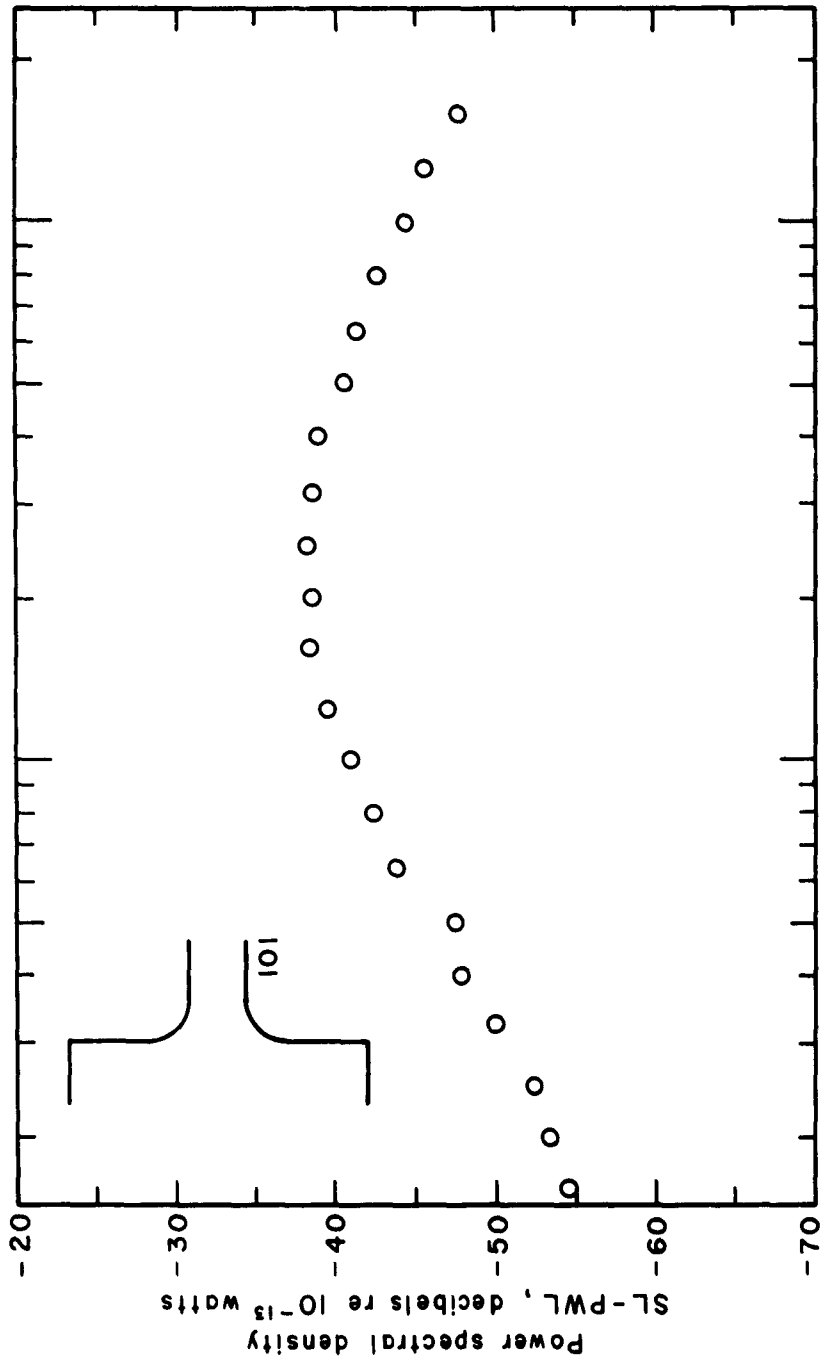

Figure 10. Frequency Analysis of Converging Nozzle 101
(a) $p_s/p_o = 1.28$

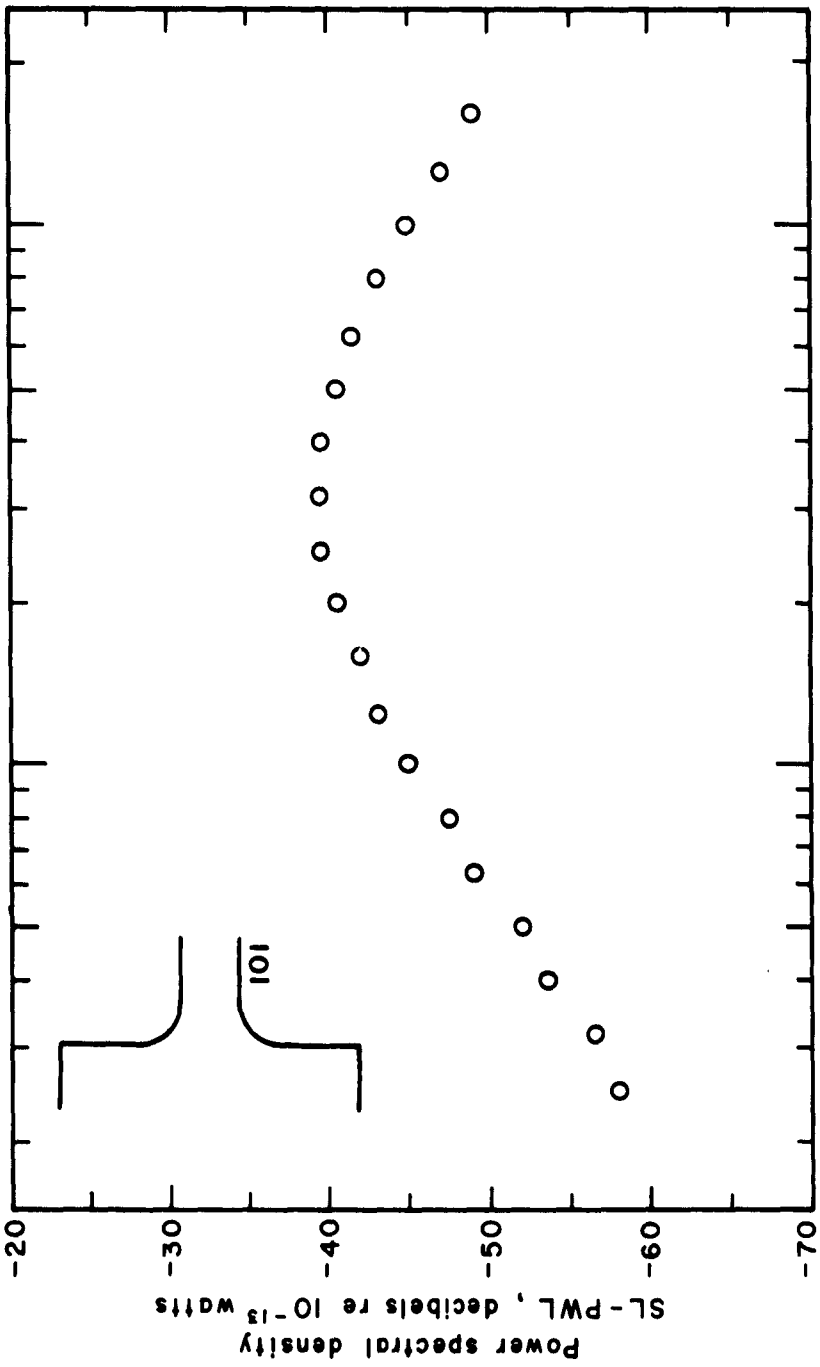

Figure 10. Frequency Analysis of Converging Nozzle 101
(b) P_s/P_o = 1.836

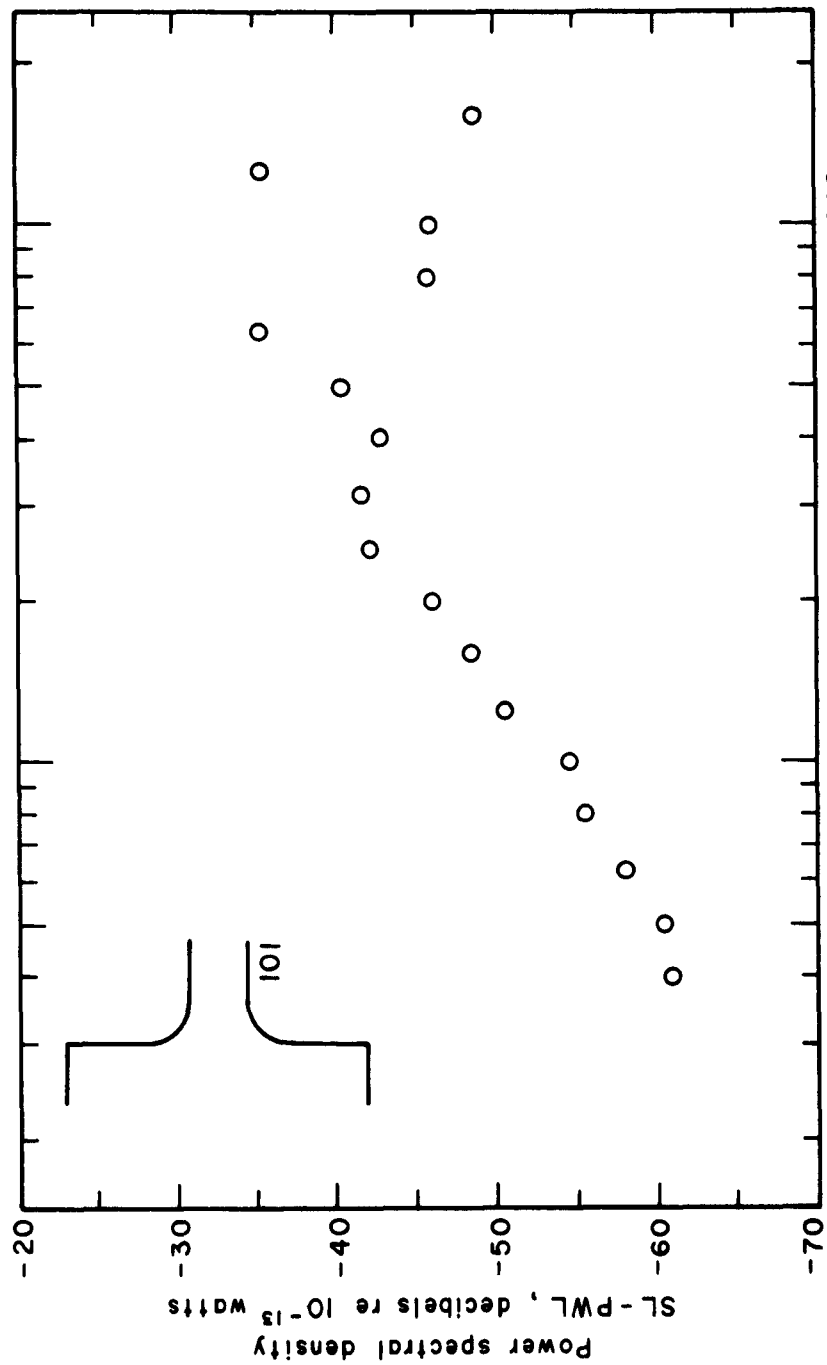

Figure 10. Frequency Analysis of Converging Nozzle 101
(c) $p_s/p_0 = 3.51$, Screech Included

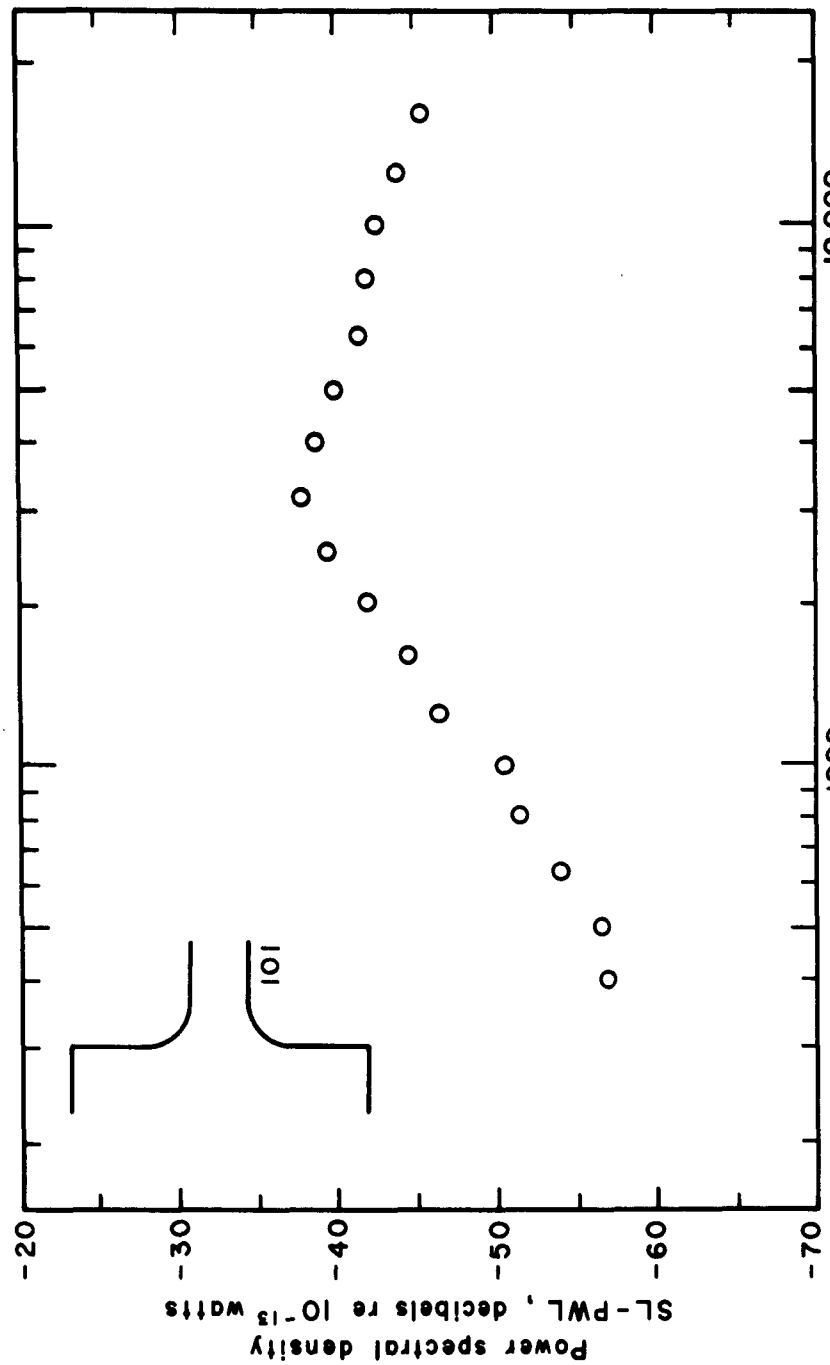

Figure 10. Frequency Analysis of Converging Nozzle 101
(d) P_s/P_o = 3.51, Screech Removed

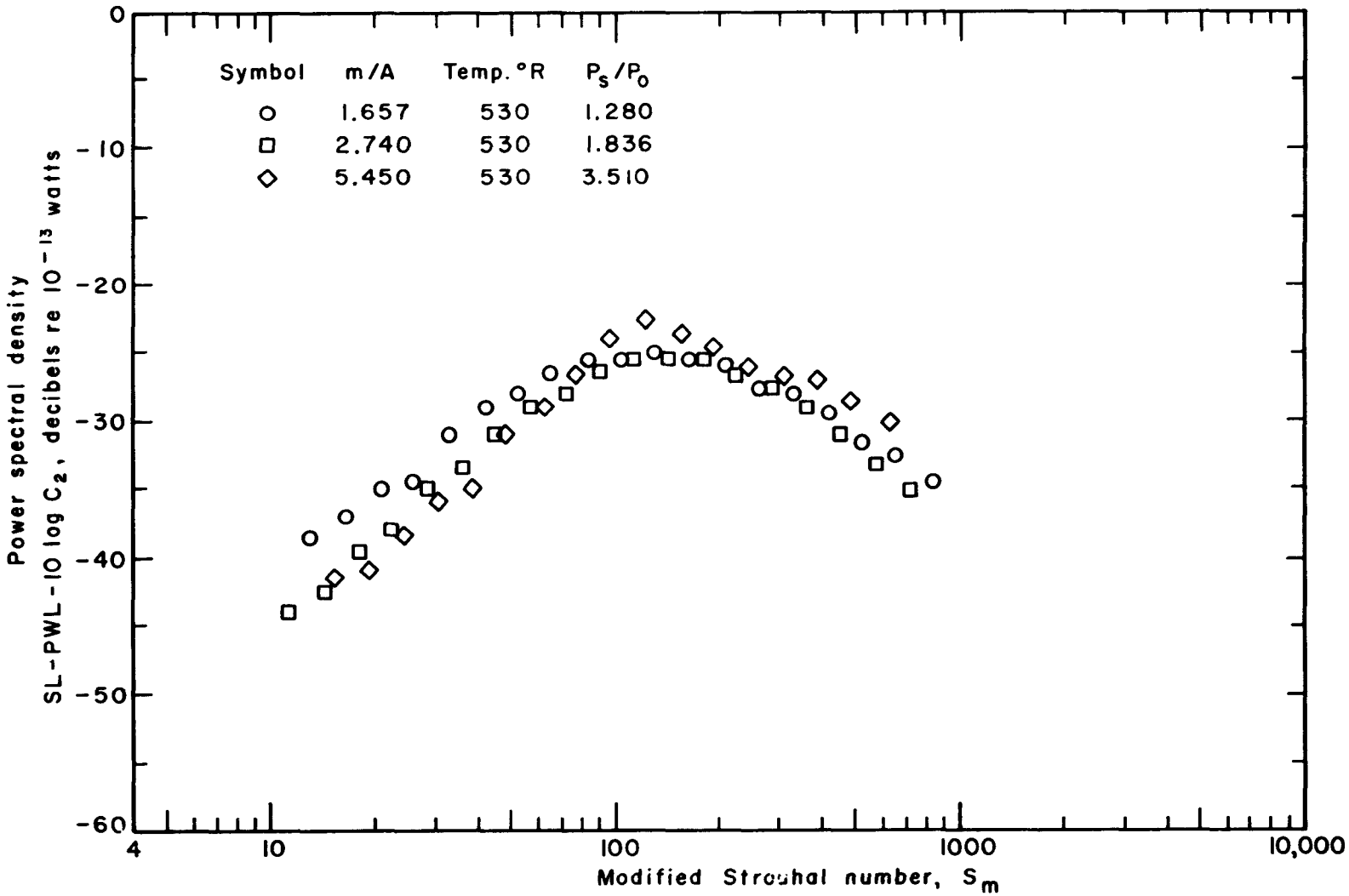

Figure 10. Frequency Analysis of Converging Nozzle 101
(e) Normalized Spectrum

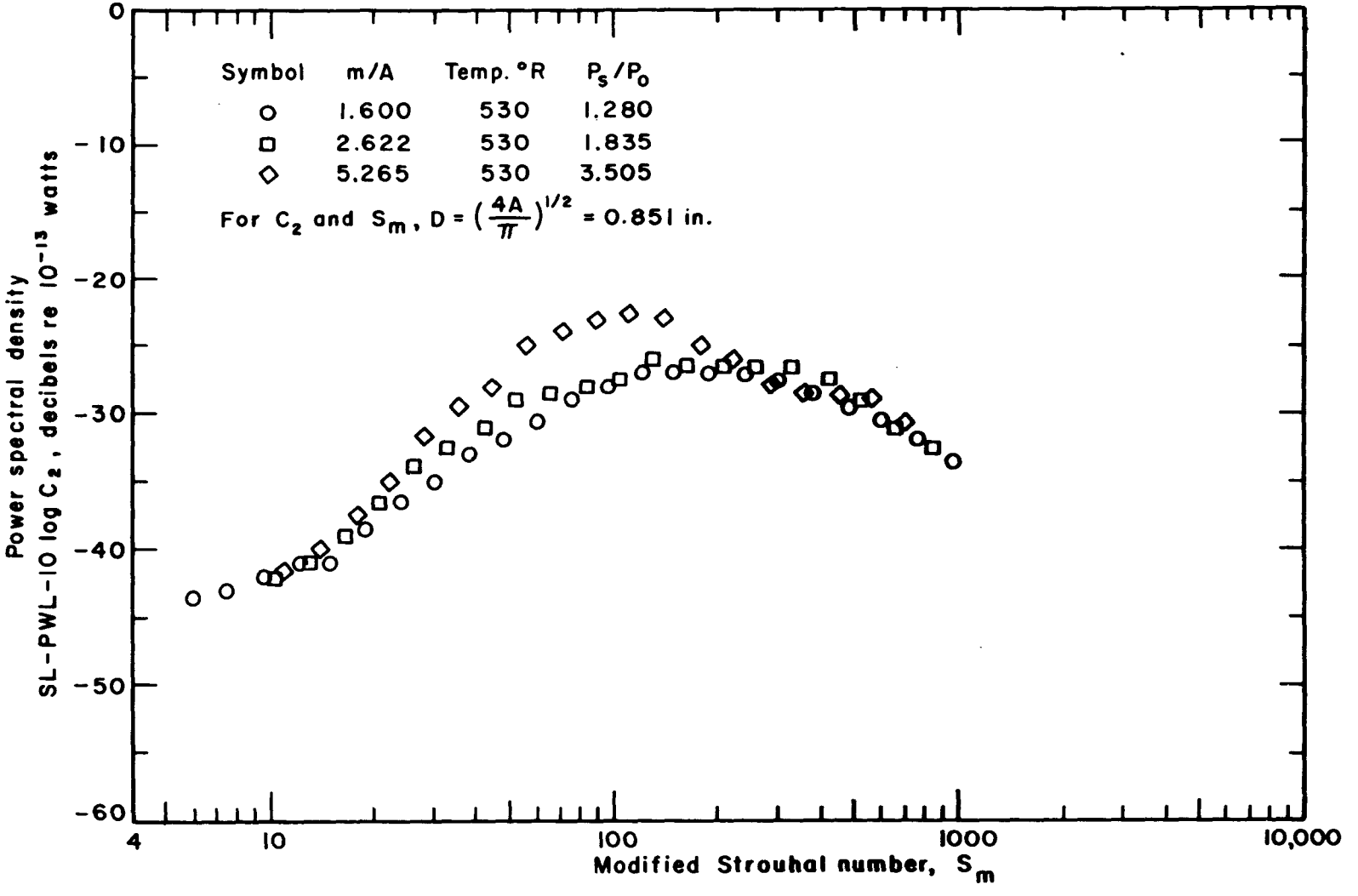

Figure 11. Normalized Frequency Analysis of Plug Nozzle 327

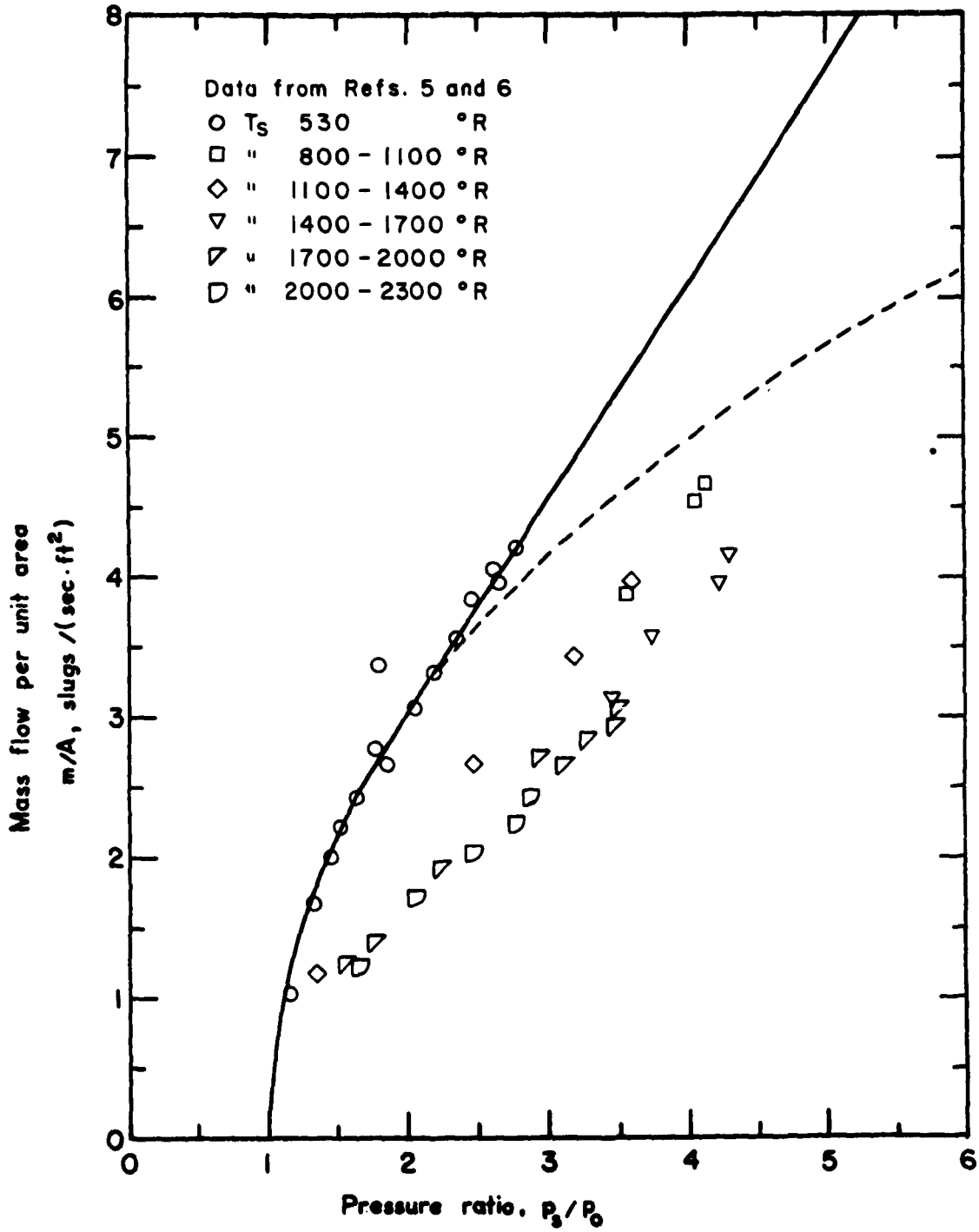

Figure 12. Flow Performance of Four-Inch Conical Nozzle

(a) Size Normalization Only

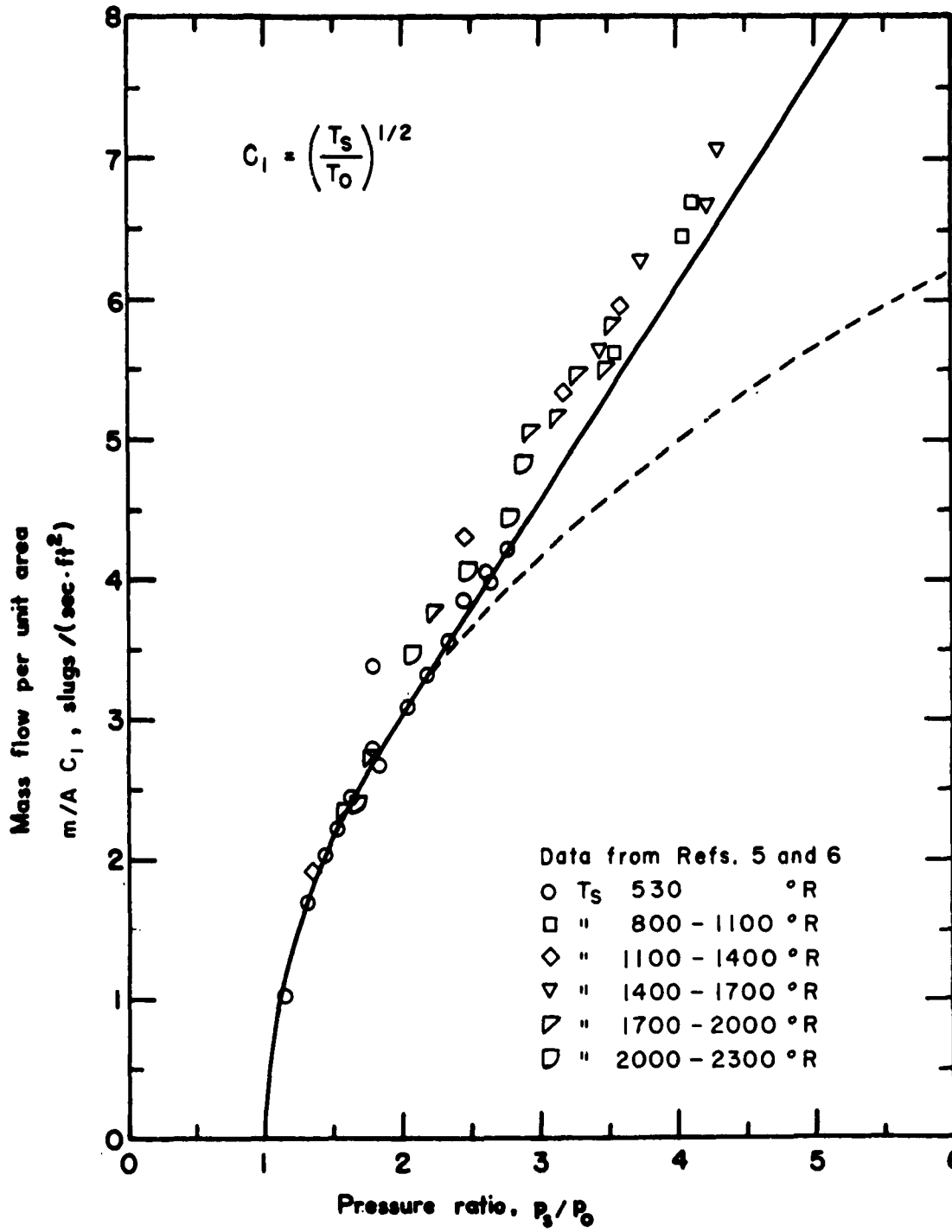

Figure 12. Flow Performance of Four-Inch Conical Nozzle

(b) Size and Partial Temperature Normalization

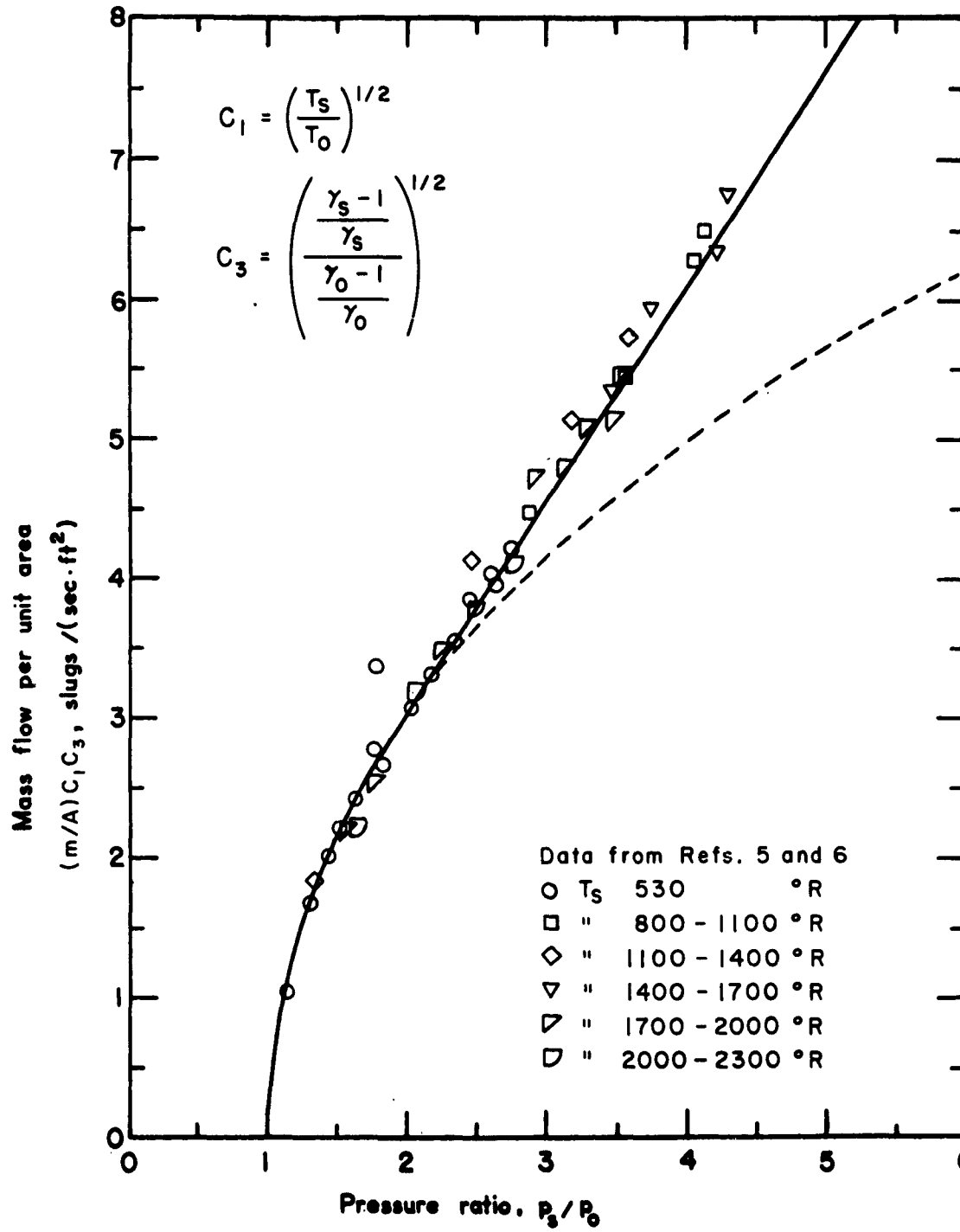

Figure 12. Flow Performance of Four-Inch Conical Nozzle

(c) Size and Temperature Normalization

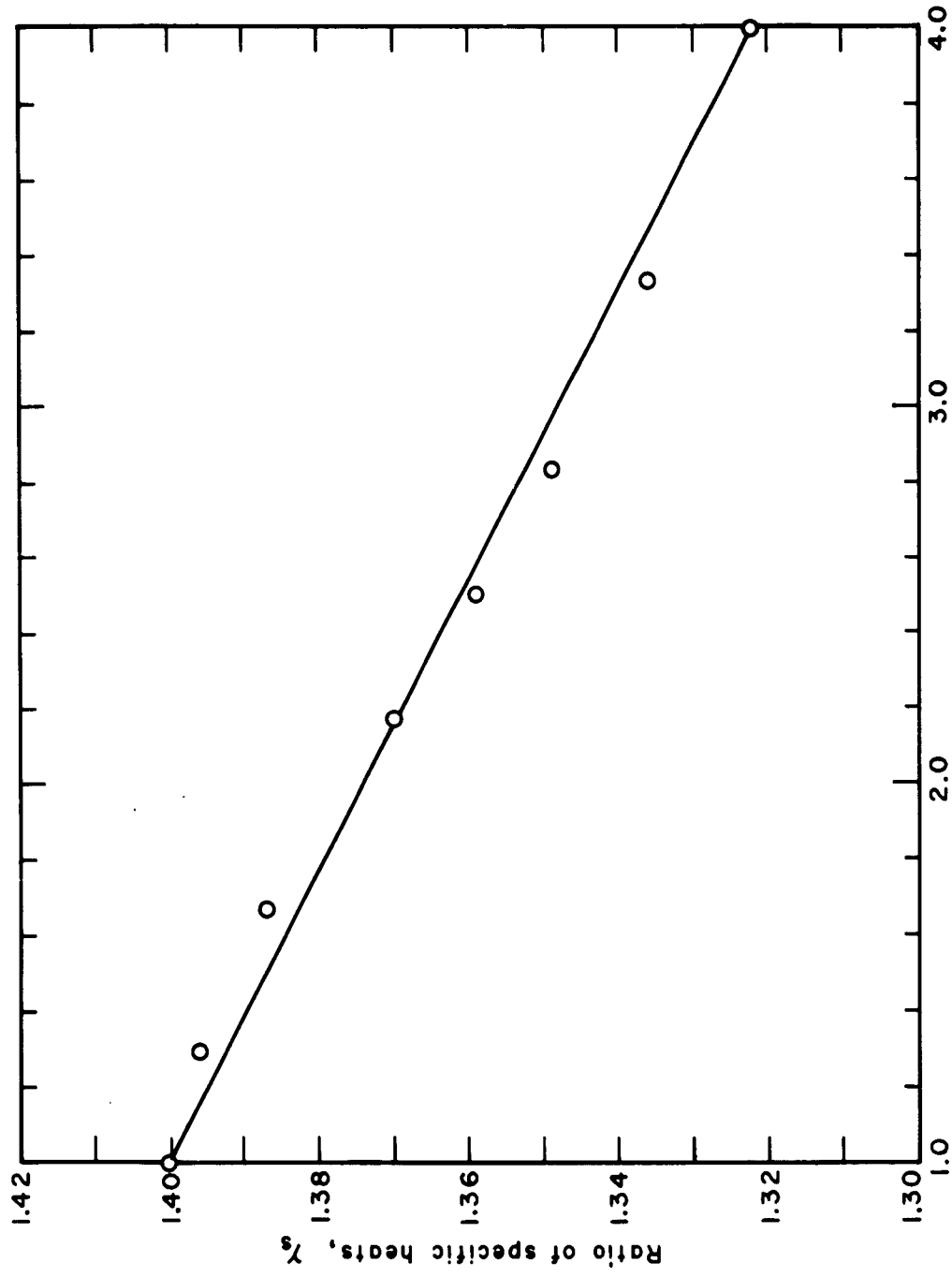

Figure 13. Variation of Specific Heat Ratio with Temperature Ratio

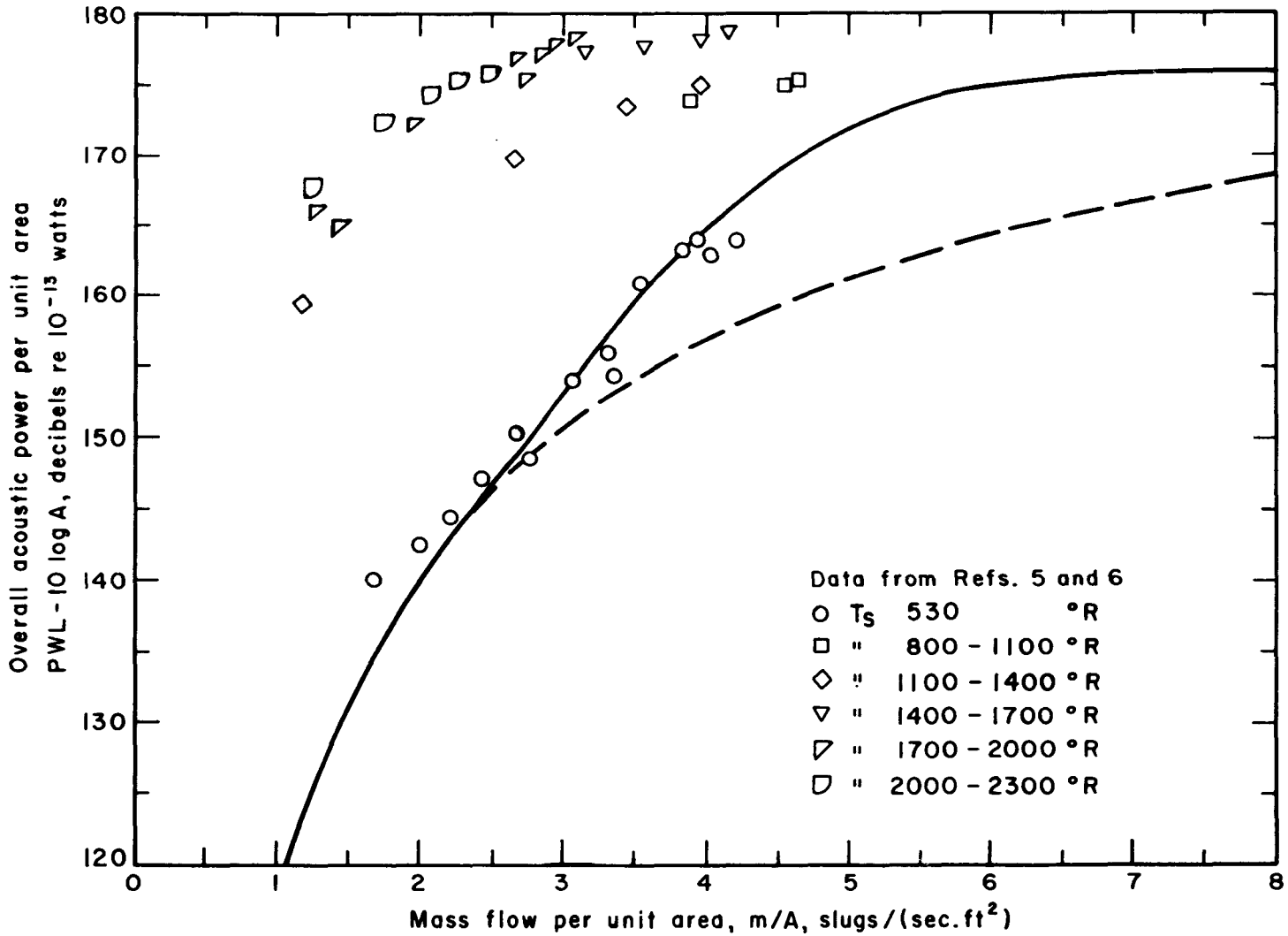

Figure 14. Acoustic Performance of Four-Inch Conical Nozzle
(a) Size Normalization Only

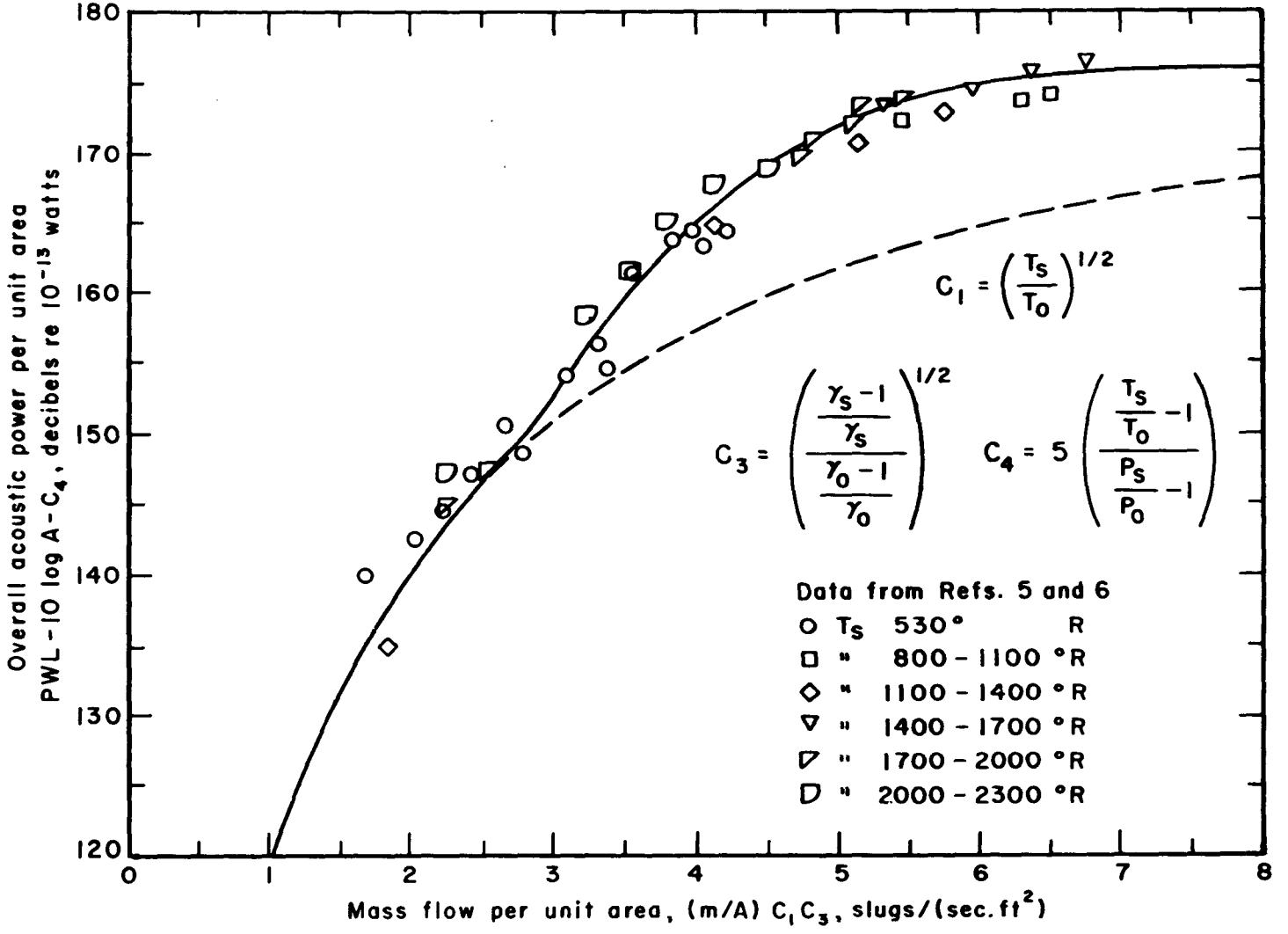

Figure 14. Acoustic Performance of Four-Inch Conical Nozzle
(b) Size and Temperature Normalization

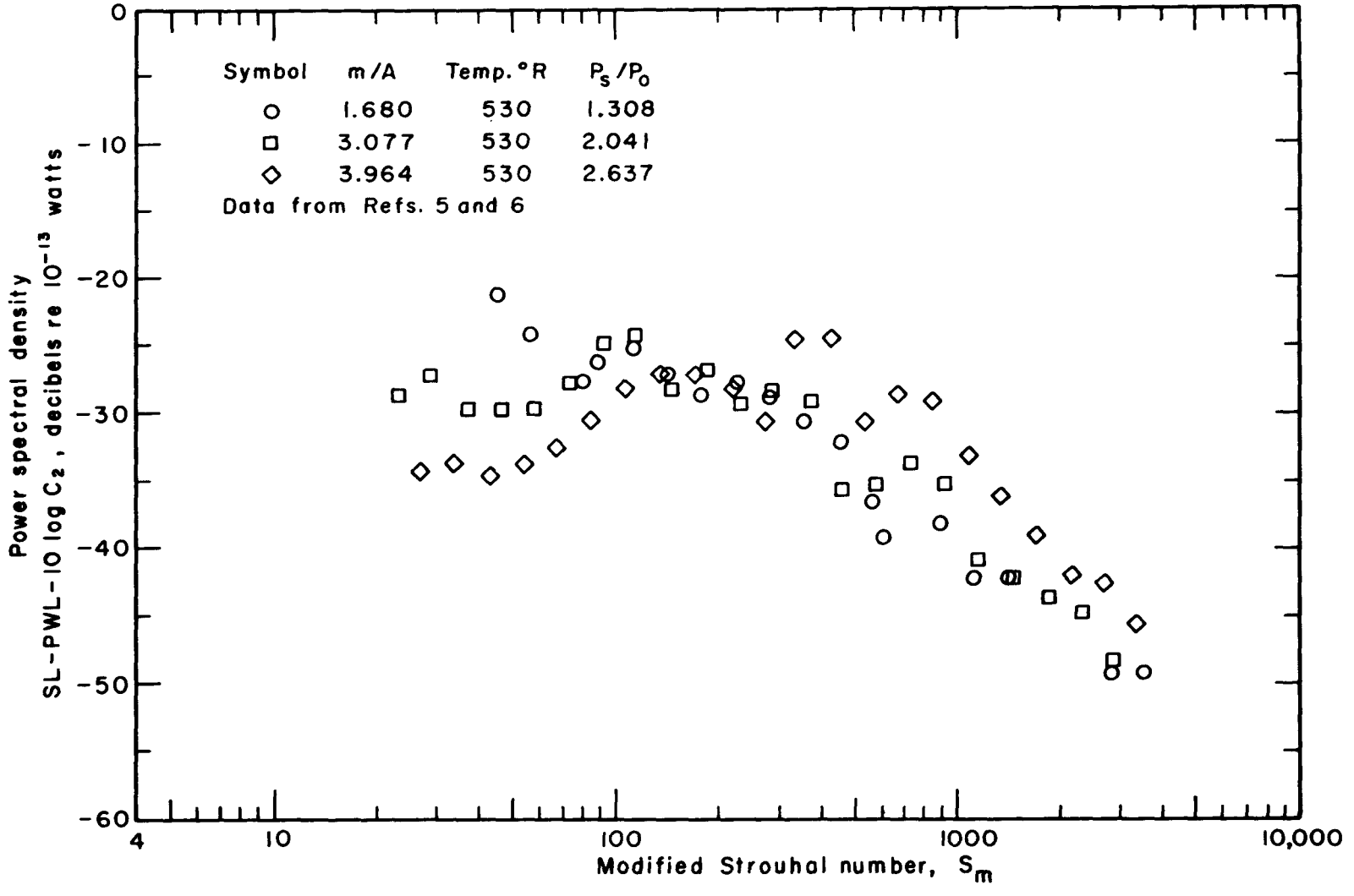

Figure 15. Normalized Frequency Spectrum of Four-Inch Conical Nozzle
(a) Run 16

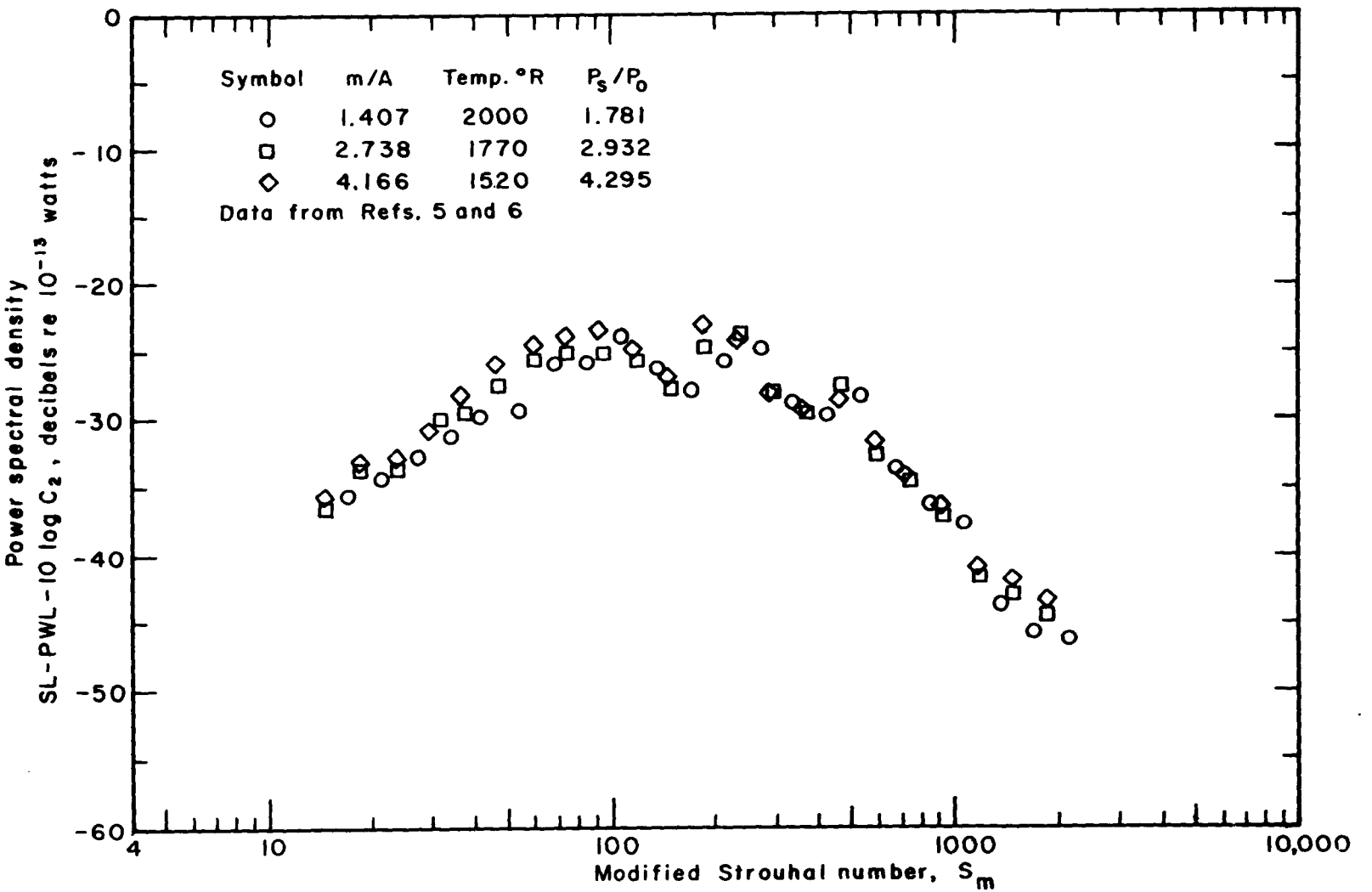

Figure 15. Normalized Frequency Spectrum of Four-Inch Conical Nozzle
(b) Run 17

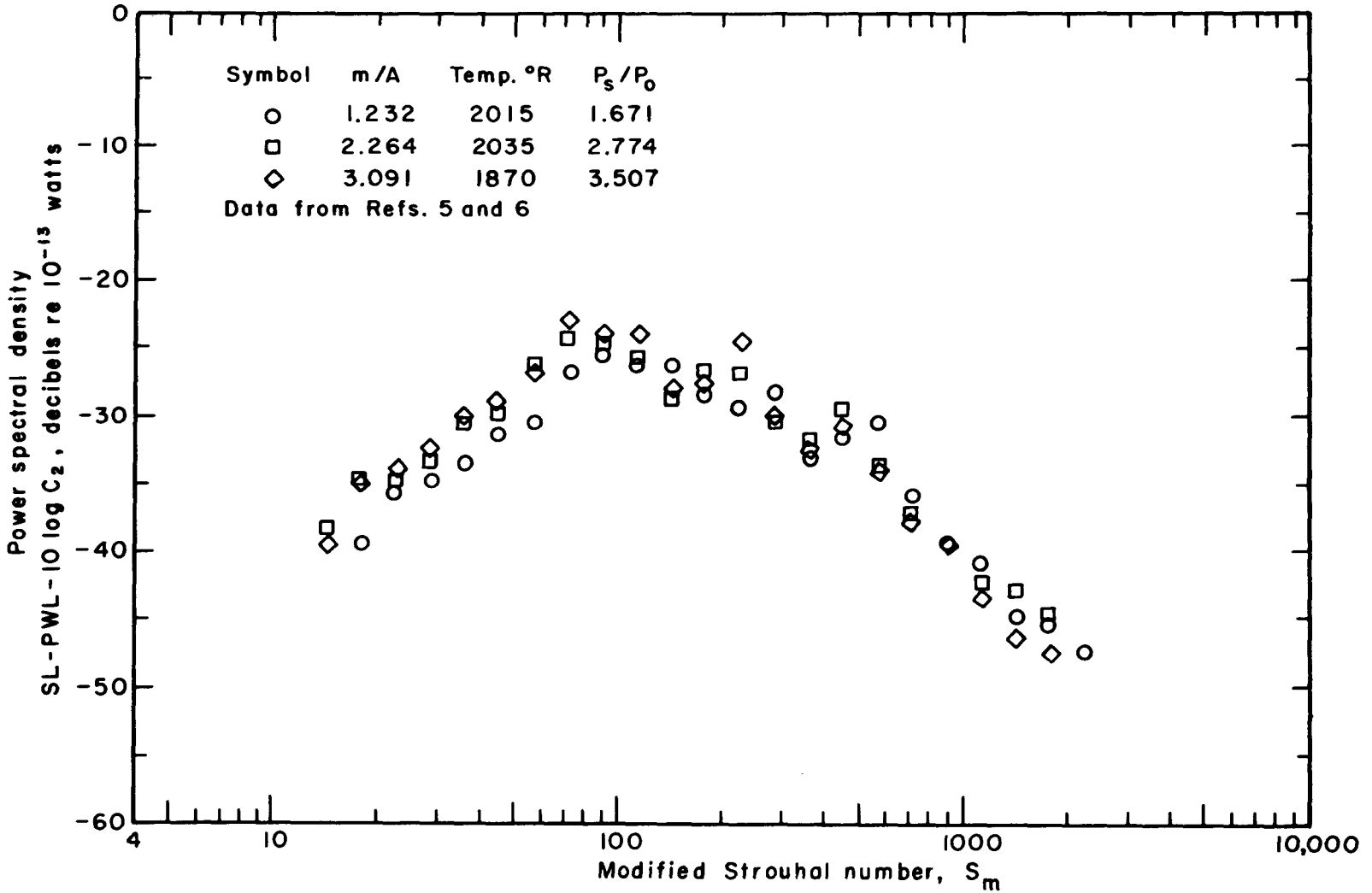

Figure 15. Normalized Frequency Spectrum of Four-Inch Conical Nozzle (c) Run 18

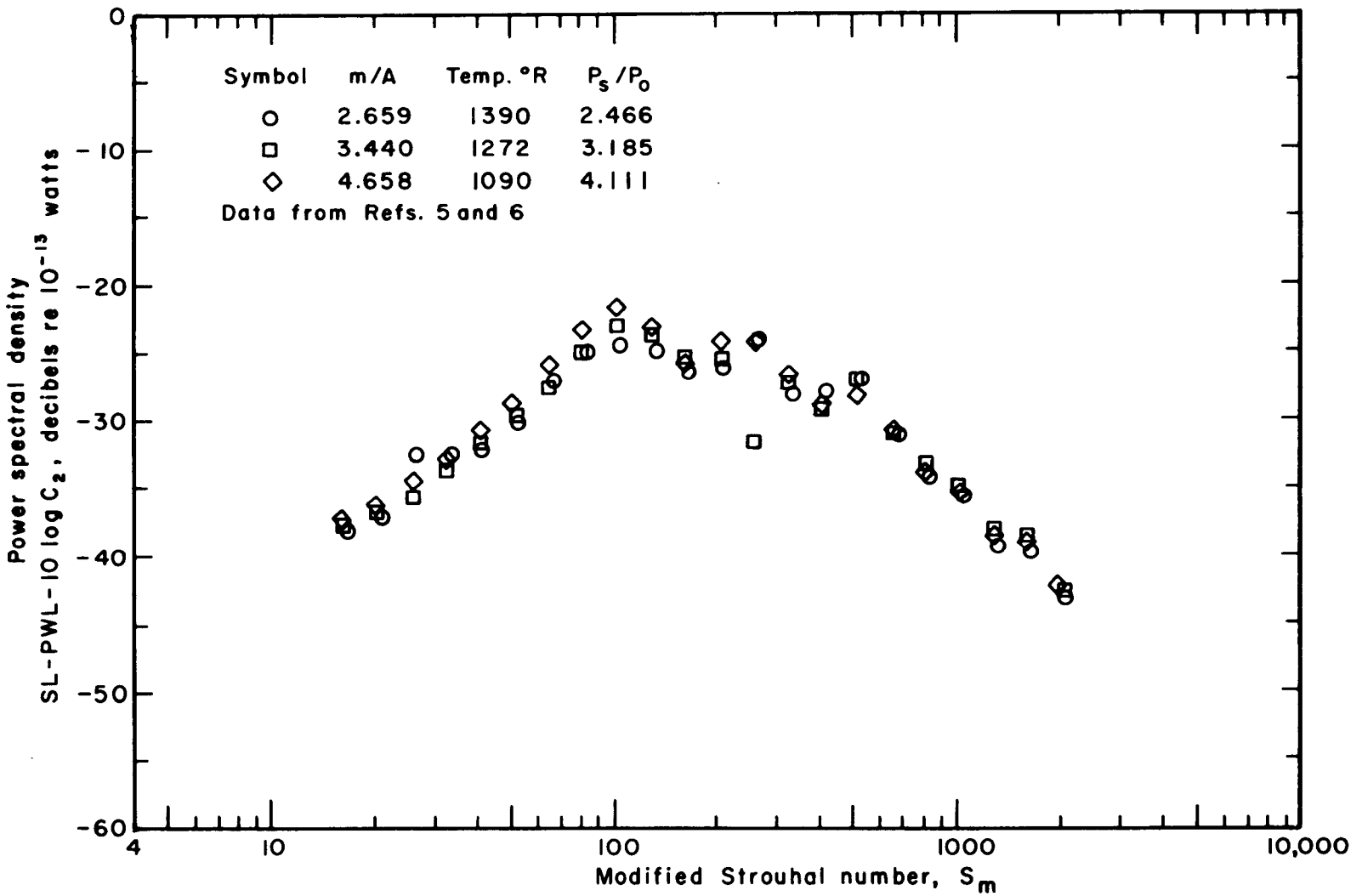

Figure 15. Normalized Frequency Spectrum of Four-Inch Conical Nozzle
(d) Run 19

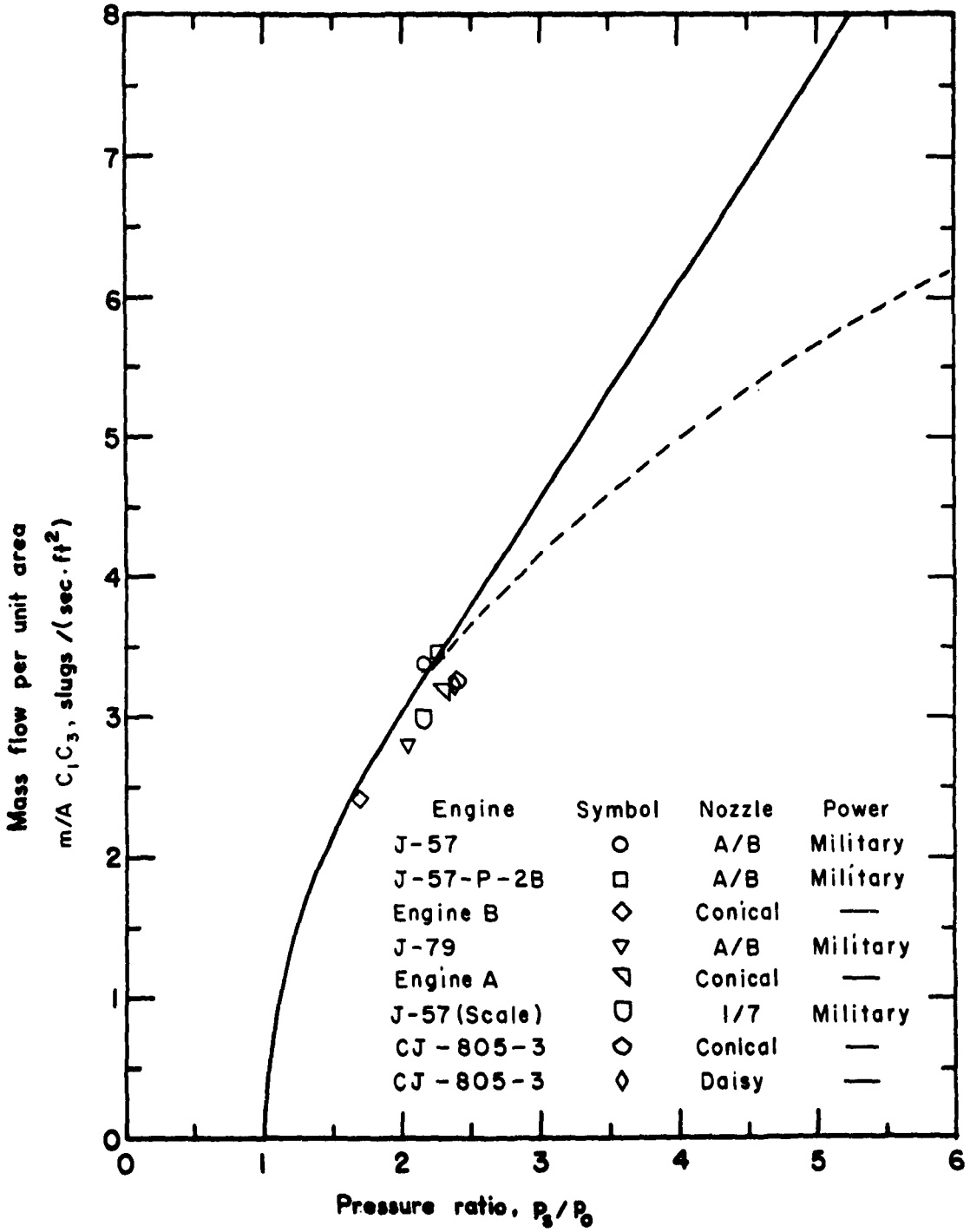

Figure 16. Normalized Flow Performance of Jet Engines

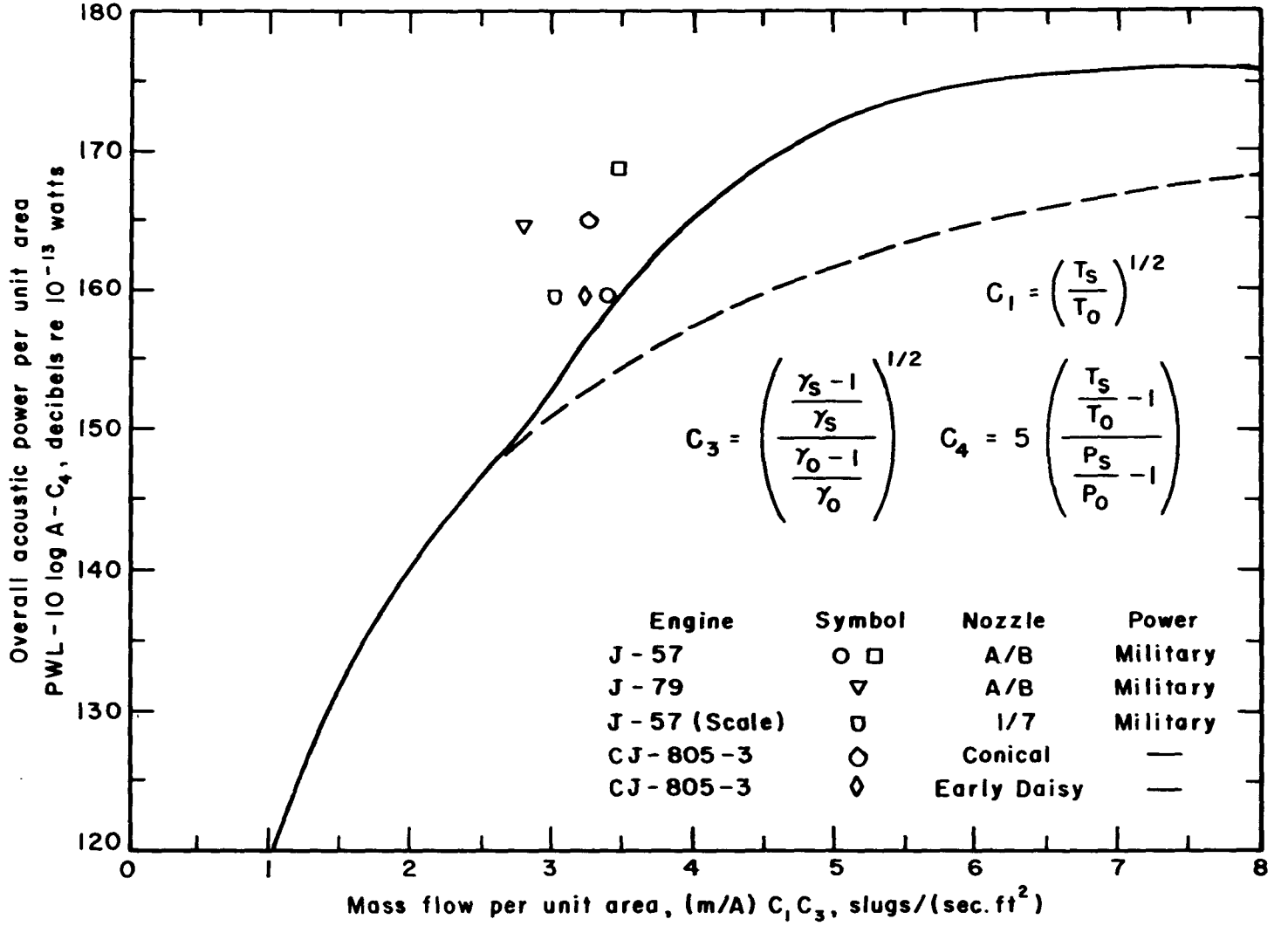

Figure 17. Normalized Acoustic Performance of Jet Engines

(a) Standard Engines

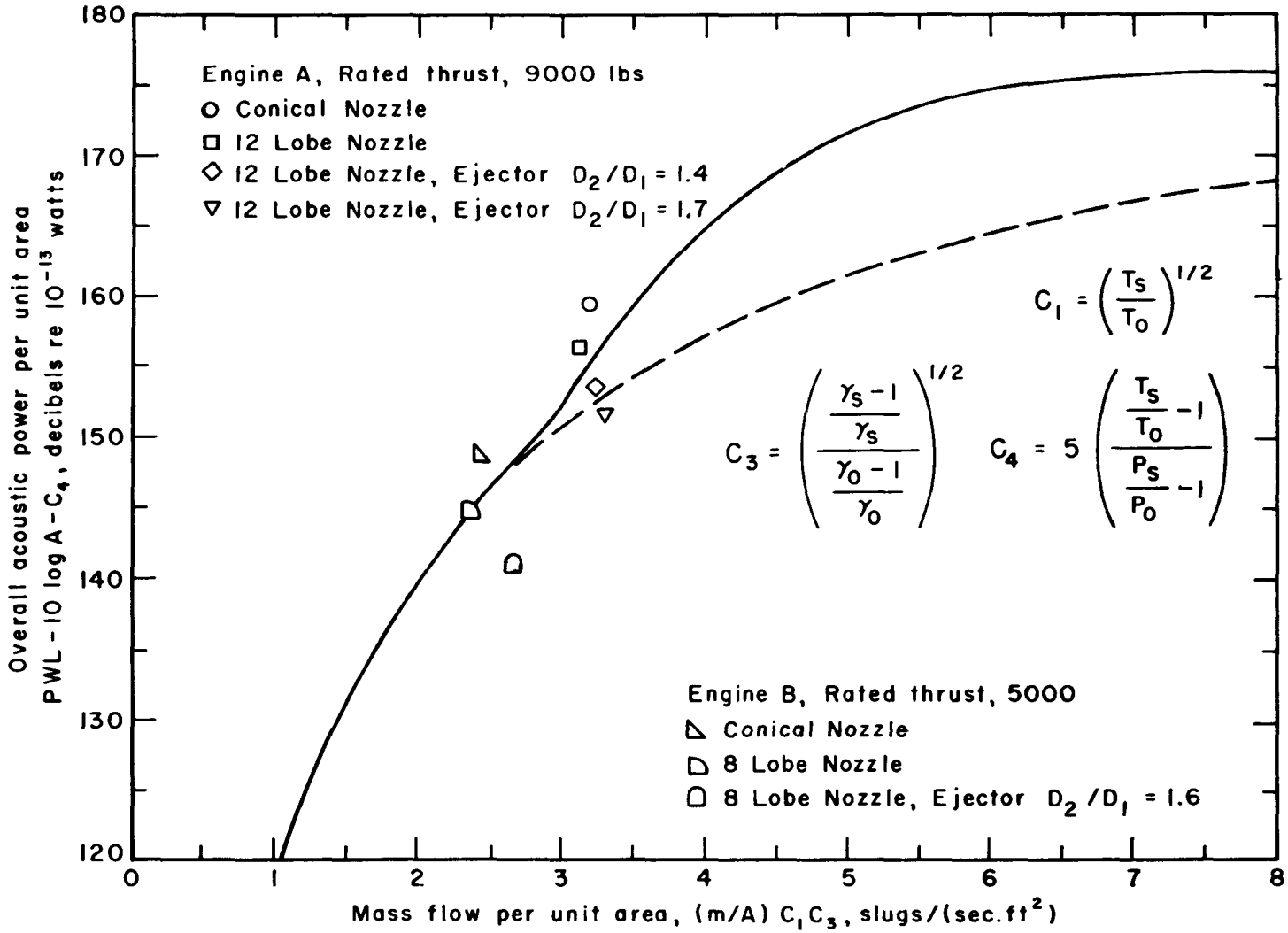

Figure 17. Normalized Acoustic Performance of Jet Engines
(b) Special Engines (Ref. 9)

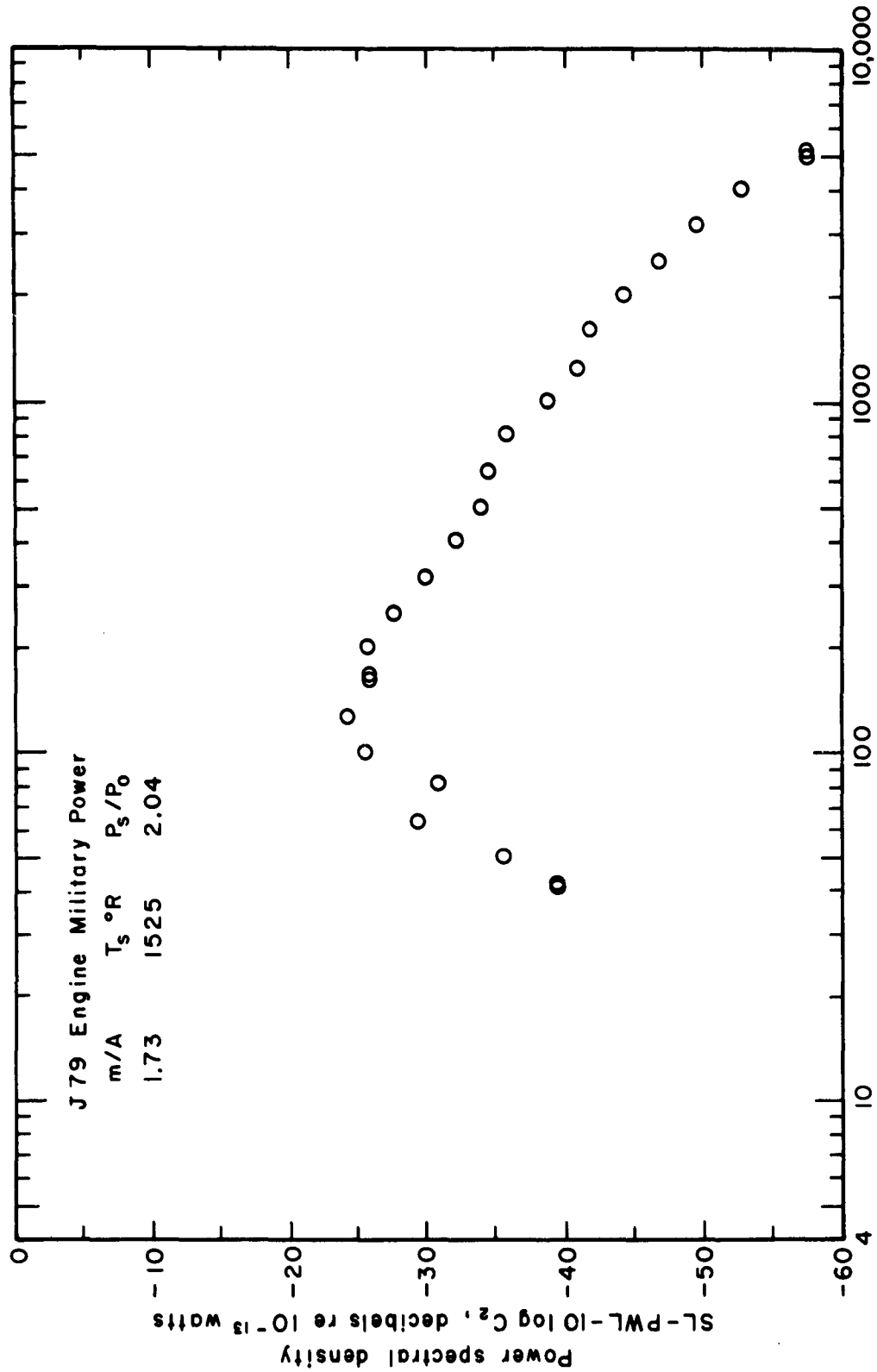

Figure 18. Normalized Frequency Spectrum of J79 Engine

FUNDAMENTAL STUDY OF JET NOISE GENERATION AND SUPPRESSION

Volume I

EXPERIMENTAL AND THEORETICAL INVESTIGATIONS OF MODEL JET EXHAUST STREAM NOISE AND THE DEVELOPMENT OF NORMALIZING PARAMETERS FOR SIZE AND TEMPERATURE

Part II

AN ACOUSTICAL SIMILARITY DERIVATION FOR SUPERSONIC PLUG NOZZLES

by

A. Peter
R. Kamo

ASD-TDR-63-326

SECTION I

THEORY

INTRODUCTION

The Dynamics of Fluids and Combustion group have continued their work on the theoretical treatment of the jet noise problem. The research effort has been expended in four main areas during the past year: (1) continued effort in seeking solution to the wave equation, (2) specific analysis of the annular plug nozzle, (3) correlation of data with cold jet experiments, and (4) laboratory set-up of hot jet facility.

The theoretical study with respect to a solution of the non-linear wave equation has thus far yielded no valid and rigorous solution to the jet noise problem. A plausible, more simple and expedient approach to the problem was investigated by the scientific personnel. The new approach to the supersonic jet noise problem is based on the similarity relationship using the shock wave as a parameter. Preliminary analysis of the extended plug nozzle and its correlation with the cold jet experiments appears very encouraging at this point. The hot jet facility was completed to obtain hot jet noise data and thrust data. However, due to breakdown of the laboratory turbo compressor, no hot jet noise or thrust data are available at this time.

THEORETICAL CONSIDERATIONS

The theoretical study of the jet noise phenomena have not, thus far, yielded a generally valid and mathematically rigorous solution of the jet noise problem by considering the non-linear wave equation. The ARF scientific personnel, who have been investigating the jet noise problem for the past three years, are of the opinion that the scarcity of data available at present for the solution of the problem is the major cause of the difficulty. To summarize this conclusion in a more mathematical way we note that the general solution of the jet noise problem must satisfy the following two basic conditions.

1) The acoustic equation governing the jet noise problem must be dissipative, i.e., the equation cannot be generated by a variational criterion. This, in turn, implies that the equation cannot be self-adjoint.

2) The eigenvalue spectrum of the solution must be continuous. Any discrete eigenvalue spectrum will not correspond to the actual physical phenomena due to the fact that the jet noise spectrum has a continuous frequency band.

From condition 1) we deduce that since the linear wave equation is generated by variational principles, the non-linearity of the jet noise

---

Manuscript released by authors 31 March 1963 for publication as an ASD Technical Documentary Report.

equation may have the physical significance of dissipation. Thus, the jet noise equation cannot be of the self-adjoint type. More precisely, since the concept of self-adjointness applies to the initial data as well, we infer that either the equation governing the jet noise problem, or its boundary data, or both, must be non-self-adjoint.

From condition 2) we infer that the given boundary data for the acoustic jet equation must generate a continuous frequency spectrum. In the case of linear equations this requirement usually indicates the presence of infinite boundaries.

On the other hand, both analytical and empirical considerations of the jet noise problem indicate the complete lack of a definite geometrical boundary, since the generating disturbances are by their very turbulent nature, in a perpetual process of change. For had we known the exact geometrical boundary of the sound-generating disturbances as well as their intensity distribution as a function of space coordinates and time, the solution of the problem could be accomplished by a single retarded-potential integration, extending over the perturbed region - a fact which was derived rigorously by M. J. Lighthill and other famous investigators in the classic jet noise literature.

As it is, the scarcity of available data relating to the above-mentioned phenomena, causes the formidable difficulties in the derivation of a rigorous basic solution of the problem.

The above considerations hold generally true for both, subsonic and supersonic flows. However, in the case of supersonic flows the appearance of a definite shock wave structure in the flow region - a structure which is a function of both - nozzle geometry and pressure ratios may have a great significance in mathematical considerations of supersonic flow noise generation.

In contrast to the characteristic parameters governing subsonic flows, the shock wave structure forms a definite geometrical pattern for a given pressure ratio and nozzle geometry.

Thus, if we decide to characterize our problem not in terms of nozzle geometry and flow parameters, but in terms of the shock wave structure caused by these unknowns, we may have gained a two-fold advantage:

Firstly, instead of considering both, the geometrical properties of the nozzle and the flow parameters, we would combine all these characteristics into one basic relationship; namely, the shock wave configuration caused by the above properties.

Secondly, the space distribution of the shock waves can be readily determined, both experimentally and to a lesser degree analytically, by the use of the steady-state solutions of the hyperbolic, quasi-linear equations of motion.

Moreover, the plausibility of such an approach is already encountered in classical literature on the subject. From the well-known Prandtl relation* we know that a sound wave is nothing but an infinitesimally weak shock. On the other hand, the present approach dictates an investigation into a finite shock condition as a conglomeration of sound waves causing a discontinuity-surface of acoustic excitations.

It should also be noted that the above approach does take into account dissipation effects. For the quasi-linear supersonic flow equations, i.e. the one dimensional unsteady wave flow as well as the Prandtl Mayer flow, are non-dissipative. This implies, that, generally, the assumption of discontinuities in the derivatives of functional variables is still compatible with a conservative field. Obviously this is not so in the case when the discontinuities are assumed to be in the variables themselves, for then dissipation takes place, and this is true for both supersonic and subsonic flows. Thus in the case of supersonic flow we get a shock condition whereas for subsonic flow we obtain a vortex sheet. Both cases introduce dissipation in the physical phenomena.

FIRST APPROXIMATION - A SIMILARITY DERIVATION

The criterion of using the shock wave structure as a noise-generating parameter immediately suggests many possibilities of attacking the jet noise problem for supersonic nozzles. Obviously, the intensity of the acoustic excitations would be a function of the shock-strength, also the shock-strength is a parameter which may be computed in terms of flow variables by known theoretical methods. Moreover, the geometry of the shock wave structure is experimentally determinable.

Considering the three dimensional shock conditions we have the following quantities that are conserved when crossing a shock surface:

$$\iint \rho u_i n_i \, ds = M \tag{1}$$

$$\iint (\rho u_i u_j n_j + p n_i) \, ds = I_i \tag{2}$$

$$\iint \left[(e + 1/2 \, u_i u_i) \rho u_j n_j + p u_j n_i \right] ds = T \tag{3}$$

---

* Refer to Appendix I

If we consider an average distribution of variables in equation (1) we have the following:

$$\overline{\rho u_i n_i} = \frac{M}{S} \tag{4}$$

It follows from equation (4) that increasing the shock wave surface while keeping the mass constant decreases the average mass flow per unit area.

Under certain assumptions regarding the distribution of the variables ρ, u_i and p before and after the shock surface, we can calculate the contributions of equations (1),(2) and (3). However, a three dimensional computation of these shock conditions demands more experimental information as well as a lengthy and tedious computational process. Thus we shall alleviate these considerations to future investigations and as a first approximation, we shall assume that the attenuation function, for a constant mass flow M and constant discharge area A is proportional to the shock wave structure surface area and intensity. Thus we can write that the attenuation function of two geometrically similar nozzles under similar flow conditions as specified above is of the general form:

$$D_A = 10 \log \frac{\iint_{s_i} f_i ds_i}{\iint_{s_j} f_j ds_j} \tag{5}$$

Where D_A is the attenuation in decibels, f_i and f_j are the given attenuation functions and s_i and s_j are the respective shock wave surfaces of the similar nozzles and under similar flow conditions (summation convention is not used).

It is again emphasized that the subsequent derivation is based upon geometrical and flow similarity. Its sole purpose is to give an indication of some possible physical trends, which take place when the shock wave surface is expanded, while keeping the flow variables constant. Also the similarity analysis should give us the physical trends resulting from an interaction of a shock wave and an expansion wave of the Prandtl Mayer type as it occurs in the case of a finite tapered plug nozzle.

SECTION II

APPLICATION OF SIMILARITY RELATION TO EXTENDED PLUG NOZZLES

We shall next apply the previously discussed similarity relation to some specific nozzle configurations and flow characteristics.

Thus let us consider two convergent and geometrically similar nozzles of radii r_o and r_1 respectively, such that $r_1 \gg r_o$. Let an infinite plug of radius c be inserted in the nozzle with the larger radii as shown in Fig. 1. We assume here that the plug extends to infinity in both directions so that the flow is not effected by its finite dimensions. Then to preserve the flow field similarity we must have the effective areas of the conventional circular and of the plugged nozzles equal, which results in the relationship:

$$r_1 = \sqrt{r_o^2 + c^2} \tag{6}$$

Referring next to Fig. 11 which is based upon shadowgraph data of the nozzles in question, we shall represent the shock wave surfaces by paraboloids whose focal distance is a function of the given mass flow M. We denote the general equation of the shock waves by

$$y^2 = a\,x \qquad \text{and} \qquad y^2 = b\,x \tag{7}$$

for the conventional circular and the plugged nozzles.

Moreover we must impose a relationship between the mass flow parameters a(m) and b (m), which in the above configurations denote the positioning of the focal distances of two shock wave surfaces. This can be immediately deduced, however, from the theoretical aspects of supersonic flows. The similarity of flow dictates that the shock detachment slopes of the two nozzles be similar. In other words the slopes of the paraboloids at r_o and $\sqrt{r_o^2 + c^2}$ must be equal. This immediately implies that:

$$b = \frac{a}{r_o} \sqrt{r_o^2 + c^2} \tag{8}$$

Now from the shock conditions shown in equations (1), (2), and (3) it can be shown that both the pressure gradients along a streamline and the curvature of the streamline are proportional to the shock wave curvature. It follows that the rate of curvature change along the shock wave is an important physical parameter to be considered in the functional relation of equation (5). To simplify our derivation we shall expand the curvature gradient function about the point of coincidence between the shock wave and the plug, i.e., y = c: Hence, if we let

$$g = \frac{dR}{dy} \tag{9}$$

where R is the radius of curvature of the shock wave, we can write:

$$g = g(c) + \left.\frac{dg}{dy}\right]_{y=c} (y - c) + \left.\frac{d^2g}{dy^2}\right]_{y=c} (y - c)^2 + \ldots \tag{10}$$

In our computation we shall use for simplicity the first term of the expansion in (10) and we shall consider some subsequent terms in the future investigations.

Thus combining equations (6) to (10) and considering relation of equation (5), we obtain the following expression for the attenuation function in (5) assuming

that $\rho = \frac{c}{r_o}$ and $K = \frac{2r_o}{a}$ are our non-dimensional variables.

$$D_A = 10 \log \frac{\left[1 + \rho^2\right]\left[\left(1 + \frac{K^2}{1 + \rho^2}\right)^{3/2}\right]\left[\left(1 + \frac{K^2}{1 + \rho^2}\right)^{3/2} - 1\right]}{\left[(1 + K^2)^{3/2} - 1\right]} \tag{11}$$

where the first term in the expansion of (10) has been considered as boundary data.

It should be noted that the first two terms in the numerator of the attenuation function in (11) represent the reciprocal of the shock wave curvature at y = c for the plugged nozzle. Thus in this first approximation we obtain that the attenuation function is directly proportional to the radius of curvature of the shock wave at y = c. Physically we obtain the result that as the plug radius c grows larger the radius of curvature of the shock wave at the point of intersection with the plug becomes larger and thus contributes to the attenuation function in equation (11).

In the practical case of finite plug extension, particularly when the given plug has a gradual taper at its end, we note that the parameter $\rho = c/r_o$ becomes a function of the mass flow. This is due to the fact that as the shock wave structure reaches the tapered plug portion, the change in ρ will be inversely proportional to the mass flow variation.

For this reason two graphs showing the attenuation of the plugged nozzle when the variable ρ is a function of the mass flow parameter K have been presented in Fig. 2 and Fig. 3 of the next section.

SECTION III

EVALUATION AND CORRELATION

The results of some experimental data and their correlation with the previously derived similarity analysis are presented in this section. A computer program on IBM 1620 was set up for equation (11). The theoretical noise attentuation was calculated for various values of ρ = constant and $\rho = \rho(K)$. Extended plug nozzle experiments which conform with theory were requested from the Acoustics Group. A series of four geometrically similar nozzles were then evaluated in the cold jet facility, and the experimental results were correlated with the theoretical derivations. The results of these studies are presented in the subsequent paragraphs.

THEORETICAL EVALUATION

Equation (11) is plotted and shown in Fig. 2 for various values of ρ = constant showing the noise attenuation as a function of the independent variable K. Note that K denotes the flow parameter. An examination of the graph reveals that for values of ρ from $\rho = 0$ to $\rho = 1$, there is an optimum attenuation of noise intensity. For the higher values of K, there is a maximum attenuation at $\rho = 2$, and any subsequent increase of ρ beyond this point causes a decrease in noise attenuation.

Figure 3 shows equation (11) plotted with ρ as a function of K, and ρ = constant/K where K is again the independent variable. Different values of the constant were chosen so as to best illustrate the trend which this attenuation function follows.

Equation (11) is again plotted with ρ as a function of K in Figure 4 ρ = constant/K^2. This figure shows the importance of the finite plug extension, particularly when the given plug has a gradual taper at the end of the plug. When the shock wave structure reaches the tapered section the change in ρ will be inversely proportional to the mass flow variation.

Figure 5 shows equation (11) plotted with ρ as the independent variable and K as a constant. This illustrates even more vividly the optimum and maximum values for ρ as mentioned for Fig. 2. The greatest attenuation takes place in the region from $\rho = 0$ to $\rho = 1$, and for the higher values of K, a very definite maximum is reached at $\rho = 2$.

EXPERIMENTAL CORRELATION

Figures 6 through 8 show the experimental results plotted together with the theoretical evaluations. All of the nozzles are geometrically

similar and the plug diameters were chosen from those available as being closest to the desired values.

A correlation was made using a 1:1 ratio between the mass flow rate, m/A, and the proportionality constant K, with m/A = 1 corresponding to K = 0. The experimental data were reproduceable to within one decibel at any given mass flow rate.

There are inequalities in the experimental data and a falling off of noise attenuation because of: (1) the mismatching of area ratios, (2) insufficient plug extension, and (3) the geometrical shapes of the plug endings.

The theoretical derivations are based upon the effective area ratio of the plugged nozzle being equal to that of the unplugged nozzle. However, in no case was this similarity ratio maintained in the experimental nozzles. Table I gives these experimental nozzle area ratios used during the tests. It will be demonstrated that as the area of the annulus approaches the area of the unplugged nozzle, the actual attenuation approaches the theoretical values and that the irregularities tend to disappear.

In two (2) cases, experimental data was obtained for a short plug and an extended plug. In both cases, the noise attenuation increased as the plug length was increased. This was accompanied by a tendency to even more closely approach the theoretical attenuation values based upon the concept of an infinite plug length.

Because of limited time, opportunity was not available to obtain experimental data for the theoretical plug end.

In Fig. 6 a combination of nozzle No. 101 and bar B10 was used. The attenuation in noise with respect to the unplugged nozzle No. 100 is plotted, using the correlation described above. Both the short plug and the extended plug experimental data are shown. For this combination, $\rho = 0.595$, and the area ratio is 1.63. The approximate constant for this combination is 8 in the function ($\rho = 8/K^2$).

As the plug length increases it can be seen that the experimental values coincide with the theoretical values for higher mass flow rates also. The irregularities of the attenuation data in the region of K = 5 are as yet unexplained in full, although it is thought to be attributed to the dissimilar area ratio and characteristic frequencies of the experimental set up.

Nozzle 102 was used with plug B20 for the experimental data shown in Fig. 7. Experimental data is available only for the short plug. Nevertheless, this combination was included because of the close value of the area ratio. For this combination, the area ratio is 1.34 and $\rho = 1.475$ using the unplugged nozzle No. 100 as the test basis. The approximate constant is 16 for the function ($\rho = 16/K^2$).

Despite the short plug length, the irregularities are considerably less and the experimental data closely approaches the theoretical values.

In Fig. 8 nozzle 103 and bar B30 were used. The experimental results are compared to the unplugged nozzle no. 100. The area ratio is 2.55 and $\rho = 2.02$. Experimental data was available for both the short and the extended plug.

The value of ρ approached the theoretical value for maximum noise attenuation in this case. The approximate constant is 25 ($\rho = 25/K^2$).

Despite insufficient plug length and the grossly dissimilar area ratios, a maximum attenuation of 15 db was obtained at the higher mass flow rates.

The representative theoretical and actual plug end shapes are shown in Fig. 9. As discussed previously the actual finite dimension of the plug and its tapered end introduce the necessity of assuming that the parameter ρ is a function of the mass flow variable parameter K. Specifically, a good approximation is obtained when we assume that ρ varies as A/K^2 where A is a constant.

SECTION IV

SHOCK WAVE STRUCTURE

Figure 10a and 10b show respectively, the shock wave structure of a supersonic jet emitted from a conventional circular nozzle and a plug nozzle. Although the pressure ratios are quite similar (3.15 vs. 3.45) obvious differences can be noted in the overall shock wave structure and its formations. We can only speculate at this early stage that the rapid dissipation of the shock wave structure can be attributed to the greater exposure of shock surface in accordance with theory. Note the number of shock formations for circular and plug nozzle configurations, respectively. This observation is of extreme interest and further investigation in this direction is highly recommended.

Figures 11 and 12 show the external shock wave formation of both an unplugged convergent circular jet nozzle, and a similar plugged nozzle. The figures are based upon shadowgraphs taken of the actual nozzles in operation as shown in Fig. 10a and 10b.

The numbered shock wave surface components illustrate the matching of these surface elements for the theoretical computation as shown in Figs. 11 and 12.

SECTION V

HOT JET FACILITY

A hot jet facility capable of providing hot jet experiments to determine the effect of temperature was set up in the Fluid Dynamics and Combustion Laboratory. Such information would be of considerable value in correlating and normalizing data with the cold jet experiments as well as determining thrust data. In addition, instrumentation has been assembled to determine other information of value such as velocity distribution, jet mixing, thrust, and shock patterns (shadowgraph).

A portable Continental gas turbine turbo compressor was contemplated for supplying the primary air. Since the compressed air supply as well as the test chamber are portable, tests can be conducted in an open field thus providing data which can be correlated with the anechoic chamber cold jet data. A damaged compressor blade and bearing have forced the hot jet facility inoperative during the contract year.

SECTION VI

DISCUSSION OF RESULTS

To verify the theoretical derivation of equation (11) an unplugged convergent circular jet nozzle was selected and 3 geometrically similar plugged nozzles were chosen for comparison. In two cases, both short and extended plugs were used, and in one case only the short plug was available.

The experimental data was correlated with the theoretical values. Despite irregularities caused by insufficient plug lengths, dissimilar area ratios, and mismatched plug end shapes (Ref. Table I), the experimental data tends to support the theoretical derivation.

Of main interest we find that the acoustic noise attenuation increases as the ratio of the plug diameter to the unplugged nozzle diameter, upon which the similarity relation is based, approaches a theoretical maximum value. The optimum noise attenuation for a given nozzle is obtained when this value approaches unity as can be seen in Fig. 2 and 4.

Equally important we observe that acoustic noise attenuation of a given nozzle increases as the plug length increases. This trend definitely confirms the theoretical derivation based upon an infinite plug length and given mass flow rate.

Furthermore, as the effective area ratios of the similar nozzles approach unity, the irregularities in the experimental data tend to lessen. The experimental noise attenuation tends to increase to a predicted theoretical value (Ref. Fig. 6,7 and 8 and Table I).

Attention is called to the fact that the preceding evaluation and correlation of experimental data was based upon an attempt to maintain the dimensionless radius ratio parameter ρ constant and realize the corresponding area ratio (i.e., condition $r_1 = \sqrt{r_o^2 + c^2}$). It is also possible to consider an 1:1 area ratio and accept the corresponding radius ratio parameter ρ. Possibly better correlation may be obtained. However, due to limited time, this aspect will be considered in future investigation.

SECTION VII

CONCLUSIONS

Based on the theoretical analyses and treatment of the extended plug nozzle for supersonic jet nozzles and further supported by preliminary experimental evidence, the following conclusions have been arrived at as a result of this research investigation.

1. A theory based on similarity relationships treating attenuation qualities of a supersonic plug nozzle with an extended plug has been developed. Preliminary correlation with experimental cold jet data are especially gratifying.

2. The modified shock wave structure and formation of the plug nozzle shows evidence of rapid shock dissipation with corresponding noise attenuation.

3. Noise reduction of 15 db has been obtained with an extended plug nozzle design. Greater noise reduction can be anticipated in conformance with optimum theoretical design parameters and design criteria.

4. Theoretical jet noise reduction parameters and criteria has been established for extended plug nozzles. A computer program was conducted.

5. A satisfactory theoretical treatment of a practical finite plug extension with tapered ends has been validated by experimental data.

6. The acoustic noise attenuation increases as the ratio of the plug diameter upon which the similarity relation is based approaches a theoretical maximum value of ρ equal to unity.

7. Greater acoustic attenuation of the plug nozzle can be obtained with increase in plug length. This is compatible with theoretical consideration of infinite plug length and mass flow rate.

8. Equivalent area ratios between conventional circular and plug nozzles are essential for maximum noise reduction in accordance with theory.

9. A patent disclosure of the extended plug nozzle has been made at the Armour Research Foundation.

10. A hot jet facility has been set up to provide basic acoustic and aerodynamic information for jet noise research investigation. However, its relative importance is questioned because of its limitation and also because of other developments in the research program.

SECTION VIII

FUTURE RESEARCH AREAS

The preliminary theoretical and experimental results obtained during the course of this research investigation have indeed shown promise. The extended plug nozzle appears both feasible and practical. Adequate jet noise attenuation without apparent loss in performance appears within the realm of realization. A simplified theory based on modification of shock structure has done much towards explaining the apparent behavior of the extended plug nozzle. The preliminary results are extremely interesting and encouraging. In view of the successful treatment of the extended plug nozzle for supersonic jet nozzle on a model scale, application to full size engines would logically be the next step. It is felt that a few more basic experiments are needed to establish definite correlation between theory and experiment. Subsequent extension of the work into full scale jet engines can then be made with confidence. To achieve the preceeding objectives, it is suggested that the following areas of research be considered in future jet noise programs.

1. Further correlation experiments are considered essential in establishing concrete trends of the correlation parameters. At the present we can only speculate as to what one might expect if certain parameters are varied. One vital point that should be considered is the maintenance of equivalent areas. Upon the completion of the proposed correlation investigations, the obtained results may further substantiate the basic approach, as postulated in the present report. It is therefore thought that the non-linear wave equation representing the supersonic jet noise problem could be attacked in the same manner.

2. More complete investigation into the shock wave structure and formation should be made by use of shadowgraph or Schlieren apparatus. For if the shock wave structure be regarded as the noise generating parameter, then its acoustic intensity must be proportional to the shock wave strength. Moreover, the geometrical pattern of the shock structures is determinable both experimentally and theoretically, and thus integration over the effective shock wave surface could be performed.

3. Performance data in terms of thrust loss or gain should be obtained for model nozzles. From theoretical consideration some gain in thrust may possibly be obtained by proper design of the extended plug.

4. More complete aerodynamic information such as velocity distribution, temperature distribution, and shock formation may lead to an aerodynamic plug nozzle. Such a nozzle can possibly do away with the solid plug.

5. Study in detail the optimum practical plug length and geometric shape of plug taper at its end.

6. Scaling of various extended plug nozzles to larger size and establish a scaling law.

7. Upon successful development of the scaling law, full size engine application will be the next step in the process of applying the extended plug nozzle design.

8. Extension of current simple supersonic theory to subsonic jets and obtain its design parameters. Whereas in supersonic flow the shock surface represents a discontinuity surface of the flow variables, in subsonic flow a contact discontinuity with no mass flow across it represents a vortex surface. May it not be possible to treat the turbulent regions in a subsonic jet as contact discontinuities which subsequently develop into vortex regions? Obviously this question is left unanswered at this stage.

BIBLIOGRAPHY

Batchelor, G. K., The Theory of Homogeneous Turbulence, Cambridge University Press, 1953

Batchelor, G. K., Proc. Cambridge Phil. Soc. 47, 359 (1951)

Batchelor, G. K., Proc. Roy. Soc. London A195, 513 (1949)

Batchelor, G. K., Proc. Roy. Soc. London A186, 480 (1946)

Courant R, Friedrichs, K. O.; Supersonic Flow and Shock Waves; Interscience Publishers Inc., London, 1948

Antonio, Ferri - Supersonic Flows with Shock Waves, Princeton -High Speed Aerodynamics, Volume VI

"Full Scale Investigation of Several Jet Engine Noise Reduction Nozzles," NACA Report 1387, 1958

Goldstein, S., Modern Developments in Fluid Dynamics, Vol. 1, Clarendon Press, Oxford, 1938

Howarth, "Modern Development in Fluid Dynamics," Oxford, pp. 34-38, 1956

Lighthill, M. J., "On Sound Generated Aerodynamically, Part I. General Theory," Proceedings of the Royal Society, Vol. A, 211, pp. 564-579

Pai, S. I., "Fluid Dynamics of Jets, D", Van Nostrand Company, 1956

Powell, "On the Noise Eminating from a Two-Dimensional Jet above the Critical Pressure," The Aeronautical Quarterly 4, February 1953, pp. 103-122

Proudman, I., "Noise Generation by Isotropic Turbulence," Cambridge, February, 1952

Proudman, I., Proc. Cambridge Phil. Soc. 47, 158 (1951)

Ribner, H. S., "Boundary Layer Induced Noise in the Interior of Aircraft" Institute of Aerophysics, Univ. of Toronto, Rept. No. 51, April 1958

Ribner, H. S., The Sound Generated by Interaction of a Single Vortex with a Shock Wave, Institute of Aerophysics, University of Toronto, June 1959

Ruden, P., "Turbulente Ausbreitungsvorgange ihn Freistrahl, Die Naturwissenschaffen, 21 No. 21/23, May 1933; pp. 375-378

Sanders, "Turbulent Noise Created by Jet Engines," General Electric Report 5761, 222, July 1957

Taylor, G. I., Proc. Roy. Soc. London A151, 421 (1935)

Taylor, G. I., Proc. Roy. Soc. London A164, 476 (1938)

Taylor, G. I., and Batchelor, G. K., Quart. J. Mech. and Appl. Math. 2, I (1949)

von Karman, Th., J. Aeronaut. Sci. 4, 131 (1937)

von Karman, Th., Compt. rend. 226, 2108 (1938)

von Karman, Th., Proc. Natl. Acad. Sci. 34, 530 (1948)

LIST OF SYMBOLS

Symbol	Definition
ρ	Dimensionless parameter, radius ratio
K	Flow parameter
D_A	Noise attenuation in decibels, overall
C	Plug radius
r_1	Plug nozzle radius
r_o	Circular nozzle radius
δ	Density
u_i	Velocity component in the $i^{\underline{th}}$ direction
n_i	Normal unit vector component in the $i^{\underline{th}}$ direction
p	Pressure
e	Internal energy
s	Shock surface
M	total mass flow
I	Total momentum flow and pressure forces
E	Total energy flow and work of pressure forces

APPENDIX I

RELATION BETWEEN SOUND WAVES AND SHOCK WAVES IN GASES *

Let the function $\varphi(x,t)$ denote any property of the fluid (e.g., pressure, density, etc.). Next let us consider that a definite process took place in which the given initial property of the fluid $\varphi_o(x,t)$ changed to $\varphi_1(x,t)$ (e.g., if the fluid went through a process its pressure changed from p_o to p_1 say; and similarly for other variables).

In the following analysis we shall assume these processes to be instantaneous, so that the actual period of duration of the process approaches $t = 0$ in the limit.

Now let us consider a function $h(x,t)$ such that

$$h(x,t) = \int_{x_o}^{x_1} \varphi(y,t)dy \qquad (1-1)$$

Then if the function $\varphi(y,t)$ has undergone a certain process at the point $x = \xi(t)$ such that

$$x_o(t) \leq \xi(t) \leq x_1(t)$$

then we can divide the integral in eq. (1-1) into the two parts

$$x_o(t) \leq y \leq \xi_{-o}(t)$$

and

$$\xi_{+o}(t) \leq y \leq x_1(t)$$

Thus relation from eq. (1-1) becomes:

$$h(x,t) = \int_{x_o}^{\xi_{-o}} \varphi(y,t)dy + \int_{\xi_{+o}}^{x_1} \varphi(y,t)dy \qquad (1-2)$$

---

* Courant and Friedrichs, Supersonic Flow and Shock Waves: Interscience Publishers; 1948

APPENDIX I

RELATION BETWEEN SOUND WAVES AND SHOCK WAVES IN GASES *

Let the function $\varphi(x,t)$ denote any property of the fluid (e.g., pressure, density, etc.). Next let us consider that a definite process took place in which the given initial property of the fluid $\varphi_o(x,t)$ changed to $\varphi_1(x,t)$ (e.g., if the fluid went through a process its pressure changed from p_o to p_1 say; and similarly for other variables).

In the following analysis we shall assume these processes to be instantaneous, so that the actual period of duration of the process approaches $t = 0$ in the limit.

Now let us consider a function $h(x,t)$ such that

$$h(x,t) = \int_{x_o}^{x_1} \varphi(y,t)dy \qquad (1\text{-}1)$$

Then if the function $\varphi(y,t)$ has undergone a certain process at the point $x = \xi(t)$ such that

$$x_o(t) \leq \xi(t) \leq x_1(t)$$

then we can divide the integral in eq. (1-1) into the two parts

$$x_o(t) \leq y \leq \xi_{-o}(t)$$

and

$$\xi_{+o}(t) \leq y \leq x_1(t)$$

Thus relation from eq. (1-1) becomes:

$$h(x,t) = \int_{x_o}^{\xi_{-o}} \varphi(y,t)dy + \int_{\xi_{+o}}^{x_1} \varphi(y,t)dy \qquad (1\text{-}2)$$

---

* Courant and Friedrichs, Supersonic Flow and Shock Waves: Interscience Publishers; 1948

Next we consider the total derivative with respect to time of the function h(x,t) which yields:

$$\frac{dh}{dt} = \frac{d}{dt}\int_{x_o}^{\xi_{-o}} \varphi(y,t)dy + \frac{d}{dt}\int_{\xi_{+o}}^{x_1} \varphi(y,t)dy \qquad (1-3)$$

and differentiating behind the integral sign we obtain:

$$\frac{dh}{dt} = \int_{x_o}^{\xi_{-o}} \frac{d\varphi}{dt}dy + \varphi(\xi_{-o},t)\frac{d\xi_{-o}}{dt} - \varphi(xo,t)\frac{dx_o}{dt} +$$

$$+ \int_{\xi_{+o}}^{x_1} \frac{d\varphi}{dt}dy + \varphi(x_1,t)\frac{dx_1}{dt} - \varphi(\xi_{+o},t)\frac{d\xi}{dt} + o\,; \qquad (1-4)$$

Now let the region under consideration be such that

$$x_o(t) \leq y \leq x_1(t) \qquad (1-5)$$

$$\lim x_o(t) = \xi_{-o}(t) \text{ and}$$

$$\lim x_1(t) = \xi_{+o}(t):$$

and we must have

$$\int_{x_o}^{\xi_{o}} \frac{d\varphi}{dt}\,dy = \int_{\xi_{+o}}^{x_1} \frac{d\varphi}{dt}\,dy = 0 \qquad (1-6)$$

And consequently eq. (1-4) yields

$$\frac{dh}{dt} = \varphi(\xi_{-o},t)\frac{d\xi_{-o}}{dt} - \varphi(x_o,t)\frac{dx_o}{dt} + \varphi(x_1,t)\frac{dx_1}{dt} - \varphi(\xi_{+o})\frac{d\xi_{+o}}{dt} \qquad (1-7)$$

Now let the surface of the jump discontinuity move with a velocity u; then

$$\frac{d\xi_{-o}}{dt} = \frac{d\xi_{+o}}{dt} = U \qquad (1-8)$$

moreover let us define:

$$\frac{dx_o}{dt} = u_o; \quad \frac{dx_1}{dt} = u_1; \quad \varphi(\xi_{-o}, t) = \varphi(x_o, t) = \varphi_o \tag{1-9}$$

$$\varphi(\xi_{+u}, t) = \varphi(x_1, t) = \varphi$$

then we have:

$$\frac{dh}{dt} = \varphi_1(u_1 - U) - \varphi_o(u_o - U): \tag{1-10}$$

Hence if we denote the velocities relative to the velocity U as:

$$u_1 - U = V_1 \tag{1-11}$$

$$u_o - U = V_o$$

We can write eq. (1-10) in the form:

$$\frac{dh}{dt} = \varphi_1 V_1 - \varphi_o V_o; \tag{1-12}$$

Where the time derivative of h(x,t) is expressed in terms of the values of the function $\varphi(y,t)$ and relative velocities before the process and after the process through which the fluid has passed instantaneously.

Let us now apply the previous derivations to the study of the equations of motion in the presence of a jump discontinuity.

From the equation of continuity we have:

$$\frac{d}{dt} \int_{x_o}^{x_1} \delta \, dx \tag{1-13}$$

which by eq. (1-12) yields

$$\delta_1 v_1 - \delta_o v_o = 0 \tag{1-14}$$

From the momentum equation we have:

$$\frac{d}{dt} \int_{x_o}^{x_1} \delta u dx = - \int_{x_o}^{x_1} \frac{\partial \delta}{\partial x} \, dx \tag{1-15}$$

which yields

$$\rho_1 u_1 v_1 = \rho_o u_o v_o = - p_1 + p_o \tag{1-16}$$

Now let us consider the mass flow m given by

$$\rho_o v_o = \rho_1 v_1 = m: \tag{1-17}$$

then equation (1-16) can be written

$$mu_1 - mu_o = p_o - p_1 \quad \text{or} \tag{1-18}$$

$$p_1 - p_o = m (U_o - u_1)$$

The above equation can also be written by eq. (1-11)

$$p_1 - p_o = mv_o - mv_1 \tag{1-19}$$

$$= m^2 \left[\frac{1}{\rho_o} - \frac{1}{\rho_1} \right]$$

$$= m^2 \left[\frac{\rho_1 - \rho_o}{\rho_1 \rho_o} \right]$$

Hence

$$\frac{p_1 - p_o}{\rho_1 - \rho_o} = \frac{m^2}{\rho_o - \rho_1} = V_o V_1 \tag{1-20}$$

Now let: ρ_o approach ρ_1 in the limit: then

$$\lim_{\rho_1 \to \rho_o} \frac{p_1 - p_o}{\rho_1 - \rho_o} = \frac{\partial p}{\partial \rho} = a^2 \tag{1-21}$$

where a is the speed of sound.

Hence we have

$$\lim_{\rho_1 \to \rho_o} V_o V_1 = a^2; \tag{1-22}$$

Consequently we see that when a fluid goes through a discontinuous process the discontinuity propagates itself in the form of a sound wave. Thus we conclude that an infinitesimally strong disturbance is propagated in the form of a sound wave.

It follows immediately that a reciprocal relation may be deduced, in which a shock wave may be regarded as a definite source of sound generation.

This in turn implies, that in the case of supersonic flows the shock wave structure could be related to the sound generating properties of the supersonic region in question.

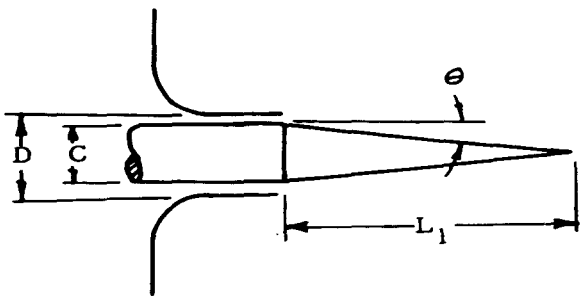

Short Plug

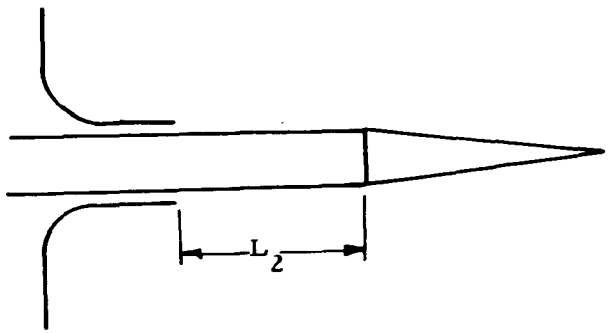

Extended Plug

Nozzle No.	Nozzle Dia. in. D_1	Nozzle Area in^2 A_1	Bar No.	Bar Dia. in C	Bar Area in^2 A_3	L_1 in	L_2	θ Degrees	$= C/D_1$	Area Ratios $\frac{A_2 - A_3}{A_1}$
1 100	0.533	0.233								
$\frac{D_2}{}$		$\frac{A_2}{}$								
2 101	0.750	0.442	B10	0.318	0.0794	1.817	2.53	10	0.595	1.63
3 102	1.000	0.785	B20	0.786	0.4850	4.82	--	9.33	1.47	1.34
4 103	1.375	1.485	B30	1.080	0.9159	6.18	2.0	9.33	2.02	2.55

TABLE I

Combinations of Nozzle and Plug Dimensions Used During Experiments

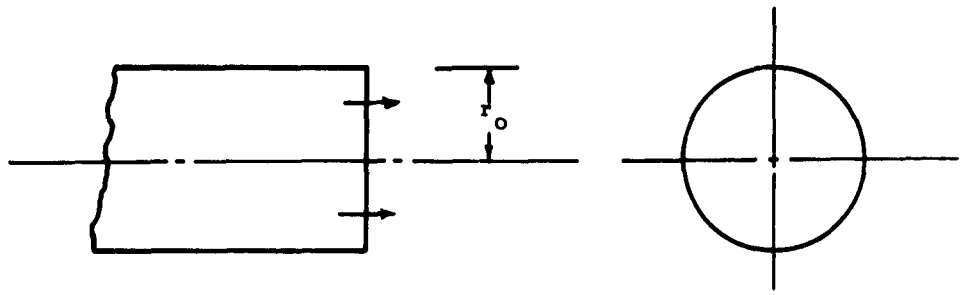

a.) Conventional Circular Nozzle with Radius r_o

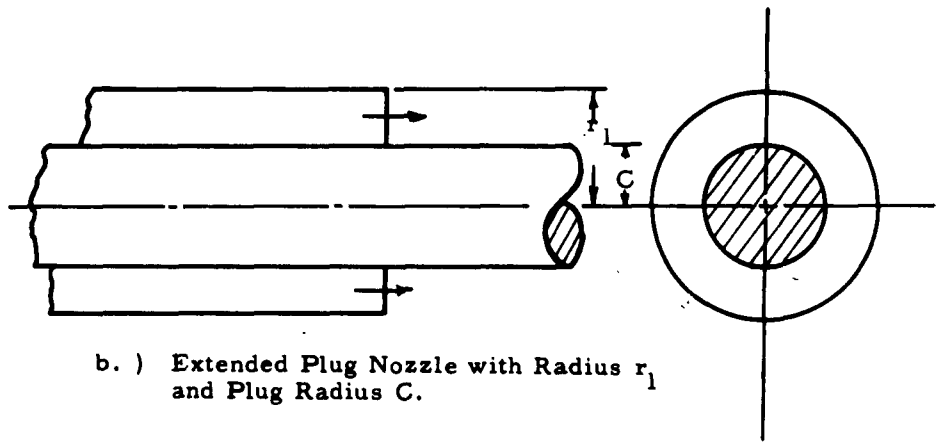

b.) Extended Plug Nozzle with Radius r_1 and Plug Radius C.

Fig. 1 GEOMETRIC CONSIDERATION OF CONVENTIONAL CIRCULAR NOZZLE AND EXTENDED PLUG NOZZLE

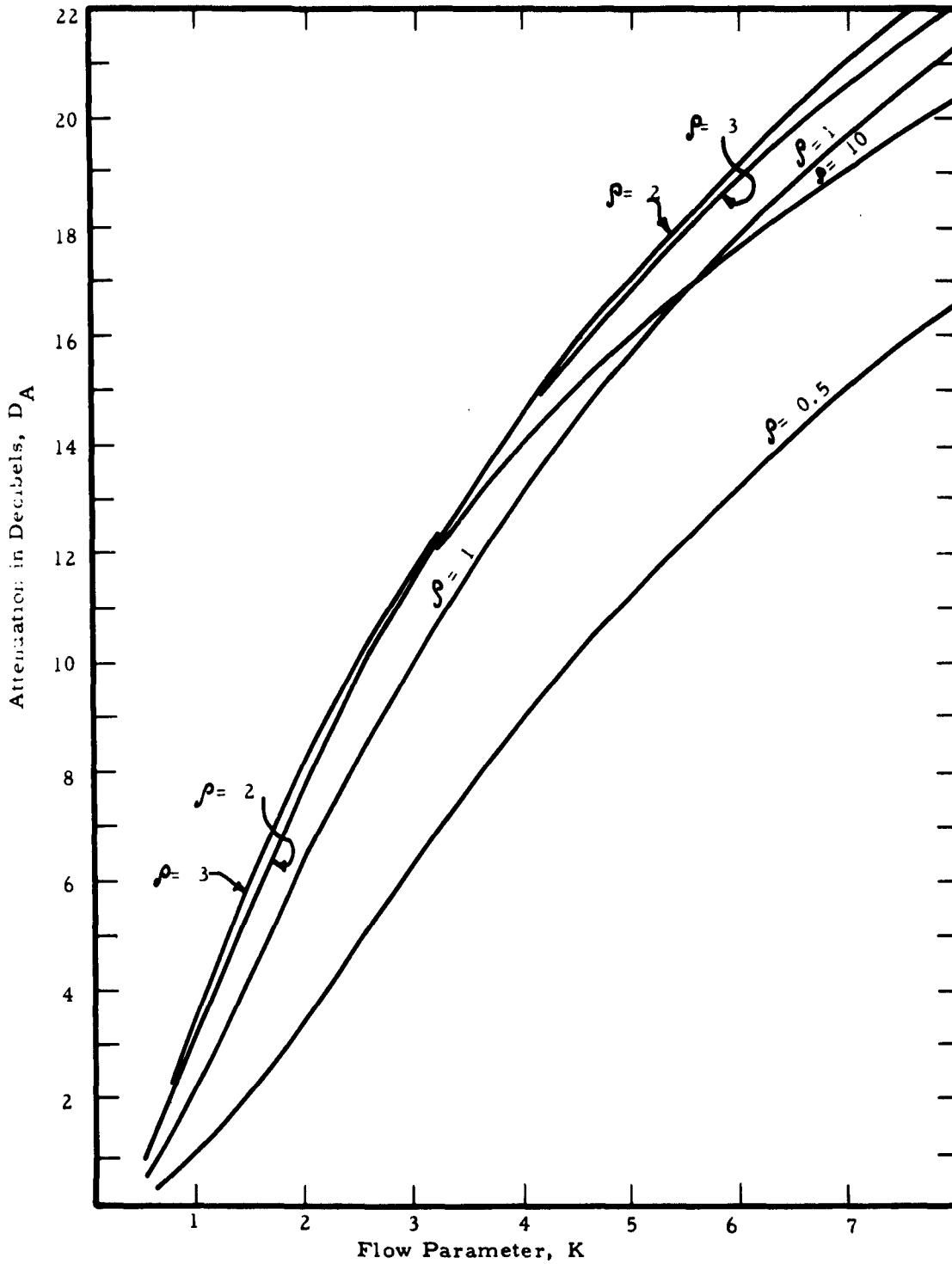

Fig. 2 THEORETICAL ATTENUATION CURVES OF AN EXTENDED PLUG NOZZLE OVER AN EQUIVALENT AREA CIRCULAR NOZZLE. FLOW PARAMETER K PLOTTED AS A FUNCTION OF D_A

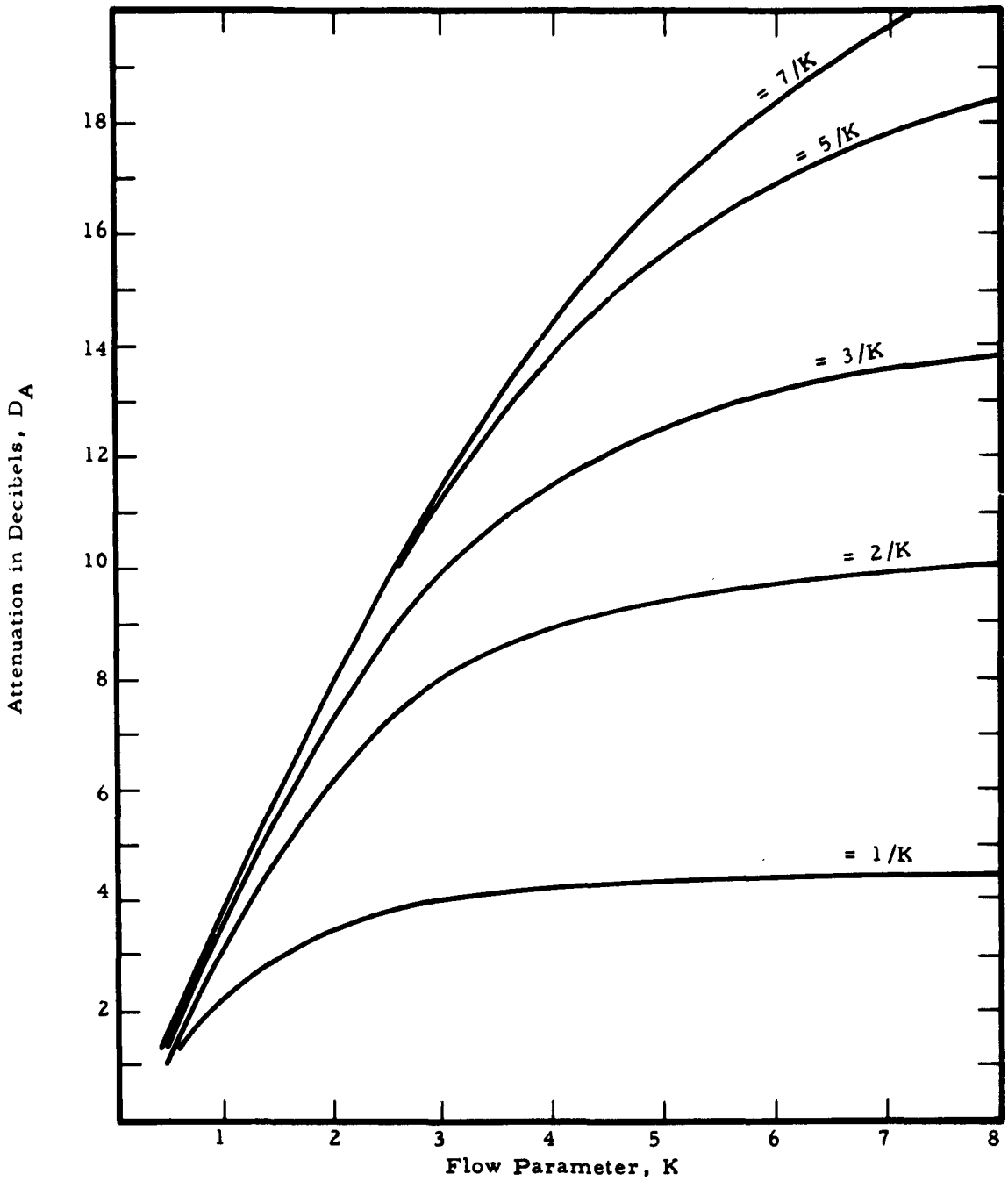

Fig. 3 Theoretical Attenuation Curves of an Extended Plug Nozzle for $\frac{\rho}{K}$ = const/K Plotted Against Attenuation D_A and Flow Parameter

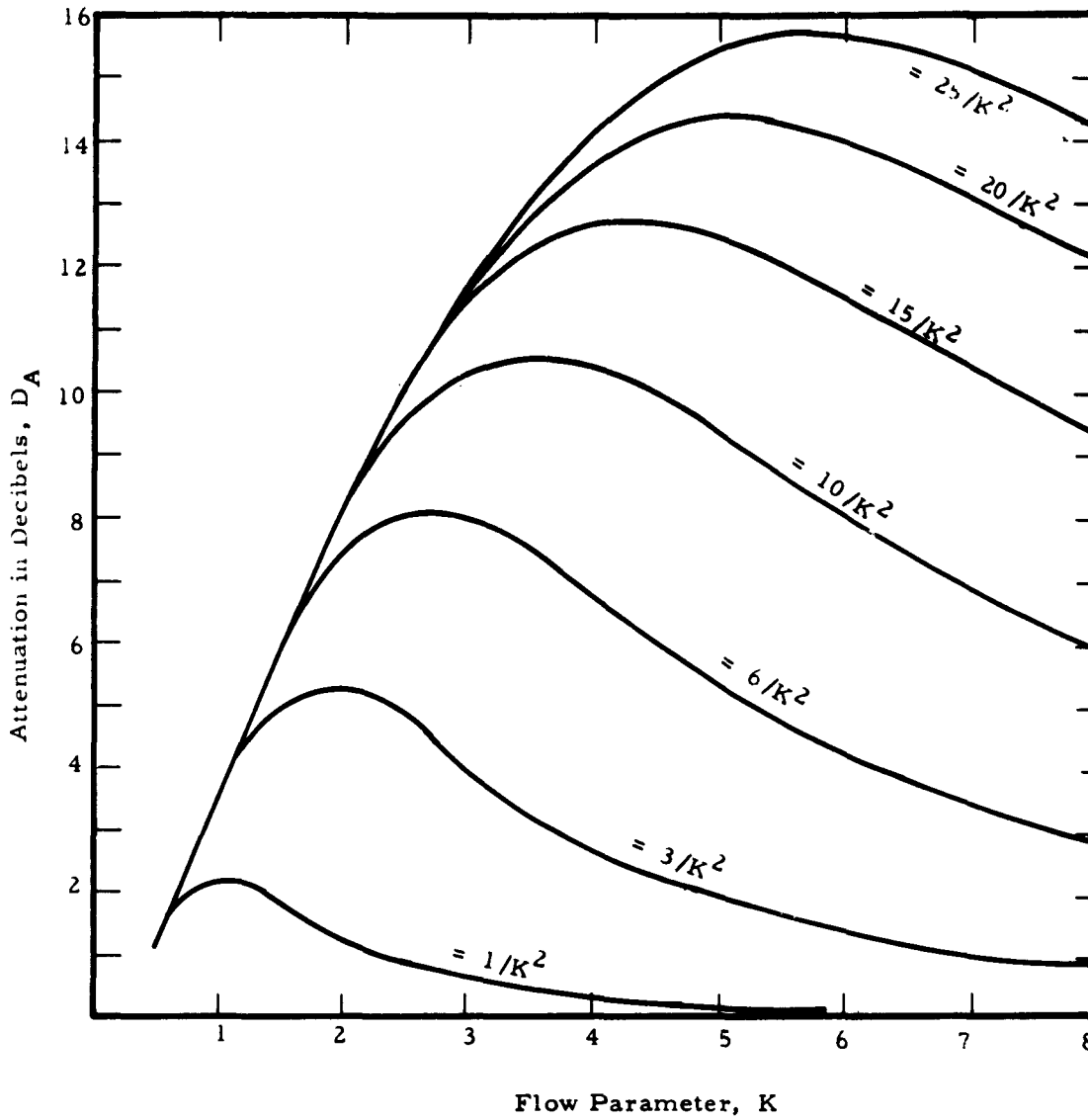

Fig. 4 Theoretical Attenuation Curves for $\rho = \text{const}/K^2$ Plotted Against Attenuation D_A and Flow Parameter K

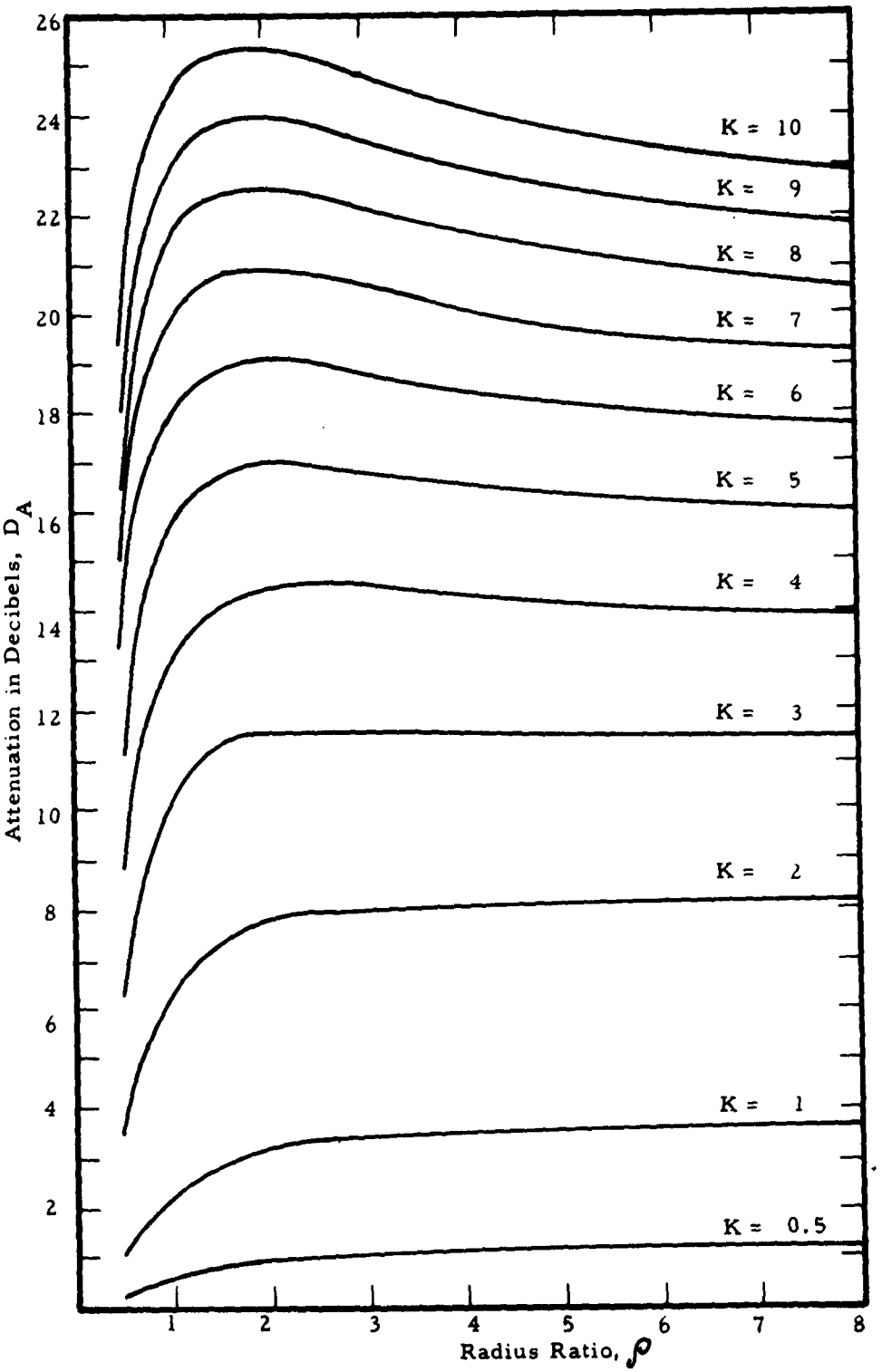

Fig. 5 THEORETICAL ATTENUATION CURVES FOR EXTENDED PLUG NOZZLE FOR VARIOUS FLOW PARAMETERS K PLOTTED AGAINST ATTENUATION D_A AND RADIUS RATIO, ρ.

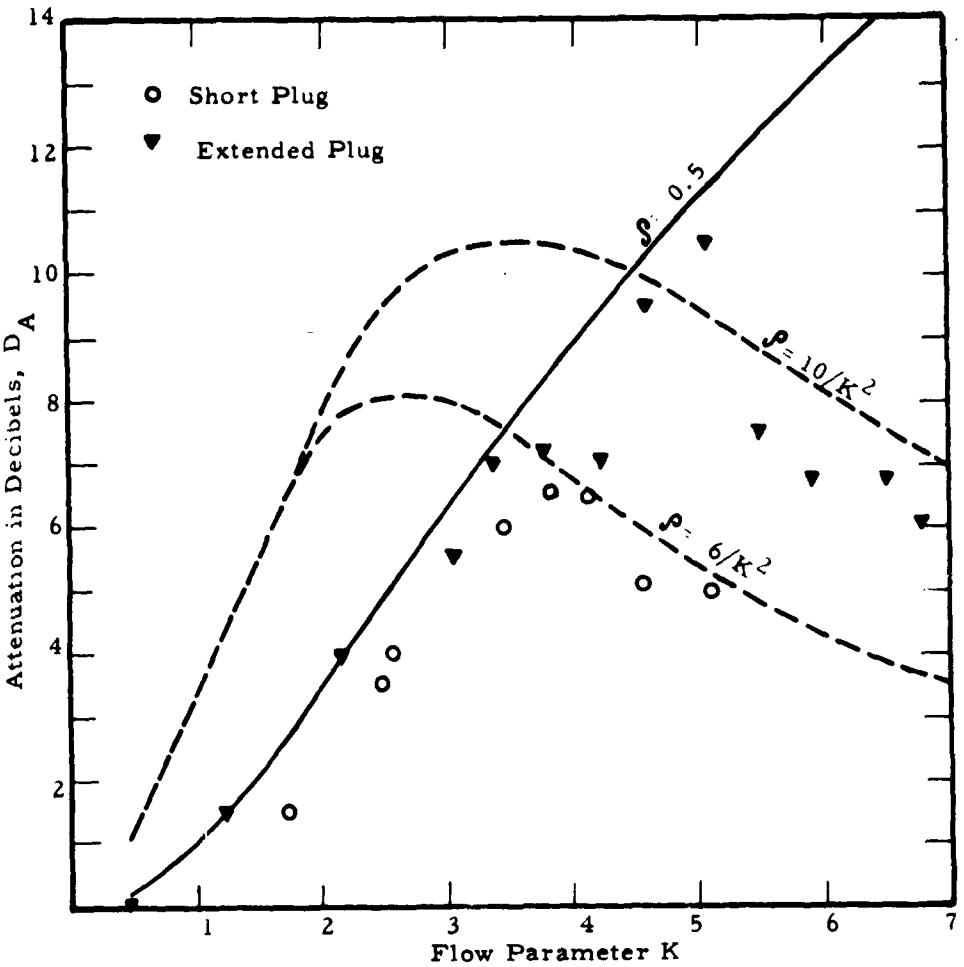

Fig. 6 EXPERIMENTAL RESULTS PLOTTED ON THEORETICAL DERIVATIONS PLUGGED NOZZLE, $\rho = 0.595$

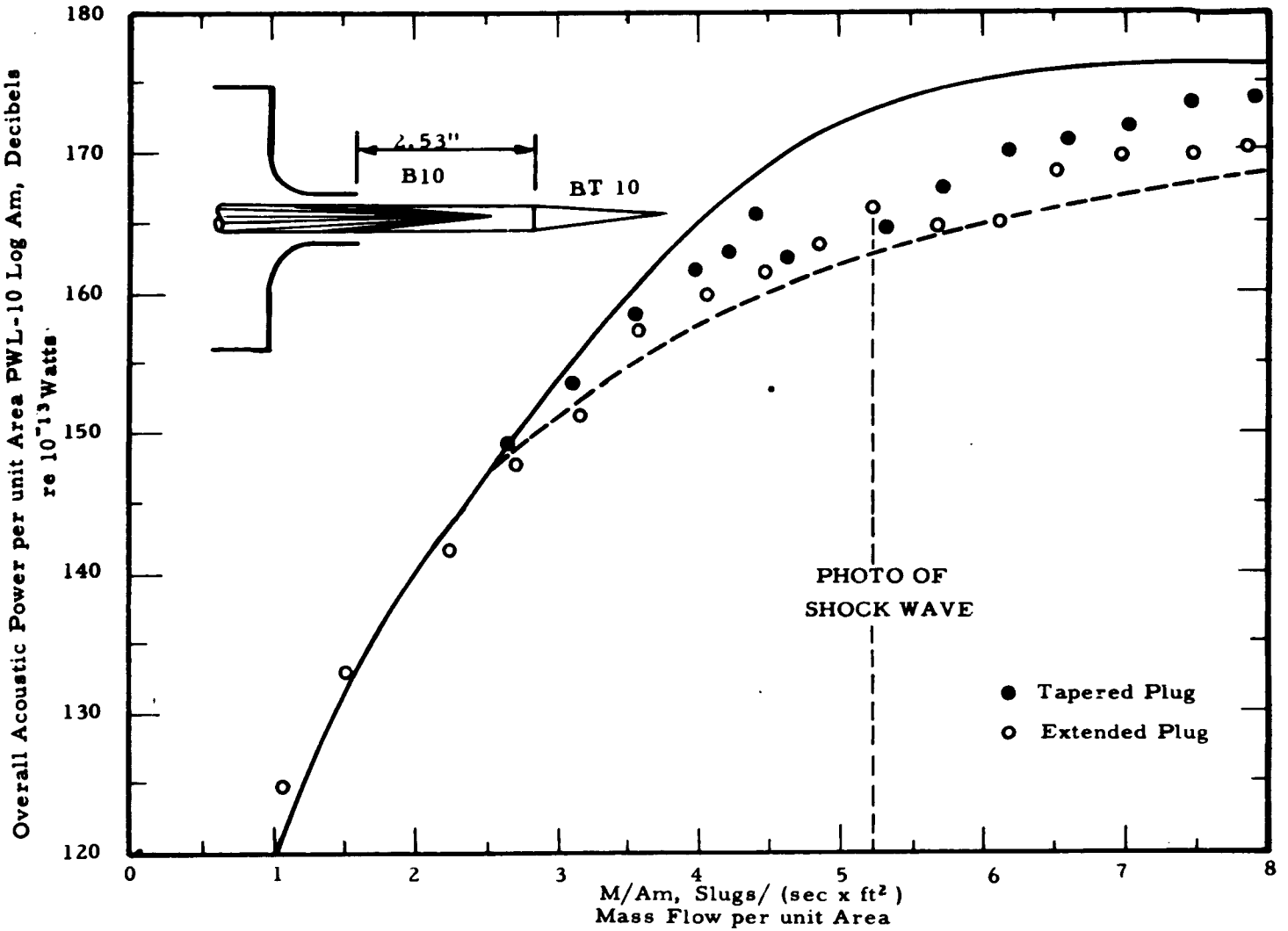

Fig.6a ACOUSTIC PERFORMANCE OF AN EXTENDED PLUG NOZZLE AS COMPARED WITH A TAPERED PLUG

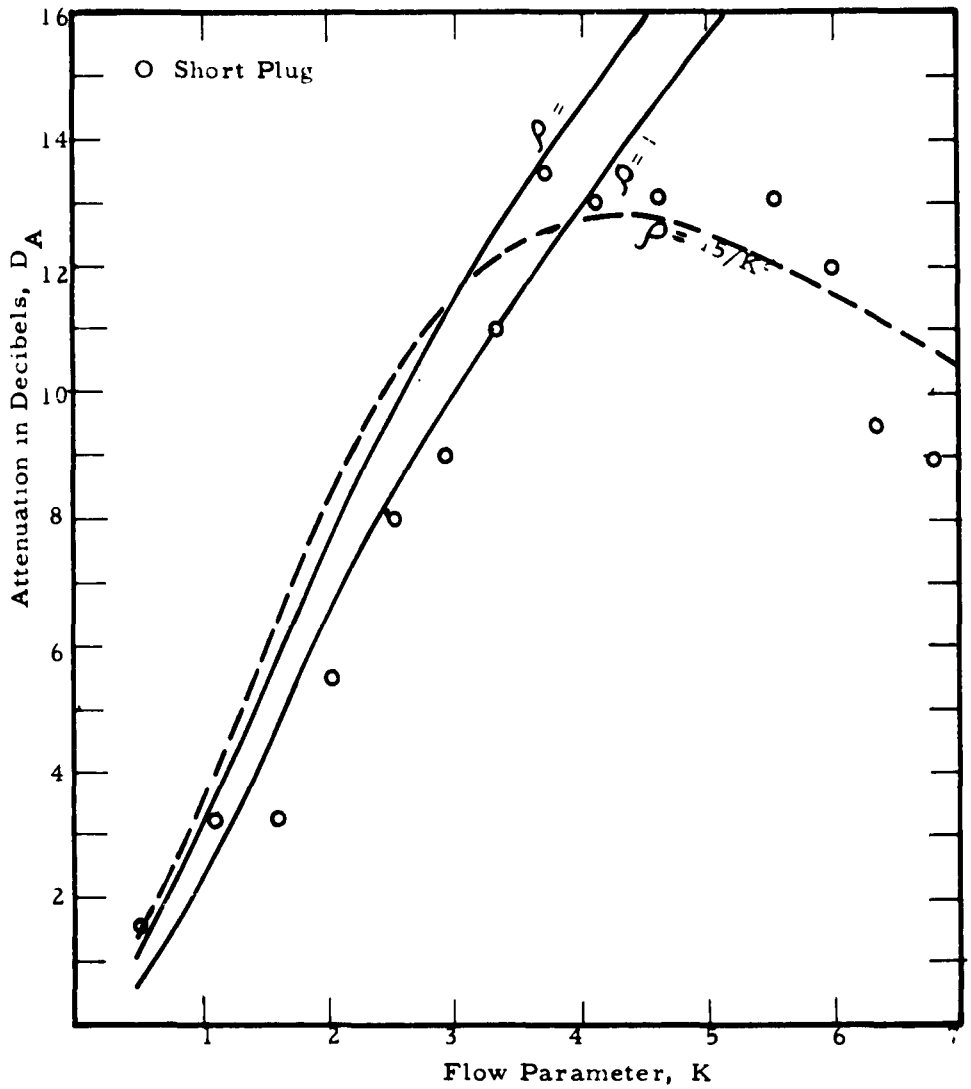

Fig. 7 EXPERIMENTAL RESULTS PLOTTED ON THEORETICAL DERIVATIONS, PLUGGED NOZZLE, ρ= 1.475

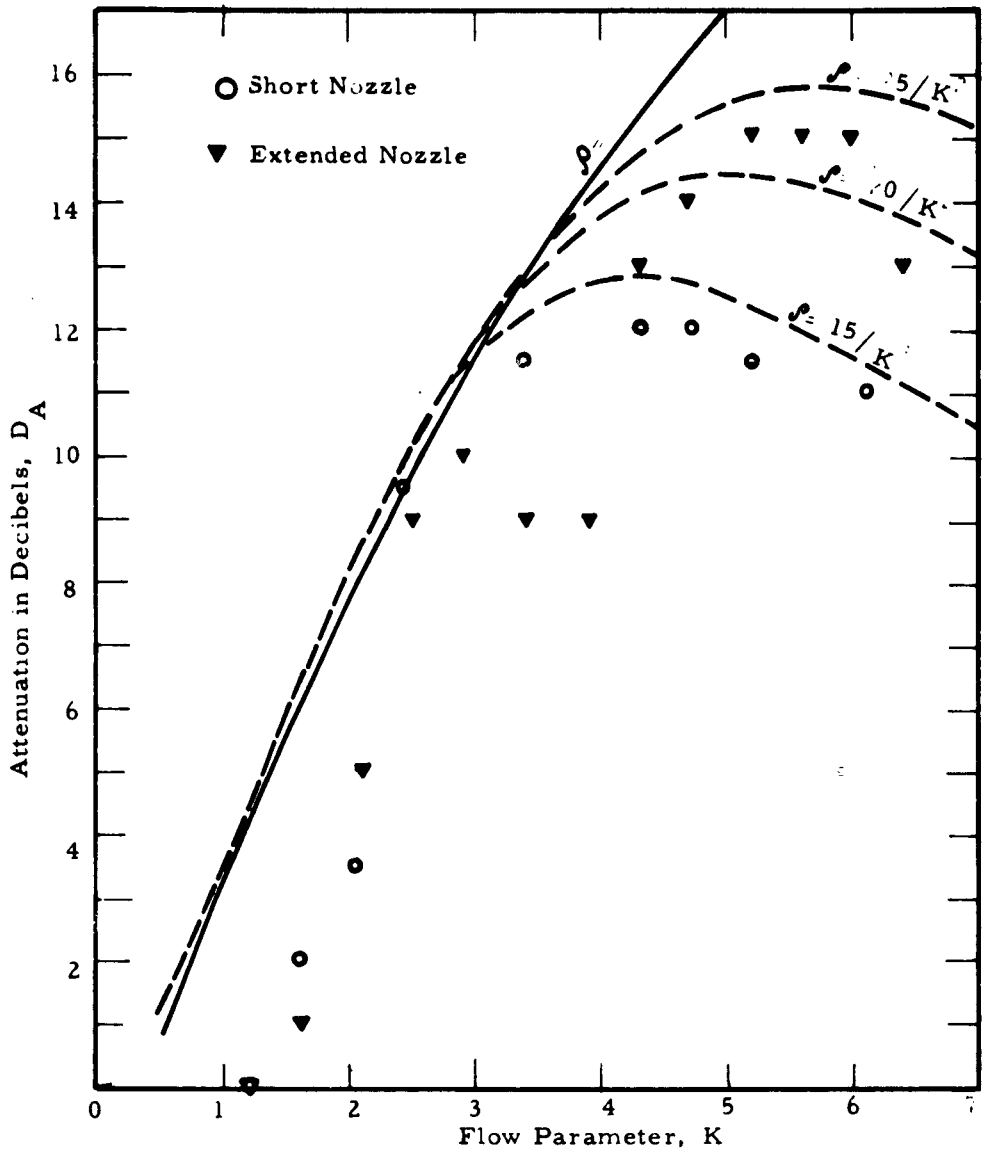

Fig. 8 EXPERIMENTAL RESULTS PLOTTED ON THEORETICAL DERIVATIONS, PLUGGED NOZZLE, $\rho = 2.02$

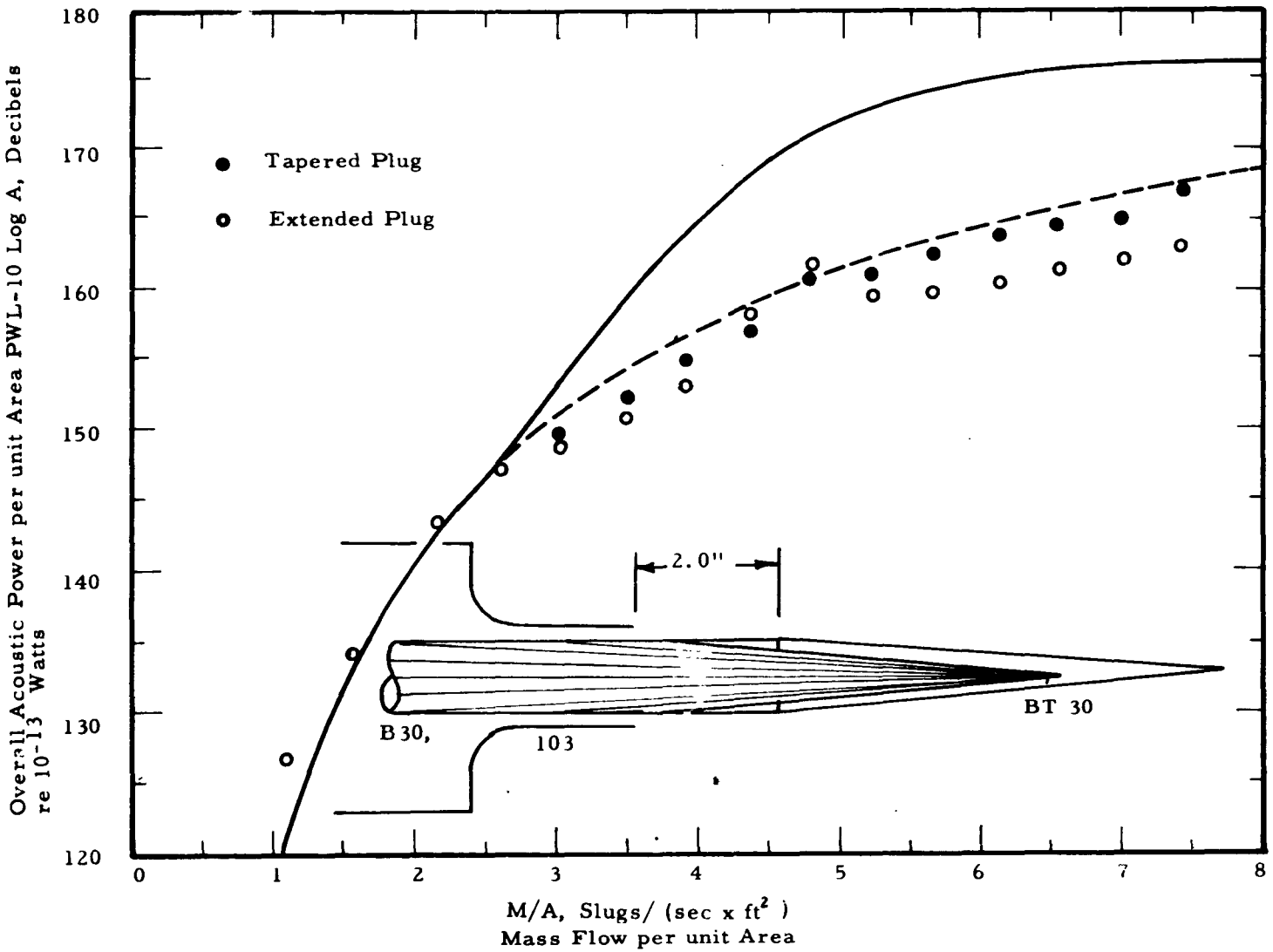

Fig 8a ACOUSTIC PERFORMANCE OF AN EXTENDED PLUG NOZZLE AS COMPARED WITH A TAPERED PLUG

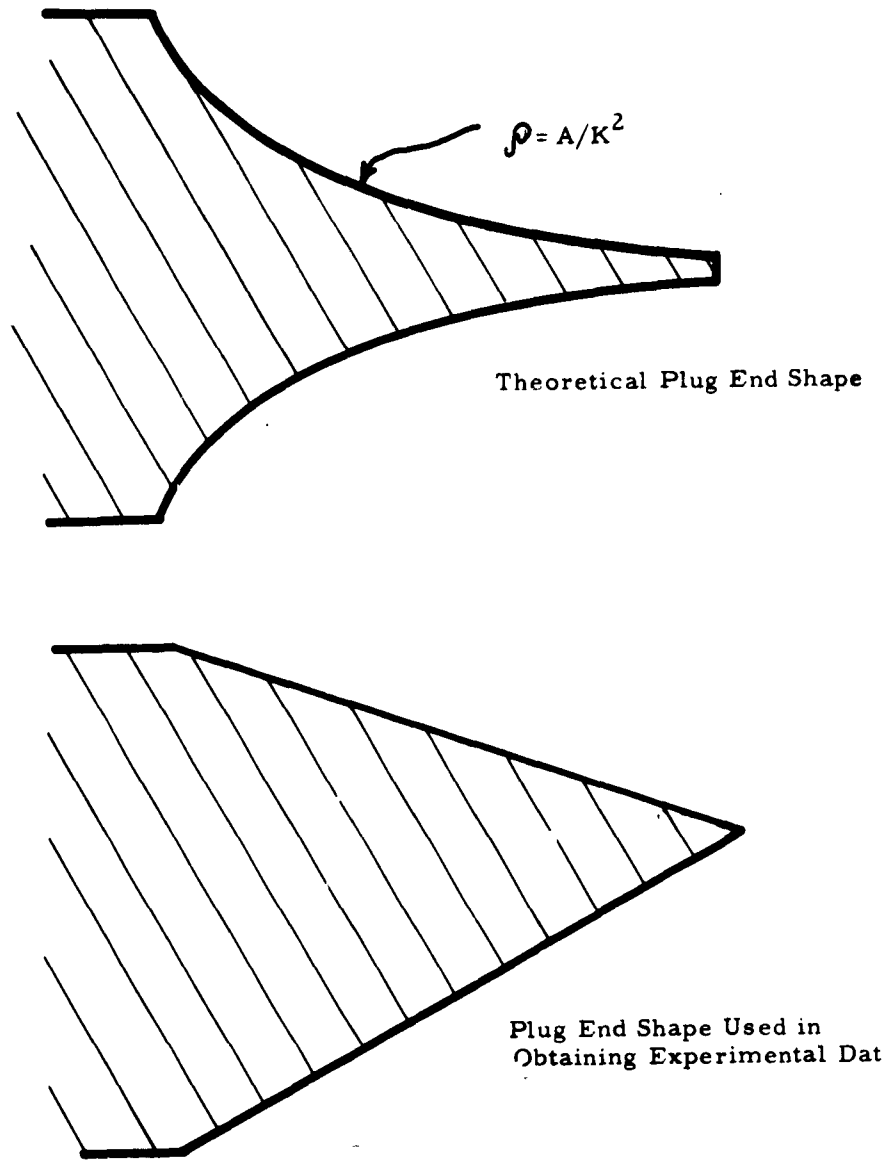

Fig 9 REPRESENTATIVE NOZZLE PLUG END SHAPES

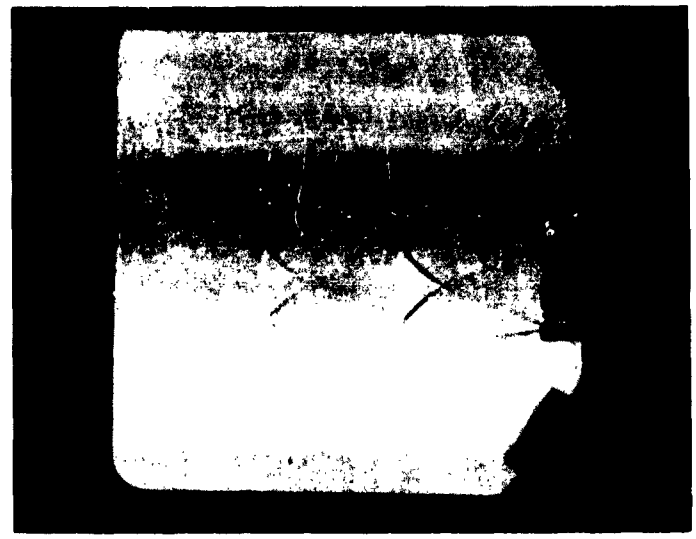

(a) Circular Jet Nozzle Shadowgraph. Pressure Ratio = 3.75
Exposure 1/500 sec.

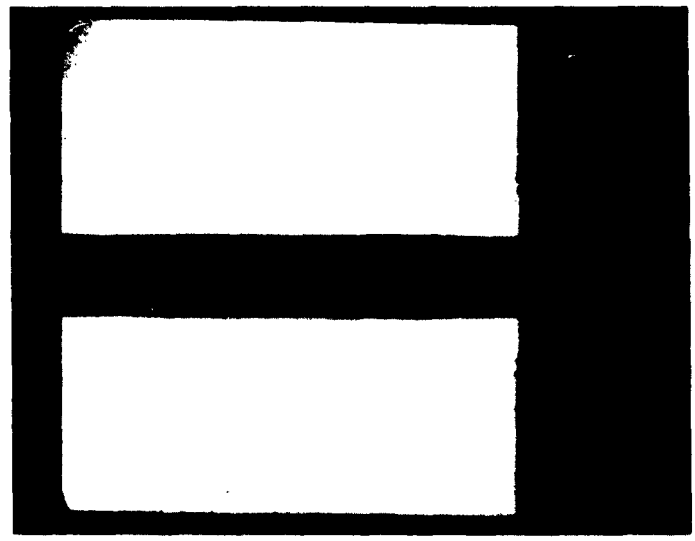

(b) Extended Plug Nozzle Shadowgraph. Pressure Ratio = 3.45;
Exposure 1/500 sec.

Figure 10. Shadowgraph Photos of Supersonic Jet Emitted from Circular and Extended Plug Nozzles.

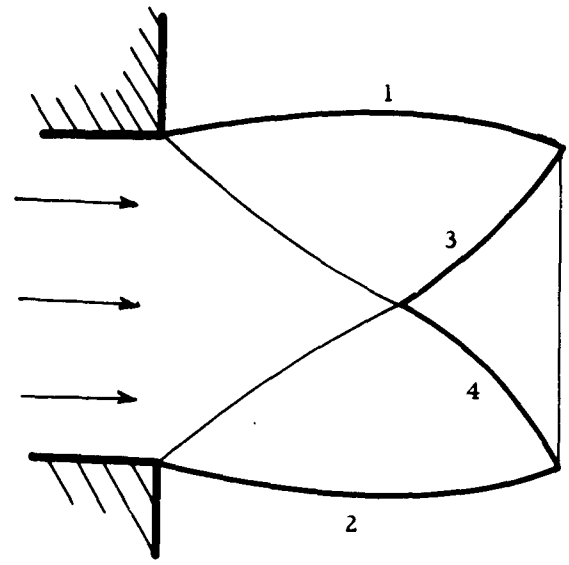

Experimental Shock Wave Formation (Shadowgraph Data)

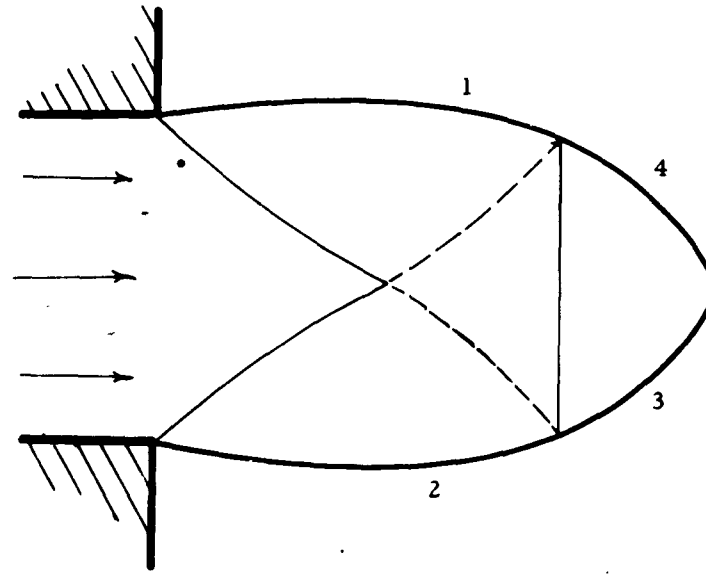

Theoretical Approximate Shock Wave Surface

Fig. 11 SHOCK WAVE FORMATION IN A CONVERGING UNPLUGGED CIRCULAR JET NOZZLE

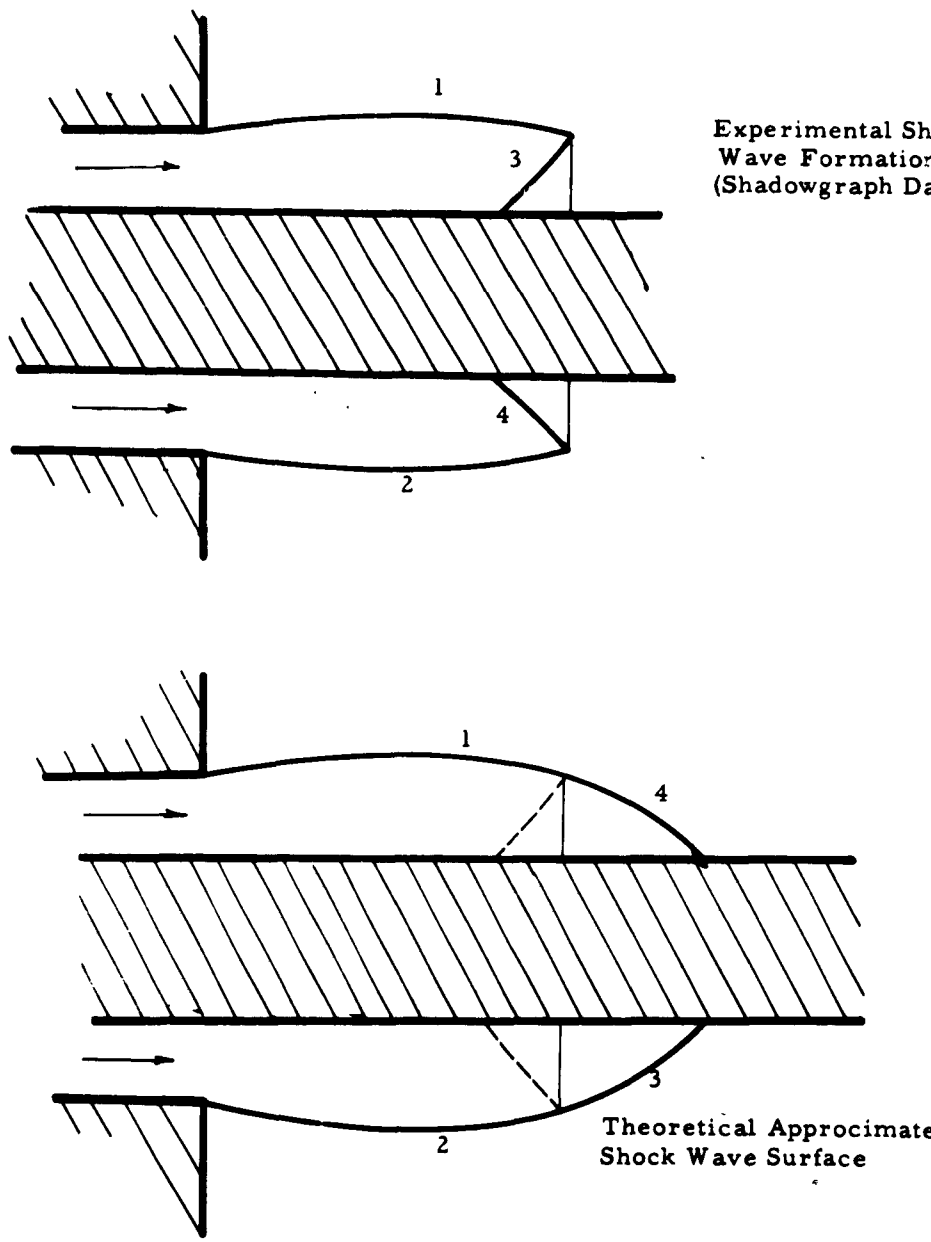

Fig. 12 SHOCK WAVE FORMATION IN A COVERGING PLUGGED CIRCULAR JET NOZZLE

Aeronautical Systems Division, Dir/Aeromechanics, Propulsion Lab, Wright-Patterson AFB, Ohio. Rpt. No. ASD-TDR-63-326. FUNDAMENTAL STUDY OF JET NOISE GENERATION AND SUPPRESSION Vol.I Experimental and Theoretical Investigations of Model Jet Exhaust Stream Noise and the Development of Normalizing Parameters for Size and Temperature. Final Report, March 1963. 191 pp. incl illus., tables, 9 refs.

Unclassified Report

Part I

Far-field sound pressure levels were measured in an anechoic room for noise generated by cold air flow through a wide variety of small nozzle configurations including converging, converging-diverging, and annular types with and without center core flow. The results are examined in terms of flow and acoustic power performance, directivity, and power spectral density. Normalization parameters are developed for both size and temperature which

(over)

1. Noise
2. Jet Exhaust Stream Noise
3. Acoustic Power
4. Noise Control
I. AFSC Project 3066, Task 306601
II. Contract AF 33(657)-8405
III. ARF Institute of Technology, Chicago, Ill.
IV. W.C.Sperry, A.Peter, R.Kamo
V. 1211-11
VI. Not aval fr OTS
VII. In ASTIA Collection

Aeronautical Systems Division, Dir/Aeromechanics, Propulsion Lab, Wright-Patterson AFB, Ohio. Rpt. No. ASD-TDR-63-326. FUNDAMENTAL STUDY OF JET NOISE GENERATION AND SUPPRESSION Vol.I Experimental and Theoretical Investigations of Model Jet Exhaust Stream Noise and the Development of Normalizing Parameters for Size and Temperature. Final Report, March 1963. 191 pp. incl illus., tables, 9 refs.

Unclassified Report

Part I

Far-field sound pressure levels were measured in an anechoic room for noise generated by cold air flow through a wide variety of small nozzle configurations including converging, converging-diverging, and annular types with and without center core flow. The results are examined in terms of flow and acoustic power performance, directivity, and power spectral density. Normalization parameters are developed for both size and temperature which

(over)

1. Noise
2. Jet Exhaust Stream Noise
3. Acoustic Power
4. Noise Control
I. AFSC Project 3066, Task 306601
II. Contract AF 33(657)-8405
III. ARF Institute of Technology, Chicago, Ill.
IV. W.C.Sperry, A.Peter, R.Kamo
V. 1211-11
VI. Not aval fr OTS
VII. In ASTIA Collection

show good agreement between flow and acoustic performance of small cold jet nozzles, large hot jet nozzles, and jet engines. A particular configuration of annular plug nozzle exhibited remarkably good acoustic performance with no measurable loss of mass flow performance.

Part II

A simplified theory on the acoustical attenuation qualities of an extended plug nozzle is presented. The theory is based upon similarity relationships and on the location of shock structure, a parameter which remains constant in supersonic flow. Theoretical curves of noise attenuation versus nozzle geometrical parameters show reasonable agreement with our experimental cold jet results for a nozzle exhibiting ten to fifteen decibels reduction over a wide mass flow range. Design criteria is given which indicate that twenty or more decibels reduction may be accomplished by an optimally designed nozzle.

show good agreement between flow and acoustic performance of small cold jet nozzles, large hot jet nozzles, and jet engines. A particular configuration of annular plug nozzle exhibited remarkably good acoustic performance with no measurable loss of mass flow performance.

Part II

A simplified theory on the acoustical attenuation qualities of an extended plug nozzle is presented. The theory is based upon similarity relationships and on the location of shock structure, a parameter which remains constant in supersonic flow. Theoretical curves of noise attenuation versus nozzle geometrical parameters show reasonable agreement with our experimental cold jet results for a nozzle exhibiting ten to fifteen decibels reduction over a wide mass flow range. Design criteria is given which indicate that twenty or more decibels reduction may be accomplished by an optimally designed nozzle.